

AD-A122 004

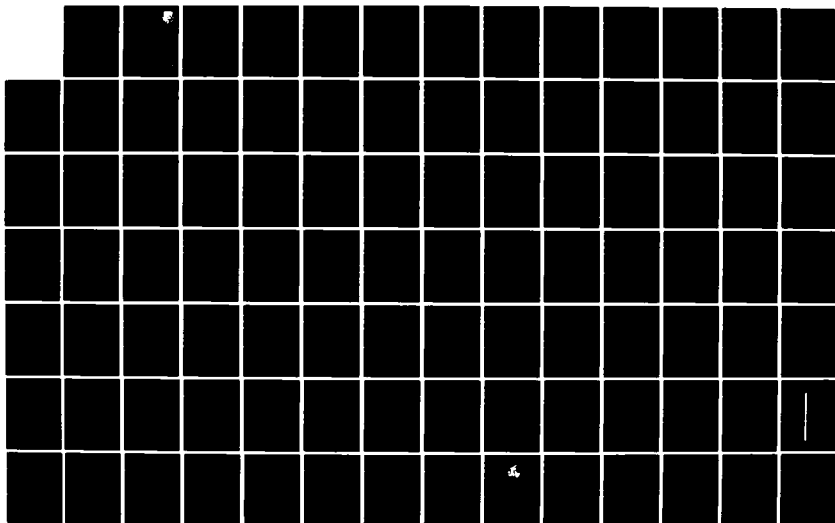
QRC EVALUATION OF MATERIALS AND PROCESSES(U) DAYTON
UNIV OH RESEARCH INST D R ASKINS ET AL OCT 82
UDR-TR-82-85 AFMAL-TR-82-4104 F33615-80-C-5011

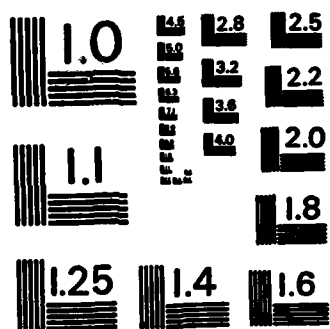
1/4

UNCLASSIFIED

F/G 14/2

NL





MICROCOPY RESOLUTION TEST CHART
NATIONAL BUREAU OF STANDARDS-1963-A

AFWAL-TR-82-4104



QRC EVALUATION OF MATERIALS AND PROCESSES

University of Dayton Research Institute
University of Dayton
Dayton, Ohio 45469

OCTOBER 1982

Final Report for Period 1 April 1980 - 14 June 1982

Approved for public release; distribution unlimited.

MATERIALS LABORATORY
AIR FORCE WRIGHT AERONAUTICAL LABORATORIES
AIR FORCE SYSTEMS COMMAND
WRIGHT-PATTERSON AIR FORCE BASE, OHIO 45433

DEC 1 1982

A

82 12 01 005

AD A122004

DTIC FILE COPY

NOTICE


When Government drawings, specifications, or other data are used for any purpose other than in connection with a definitely related Government procurement operation, the United States Government thereby incurs no responsibility nor any obligation whatsoever; and the fact that the government may have formulated, furnished, or in any way supplied the said drawings, specifications, or other data, is not to be regarded by implication or otherwise as in any manner licensing the holder or any other person or corporation, or conveying any rights or permission to manufacture, use, or sell any patented invention that may in any way be related thereto.

This technical report has been reviewed by the Office of Public Affairs (ASD/PA) and is releasable to the National Technical Information Service (NTIS). At NTIS, it will be available to the general public, including foreign nations.

This technical report has been reviewed and is approved for publication.


ALBERT OLEVITCH
Project Engineer

FOR THE COMMANDER:


WARREN P. JOHNSON, Chief
Systems Support Division
Materials Laboratory

"If your address has changed, if you wish to be removed from our mailing list, or if the addressee is no longer employed by your organization, please notify AFWAL/MLS, WPAFB, OH 45433 to help us maintain a current mailing list."

Copies of this report should not be returned unless return is required by security considerations, contractual obligations, or notice on a specific document.

UNCLASSIFIED

SECURITY CLASSIFICATION OF THIS PAGE (When Data Entered)

REPORT DOCUMENTATION PAGE		READ INSTRUCTIONS BEFORE COMPLETING FORM
1. REPORT NUMBER AFWAL-TR-82-4104	2. GOVT ACCESSION NO. AD-A122004	3. RECIPIENT'S CATALOG NUMBER
4. TITLE (and Subtitle) QRC Evaluation of Materials and Processes		5. TYPE OF REPORT & PERIOD COVERED Final Report 1 April 1980-14 June 1982
		6. PERFORMING ORG. REPORT NUMBER UDR-TR-82-85
7. AUTHOR(s) D. R. Askins, R. R. Cervay, K. A. Davis, D. L. Hart, K. L. Lindsay, and B. H. Wilt		8. CONTRACT OR GRANT NUMBER(s) F33615-80-C-5011
9. PERFORMING ORGANIZATION NAME AND ADDRESS University of Dayton Research Institute 300 College Park Avenue Dayton, Ohio 45469		10. PROGRAM ELEMENT, PROJECT, TASK AREA & WORK UNIT NUMBERS 2421-03-15
11. CONTROLLING OFFICE NAME AND ADDRESS Materials Laboratory (AFWAL/MLSE) Air Force Wright Aeronautical Laboratories, AFSC Wright-Patterson Air Force Base, Ohio 45433		12. REPORT DATE October 1982
		13. NUMBER OF PAGES 300
		15. SECURITY CLASS. (of this report) Unclassified
14. MONITORING AGENCY NAME & ADDRESS (if different from Controlling Office)		15a. DECLASSIFICATION/DOWNGRADING SCHEDULE
16. DISTRIBUTION STATEMENT (of this Report) Approved for public release; distribution unlimited.		
17. DISTRIBUTION STATEMENT (of the abstract entered in Block 20, if different from Report)		
18. SUPPLEMENTARY NOTES		
19. KEY WORDS (Continue on reverse side if necessary and identify by block number)		
Crack initiation	Dielectric constant	Reticulated foams
Slack-quenched	O-ring seals	Adhesion promoter
Mechanical properties	Sealants	Thermophysical properties
Fatigue crack growth rate	Chalking	Transparent plastics
Failure analysis	Hydrolytic stability	Honeycomb core
20. ABSTRACT (Continue on reverse side if necessary and identify by block number)		
<p>This report is comprised of six sections which summarize the engineering studies completed under contract to the Air Force Wright Aeronautical Laboratories, Materials Laboratory System Support Division. Materials evaluations under the categories of Alloys and Composites; Electronic Failure Analysis; Fibrous Materials; Elastomers; Plastics, Adhesives and Composites; and Lubricants were completed during the contract period.</p> <p>(Continued on reverse side)</p>		

DD FORM 1 JAN 73 1473

UNCLASSIFIED

SECURITY CLASSIFICATION OF THIS PAGE (When Data Entered)

19. Key Words (Concluded)

Adhesives	Injection molding
Stress cracking	Lubricating oils
Composites	Hydraulic fluids
Environmental aging	

20. Abstract (Concluded)

→ The section entitled Engineering Data on Alloys and Composites includes materials properties evaluations of metal alloys and composite structural components. These include data on fatigue crack growth data on Titanium at elevated temperatures, the degradation of Kevlar-29 at elevated temperatures, evaluation of the mechanical properties of Aluminum 7010 and X7091 alloys, and an evaluation of parachute shroud release mechanisms.

Other engineering evaluations in this section include strain rate effects on Aluminum weld joints, fatigue-crack growth of improperly quenched Aluminum, the development of an automated system for fatigue crack growth rate data acquisition, and the effect of spectrum modifications to FALSTAFF on fatigue life and fracture face morphology.

This section of the report also includes the results of a Navy round robin program to determine corrosion fatigue crack growth rates on HY-80 and a C-1 compressor stage material and adhesive evaluation for the Arnold Engineering and Development Center (AEDC).

→ The next section, Electronic Failure Analysis, presents the results of failure analyses of a number of aircraft electronic components. These include transducers, potentiometers, resistors, switches, a Cathode Ray Tube (CRT) geometry focus correction module. A method to remove residue from a fiber optic terminal and repairability of an encapsulated electronic module are also discussed.

→ Section 3, Fibrous Materials, presents the results of testing of carpeting materials for use in aircraft and the results of tensile tests conducted on Kevlar-29 parachute cord.

→ The section on Elastomers discusses the evaluations of a number of aircraft sealants and foams, including fluorosilicones, polysulfides, channel and firewall sealants, fuel tank foams, polyurethane potting compound, external coatings, and a fuel tank bladder. It also discusses a method for the determination of air entrapped in a sealant.

This section also presents the results obtained from evaluations of various cleaning solvents and adhesion promoters on the adhesive properties of fuel tank sealants. Compatibility determinations of a number of O-ring seal materials, a polysulfide sealant, and two impregnants are also presented.

→ The fifth section, Plastics, Adhesives and Composites, summarizes the results of mechanical testing of shelter honeycomb core materials, NORYL EN-265 aircraft plastic, and characterization of NEAT resin matrix systems. It also discusses the assistance provided in the preparation of a primer specification and the evaluation of a number of plastics including windshield material, reinforced injection molded urethane resin, expandable sleeving, polyetherimide, Kevlar-29, and glass-filled polyphenylene sulfide. Mechanical, physical and thermophysical properties of various radome materials are also presented.

Surface treatments, adhesive bonding, coating developments, and a comparison of multi-joint and single-lap adhesive specimens are also discussed.

→ The last section, entitled Lubricants, presents the results of physical properties determined for a number of aircraft hydraulic fluids and lubricating oils.

PREFACE

This summary report covers work performed under Air Force Contract F33615-80-C-5011 during the period from 1 April 1980 through 14 June 1982. The contract was initiated under Project Number 2421-03-15, "Materials Application." The work was administered under the direction of the Air Force Wright Aeronautical Laboratories, Materials Laboratory, Materials Support Division, Wright-Patterson Air Force Base, Ohio. Mr. A. Olevitch (AFWAL/MLSE) acted as Project Engineer.

This work was conducted under the general supervision of Mr. D. Gerdeman, Project Supervisor. University of Dayton personnel who made major contributions to the program include: D. R. Askins, R. R. Cervay, K. A. Davis, D. L. Hart, J. J. Ruschau, M. Stropki, B. H. Wilt, Research Engineers; and D. Anderson, D. R. Byrge, J. R. Conner, J. N. Dues, T. Dusz, J. H. Eblin, T. A. Elmore, G. W. Fultz, W. Gaskins, K. Kowan, R. J. Kuhbander, K. L. Lindsay, A. L. Logue, S. C. Macy, R. J. Marton, J. C. McKiernan, D. S. Opela, L. D. Pike, P. J. Proshek, R. A. Rondeau, D. W. Wolesslagle, Research Technicians. Jeanne Drake, Secretary, organized and typed this summary report. This report was submitted in July 1982. The contractor's report number is UDR-TR-82-85.



Project No.	
Contract No.	
Report No.	
Date	
Author	
Reviewer	
Approved	
Signature	
Initials	
Comments	

A

TABLE OF CONTENTS

<u>SECTION</u>	<u>PAGE</u>
1 ENGINEERING DATA ON ALLOYS AND COMPOSITES	1
1.1 Ti 6-2-4-6 ELEVATED TEMPERATURE MODELING OF FATIGUE CRACK GROWTH RATE DATA	1
1.2 TEMPERATURE DEGRADATION OF KEVLAR-29 TENSILE STRENGTH	12
1.3 MECHANICAL PROPERTY EVALUATION OF ALUMINUM ALLOY 7010-T73651	18
1.4 AN EMPIRICAL MODEL FOR LOADING RATIO EFFECT ON FATIGUE CRACK GROWTH RATE DATA	31
1.5 PARACHUTE SHROUD RELEASE EVALUATION	43
1.6 STRAIN RATE EFFECT ON ALUMINUM WELD JOINTS	57
1.7 FATIGUE CRACK GROWTH INVESTIGATIONS OF IMPROPERLY-QUENCHED (SOFT) ALUMINUM UNDER A TRANSPORT AIRCRAFT LOAD HISTORY	60
1.8 MECHANICAL PROPERTY INVESTIGATION OF ALUMINUM X7091-T7E69 EXTRUSION	69
1.9 FATIGUE CRACK GROWTH RATE DATA ACQUISITION SYSTEM FOR LINEAR AND NONLINEAR FRACTURE MECHANICS APPLICATIONS	76
1.10 EFFECT OF SPECTRUM MODIFICATIONS TO FALSTAFF ON FATIGUE LIFE AND FRACTURE FACE MORPHOLOGY	92
1.11 NAVY ROUND ROBIN CORROSION FATIGUE CRACK GROWTH RATE TEST RESULTS FOR HY-80	104
1.12 EVALUATION OF AEDC C-1 STAGE MATERIAL AND ADHESIVE SYSTEMS	112
2 ELECTRONIC FAILURE ANALYSIS	127
2.1 FAILURE ANALYSIS OF A LINEAR POSITION TRANSDUCER	127
2.2 FAILURE ANALYSIS OF AN EJECTION SEAT ARMING SWITCH	127
2.3 FAILURE ANALYSIS OF TWO STEERING CONTROL FEEDBACK POTENTIOMETERS	128
2.4 INVESTIGATION OF A METHOD FOR THE REMOVAL OF THE RESIDUE IN A FIBER OPTIC TERMINAL	129
2.5 REPAIRABILITY ANALYSIS OF AN ENCAPSULATED ELECTRONIC MODULE	130

TABLE OF CONTENTS (Continued)

<u>SECTION</u>		<u>PAGE</u>
2.6	INTEGRATED CIRCUIT LEAD SOLDERABILITY	131
2.7	FAILURE INVESTIGATION OF A CRT GEOMETRY/FOCUS CORRECTION MODULE	131
2.8	FAILURE INVESTIGATION OF A PRECISION VARIABLE RESISTOR	132
2.9	FAILURE ANALYSIS OF LANDING GEAR DOWN LOCK SWITCH	133
2.10	FAILURE INVESTIGATION OF AN ANGLE OF ATTACK TRANSMITTER	134
2.11	FAILURE ANALYSIS OF TIP TANK AUTO-DROP SWITCHES	135
2.12	FAILURE ANALYSIS OF A LINEAR SERVO ACCELEROMETER	137
2.13	CERT (COMBINED ENVIRONMENTS RELIABILITY TEST) FAILURE ANALYSIS	139
3	FIBROUS MATERIALS	142
3.1	AIRCRAFT CARPETING	142
3.2	PARACHUTE CORD	142
3.3	FLAME RESISTANT MATERIALS	144
4	ELASTOMERS	145
4.1	EVALUATION OF SEALANTS AND FOAMS	145
4.1.1	Fluorosilicone Sealants	145
4.1.2	Polysulfide Sealants	146
4.1.3	Channel Sealants	147
4.1.4	Firewall Sealants	148
4.1.5	Air Content in Sealant	150
4.1.6	Foam Materials	155
4.2	EVALUATION OF CLEANING SOLVENTS AND ADHESION PROMOTERS	162
4.3	PEEL STRENGTH EVALUATIONS	166
4.3.1	MIL-C-5541 Alodine Coating	166
4.3.2	Ion Vapor Deposited Coating	167
4.3.3	Peel Test Methods	168
4.3.4	Peel Test Differences	170
4.4	EVALUATION OF O-RINGS	173
4.4.1	MIL-P-25732 O-Ring Seals	173
4.4.2	PNF O-Ring Seals	175

TABLE OF CONTENTS (Continued)

<u>SECTION</u>		<u>PAGE</u>
	4.4.3 Corrosion Test of Hydraulic Seals	177
4.5	MATERIALS COMPATIBILITY IN JP-10 FUEL	178
4.6	MATERIALS COMPATIBILITY WITH SHALE OIL DERIVED FUEL	179
4.7	POLYURETHANE POTTING COMPOUND	179
4.8	BOSTIK NO. 7102 USING THE "MERCER HOT MELT APPLICATOR"	187
4.9	GENERAL ELECTRIC TUFEL SILICONE	188
4.10	EVALUATION OF F-16 FUEL BLADDER	189
4.11	EXTERIOR FUEL TANK COATINGS	191
5	PLASTICS, ADHESIVES, AND COMPOSITES	200
5.1	SHELTER HONEYCOMB CORE SHEAR TESTING	200
5.2	TENSILE PROPERTIES OF NORYL EN-265	219
5.3	CHARACTERIZATION OF NEAT RESIN MATRIX SYSTEMS	219
5.4	ASTM-E-TBD-5 PRIMER SPECIFICATION	219
5.5	FIELD PERFORMANCE PANELS	219
5.6	OPTICAL PROPERTIES OF TRANSPARENT SPECIMENS	223
5.7	EVALUATION OF REINFORCED RIM 120	223
5.8	COLD TEMPERATURE TESTS FOR EXPANDABLE SLEEVING	226
5.9	POLYETHERIMIDE (G.E.) TENSILE TESTING	226
5.10	KEVLAR-29 RECOVERY SYSTEMS	226
5.11	ANISOTROPY OF GLASS FILLED POLYPHENYLENE SULFIDE	229
5.12	STANDARD WORK PROCEDURE REQUESTS	229
5.13	SUPPORT OF JANAF FIBERGLASS LAMINATE TESTING	229
5.14	NEW SURFACE TREATMENTS	241
5.15	BONDING PANELS FOR STRESS-DURABILITY	241
5.16	EVALUATION OF SCAR SPECIMEN DESIGN	243
5.17	CHARACTERIZATION OF A "SILICADIZED COATING" AS A BONDING SURFACE	249

TABLE OF CONTENTS (Continued)

<u>SECTION</u>		<u>PAGE</u>
5.18	DURABILITY TESTING OF FM400/BR400 ADHESIVE JOINTS	251
5.19	COMPATIBILITY OF PHOSPHORIC ACID ANODIZING WITH 350°F (177°C) CURING ADHESIVE PRIMERS	251
5.20	TENSILE SHEAR EVALUATION OF FUEL TANK ADHESIVES	263
5.21	SHELTER REPAIR ADHESIVES	267
5.22	COPPER CONTENT OF FPL ETCH SOLUTIONS	267
5.23	STATISTICAL STUDY OF RYTON R-4 INJECTION MOLDING	270
5.24	TENSILE CREEP TESTING OF RYTON R-4	271
5.25	HIGH TEMPERATURE ADHESIVE EVALUATION	272
6	LUBRICANTS	276
6.1	HYDRAULIC FLUID	276
6.2	LUBRICATING FLUIDS	278
6.3	ADDITIVES	280
6.4	INSTRUMENT OIL CANDIDATE FLUIDS	280
7	REFERENCES	281

LIST OF ILLUSTRATIONS

<u>FIGURE</u>		<u>PAGE</u>
1	Tensile Specimen Configuration	2
2	Fatigue Crack Growth Rate CT Test Specimen	2
3	Room Temperature Fatigue Crack Growth Test Results	5
4	Linear Region of Room Temperature Fatigue Crack Growth Rate Test Data	6
5	R-ratio Equal to 0.1, 800°F (427°C), Fatigue Crack Growth Test Data	7
6	R-ratio Equal to 0.3, 800°F (427°C), Fatigue Crack Growth Test Data	8
7	R-ratio Equal to 0.5, 800°F (427°C), Fatigue Crack Growth Test Data	9
8	R-ratio Equal to 0.7, 800°F (427°C), Fatigue Crack Growth Test Data	10
9	R-ratio Equal to 0.1, Room Temperature and 800°F (427°C) Fatigue Crack Growth Test Data	11
10	R-ratio Versus Log-Paris Coefficient for 800°F (427°C) Ti6-2-4-6 Fatigue Crack Growth Test Data	13
11	Constant Amplitude Loading Cyclic Crack Growth Test Results for CT Specimens Loaded in the Longitudinal Grain Direction at 72°F (22°C)	24
12	Constant Amplitude Loading Cyclic Crack Growth Test Results for CT Specimens Loaded in the Long-Transverse Grain Direction at 72°F (22°C)	25
13	Constant Amplitude Loading Cyclic Crack Growth Test Results for L-T and T-L Oriented CT Specimens at 72°F (22°C)	26
14	Constant Amplitude Loading Cyclic Crack Growth Test Results for Longitudinal Grain Loaded CT Specimens at 250°F (121°C)	28
15	Constant Amplitude Loading Cyclic Crack Growth Test Results for Long-Transverse Grain Loaded CT Specimens at 250°F (121°C)	29

LIST OF ILLUSTRATIONS (Continued)

<u>FIGURE</u>		<u>PAGE</u>
16	Constant Amplitude Loading Cyclic Crack Growth Test Results for L-T Oriented CT Specimens at 72°F, 250°F, and 350°F (22°C, 121°C, and 177°C)	30
17	Room Temperature, Loading Ratio = 0.10 FCGR Test Data for Al 7010-T73651	33
18	Room Temperature, Loading Ratio = 0.30 FCGR Test Data for Al 7010-T73651	34
19	Room Temperature, Loading Ratio = 0.5 FCGR Test Data for Al 7010-T73651	35
20	Room Temperature, Loading Ratio = 0.8 FCGR Test Data for Al 7010-T73651	36
21	Loading Ratio, R, Versus Log-Paris Coefficient, Log C, for Al 7010-T73651 at 72°F (22°C)	38
22	Fast Crack Growth Rate Region, Room Temperature Loading Ratio = 0.65, FCGR Test Data for Al 7010-T73651	41
23	Full Velocity Range, Room Temperature, Loading Ratio = 0.65 FCGR Data for Al 7010-T73651	42
24	Center-Cracked Panel Test Geometry	62
25	Portion of Load-versus-Time Record for TWIST Load History	63
26	Spectrum Fatigue Crack Growth Data for Normal and "Soft" Aluminum 2024-T351	65
27	Spectrum Fatigue Crack Growth Data for Normal and "Soft" Aluminum 7075-T651	66
28	Constant Amplitude FCGR Data for Normal and "Soft" Aluminum 2024-T351	67
29	Constant Amplitude FCGR Data for Normal and "Soft" Aluminum 7075-T651	68
30	Typical Fraction Appearance for Aluminum X7091-T7E69 Toughness Specimens	72
31	Smooth Axial Fatigue Results for Aluminum X7091-T7E69 Extrusion	73

LIST OF ILLUSTRATIONS (Continued)

<u>FIGURE</u>		<u>PAGE</u>
32	Notched ($D_t = 3$) Axial Fatigue Results for Aluminum X7091-T7E69 Extrusion	74
33	Constant Amplitude Fatigue Crack Growth Data for X7091-T7E69 for Room Temperature and 250°F (121°C) Test Environments	75
34	Schematic of FCGR Acquisition System	78
35	Compact Type (CT) Specimen Geometry	80
36	Flow Chart for FCGR Acquisition System	81
37	Graphical Method for Determining Area Under Load-Displacement Record for nth Cycle	84
38	LEFM Crack Growth Data Obtained via Acquisition System and Visual Methods	89
39	NLFM Crack Growth Data Obtained via Acquisition System and Analytical Methods	91
40	Center-Cracked-Panel Specimen Geometry	96
41	Fatigue Crack Growth Data for Standard FALSTAFF	97
42	Fatigue Crack Growth Data for FALSTAFF with Negative Loads Clipped	100
43	Fatigue Crack Growth Data for FALSTAFF with Loose Pin at Load Level 34	101
44	Fatigue Crack Growth Data for FALSTAFF with Tight Pin and Load Level 34	103
45	WOL Specimen Geometry	105
46	Horizontal Stressing Frame Installed in Vertical Loading Fatigue Machine	106
47	Crack Length vs. Cycles Record for Specimen X1-41	109
48	Crack Length vs. Cycles Record for Specimen X1-5	110
49	Fatigue Crack Growth Rate Results Based on Graphical Method	111
50	Fatigue Crack Growth Rate Results Based on Graphical, Acquisition System, and Optical Methods	113

LIST OF ILLUSTRATIONS (Concluded)

<u>FIGURE</u>		<u>PAGE</u>
51	Interlaminar Type Failure Experienced During Flexural Testing for Panels #3F and #4F	122
52	Typical Failure Mode for Edgewise Compression Testing	123
53	Hydrolytic Stability of MIL-B-83054, Type I (Orange) Foam	156
54	Hydrolytic Stability of MIL-B-83054, Type II (Yellow) Foam	157
55	Hydrolytic Stability of MIL-B-83054, Type III (Red) Foam	158
56	Hydrolytic Stability of MIL-B-83054, Type IV (Dark Blue) Foam	160
57	Hydrolytic Stability of MIL-B-83054, Type V (Light Blue) Foam	161
58	Standard Peel Test Panel	169
59	Peel Test Panel and Adapter	169
60	Peel Panel Lay-Up Order	197
61	Photomicrographs of Quartz/Polyimide Laminates	233
62	Laminate Photomicrographs	234
63	Thermal Conductivity Curves on EG/Epoxy Type 1 and 2 and Quartz 581/PMR-15 Laminates	237
64	Thermal Conductivity Curves on SG/Epoxy Type 1 and 2 and Cordopreg Laminates	238
65	Specimen Configurations for SCAR Design Evaluation	245
66	Wedge Crack Propagation Results for Reliabond 398 Adhesive on 2024T81 Aluminum Adherends in Salt Fog Environment	261
67	Wedge Crack Propagation Results for MB329-1 Adhesive on 2024T81 Aluminum Adherends in Salt Fog Environment	262
68	Fuel Tank Lap Shear Specimen	266

LIST OF TABLES

<u>TABLE</u>		<u>PAGE</u>
1	Chemical Constituent Analysis	1
2	Tensile Test Results for Ti6-2-4-6 Extruded Shaft	4
3	Load Carrying Capability of Kevlar-29 Aramid Fiber Woven Ribbon	15
4	Time-Temperature Exposure Degradation of Kevlar Ribbon	16
5	Tensile Properties of Al 7010-T73651	21
6	Fracture Toughness Test Results for Aluminum 7010-T73651	22
7	Parachute Harness Shroud Release Clasp Test Results	46
8	Frost Engineering Parachute Shroud Release Clasp Test Results	49
9	A-10 Aircraft Shroud Release Evaluation	52
10	Capwell Shroud Release Weight-Pan-Loaded Trigger Release	54
11	Parachute Shroud Release Test Group	55
12	Test Group's Fractional Success of Triggering The Shroud Release	56
13	Butt Weld Tensile Test Results	58
14	Longitudinal Tensile Data for Aluminum X7091-T7E69 Extrusion	71
15	Fracture Results for Aluminum X7091-T7E69 Extrusion (L-T Orientation)	71
16	Comparison of Acquisition System Output Data to Measure Crack Length and Area for J-Analysis	87
17	Comparison of Acquisition System Output Data to Measure Crack Length for K-Analysis	88
18	FALSTAFF Load Histogram	95

LIST OF TABLES (Continued)

<u>TABLE</u>		<u>PAGE</u>
19	Average Tensile Test Results for E293/E-Glass Material	114
20	Average Flexural Test Results for E293/E-Glass Material	116
21	Average Interlaminar Shear Test Results for E293/E-Glass	116
22	Average Single-Lap-Shear Results of Steel-Composite Specimens	117
23	Average Single-Lap-Shear Results for Composite-Composite Specimens	119
24	Test Results of Single-Lap-Shear Foam Adhesive Specimens	119
25	Flexural Test Results for E293-Aluminum Honeycomb Sandwich Panels	121
26	Edgewise Compression Results for E293-Aluminum Honeycomb Sandwich Panels	124
27	Individual Peel Test Results for Composite-Viton Peel Specimens	126
28	Aircraft Carpet Test Data	143
29	Visual Appearance of CS 3204 B-2 Sealant Base	151
30	Sealant Air Content Determinations	154
31	F-15 Foam	162
32	Peel Test Results	172
33	Physical Properties of O-Rings in MIL-H-5606 With and Without MLO-79-483 Additive After Aging for 70 hrs. at 275°F (135°C)	174
34	Materials Compatibility in JP-10 Fuel MIL-P-5315 Buna-N N602 O-rings	180
35	Materials Compatibility in JP-10 Fuel MIL-R-83248 Fluoroelastomer V747-75 O-rings	181

LIST OF TABLES (Continued)

<u>TABLE</u>		<u>PAGE</u>
36	Materials Compatibility in JP-10 Fuel MIL-R-25988 Fluorosilicone L677-70 O-rings	182
37	Materials Compatibility in JP-10 Fuel MIL-R-1149 Neoprene O-rings	183
38	Materials Compatibility in JP-10 Fuel MIL-S-8802 Polysulfide PS-890B-2	184
39	Materials Compatibility in JP-10 Fuel Imprex (Ultraseal PC504 Impregnant)	185
40	Materials Compatibility in JP-10 Fuel Loctite (Loctite PMS 10E Impregnant)	186
41	F-16 Fuel Bladder Evaluation	190
42	PR-1196 Tensile Strength, Elongation and Volume Swell	192
43	Bostik 473-13 Tensile Strength, Elongation and Volume Swell	193
44	Low Temperature Flexibility	194
45	Dynamic Cycling - With JP-4	195
46	PR-1196 Peel Strength	198
47	Bostik 473-13 Peel Strength	199
48	Shelter Core Material Characteristics	201
49	HRH-10 Core Shear Strength by Plate Test Method	203
50	WR-II Core Shear Strength by Beam Method, "L" Direction, 0.5 inch (1.27 cm) Thick	204
51	WR-II Core Shear Strength by Beam Method, "W" Direction, 0.5 inch (1.27 cm) Thick	205
52	WR-II Core Shear Strength by Beam Method, "L" Direction, 2 inch (5.08 cm) Thick	206
53	WR-II Core Shear Strength by Beam Method, "W" Direction, 2 inch (5.08 cm) Thick	207

LIST OF TABLES (Continued)

<u>TABLE</u>		<u>PAGE</u>
54	HRH-10 Core Shear Strength by Beam Method, "L" Direction, 0.5 inch (1.27 cm) Thick	208
55	HRH-10 Core Shear Strength by Beam Method, "W" Direction, 0.5 inch (1.27 cm) Thick	209
56	HRH-10 Core Shear Strength by Beam Method, "L" Direction, 2 inch (5.08 cm) Thick	210
57	HRH-10 Core Shear Strength by Beam Method, "W" Direction, 2 inch (5.08 cm) Thick	211
58	HRH-10 Core Shear Strength by Beam Method, "L" Direction, 3 inch (7.62 cm) Thick	212
59	HRH-10 Core Shear Strength by Beam Method, "W" Direction, 3 inch (7.62 cm) Thick	213
60	HRP Core Shear Strength by Beam Method, "L" Direction, 1.5 inch (3.81 cm) Thick	214
61	HRP Core Shear Strength by Beam Method, "W" Direction, 1.5 inch (3.81 cm) Thick	215
62	HTP Core Shear Strength by Beam Method, "L" Direction, 0.87 inch (2.22 cm) Thick, 3.2 lbs/ft ³ (51.3 kg/m ³) Density	216
63	HTP Core Shear Strength by Beam Method, "W" Direction, 0.87 inch (2.22 cm) Thick, 3.2 lbs/ft ³ (51.3 kg/m ³) Density	217
64	HTP Core Shear Strength by Beam Method, 0.87 inch (2.22 cm) Thick, 4.5 lbs/ft ³ (72.1 kg/m ³) Density	218
65	Tensile Properties of A-10 Plastic Parts	220
66	Tensile Properties of Virgin EN-265 and Polycarbonate	221
67	Properties of Cast Epoxy Resin Systems	222
68	Windshield Haze Measurements	224
69	Tensile Properties of RIM 120 (6LPT97-18) With 25% Glass Reinforcement	225

LIST OF TABLES (Continued)

<u>TABLE</u>		<u>PAGE</u>
70	Polyetherimide (G.E.) Tensile Specimens	227
71	Tensile Strength and Load Loss of Kevlar-29 Recovery Systems	228
72	Tensile Properties of Injection Molded Polyphenylene Sulfide	230
73	Physical Properties of JANAF Laminates	232
74	Specific Heat of JANAF Laminates	236
75	Tensile Properties of JANAF Laminates	239
76	Flexural Properties of JANAF Laminates	240
77	Lap Shear Properties of Bonds Incorporating Reacted Surface vs. Optimized FPL Etched Surface Treatments	242
78	Lap-Shear Control Properties of Bonded Panels for Stress-Durability	244
79	Static Lap-Shear Test Results for SCAR Design Evaluation	246
80	Stress-Durability Test Results Using the Sharp Fixture for SCAR Design Evaluation @ 140°F (60°C), 95-100% R.H.	247
81	Stress-Durability Test Results Using the Durability Test Apparatus for SCAR Design Evaluation @ 140°F (60°C), 95-100% R.H.	248
82	Lap Shear Results on Silicadized Coatings Tested at Room Temperature	250
83	FM400 Adhesive Durability Test Matrix	252
84	Static Thick Adherend Lap-Shear Strength of Commercial FM400 Adhesive System	253
85	Static Thick Adherend Lap-Shear Strength of UD-1 (with aluminum filler and no scrim)	254
86	Static Thick Adherend Lap-Shear Strength of UD-2 (with no scrim or aluminum filler)	255

LIST OF TABLES (Continued)

<u>TABLE</u>		<u>PAGE</u>
87	Environmental Stress-Durability Behavior of Lap-Shear Adhesive Joints	256
88	Lap Shear Property Summary	259
89	Floating Roller Peel Data Summary	260
90	Stress-Durability Test Results After 2400-Hour Exposure to 95°F (35°C), 5% Salt Spray Environment	264
91	Fuel Tank Adhesive Data	265
92	Atomic Absorption Analyses of Acid Solutions for Copper	269
93	Room Temperature Tensile Properties of Ryton R-4	272
94	Lap Shear Properties of FM-34 and PMR-15 Steel-to-Composite Panels	275

SECTION 1
ENGINEERING DATA ON ALLOYS AND COMPOSITES

1.1 Ti 6-2-4-6 ELEVATED TEMPERATURE MODELING OF FATIGUE CRACK GROWTH RATE DATA

The purpose of this program was to evaluate the constant amplitude loading fatigue crack growth resistance of titanium alloy 6Al-2Sn-4Zr-6Mo at an elevated temperature the material would encounter in service, e.g., jet engine application. The material is commonly used in-service where the environmental temperature can be up to 1000°F (538°C). A small amount of material was provided as an extruded shaft product form. The findings of a chemical constituent analysis performed on the test material are presented in Table 1.

TABLE 1
CHEMICAL CONSTITUENT ANALYSIS

<u>Al</u>	<u>Sn</u>	<u>Zr</u>	<u>Mo</u>	<u>Fe</u>	<u>Ti</u>
6.0	1.8	4.4	5.3	0.1	Balance

The molybdenum content is slightly low at 5.3 percent. Specifications call for a nominal 6.0 percent by weight content or a minimum of 5.5 percent by weight content.

Duplicate tensile tests were conducted at 72°F (22°C) and 800°F (427°C) on specimens cut from the test material and machined in accord with Figure 1. The specimens' loading axes were the circumferential direction of the shaft.

Constant amplitude loading fatigue crack growth rate (FCGR) tests were conducted on CT specimens machined from the test material in compliance with Figure 2. All of the specimens were removed from the test piece of material with circumferential-radial (C-R) grain orientation as defined by ASTM E-399.[1]

Room temperature FCGR tests were conducted at one loading ratio, R, equal to 0.1; 800°F (427°C) tests were conducted at four loading ratios: 0.1, 0.3, 0.5, and 0.7.

Tensile test results are presented in Table 2. With the 728°F (404°C) increase in temperature there is a 21.5 percent decrease in the tensile strength and a 35.0 percent decrease in the yield strength, along with a large increase in ductility.

The room temperature constant amplitude loading FCGR test results are presented in Figure 3. The linear region of the room temperature data set is represented in Figure 4 along with the best fit Paris equation (1) calculated for this smaller data set:

$$\frac{da}{dn} = C\Delta K^m \quad (1)$$

where da/dn is the crack growth rate, ΔK is the stress intensity, range, and C and m are the Paris coefficient and Paris exponent, respectively.

The 800°F (427°C) FCGR test data for the four loading ratios 0.1, 0.3, 0.5, and 0.7 are presented in Figures 5 through 8. In general, the FCGR increases with increasing R-ratio. The best fitting Paris equation calculated for each loading ratio data set is also presented in each respective figure. The Paris exponents for the four calculated best fit equations associated with the 800°F (427°C) data sets are 2.52, 2.49, 2.47, and 2.38. The average value exponent, \bar{m} , is 2.47; the scatter in these four exponents is ± 4 percent. In contrast the exponent, m , calculated for the best fitting equation to the room temperature data set (Figure 4) was 2.97 which is larger than any of the exponents calculated for the elevated temperature data sets. Figure 9 presents the 72°F (22°C) and 800°F (427°C) data sets generated with the loading ratio equal to 0.1. As would be indicated by the difference in the exponents the two sets of data cross. At a high stress intensity range the room temperature crack growth rate is greater than that at 800°F (427°C).

Reference 2 presents room temperature fatigue crack growth rate data where the loading ratio and the log-Paris coefficient

TABLE 2
TENSILE TEST RESULTS FOR Ti6-2-4-6
EXTRUDED SHAFT

Test Temperature °F (°C)	Ultimate Strength KSI (MPa)	0.2% Yield Strength KSI (MPa)	Elongation 0.5 in. (12.7 mm) G.L. (%)	Reduction of Area (%)
72 (22)	159.3 (1098)	147.5 (1016)	10.5	23.3
	160.5 (1106)	148.1 (1020)	14.0	23.3
	<u>157.4 (1084)</u>	<u>146.1 (1006)</u>	<u>10.2</u>	<u>24.7</u>
	Avg. 159.1 (1096)	147.2 (1014)	11.6	23.8
800 (427)	123.0 (847)	95.1 (655)	19.0	51.0
	125.6 (863)	95.9 (661)	16.7	45.8
	<u>126.0 (868)</u>	<u>96.3 (664)</u>	<u>16.4</u>	<u>46.6</u>
	Avg. 124.9 (860)	95.7 (659)	17.4	47.8

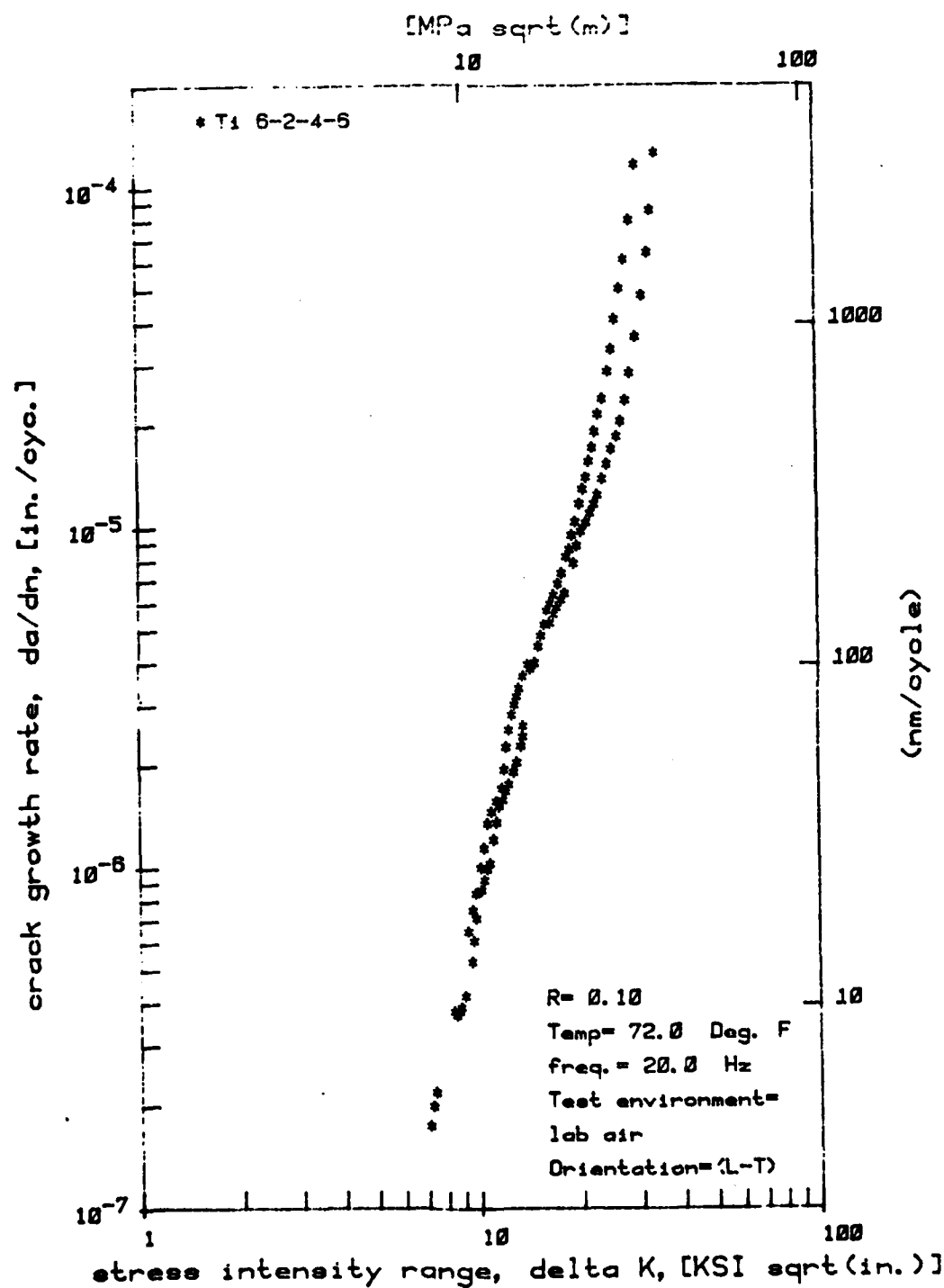


Figure 3. Room Temperature Fatigue Crack Growth Test Results.

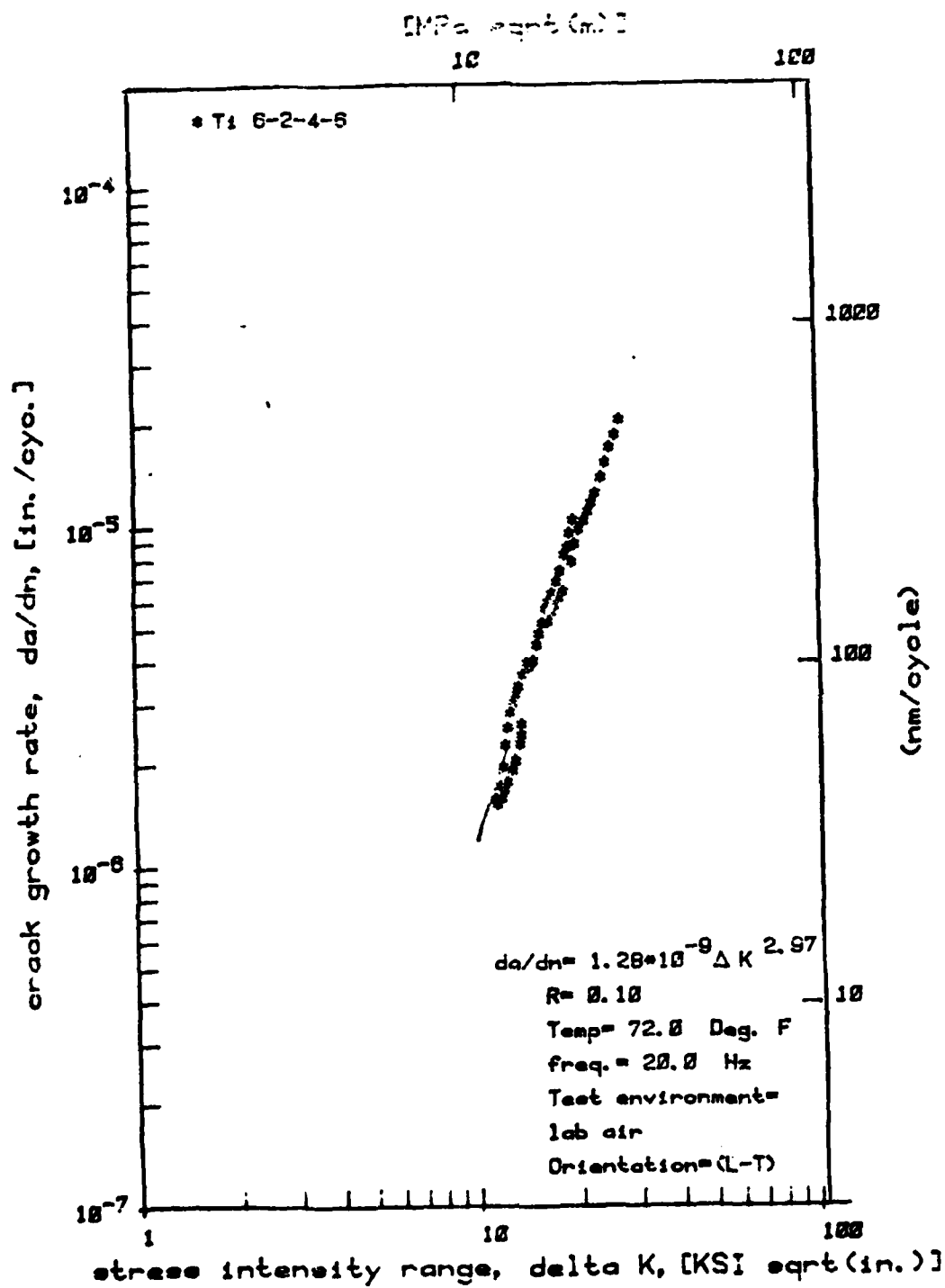


Figure 4. Linear Region of Room Temperature Fatigue Crack Growth Rate Test Data.

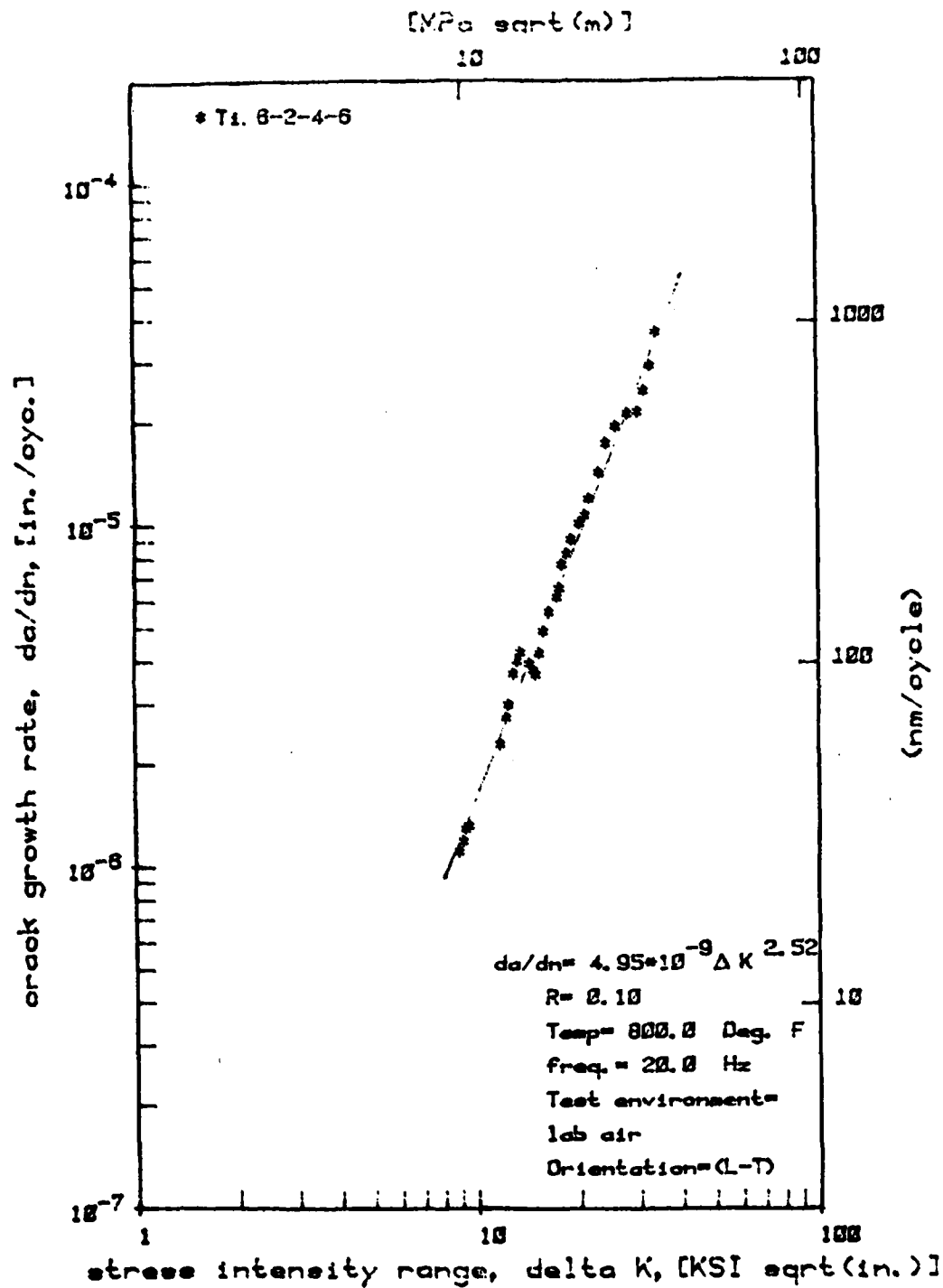


Figure 5. R-ratio Equal to 0.1, 800°F (427°C), Fatigue Crack Growth Test Data.

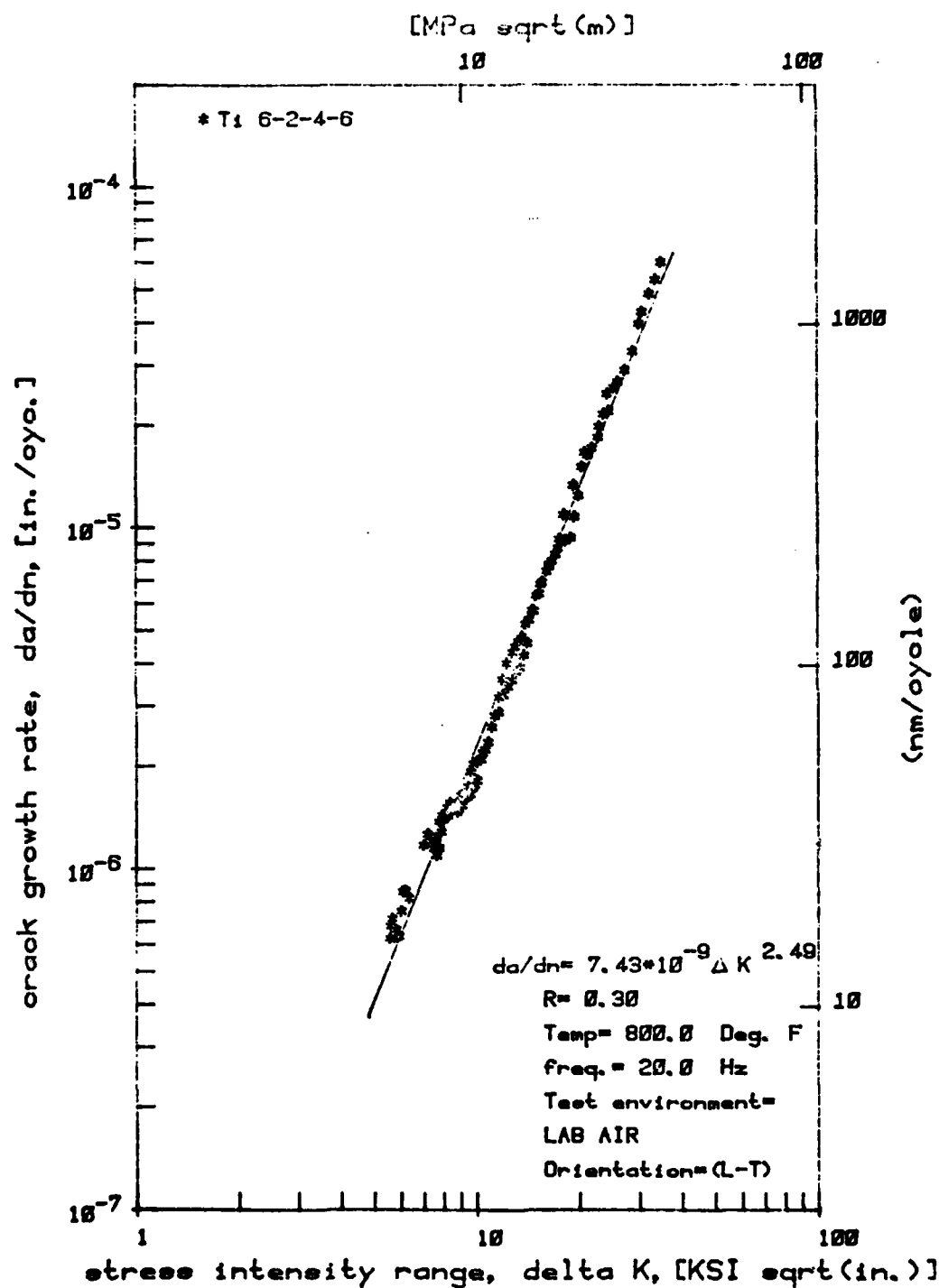


Figure 6. R-ratio Equal to 0.3, 800°F (427°C) Fatigue Crack Growth Test Data.

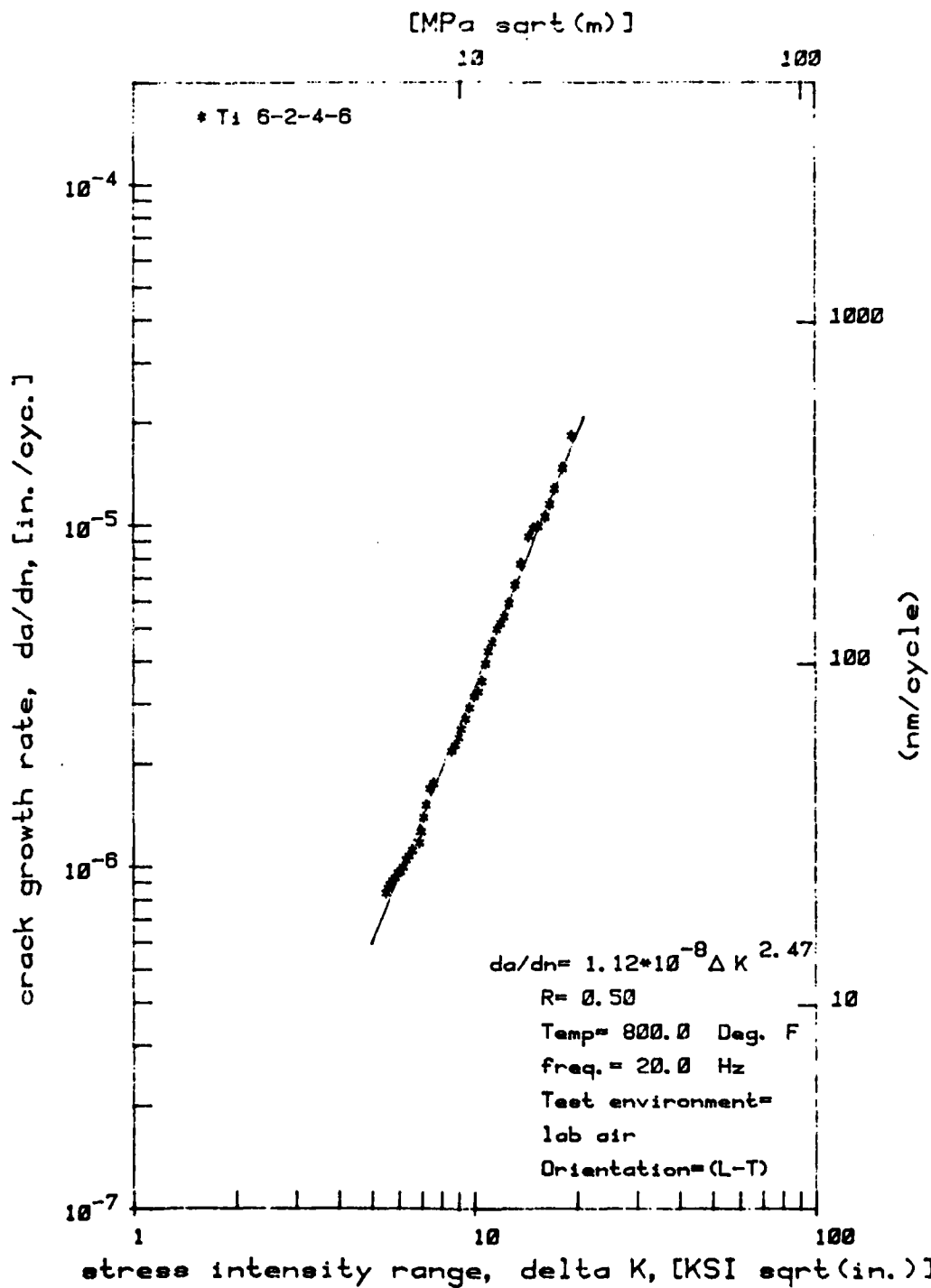


Figure 7. R-ratio Equal to 0.5, 800°F (427°C) Fatigue Crack Growth Test Data.

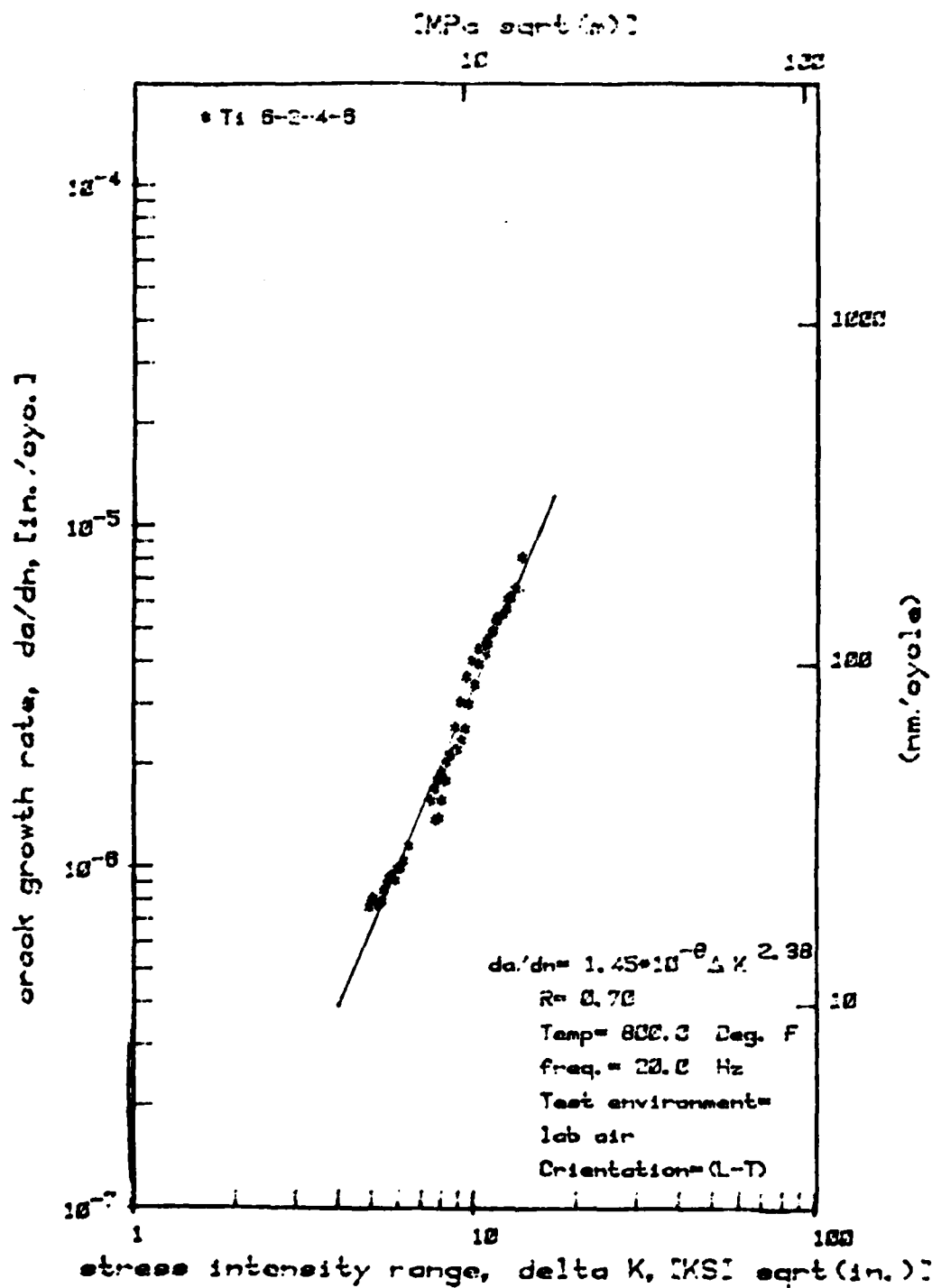


Figure 8. R-ratio Equal to 0.7, 800°F (427°C) Fatigue Crack Growth Test Data.

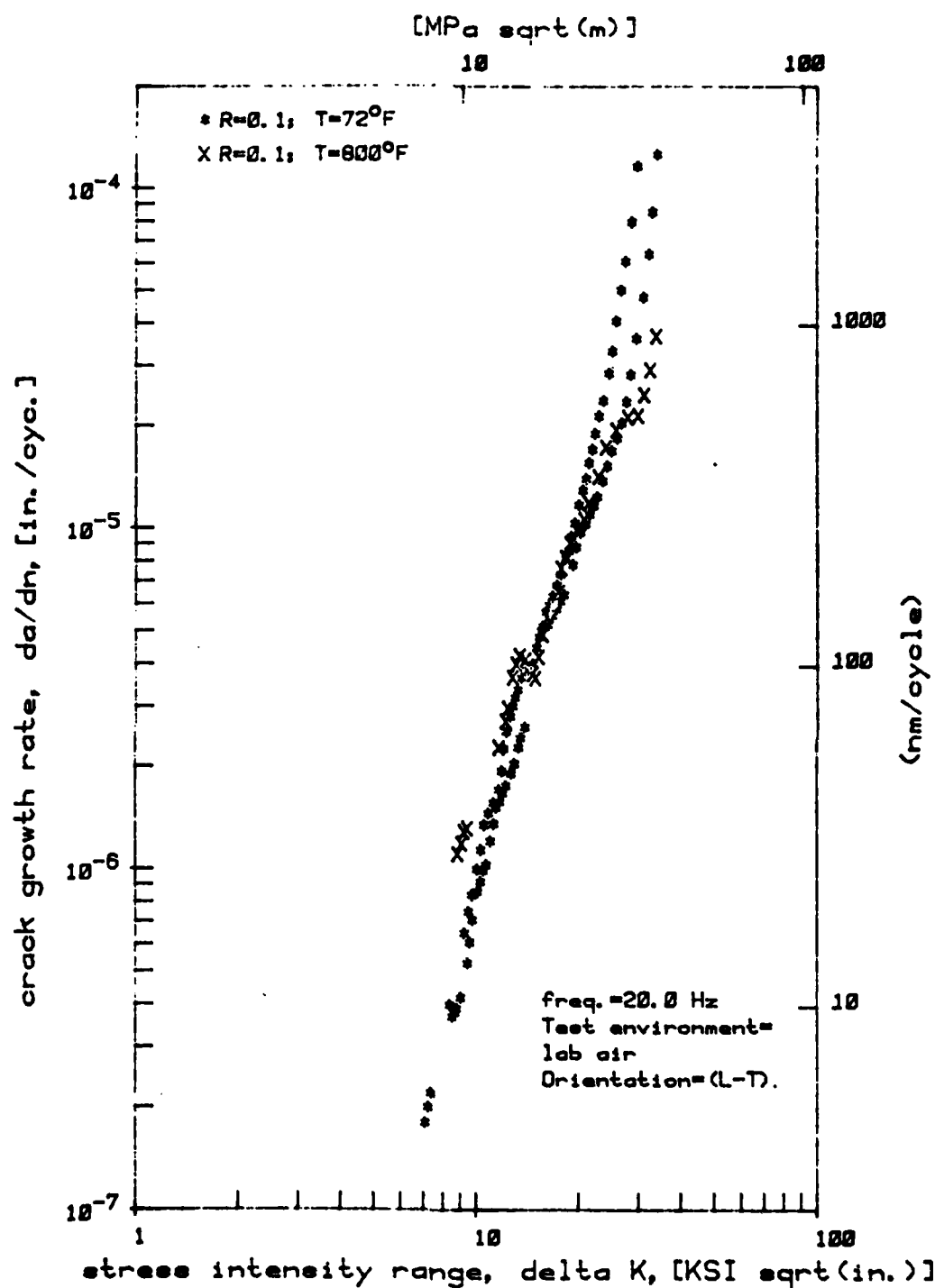


Figure 9. R-ratio Equal to 0.1, Room Temperature and 800°F (427°C) Fatigue Crack Growth Test Data.

are linearly related for data sets generated at constant loading frequency and test temperature. Figure 10 presents the loading ratio versus the log-Paris coefficients taken from Figures 5 through 8 for the four 800°F (427°C) data sets. Here too, the log-Paris coefficient can fairly be represented as linearly related to the loading ratio for constant loading frequency and an elevated temperature test parameter.

1.2 TEMPERATURE DEGRADATION OF KEVLAR-29 TENSILE STRENGTH

Drag parachutes constructed of Aramid fiber woven ribbon are often employed to deploy the main chute which in turn perform a variety of functions such as slowing down a landing aircraft, arresting a rocket sled, or allowing the recovery of an air vehicle. The various applications for the chutes involve storage of the units for up to ten years in worldwide weather environments. Ultraviolet light as in sunlight, moisture, and heat all degrade the material's load carrying ability. This program concentrates on the effect of one of these variables, prolonged exposure to a constant elevated temperature.

This program was initiated to determine how rapidly the material's tensile strength deteriorates due to prolonged furnace exposure at different elevated temperatures. The test material was Kevlar-29 which is a DuPont para-aramid fiber. Nominal load-carrying ability of the particular size and weave test ribbon was reported to be 600 pounds (2,669 N). The four temperatures under consideration were: 437°F (225°C), 347°F (175°C), 257°F (125°C), and 212°F (100°C). The high temperature, 437°F (225°C), was included because of application in a particular system where the chute is packed very close to the rocket engine exhaust nozzles and experiences a service temperature of up to 400°F (204°C). All tests were conducted at room temperature in accord with Method 4108, Federal Test Method Standard 191A. The minimum crosshead velocity called for in the test standard, 2 inches per minute (51 mm/min), was employed

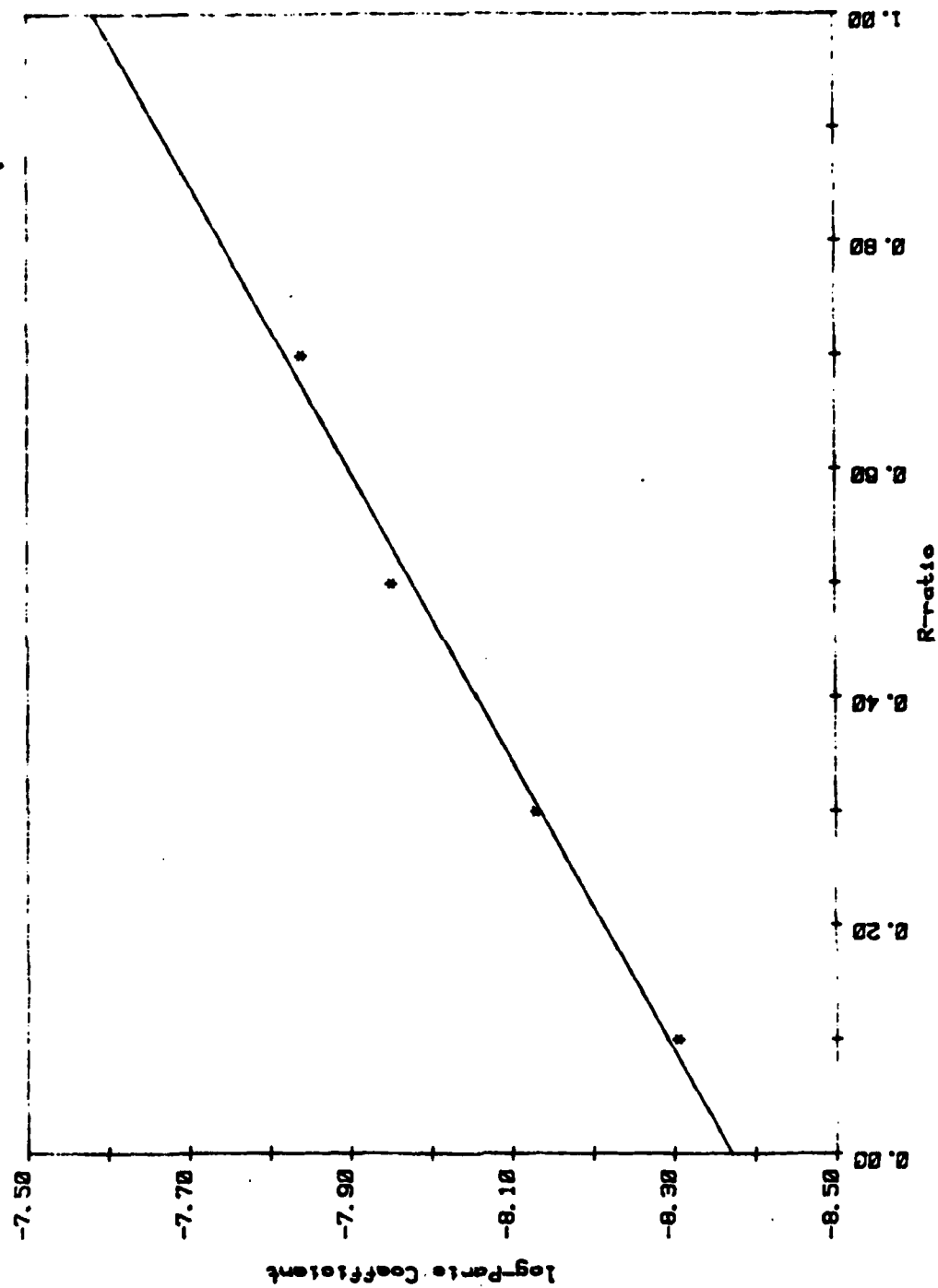


Figure 10. R-ratio Versus Log-Paris Coefficient for 800°F (427°C) Ti6-2-4-6 Fatigue Crack Growth Test Data.

for all tests. The test standard's recommended test fixtures were not used; the gripping fixtures described in Reference 3 were used for all testing. Upon removal of the test ribbon from the ovens, sufficient time was allowed for the material to stabilize at the 72°F (22°C) test temperature. The material was exposed to temperature for 28 days or until the average tensile strength degradation fell to less than 85 percent of the unexposed material's average load-carrying capability.

For a baseline data set, 12 specimens of the test material in the as-received condition were tensile pulled to failure. The test results are presented in Table 3. The average strength of the ribbon was found to be 676 pounds (3,006 N) which is 12 percent above the nominal load carrying ability. There were found to be some scatter in the failure load among the baseline set of specimens. The maximum failure load was 722 pounds (3,211 N) and the minimum failure load was 646 pounds (2,873 N), representing a 76 lbf scatter range for the set of 12 tests. The smallest failure load within the baseline set was 7.7 percent in excess of the nominal 600 pound (2,669 N) load carrying capability the ribbon was made to carry. 85 percent of the average baseline tensile strength is 575 pounds (2,558 N); this value was used as a minimum value termination criteria for the series of time-temperature exposures being conducted at 437°F (225°C) and 347°F (175°C).

A summary table containing the average value for each set of specimens that underwent the same time-exposure are presented in Table 4.

The 437°F (225°C) exposure temperature is too high a temperature for Kevlar-29 ribbon. The average test result failed the 85 percent retained tensile strength criteria following a mere 0.5 hour furnace exposure. In fact, limited service life could be anticipated where the material was subjected to 347°F (175°C). At this temperature the ribbon failed the 85 percent retained strength criteria after 24 hours.

TABLE 3
LOAD CARRYING CAPABILITY OF
KEVLAR-29 ARAMID FIBER WOVEN RIBBON

Specimen No.	Failure Load*	
	Pounds	Newtons
1	662	2945
2	722	3111
3	690	3069
4	652	2909
5	664	2953
6	684	3042
7	682	3034
8	652	2900
9	688	3066
10	676	3007
11	696	3096
12	<u>646</u>	<u>2873</u>
	Avg. 676	3006

* Test temperature was 72°F (22°C) .

TABLE 4
TIME-TEMPERATURE EXPOSURE DEGRADATION
OF KEVLAR RIBBON

Exposure Temperature °F (°C)		Exposure Time (Hours)	Avg. Tensile Load Lbs (N)		No. of Specimens	% Retained Strength
72	22	0	676	(3007)	12	100
437	225	0.5	557	(2478)	12	82
		1.0	591	(2629)	3	87
		1.3	535	(2380)	3	79
		2.3	551	(2451)	3	81
		3.0	519	(2309)	3	77
347	175	8.0	605	(2691)	3	89
		16.0	595	(2647)	3	88
		24.0	559	(2486)	3	83
		96.0	568	(2526)	3	84
		120.0	556	(2473)	5	82
257	125	8.0	584	(2598)	3	86
		16.0	621	(2762)	3	92
		24.0	600	(2669)	3	89
		48.0	575	(2558)	3	85
		72.0	593	(2637)	3	88
		96.0	574	(2553)	3	85
		168.0	591	(2628)	3	87
		336.0	603	(2682)	6	89
		504.0	577	(2566)	3	85
		672.0	581	(2584)	3	86
212	100	24.0	659	(2931)	3	98
		48.0	650	(2891)	3	96
		72.0	656	(2918)	3	97
		168.0	646	(2873)	3	96
		336.0	603	(2682)	3	89
		504.0	623	(2771)	3	92
		672.0	618	(2749)	3	92

The series of tests conducted on specimens undergoing an oven exposure at 257°F (125°C) was carried out for the full 28 days. The average tensile strength for specimens removed from the oven after 28 days (672 hours) was equal to 86 percent of the strength of the material in the as-received condition. The strength was not appreciably decreasing when the test series was terminated.

The 212°F (100°C) oven exposure tests were also carried out for the full 28-day test period allocated to this program. Over that period the tensile strength decreased to 92 percent of the as-received material's average tensile strength and appears to have leveled off at that value, showing little or no signs of further degradation for the final 200 hours of the exposure period.

Looking at Table 4, the test material responded much more dramatically to the exposure temperature it was subjected to than to the duration of the exposure. For the 257°F (125°C) exposure there is very little change in the average strength for the exposures varying in length from 8 to 672 hours. For the other three series of time-temperature exposures there appears to be an initial short period of rapid strength degradation followed by little or no change in the strength with further increasing exposure time. For the 347°F (175°C) exposure temperature following 24 hours, the material's average load carrying ability had decreased to 83 percent of the as-received material's. The additional 100 hours of oven exposure caused little further strength degradation. Similarly, for the 212°F (100°C) oven exposed material following 168 hours, the material's average strength had decreased to be 96 percent that of the as-received materials. After an additional 500 hours the material's average load carrying capability had dropped only an additional 4 percent.

The scatter observed in the baseline set failure loads continued in the data sets for specimens subjected to the same

time-temperature exposure. The amount of scatter broadened for some of the specimen sets subjected to long exposure periods, (336 to 672 hours) at the two lower temperatures of 257°F (125°C) and 212°F (100°C). For example, a failure load range of 142 pounds was obtained for the three specimens subjected to 257°F (125°C) for 672 hours, and a failure load range of 130 pounds was obtained for the three specimens oven exposed to 212°F (100°C) for 672 hours. The diverging data scatter band is approaching one-quarter of the average test result. It is difficult to make any further generalized observation because the wide failure load scatter band for the baseline data set and diverges to be even wider for the lower temperature/long term exposure specimen test results. Further analysis would require: (1) a much larger specimen sampling to be representative of the material, (2) a statistical analysis of the larger samplings, and (3) consideration of a minimum guaranteed retained strength.

1.3 MECHANICAL PROPERTY EVALUATION OF ALUMINUM ALLOY 7010-T73651

Aluminum alloy 7010 was developed by Alcan Plate Limited, Birmingham, England. The material is of interest to the Air Force because it has been accepted by several European sources as being an equivalent substitute for alloy 7050 and has been proposed for use in those countries. There are limited mechanical property test data available in the literature for alloy 7010. Both alloys 7050 and 7010 were developed for applications requiring high strength, high fracture toughness, exfoliation resistance, and stress corrosion cracking resistance in thick section product forms, e.g., 2 to 4 inch (50.8 to 101.6 mm) thick rolled plate.

Alcan Plate Limited produced the test material which they provided in the form of a 2 inch (50.8 mm) thick rolled plate. It was provided in the T73651, overaged and cold-worked heat treatment. The material is a high purity aluminum alloy with very small amounts of iron and silicon impurities present. The

findings of a chemical constituent analysis are presented below. The alloy's copper content is high for a 7000 series aluminum alloy and is intended to improve stress corrosion cracking resistance. Except for a slightly higher copper content, the two alloys, 7010 and 7050, are similar in chemical composition. Both alloys use zirconium rather than chromium as the grain refiner. Zirconium provides high strength and toughness while retaining good corrosion resistance.

CHEMICAL COMPOSITION, WT. PERCENT

	<u>Zn</u>	<u>Mg</u>	<u>Cu</u>	<u>Zr</u>	<u>Si</u>	<u>Fe</u>	<u>Ti</u>	<u>Mn</u>	<u>Cr</u>	<u>Other</u>	<u>Al</u>
7010 Test Material	6.0	2.3	1.9	0.12	0.09	0.07	0.01	<0.01	<0.01	<0.01	Balance
Alcan	5.7-	2.2-	1.5-	0.11-	0.10	0.15	0.05	0.03	0.05	0.05	Balance
7010 Spec.	6.7	2.7	2.0	0.17	Max	Max	Max	Max	Max	0.15 tot.	
7050	5.7-	1.9-	2.0-	0.08-	0.12	0.15	0.06	0.10	0.04	0.05	Balance
Mil Spec.	6.7	2.6	2.6	0.15	Max	Max	Max	Max	Max	0.15 tot.	

Included in the test program are test data for the following mechanical properties: tensile strength, fracture toughness, stress corrosion cracking threshold in a 3.5 percent by weight NaCl solution, and constant amplitude fatigue crack growth rate. Duplicate tests were performed for the fracture toughness data at both 72°F (22°C) and 250°F (121°C). All tensile tests were conducted at 72°F (22°C). For the tensile and fracture toughness tests, duplicate specimens were machined from the plate with specimen loading directions parallel to each of the three principal grain orientation directions. Specimens for the fatigue crack growth tests were loaded in one of two principal grain directions, longitudinal and long-transverse, both at room temperature and 250°F (121°C). A single crack growth test was conducted at 350°F (177°C); this specimen had the L-T grain orientation. Only short-transverse (S-L) loading direction specimens were used for the stress corrosion threshold tests.

All tests were conducted in compliance with the applicable ASTM testing procedure: E-399-78, "Plane Strain Fracture Toughness of Metallic Materials;" E-8-78, "Tension Testing of Metallic

Materials;" and E-647-78T, "Constant-Load-Amplitude Fatigue Crack Growth Rate Above 10^{-8} m/cycle." Where test standards are nonexistent, as in the case of stress corrosion cracking, current practices employed throughout the technical community were used.

Room temperature tensile test results are presented in Table 5. The alloy is a high strength 7000 series aluminum alloy comparable to alloy 7175, 7050, and 7475 in the T73 heat treated condition. There is little variation in the ultimate and yield strength data obtained from the specimens with the three various grain orientations. The material's ductility as indicated by the elongation and reduction of area are approximately equal to the same 7000 series aluminum alloys listed above in the T73 heat treatment. The short transverse tensile specimens demonstrated lower ductility than the other two grain orientations.

Room temperature and 250°F (121°C) fracture toughness test results are presented in Table 6. Those tests that are shown as not valid do not meet the ASTM E-399-78 specimen thickness criteria which calls for a minimum thickness of approximately 0.84 inch (21 mm). Naturally, those specimens loaded in the longitudinal grain direction displayed the highest conditional toughness, K_Q , while those loaded in the short transverse grain direction have the lowest fracture toughness. Of the longitudinal specimen data those with the L-S orientation possess the highest K_Q test results at both room temperature and at 250°F (121°C). Generally the increase in environmental temperature from 72°F (22°C) to 250°F (121°C) had little effect on the material's conditional toughness, K_Q .

Because of the large number of invalid toughness data, primarily caused by insufficient specimen thickness, four additional compact specimens (A1-A4) were fabricated from the remnant of the test plate but with thickness, B, equal to 1.50 inches (31.8 mm). Two of the specimens underwent tests at 72°F (22°C) and the other two were tested at 250°F (121°C).

TABLE 5
TENSILE PROPERTIES OF Al 7010-T73651
(All tests performed at 72°F (22°C))

Specimen No.	Grain Orientation	Ultimate Tensile Str. KSI (MPa)	0.2% Yield Strength KSI (MPa)	% Elong.	% R.A.
L1	Longitudinal	72.4 (499)	61.9 (426)	14.4*	43.0
L2	Longitudinal	72.8 (501)	65.1 (449)	13.4*	35.8
L3	Longitudinal	74.9 (516)	65.4 (450)	12.4*	38.0
L4	Longitudinal	74.5 (513)	65.2 (449)	11.2*	27.8
T1	Long-Transverse	73.5 (506)	62.6 (431)	10.5*	25.6
T2	Long-Transverse	73.7 (508)	62.5 (431)	12.0*	38.7
T3	Long-Transverse	73.0 (503)	62.2 (429)	12.6*	34.0
T4	Long-Transverse	74.5 (513)	64.2 (442)	12.5*	26.9
ST1	Short-Transverse	72.4 (499)	64.3 (443)	8.1**	19.5
ST2	Short-Transverse	73.4 (506)	66.2 (456)	7.7**	13.3
ST3	Short-Transverse	72.9 (502)	65.2 (449)	8.9**	10.6
ST4	Short-Transverse	74.7 (515)	64.1 (442)	7.0**	8.7

* Elongation in a 1 inch (25.4 mm) gage length.

** Elongation in a 0.5 inch (12.7 mm) gage length.

TABLE 6
FRACTURE TOUGHNESS TEST RESULTS FOR
ALUMINUM 7010-T73651

Specimen No.	Orientation	Test Temperature		K _Q		ASTM Valid?
		(°F)	(°C)	KSI $\sqrt{\text{in}}$	(MPa $\sqrt{\text{m}}$)	
TL1	L-T	72	22	39.0	(42.9)	No
TL2	L-T	72	22	36.4	(40.0)	No
TL3	L-T	72	22	35.6	(39.1)	No
LT1	T-L	72	22	29.9	(32.9)	Yes
LT2	T-L	72	22	29.0	(31.9)	Yes
LT3	T-L	72	22	30.8	(33.8)	Yes
LS1	T-S	72	22	30.3	(32.3)	Yes
LS2	T-S	72	22	31.8	(34.9)	Yes
TS4	L-S	72	22	39.9	(43.9)	No
SL10	S-L	72	22	23.4	(25.7)	Yes
SL11	S-L	72	22	22.7	(24.9)	Yes
TL4	L-T	250	121	37.3	(41.1)	No
TL5	L-T	250	121	35.8	(39.3)	No
TL6	L-T	250	121	33.1	(36.4)	No
LT4	T-L	250	121	28.0	(30.8)	Yes
LT5	T-L	250	121	29.5	(32.4)	No
LT6	T-L	250	121	29.6	(32.5)	No
LS3	T-S	250	121	32.8	(36.0)	No
TS5	L-S	250	121	39.2	(43.1)	No
TS6	L-S	250	121	42.4	(46.6)	No
A1	L-T	72	22	37.8	(41.5)	Yes
A3	L-T	72	22	37.1	(40.8)	Yes
A2	L-T	250	121	38.0	(41.8)	Yes
A4	L-T	250	121	39.4	(43.3)	Yes

The results for all four of these tests are valid by the ASTM test standard and are presented at the bottom of Table 6.

Only two precracked short transverse (S-L) orientation compact type specimens were statistically loaded in the 3.5 percent by weight sodium chloride corrosive solution. This loading orientation is the most sensitive to stress corrosion cracking for the following reasons: first, it has the lowest tensile strength; secondly, corrosion cracking is an intergranular phenomena, and with S-L specimen orientation the crack is moving in the longitudinal grain direction. These concomitant factors for this particular specimen orientation have a synergistic effect of accelerated corrosion crack propagation, thus causing the stress corrosion cracking sensitivity. The first specimen was loaded at $20 \text{ KSI}/\sqrt{\text{in}}$ ($22.0 \text{ MPa}/\sqrt{\text{m}}$) which is 87 percent of the material's average room temperature fracture toughness (S-L orientation); the test specimen sustained the load for 885 hours when failure occurred. The second stress corrosion cracking test specimen was initially loaded at $17 \text{ KSI}/\sqrt{\text{in}}$ ($18.8 \text{ MPa}/\sqrt{\text{m}}$), 73.8 percent of the material's average fracture toughness. The test was on line for 2,762 hours when it was terminated; specimen failure had not occurred. The fact that the threshold for corrosion cracking is in excess of 70 percent of the material's K_{IC} , indicated the material is insensitive to corrosion cracking in the type of environment investigated.

The room temperature fatigue crack growth test results are presented in Figures 11 to 13. Figure 11 presents the results for specimens loaded in the longitudinal grain direction (L-T and L-S); Figure 12 is a plot of the test data for specimens loaded in the long-transverse grain direction (T-L and T-S). There is much more scatter in the data derived from specimens where the crack propagated in the short-transverse grain direction compared to the data representing test specimens with the crack moving in the longitudinal or the long-transverse grain directions. In both figures (see Figures 11 and 12) the specimens

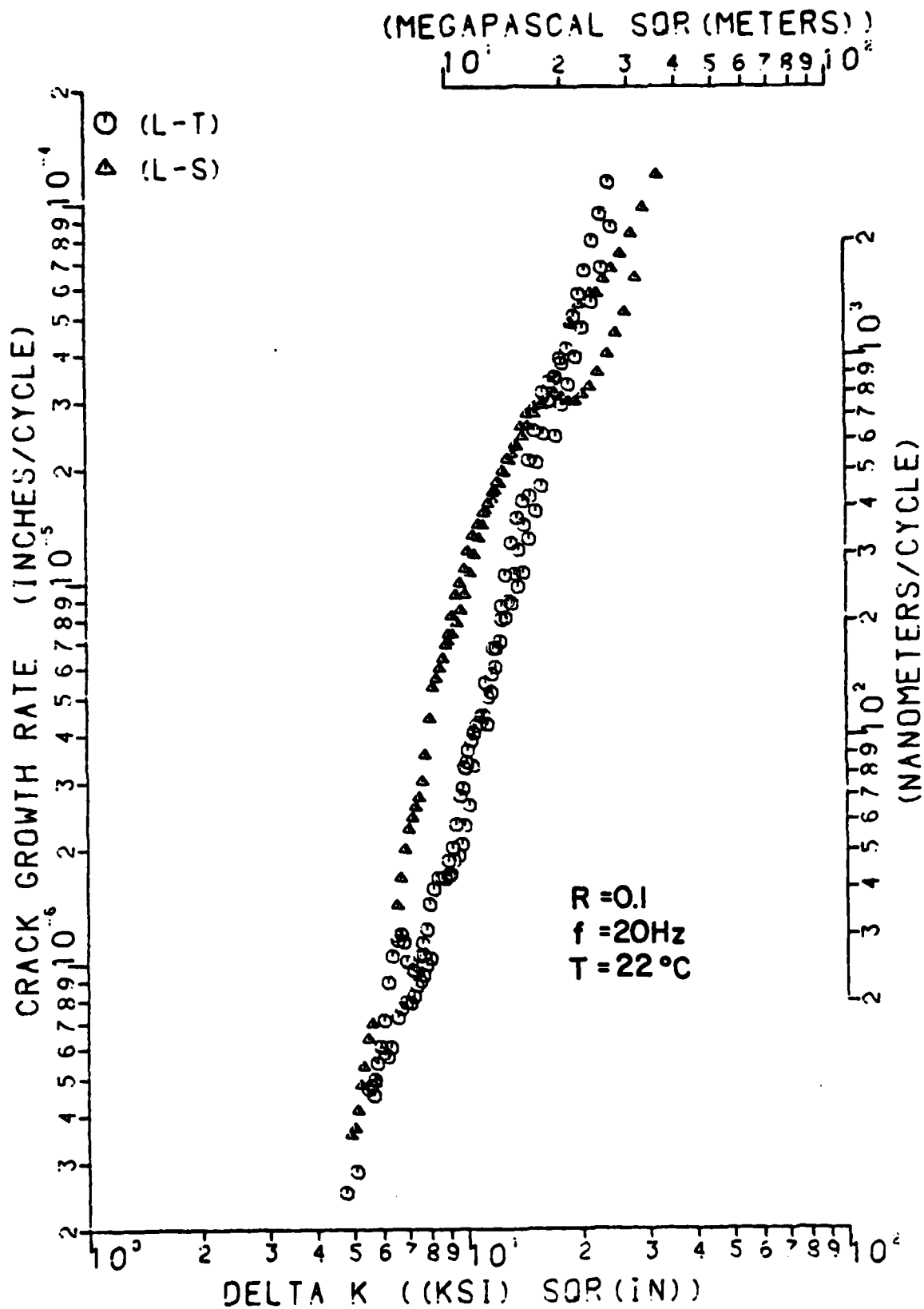


Figure 11. Constant Amplitude Loading Cyclic Crack Growth Test Results for CT Specimens Loaded in the Longitudinal Grain Direction at 72°F (22°C).

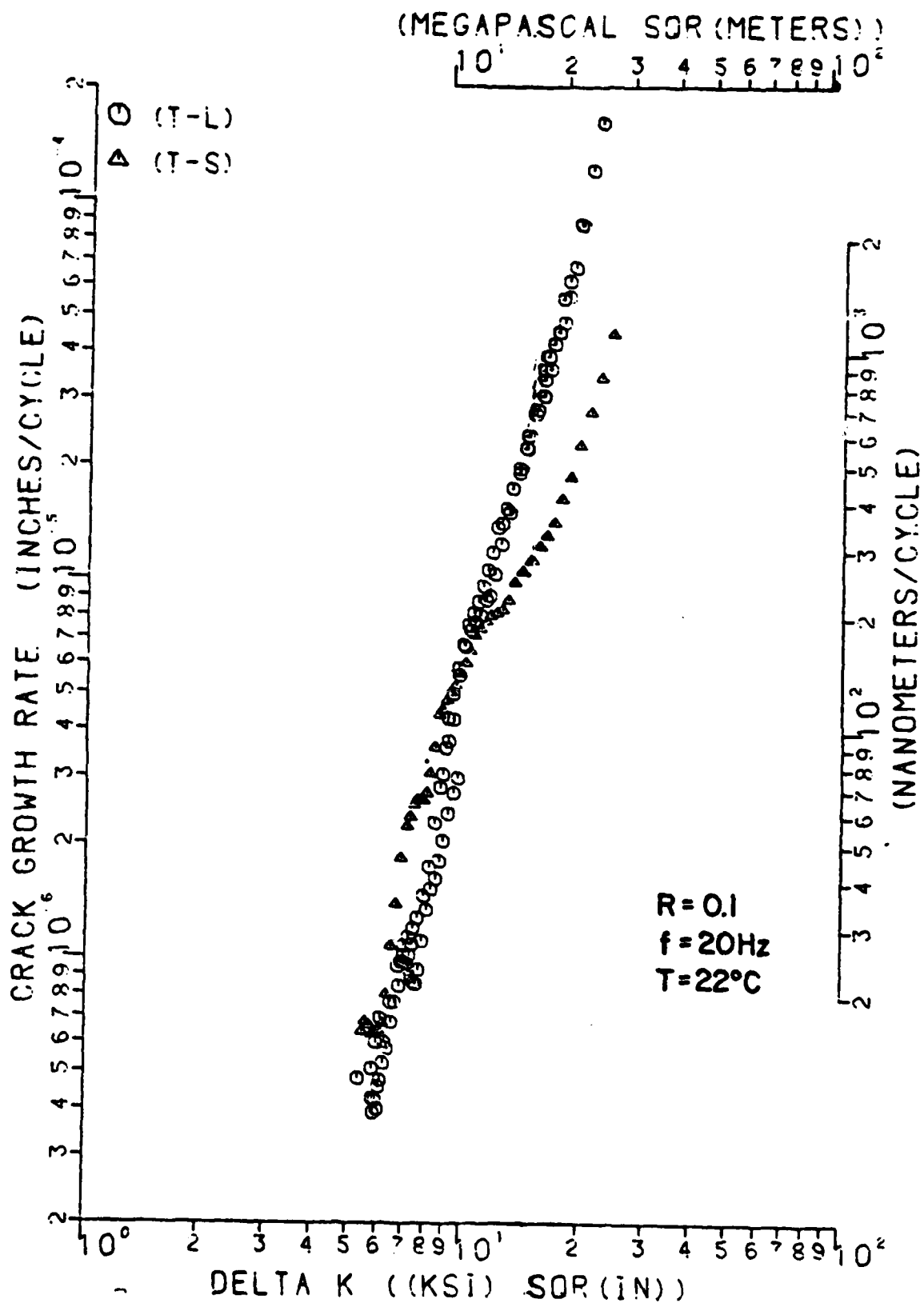


Figure 12. Constant Amplitude Loading Cyclic Crack Growth Test Results for CT Specimens Loaded in the Long-Transverse Grain Direction at 72°F (22°C).

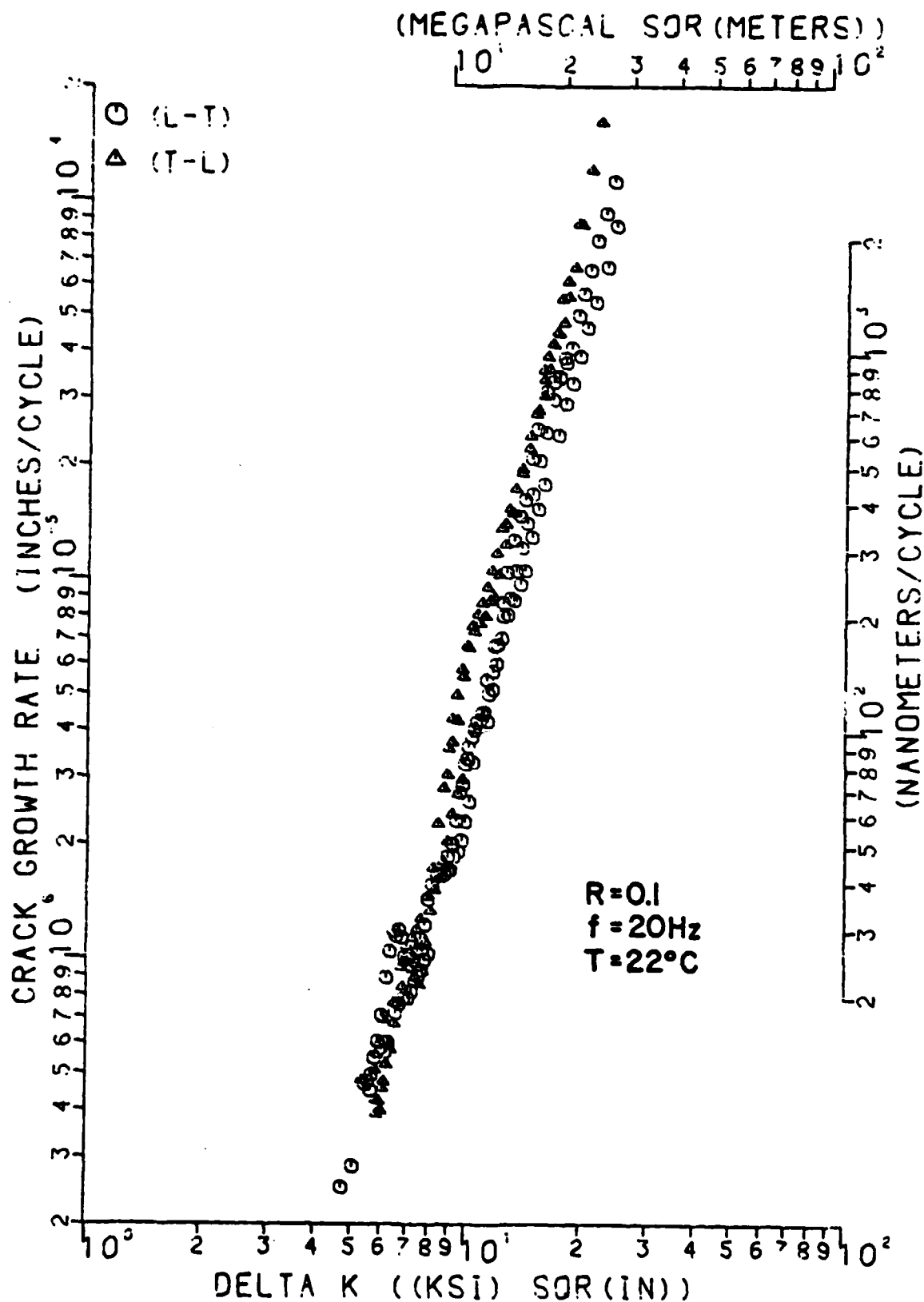
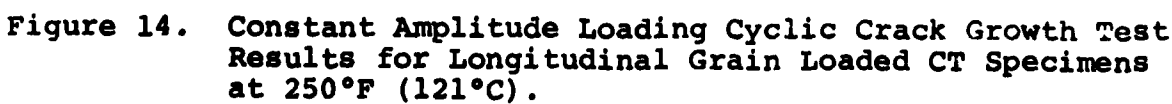


Figure 13. Constant Amplitude Loading Cyclic Crack Growth Test Results for L-T and T-L Oriented CT Specimens at 72°F (22°C).

with L-S and T-S orientations have wide scatter bands and cross over the data derived from specimens with L-T or T-L grain orientations which plotted in a narrow, well defined data scatter band. This point is better illustrated in Figure 13 where the same 72°F (22°C) L-T and T-L specimen orientation data is replotted together. Only at the slower crack growth rate do the data sets plot on top of each other. For most of the data for a constant stress intensity range the material loaded in the longitudinal grain direction was more crack growth resistant.

The 250°F (121°C) crack growth test results are presented in Figures 14 and 15. All of the elevated temperature crack growth tests used a loading frequency of 25 Hz. Figure 14 is a plot of the data obtained from the specimens loaded in the longitudinal grain direction (L-T and L-S), and Figure 15 presents the data for specimens loaded in the long-transverse grain direction (T-L and T-S). All of the data plots in a narrow scatter band. For the elevated temperature data associated with the crack moving in the short-transverse grain direction (L-S and T-S) there is not near as wide of a data scatter band as occurred in the data generated at 72°F (22°C) for these same two specimen grain orientations. For a constant stress intensity range, ΔK , the crack growth rate at 250°F (121°C) is two to five times faster than that at 72°F (22°C). This point is better illustrated in Figure 16 where the 72°F (22°C), 250°F (121°C), and 350°F (177°C) test results, for (L-T) specimen orientation, are presented together. There is a well defined shift between the crack growth data generated at 72°F (22°C) and that conducted at 250°F (121°C). The data obtained from the single crack growth specimen tested at 350°F (177°C) plots on the left side of the 250°F (121°C) data scatter band and for a constant stress intensity range represents approximately a 30-50 percent increase in the crack growth rate over that existing at 250°F (121°C).





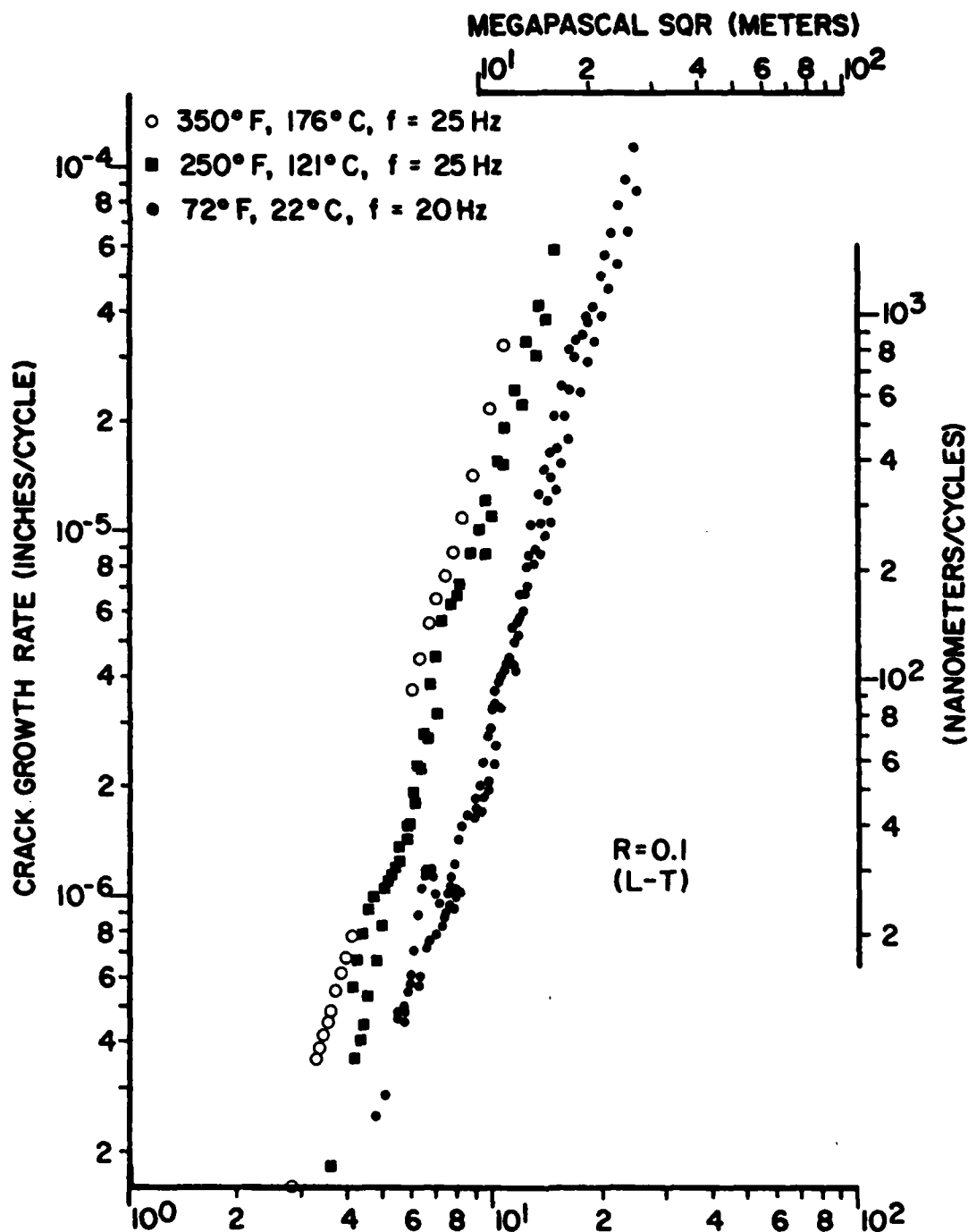


Figure 16. Constant Amplitude Loading Cyclic Crack Growth Test Results for L-T Oriented CT Specimens at 72°F, 250°F, and 350°F (22°C, 121°C, and 177°C).

Conclusions that can be drawn from this evaluation are as follows.

1. The test plate was a high purity aluminum alloy with very low Si and Fe content.
2. The alloy has high strength, high toughness, and good ductility comparable to alloys 7050-T73, 7175-T73, and 7475-T73.
3. The increase in test temperature from 72°F (22°C) to 250°F (121°C) had little effect on the conditional toughness, K_Q , test results.
4. The material is insensitive to stress corrosion cracking in a 3.5 percent by weight NaCl solution.
5. The test material's room temperature constant amplitude loading crack growth resistance is comparable to other high strength, high toughness, 7000 series aluminum alloys, e.g., 7050, 7175, and 7475.
6. There was an increase in the constant amplitude loading crack growth rate when the test temperature was increased from 72°F (22°C) to 350°F (177°C).

1.4 AN EMPIRICAL MODEL FOR LOADING RATIO EFFECT ON FATIGUE CRACK GROWTH RATE DATA

The empirical mathematical model for FCGR test data examined in this program is found in the Paris model; for that reason it can only be extended to the Paris data region, i.e., that portion of the test data where a straight line can fairly represent the FCGR data when it is plotted on a log-stress intensity range versus a log-crack growth rate set of axes. The threshold and the rapid crack velocity regions are not considered in this effort.

The mathematical model for room temperature FCGR test data discussed herein is based on the Paris equation (2).

$$da/dn = C\Delta K^m \quad (2)$$

Here, da/dn is the crack extension per load cycle, ΔK is the stress intensity range. This program examines the variation in the constants, exponent m , and coefficient C , in response to varying loading ratio, R , using aluminum alloy 7010-T73651 plate as test material. The test results of a more extensive mechanical property test program conducted on this particular plate are presented in Reference 4. The questions to be addressed in this program are: (1) If the exponent, m , is allowed to freely vary along with the coefficient, C , in determining the best-fit Paris straight line to a data set at various loading ratios, will a straight line still model a plot of loading ratio versus the log of the calculated Paris coefficients? and (2) If the answer to question (1) is yes, can the mathematical model be made more tractable by fitting a straight line to those same R -ratio data sets with the Paris exponent, m , fixed equal to the average value of the exponents derived in answering question (1)?

Tests were conducted at loading ratios, R , equal to 0.1, 0.3, 0.5, and 0.8. Based on these test results a predictive Paris equation was formulated for a loading ratio equal to 0.65 prior to generating test data at that loading ratio.

The constant amplitude loading fatigue crack growth test results for loading ratios equal to 0.1, 0.3, 0.5, and 0.8 are presented in Figures 17 through 20. The crack growth rate range that was considered for fitting the straight line was from 1.0×10^{-7} in./cycle (2.54 nm/cycle) to 1.0×10^{-4} in./cycle (2540 nm/cycle). For the remainder of the discussion the crack growth rates are in terms of inches per cycle, while the stress intensity range is in KSI/\sqrt{in} . In determining the best fit Paris straight line, as illustrated in Figures 17 through 20, both the Paris exponent, m , and the Paris coefficient, C , were

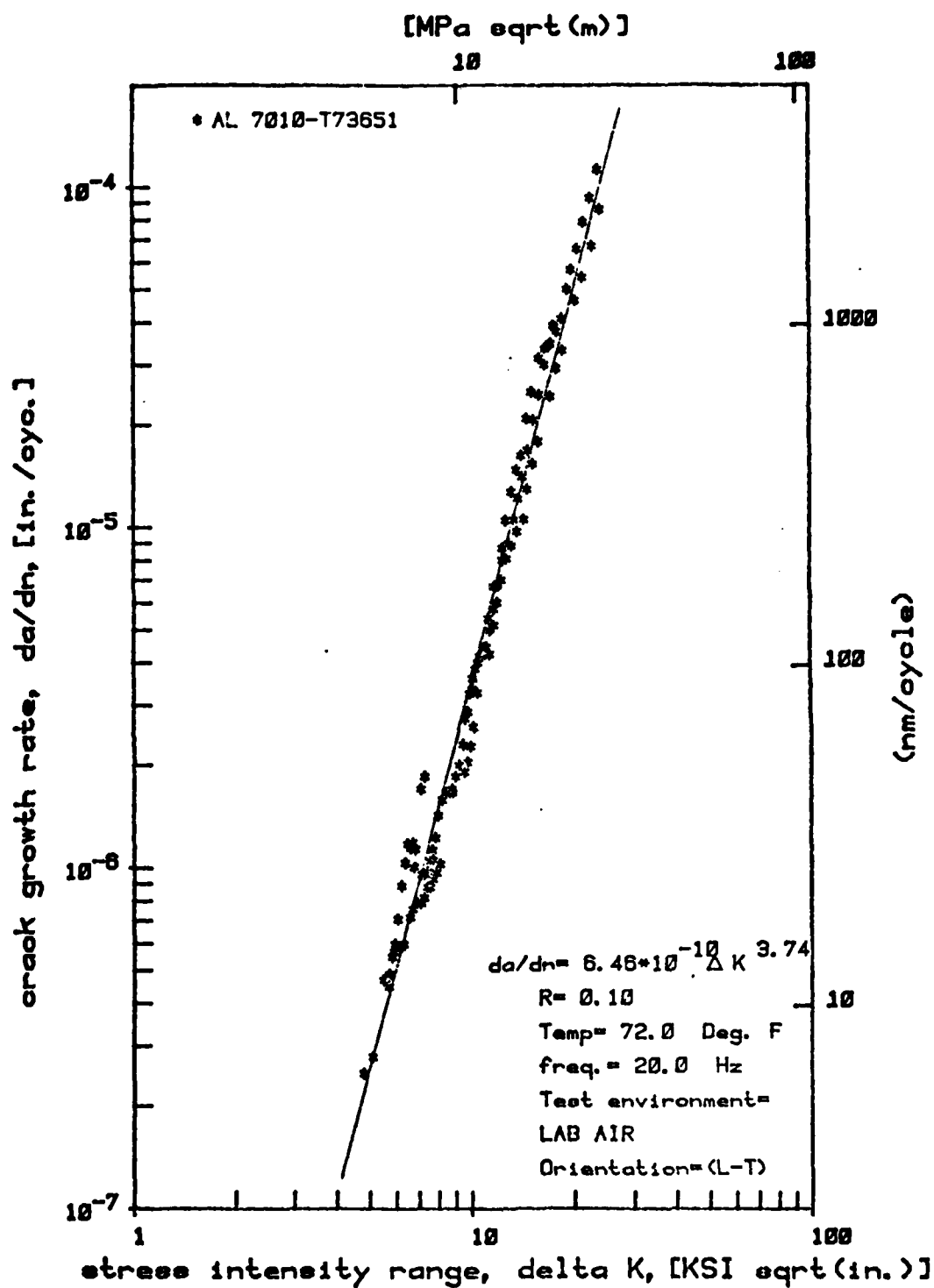
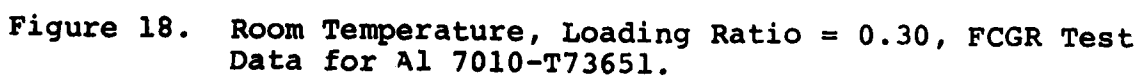


Figure 17. Room Temperature, Loading Ratio = 0.10 FCGR Test Data for Al 7010-T73651.



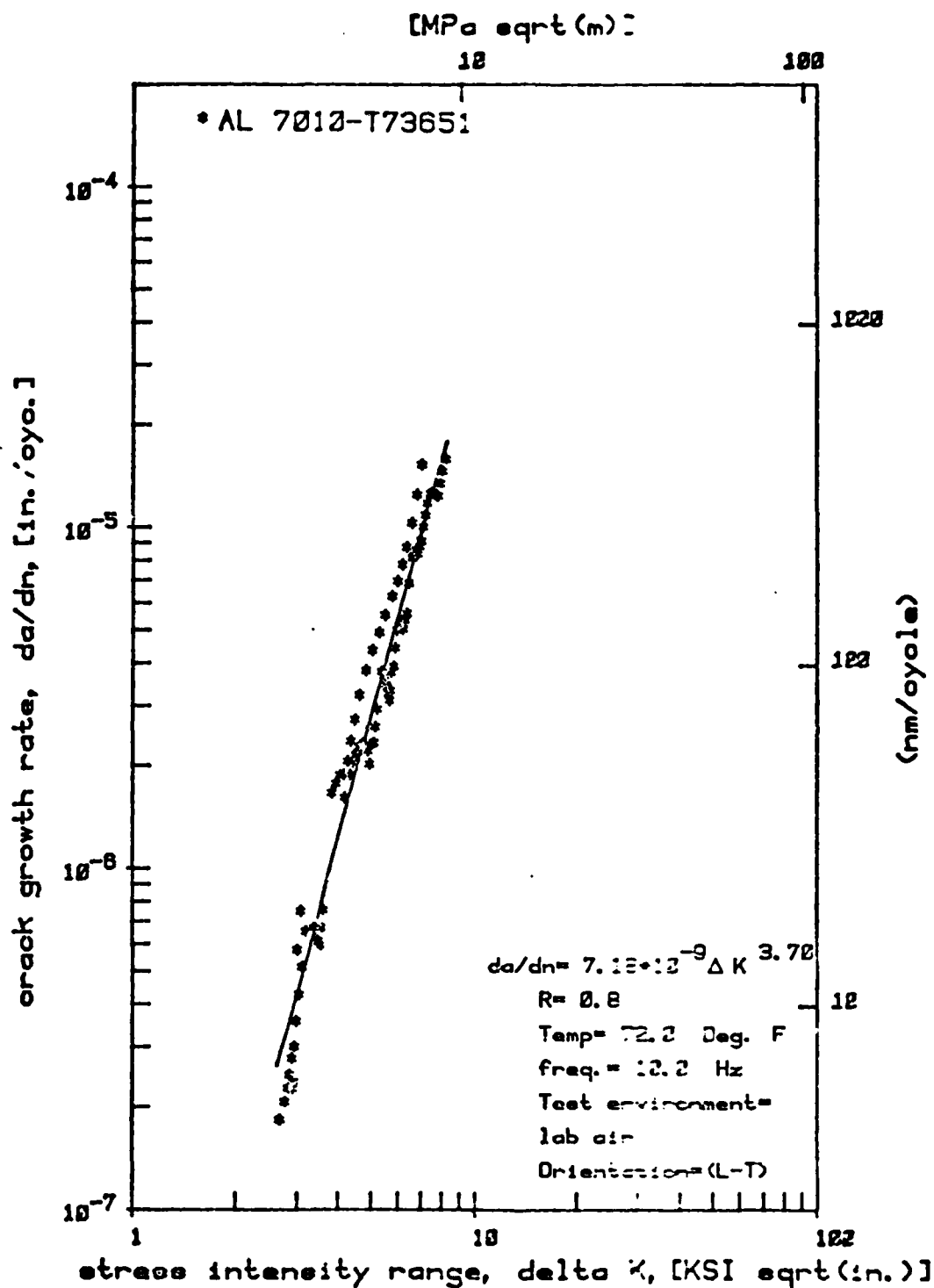


Figure 20. Room Temperature, Loading Ratio = 0.8 FCGR Test Data for Al 7010-T73651.

allowed to freely vary. The four Paris equations (3 through 6) representing each data set are presented below.

<u>Loading Ratio</u>	<u>Paris Equation</u>	
0.1	$da/dn = 6.46 \times 10^{-10} \Delta K^{3.74}$	(3)
0.3	$da/dn = 1.74 \times 10^{-9} \Delta K^{3.60}$	(4)
0.5	$da/dn = 2.67 \times 10^{-9} \Delta K^{3.67}$	(5)
0.8	$da/dn = 7.18 \times 10^{-9} \Delta K^{3.70}$	(6)

The log-Paris coefficient, $\log C$, for the four data sets are plotted in Figure 21 as a function of loading ratio, R . The four points are distributed around a straight line defined by equation (7).

$$\log C = 1.438R - 9.277 \quad (7)$$

If the logarithm of both sides of the Paris equation (2) is taken it becomes equation (8).

$$da/dn = C \Delta K^m \quad (2)$$

$$\log da/dn = \log C + m \log \Delta K \quad (8)$$

The empirical equation just derived for the Paris coefficient as a function of loading ratio, equation (7), can now be substituted into equation (8),

$$\log da/dn = 1.438R - 9.277 + m \log \Delta K \quad (9)$$

Again the Paris exponent, m , for the four best-fit straight lines corresponding to the four loading ratios under consideration are presented below.

PARIS EXPONENTS
[All Tests Conducted at 72°F (22°C)]

<u>Loading Ratio, R</u>	<u>Paris Exponent, m</u>
0.1	3.74
0.3	3.60
0.5	3.67
0.8	3.70

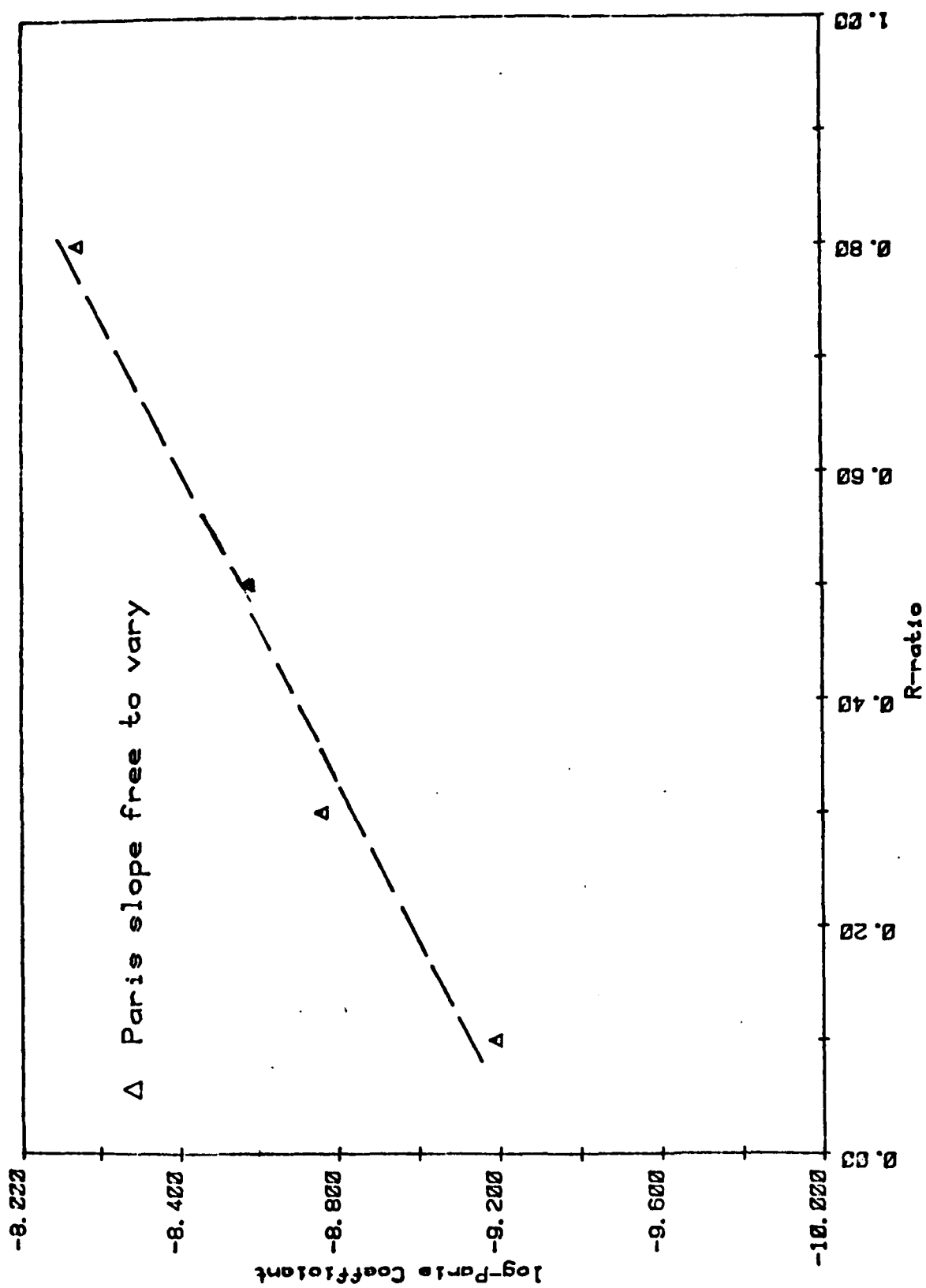


Figure 21. Loading Ratio, R, Versus Log-Paris Coefficient, Log C, for Al 7010-T73651 at 72°F (22°C).

The average value, \bar{m} , is equal to 3.68. The maximum value among the four exponents is 3.74 and the minimum value is equal to 3.60, representing a range equal to ± 2 percent of the average value Paris exponent, \bar{m} . By substituting the average Paris exponent, $\bar{m} = 3.68$, into equation (9) and taking the antilogarithm of both sides of the resulting expression a generalized expression, equation (10) is derived:

$$\begin{aligned}\log da/dn &= 1.438R - 9.277 + 3.68 \log \Delta K \\ da/dn &= 10^{(1.438R-9.277)} \Delta K^{3.68}\end{aligned}\quad (10)$$

This expression for the test material aluminum alloy 7010-T73651 is applicable for a loading ratio range from 0.1 to 0.8 in a 72°F (22°C) laboratory air test environment.

The largest gap in the R-ratio data sets was between the loading ratios equal to 0.5 and 0.8; a loading ratio in the middle of this gap, $R = 0.65$, was selected as a test case for the two generalized expressions, equation (10) the resulting prediction is equation (11).

$$da/dn = 10^{(1.438R-9.277)} \Delta K^{3.68} \quad (10)$$

$$R = 0.65; da/dn = 4.547 \times 10^{-9} \Delta K^{3.68} \quad (11)$$

Two experimental approaches were taken to verify that the prediction, equation (11), would accurately represent data at the test-case an R-ratio equal to 0.65.

First, since the exponent \bar{m} of the series of Paris equations has already been satisfactorily determined. to empirically establish a verifying equation with a set of data only the Paris coefficient need to be accurately determined experimentally. This curtails the necessity for generating a large range of data at an R-ratio of interest. Using this approach, two specimens were tested at a loading ratio equal to 0.65. To minimize test time an initially high stress intensity range received primary attention with the sole

exception of one data point at a low stress intensity range that was established immediately following crack initiation of one of the specimens. The combined test results are presented in Figure 22. The line in Figure 22 represents the best-fit equation with the exponent fixed equal to $\bar{m} = 3.68$. The equation that defines the line in Figure 22 is:

$$da/dn = 4.28 \times 10^{-9} \Delta K^{3.68} \quad (12)$$

The lines representing the predictive equation (11) and the best-fit, fixed-exponent equation (12) to the actual test data are virtually indistinguishable.

Encouraged by this success an alternate approach was undertaken to verify the prediction equation (11). A third specimen was tested at a loading ratio equal to 0.65 but with an initial crack velocity of approximately 4×10^{-7} in/cycle (11.18 nm/cycle). The test results for this single specimen are presented in Figure 23. The solid line in Figure 23 represents the best-fit equation to this second data set which is:

$$da/dn = 4.09 \times 10^{-9} \Delta K^{3.65} \quad (13)$$

and was calculated with both the Paris exponent and coefficient free to vary. The dashed line represents the predictive equation (11) which plots very close to and almost parallel to the solid line representing equation (13). The shift from the line representing the prediction, equation (12) to that line representing the best-fit equation to the data set, equation (13), is small when compared to the large shift from the best-fit line to the 0.5 R-ratio data set to that of the 0.8 R-ratio data set.

For constant amplitude loading FCGR data for various positive loading ratios, the Paris coefficient for the linear region of the growth rate curve can satisfactorily be modeled as a log-linear straight line relationship, i.e., R-ratio versus log-Paris coefficient.

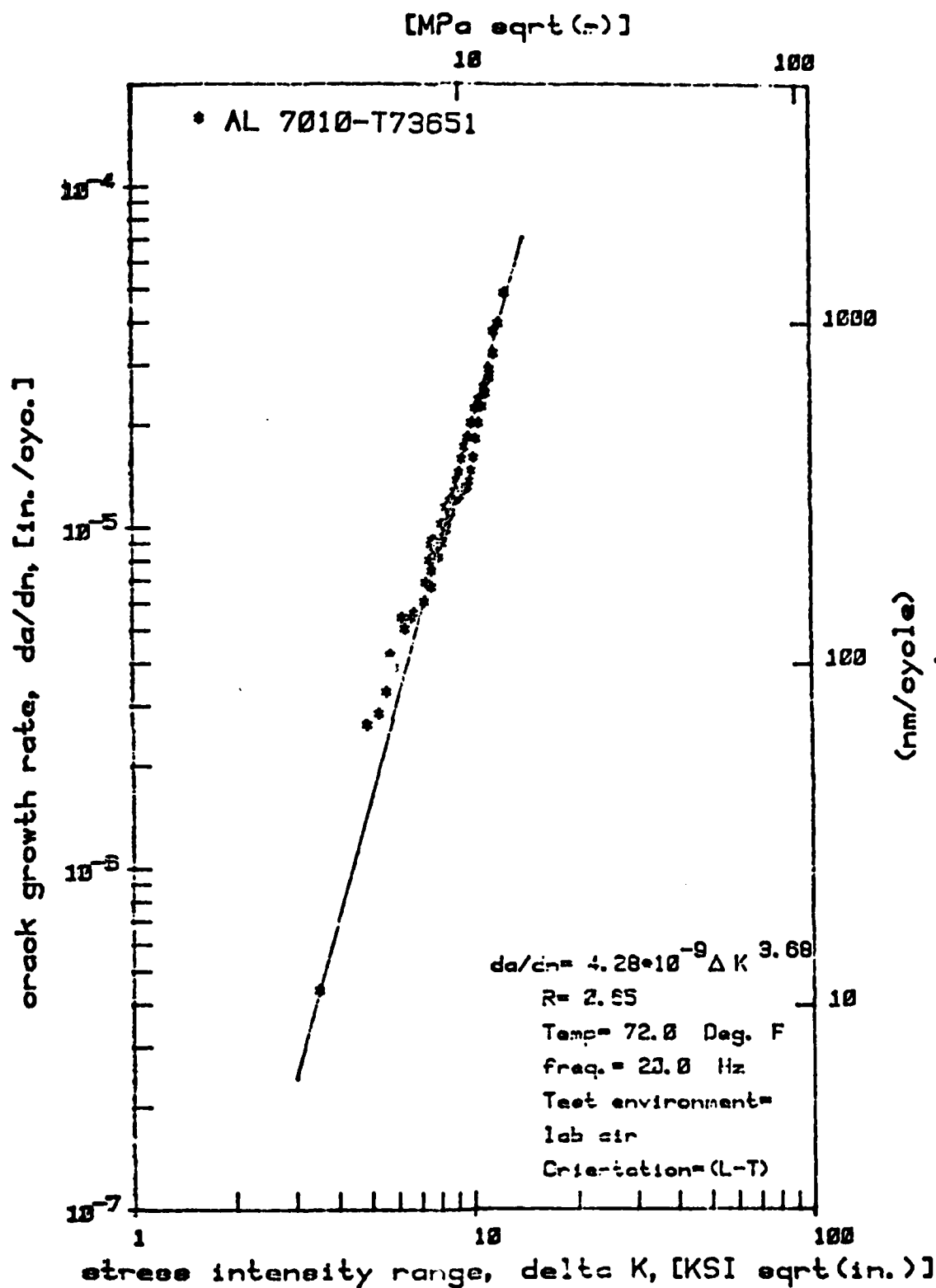


Figure 22. Fast Crack Growth Rate Region, Room Temperature, Loading Ratio = 0.65, FCGR Test Data for AL 7010-T73651.

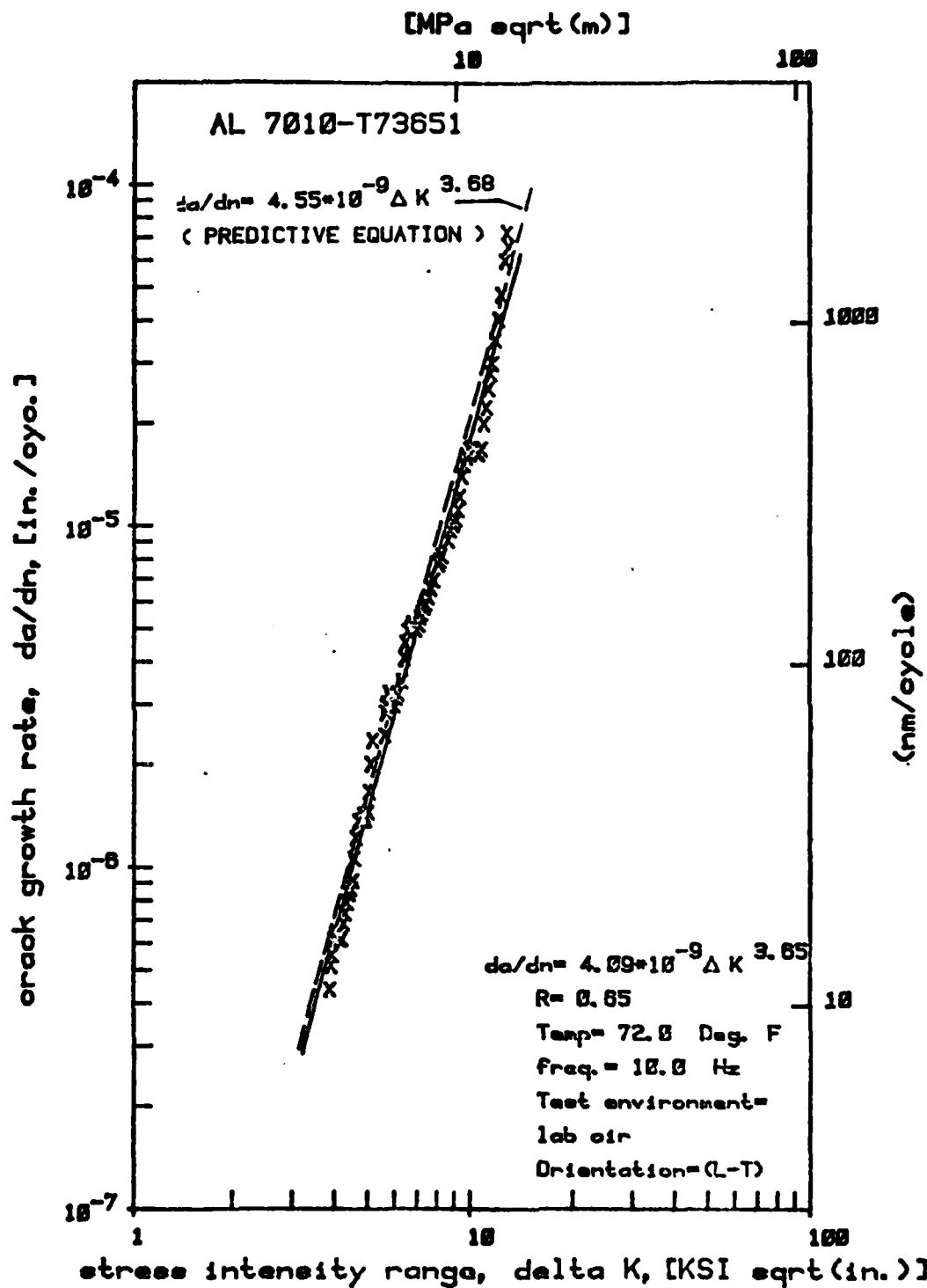


Figure 23. Full Velocity Range, Room Temperature, Loading Ratio = 0.65 FCGR Data for Al 7010-T73651.

1.5 PARACHUTE SHROUD RELEASE EVALUATION

During October 1980, two A-10 aircraft collided over the English coast. Both pilots successfully ejected from their aircraft. Weather conditions were severe; the average wind velocity was 35 knots (17.5 m/s) with frequency gusts up to 45 knots (23.1 m/s). Although both men ejected over land, due to the tremendous wind one of the men was carried and dropped into the sea; the second pilot was successfully dropped onto land. The latter individual was pulled over the terrain, receiving cuts and contusions until he was able to trigger one of his two shroud release clasps allowing the parachute to dump the air and collapse. The clasps attaching the airman's harness to his parachute shroud could not be triggered by using only one hand. It was necessary for the airman to grab the shroud above the clasp and pull the shroud toward his shoulder relieving some of the load carried by the clasp. Only in this manner was the other hand strong enough to activate the shroud clasp release trigger.

The second pilot that landed in the sea was joined by an English Navy para-rescue seaman who immediately latched himself to the pilot's parachute harness. Neither the pilot nor the para-rescue seaman could activate the shroud release clasps. An attempt was made to haul the two men in the water up to the hovering helicopter with the pilot's chute still attached and deployed. The large load caused by the deployed chute in the severe wind conditions destroyed the helicopter's winch, dropping the two men back into the sea. The deployed chute dragged the two men, at an estimated average velocity of 11 knots (5.7 m/s) through a 17 foot (5.2 m) rolling surf until an American helicopter dropped a U.S. Navy para-rescue serviceman into the water who immediately cut the chute with a large knife. The cut chute collapsed and the American helicopter was then able to winch its seaman and the two drowned individuals aboard the craft.

The above incident called attention to the large force necessary to trigger release of the heavily loaded shroud clasp when the chute is deployed in severe weather conditions. The subject clasp is in widespread usage; it is used in the A-10, F-15, A-7, and F-4 aircrafts. During ordinary circumstances, i.e., moderate wind, the shroud/clasp is carrying no more than 300 pounds (1334 N) with the chute deployed. An airman attempting to free himself can trigger release of the clasp by exerting a force of 20 to 30 pounds (89 to 133 N) with the two finger tips that fit onto the trigger, not too difficult a feat. These clasps were purchased to a specification that requires that a force no greater than 35 pounds (156 N) be required to release the clasps when a shroud and mating clasp are carrying 500 pounds (2224 N). The 35 pounds (156 N) represents approximately the maximum force an average adult male can exert with the two finger tips that fit on the clasp trigger, provided the hand is uninjured.

By estimating both the distance the two drowned men were pulled through the surf and the time between them being dropped back into the sea until the second para-rescue was able to cut the chute, their average velocity of 11 knots (5.7 m/s) was estimated. The average horizontal drag force the two bodies exerted onto the parachute shrouds was proportional to the square of the average velocity of the bodies moving through the water. The chute and shrouds were estimated by the helicopter crew to be orientated at 30° from the horizon which made the load carried by the shrouds and connecting clasps 1.7 times larger than the calculated drag force. The estimated average load carried by each shroud and clasp was 700 pounds (3117 N). The maximum estimated load to be carried by each shroud and clasp during the 45 knot (21.3 m/s) wind gusts was 1100 pounds (4893 N). No trigger activator force test data existed on the involved clasp design at these high loading conditions.

Because of the loss of life and the non-existence of trigger activation load data for a highly loaded shroud and

clasp of this particular design, the Life Support Branch, ASD/AESE, requested that a series of tests be performed on shroud release clasps identical to the hardware involved in the accident and on similar clasps that are also used in service. A series of tests were designed to determine the activation loads required to trigger release of the clasps when the shroud/clasp was carrying loads normally encountered in service, 100 to 300 pounds (445 to 1334 N). Static loads were then incrementally increased to be equal to those estimated to exist during the average wind condition, [700 lbs (3117 N)] and then the gust loading [1100 lbs (4893 N)] conditions on the day of the accident.

Two complete parachute shroud release clasp assemblies fabricated by H. Coch and Sons Inc., were furnished by the Life Support Branch for evaluation. Also two substitute male components fabricated by Teledyne Co. were furnished. The Teledyne Co. manufactured male components are used in service interfaced to the H. Coch and Sons Inc. produced female half of the clasps. This particular arrangement was identical to what the two airmen involved in the accident had in their chute. The clasps were statically loaded in a tensile testing machine to be carrying: 100, 300, 500, 700, 900, and 1100 pounds (444, 1334, 2224, 3114, 4003, 4893 N). With the assembly loaded to each of the above nominal loads a weight pan was attached to the clasp's release trigger. The trigger was then manually loaded by adding weights to the pan in 1 pound (4.448 N) increments until the release trigger was activated and separation of the clasps occurred. The loads required to trigger release of the clasps are presented in Table 7. For the two H. Coch produced female components the one with S/N ADA 19 required larger loads to trigger release than did the one with S/N 0274, using either the H. Coch or the Teledyne produced male mating components.

Seven adult men next attempted to trigger the release of one clasp while it was statically loaded to the same nominal loads used in the previous series of tests. The female clasp component (S/N ADA 19) and the Teledyne produced male component

TABLE 7
PARACHUTE HARNESS SHROUD RELEASE
CLASP TEST RESULTS

Component Manufacturer		Shroud Load	Trigger-Release-Load	
Female (S/N)	Male (S/N)	lbf (N)	lbf	(N)
H. Coch (0274)	Teledyne (728)	100 (445)	8	(36)
		300 (1334)	18	(80)
		500 (2224)	26	(116)
		700 (3117)	36	(160)
		900 (4003)	46	(205)
		1100 (4893)	53	(235)
H. Coch (ADA19)	Teledyne (833)	100 (445)	9	(40)
		300 (1334)	21	(93)
		500 (2224)	32	(142)
		700 (3117)	43	(191)
		900 (4003)	53	(236)
		1100 (4893)	65	(289)
H. Coch (ADA19)	Teledyne (728)	100 (445)	8	(36)
		300 (1334)	21	(93)
		500 (2224)	30	(133)
		700 (3117)	42	(187)
		900 (4003)	54	(240)
		1100 (4893)	64	(285)
H. Coch (0274)	Coch (#1)	100 (445)	8	(36)
		300 (1334)	17	(76)
		500 (2224)	26	(116)
		700 (3117)	33	(147)
		900 (4003)	38	(169)
		1100 (4893)	42	(187)
H. Coch (ADA19)	Coch (#2)	100 (445)	9	(40)
		300 (1334)	20	(89)
		500 (2224)	29	(129)
		700 (3117)	40	(178)
		900 (4003)	51	(227)
		1100 (4893)	61	(271)

(S/N 833) were employed for this series of tests. This particular combination of components was selected because they demonstrated the largest magnitude set of triggering loads during the previous weight-pan-loaded-trigger series of tests. All seven members of the group could activate the release trigger when the unit was loaded to 300 pounds (1334 N). Only one individual in the group could activate the trigger when the clasp was loaded to 500 pounds (2224 N). None of the seven individuals constituting the test group could release the clasp when it was loaded to 700 pounds (3114 N). This clasp was difficult to activate because: (1) the release trigger provided too small of bearing area, an area that would allow loading the trigger with only two finger tips, (2) the safety catch had to be simultaneously pushed out of the way to uncover the trigger by a third finger, a feat that requires some dexterity, (3) simultaneously watching the release hand was an asset, blind activation of the clasp was difficult, and (4) finger nail length was determined due to clearance.

The test results indicate that the trigger activation load on the day of the incident was at best, the maximum load an average male was capable of exerting under the most ideal environmental conditions. These conditions worked concomitantly with additional adverse environmental conditions: (1) the two men were being pulled at a high velocity through a 17 foot (5.2 m) rolling sea, (2) the water temperature was 42°F (5.6°C), and (3) the maximum load an average adult male can exert with two fingers, 30-35 pounds (133-156 N), had to be applied to the water lubricated trigger surface. All of these factors acting together created a circumstance that was very unlikely for the airman or para-rescue seaman to be capable of releasing the deployed parachute.

After completion of the series of tests described above, the Life Support Branch furnished two additional parachute release clasps manufactured by Frost Engineering. These two

clasps were of an entirely different design concept than the H. Coch/Teledyne design clasps used in the previous series of tests. The Frost Engineering parachute shroud release clasps are used exclusively throughout the F-16 fighter aircraft fleet.

These two Frost Engineering clasps differed slightly in that one was a first generation prototype (henceforth referred to as the "old" design) and the other clasp was a second generation design refinement of the first clasp (henceforth referred to as the "new" design). The new design clasp was: (1) smaller and (2) had a dry film lubricant coating on the mating surface of the female component. The male components of the old and new designs are interchangeable in the two Frost designed female halves of the clasps. The two clasps were subjected to the same two series of tests as were the H. Coch/Teledyne clasps.

The results of the weight-pan-loaded-trigger release tests are presented in Table 8. At the higher static loading conditions, the trigger activation forces for the old design are approximately equal to those necessary to trigger the H. Coch/Teledyne produced clasps. However, at low loading conditions, 100 and 300 pounds (445 and 1334 N), the H. Coch/Teledyne clasps required much smaller loads to trigger release.

For the static loading test conditions, the new design Frost Engineering produced clasp requires much smaller loads to trigger release than did the old design, most probably due to the dry film lubricant coating on the female half of the clasp. Also, the loads required to trigger release of the new design clasp for a given static loading condition were consistently reduced during the second, repeat, series of tests.

Eight adult males again attempted to trigger the release of the two Frost Engineering produced clasps while the clasps were transmitting the nominal loads employed during the weight-pan-loaded-trigger series of tests. Except where noted, the ASD/AESE recommended gripping technique was employed during

TABLE 8
FROST ENGINEERING PARACHUTE SHROUD
RELEASE CLASP TEST RESULTS

Female Component Design	Male Component Design	Shroud	Load	Trigger-Release-Load	
		lbf	(N)	lbf	(N)
Old (1st Run)	Old	100	(445)	16	(71)
		300	(1334)	25	(111)
		500	(2224)	32	(142)
		700	(3117)	41	(182)
		900	(4003)	48	(214)
		1100	(4893)	53	(236)
Old (2nd Run)	Old	100	(445)	18	(80)
		300	(1334)	26	(116)
		500	(2224)	32	(142)
		700	(3117)	43	(191)
		900	(4003)	56	(249)
		1100	(4893)	66	(234)
Old	New	100	(445)	15	(67)
		300	(1334)	24	(108)
		500	(2224)	33	(147)
		700	(3117)	44	(196)
		900	(4003)	53	(236)
		1100	(4893)	61	(271)
New (1st Run)	New	100	(445)	14	(62)
		300	(1334)	19	(85)
		500	(2224)	25	(111)
		700	(3117)	31	(138)
		900	(4003)	37	(165)
		1100	(4893)	39	(173)
New (2nd Run)	New	100	(445)	10	(44)
		300	(1334)	15	(67)
		500	(2224)	23	(102)
		700	(3117)	28	(125)
		900	(4003)	33	(147)
		1100	(4893)	38	(169)

these tests. All eight members of the test group could trigger the new Frost Engineering design clasp while it was carrying the maximum static test load, 1100 pounds (4893 N).

For the old Frost designed clasp, all eight members of the group could trigger the clasp when it was carrying 500 pounds (2224 N), six individuals could activate the release trigger when this clasp was transmitting 700 pounds (3114 N), half of the group, four people, could trigger the release when it was carrying 900 pounds (4003 N), and only two individuals could trigger release of the old design clasp when it was statically loaded to be transmitting 1100 pounds (4893 N) (one of these successful individuals was not using the recommended gripping technique).

None of the clasps manufactured by H. Coch/Teledyne, or Frost Engineering and tested in this effort could be readily triggered to release with an injured hand if the clasp was transmitting a load in excess of 500 pounds (2224 N).

Following the initial evaluation of the various shroud releases that are currently in service, the actual shroud releases worn by the two pilots on the day of the accident were furnished by the Life Support Branch. These four clasps (two pair) were subjected to the same static loads in a tensile testing machine, along with the trigger's dead-weight-loading procedure, as were the identical clasps in the previously described effort. The test results for the four clasps were then compared to the baseline data generated in the preceding test effort. This same test procedure was used to determine activation loads required to trigger an alternate shroud release manufactured by Capwell and used in service for the past 20 years in various aircraft systems: B-52, T-38, F-5, and C-135.

In the previous program with the shroud releases mounted in a tensile testing machine, the hand-activated release gripping posture did not closely resemble the attitude an airman experiences when the releases are mounted on his/her personal parachute harness.

The Life Support Branch felt that this discrepancy in posture may have a serious effect on the maximum shroud loading condition an individual would be successful in triggering the shroud release. They requested a similar series of tests be performed where a test group of individuals attempts to activate the test shroud release that was mounted on the personal parachute harness the test subject was wearing. The Life Support Branch chose a test group of six subjects made up of crewmen on active flight status. All four clasp designs included in the previous program were tested in this manner. One additional shroud release design manufactured by Capwell Manufacturing Company, previously described, was also included in this series of tests.

The four shroud releases worn by the two airmen involved in the accident had a female portion manufactured by H. Koch and Sons Inc. The mating male part was made by Teledyne Co. The clasps were tested with the parts interfaced to the same mating components as they were on the day of the accident. These clasps were statically loaded in a tensile testing machine to the following load levels: 100, 300, 500, 700, 900, and 1100 pounds (444, 1334, 2224, 3114, 4003, and 4893 N). With the assembly loaded to each of the above loads a weight pan was attached to the clasps release trigger. The trigger was manually loaded by adding weights to the pan in 1 pound (4.4 N) increments until the release trigger was activated and separation of the clasps occurred.

The loads required to trigger release of the clasps are presented in Table 9. Clasps with identification numbers 1 and 2 were the two releases removed from the drowned airman's harness. The releases with identification numbers 3 and 4 were removed from the airman's harness that was drug over land. Generally for a low shroud load level, the corresponding trigger-release-load required for the four clasps associated with the accident were slightly higher than the baseline data set previously generated. In contrast, for the higher nominal shroud load levels the four releases involved in the accident required trigger release loads

TABLE 9
A-10 AIRCRAFT SHROUD RELEASE EVALUATION

Teledyne/Koch Shroud Releases Involved in October 1980 Accident
at English coast line

I.D. No.	Shroud Load lbf (N)	Trigger Release Load lbf (N)
<u>(Drown Airman's Shroud Releases)</u>		
1	100 (445)	10 (44)
	300 (1334)	23 (102)
	500 (2224)	29 (129)
	700 (3117)	41 (182)
	900 (4003)	48(213), 45(200), 43(191)
	1100 (4893)	53(236), 53(236), 49(218), 52.5(234)
2	100 (445)	8(36), 9(40)
	300 (1334)	21(93), 14.5(64), 15.5(69)
	500 (2224)	28(125), 23(102), 25(111)
	700 (3117)	43(191), 28(125), 27(120), 27.5(122)
	900 (4003)	48(214), 51(227), 33(147), 33(147), 35(156)
	1100 (4893)	38(169), 38(169), 37(165), 40.5(180), 43(191)
<u>(Survived Airman's Shroud Releases)</u>		
3	100 (445)	11(49), 11(49)
	300 (1334)	23(102), 21.5(96)
	500 (2224)	30(133), 28(125)
	700 (3117)	41(182), 40(178)
	900 (4003)	50(222), 48(214)
	1100 (4893)	50(222), 53(236)
4	100 (445)	10.5(47), 9.5(42)
	300 (1334)	20(89), 19(85)
	500 (2224)	28(125), 28(125)
	700 (3117)	38(169), 37(165)
	900 (4003)	46(205), 44(195)
	1100 (4893)	52(231), 56(249)

that were at the lower end of the baseline data range or below the lowest load previously obtained in the baseline data. Release number 2 (worn by the drowned airman) behaved in a peculiar manner. In going through the test sequence of increasing the shroud load, 300, 500, 700, etc., pound force, this release behaved as the others, baseline or accident involved clasps, requiring a gradually increasing trigger-release-load until the largest shroud load, 1100 pounds (4893 N), was reached. At this test condition there was a 10 pound (44 N) decrease in the trigger-release-load, requiring only 38 pounds (169 N) to activate the release whereas the previous test on this clasp with a shroud load of 900 pounds (4003 N) required 48 pounds (215 N) to trigger release. For this unit all of the test points were repeated; tests at some of the higher levels were repeated several times. Release number 3 behaved in a similar manner requiring about the same load to trigger the release when loaded to 1100 pounds (4893 N) as was required at the previous test condition of a 900 pound (4003 N) shroud load. There appears to be a seating or wearing in of the parts; for most of the repeat tests conducted on release number 2 there was a considerable reduction in the trigger release loads when compared to the first test result obtained for a given load level. When the Life Support Branch was informed of this peculiar behavior they indicated that such behavior had been observed in previous testing of this model shroud release. As a consequence the manufacturer is now required to trigger the loaded finished unit ten times prior to shipment.

The test results for the Capwell manufactured shroud release loaded in the tensile testing machine are presented in Table 10. The safety cover was restrained out of the way to prevent its interference with the weight-pan-loading of the trigger.

Generally the loads required to trigger the Capwell release with the shroud loaded to any of the nominal test loading conditions, except the smallest, 100 pounds (445 N), were much

TABLE 10
CAPWELL SHROUD RELEASE
WEIGHT-PAN-LOADED TRIGGER RELEASE

Shroud Load		Trigger-Release-Load	
lbf	(N)	lbf	(N)
100	(445)	12	(53)
300	(1334)	13	(58)
500	(2224)	13	(58)
700	(3117)	13	(58)
900	(4003)	22	(98) *
1100	(4893)	23	(102) *

* Average of two tests.

smaller than the trigger loads required for the Koch/Koch, Koch/Teledyne, or the two Frost Engineering designed releases.

The Life Support Branch selected six members of flight crews on active flight status as a test group. The heights and weights of the test group are presented in Table 11. In this series of tests the parachute harness, worn by a test subject with the test shroud releases mounted in place, had the harness loaded, via a creep frame, from the bottom attachment fitting to the shroud webbing. The loading condition was incrementally increased to the same nominal load values as used in the previous series of tests. The procedure was continued for each test subject until a harness/shroud load level was reached where the test subject was incapable of triggering the test clasp or a maximum load level of 1100 pounds (4893 N) was reached with a successful release. For every test the shroud/release on the left shoulder was examined. All test subjects were wearing their personal gloves normally worn in flight.

A summary of the test results are presented in Table 12. The letter "R" in the table indicates the right hand was crossed

TABLE 11
PARACHUTE SHROUD RELEASE TEST GROUP

Subject	Height		Weight		Sex
	ft/in	(m)	lbf	(N)	
J. Botka	5'2.5"	(1.59)	104	(463)	F
Dr. Raddin	6'0"	(1.83)	200	(890)	M
J. Bainter	6'0"	(1.83)	190	(845)	M
Sgt. Beavers	6'0"	(1.83)	197	(876)	M
Dr. Hoffman	6'3"	(1.91)	210	(934)	M
C. Pickell	6'1"	(1.85)	180	(800)	M

over the chest to trigger the release mounted on the left shoulder; the letter "L" indicates the left hand was used to trigger the left shroud release. The letter "B", only occurring for the old Frost Engineering designed release, indicates both hands were used in unison on the safety and trigger to successfully activate the release. The clasp with both Koch manufactured parts and the clasp with mating Koch female and Teledyne male components are clearly the more difficult releases to activate. Only the largest male members of the test group successfully triggered these releases while they were carrying 900 pounds (4003 N); no one triggered these releases when the shroud load was 1100 pounds (4893 N). The old Frost Engineering design clasp test record was slightly better than that of the Koch/Koch or Koch/Teledyne produced clasps. The new Frost Engineering design and the Capwell Company produced shroud releases had a vastly superior test record compared to the other shroud releases; all members of the test group were capable of triggering these two shroud releases at the maximum shroud loading test condition, 1100 pounds (4893 N).

TABLE 12

TEST GROUP'S FRACTIONAL SUCCESS OF TRIGGERING THE SHROUD RELEASE
(Test Group - Six Active Flight Crew Members)¹

Manufacturer, Aircraft Systems, Successful Fraction											
Shroud Load ² lbf (N)	Koch/Koch A-7		Koch/Teledyne A-10, F-15		Frost (Old) F-16		Frost (New) F-16 ⁶		Capwell B-52, T-38, F-5		
	R ⁴	L ³	R	L	R	B ⁵	L	R	L	R	L
100 (445)	6/6	6/6	6/6	6/6	6/6		6/6	6/6	6/6	6/6	6/6
300 (1334)	6/6	6/6	6/6	6/6	6/6		6/6	6/6	6/6	6/6	6/6
500 (2224)	5/6	5/5	5/6	5/6	5/6	1/6	5/6	6/6	6/6	6/6	6/6
700 (3117)	4/6	5/6	4/6	3/6	2/6	2/6	4/6	6/6	6/6	6/6	6/6
900 (4003)	0/6	2/6	1/6	1/6	2/6	1/6	3/6	6/6	6/6	6/6	6/6
1100 (4893)	0/6	0/6	0/6	0/6	1/6	1/6	0/6	6/6	6/6	6/6	6/6

¹All test subjects wore standard issue flight gloves during the laboratory test.

²Left shroud and release were loaded for all tests.

³Left hand triggering of left release; "L".

⁴Right hand crossed over chest to trigger left release; "R".

⁵Successful in triggering release using both hands together; "B".

⁶Very limited usage in service, used only on ten F-16 aircraft stationed at Hill Air Force Base.

1.6 STRAIN RATE EFFECT ON ALUMINUM WELD JOINTS

A test program was undertaken to investigate the weld joints typically used in the fabrication of the portable shelter for the Ground Launch Cruise Missile (GLCM). All of the test specimen welds join together an aluminum alloy 6061-T6 plate to an aluminum alloy 5083-H321 plate. Both plates are 0.375 inch (9.5 mm) thick. The program was initiated to determine:

(1) the effect of loading rate on the load carrying ability of butt and overlap weld joints, (2) any difference in the two materials' strain rate response to loading, and (3) any difference in alloy 6061 local strain rate in moving from the weld heat effected zone to a local remote from the weld zone.

All of the butt and lap weld specimen test results are presented in Table 13.

The first series of butt weld specimens (I.D. Nos. 1-4) were fabricated with filler alloy 5356. Specimens 1-3 were loaded at the fastest ram velocity, approximately 3.8 in/sec (97 mm/sec), the test machine was capable of providing. For this series of specimens a strain gage was attached to each side of the weld in the heat affected zone, approximately 6 mm from the weld bead. The strain response of the alloy 5083 material was always faster and larger than that of the alloy 6061 plate. All of the butt weld test samples failed in the heat affected zone of alloy 6061 adjacent to the weld bead; the failure sight was not in the weld itself. Specimen number 4 was loaded at a slower ram velocity than the other three specimens of the series; due to instrumentation malfunctions the exact loading rate and weld zone strain rate responses are not known.

The second set of butt weld test samples (5BB-1,2,3,4) were also fabricated with alloy 5356 filler material. Two of these samples, (5BB-2, and -4), were loaded in tension at a slow ram velocity and one specimen, 5BB-3, was loaded in tension at maximum ram velocity. Typical of a standard coupon tensile test a higher fracture load resulted from the faster ram velocity.

TABLE 13
BUTT WELD TENSILE TEST RESULTS

Specimen I.D.	Weld Filler Alloy	Ram Velocity		ϵ l/sec Al6061 Heat Effected Zone	ϵ l/sec Al5083 Heat Effected Zone	ϵ l/sec Al6061 Heat Unaffected Zone	Max. Load KIP (kN)	Yield Load KIP (kN)
		in/sec	(mm/sec)					
1	5356	3.75	95	0.053	0.216		11.5 (51.1)	6.0 (26.7)
2	5356	3.83	97	0.043	0.360		11.10(49.4)	8.5 (37.8)
3	5356	3.9	99	0.056	0.360		11.30(50.3)	7.0 (31.1)
4	5356	---	--	---	---		12.00(53.4)	6.5 (28.9)
SBB-1*	5356	3.53	89	0.188	---	0.035	0.7 (3.1)	---
SBB-2	5356	0.002	0.05	0.0006		0.0003	10.7 (47.6)	6.0 (26.7)
SBB-3	5356	5.3	134	0.156		0.027	11.8 (52.5)	8.2 (36.9)
SBB-4	5356	0.002	0.05	0.0008		0.0003	11.0 (48.9)	6.5 (28.9)
LAP WELD TENSILE TEST RESULTS								
1-5TA	5356	3.90	99	---	---		10.8 (48.0)	8.3 (36.9)
3-5TA	5356	2.20	56	0.037	0.252		10.8 (48.0)	7.5 (33.4)
15-5TB	5356	0.0008	0.02	0.0001	---		12.5 (55.6)	7.5 (33.4)
4-5TA	5356	0.0013	0.03	0.00015	0.00014		11.8 (52.5)	8.3 (36.9)
13-5TB	5356	3.75	95	0.275	0.425		13.3 (59.2)	5.8 (25.8)
10-5TB	5356	4.16	106	0.150	0.195		12.2 (54.3)	7.1 (31.6)
2-5TA	5356	0.0013	0.03	0.00025	0.00019		11.0 (48.9)	8.3 (36.9)
14-5TB	5356	2.13	54	0.1818	0.2700		---	---
5-4TA	4043	0.0008	0.02	0.0002	0.0003		9.4 (41.8)	---
7-4TA	4043	2.04	52	0.324	0.498		9.5 (42.3)	7.5 (33.4)
8-4TA	4043	3.3	83	0.156	0.298		9.6 (42.7)	7.0 (31.1)
10-4TA	4043	2.31	59	0.138	0.294		9.4 (41.8)	8.0 (35.6)
6-4TA	4043	0.0013	0.03	0.00017	0.00018		9.5 (42.3)	6.3 (28.0)
12-4TA	4043	3.60	91	1.59	0.321		9.0 (40.0)	7.0 (31.1)
11-4TA	4043	3.53	90	0.144	0.272		9.3 (41.4)	6.8 (30.2)

* 3 Point Bend Loading to Failure Span = 8.0 Inches

For this series of specimens two strain gages were bonded onto the alloy 6061 plate material. One gage was mounted in the weld heat affected zone and the other strain gage was mounted remote from the weld heat affected zone. Specimen 5BB-1 was loaded to failure in a three point bend fixture at maximum ram velocity, 3.53 in/sec (89 mm/sec). In all cases the material adjacent to the weld bead, where failure occurred, demonstrated a higher strain rate than the material remote to the weld and heat affected zone. When failure occurred a much larger strain was indicated by the gage adjacent to the weld bead for three of the test specimens. For the one specimen, 5BB-2, where a larger strain indication was registered by the remotely located gage it was assumed that the strain gage adjacent to the weld bead delaminated as the material was yielding.

The rest of the test data presented in the table were from an overlap weld joint specimen configuration with two weld seams per specimen. The overlap weld joint specimens were fabricated using one of two different weld filled alloys, 5356 or 4043 aluminum. Doublers were added so as to not induce a large bending moment into the specimen when they were gripped. A strain gage was bonded to each of the two plates in the heat affected zone approximately 6 mm from the weld bead. No strain gages were mounted onto the material remote from the weld beads for any of the overlap weld test specimens. The dash entries in the table represent debonding of the strain gage or instrumentation failure. The lap weld specimens always show a faster strain rate response in the alloy 5083 plate material regardless of the ram velocity used during the test. The ram velocity had very little influence on the resulting ultimate and yield load levels for the overlap weld specimen configuration. All failures were in the weld beads. The load level where yielding occurred was approximately 80 percent of the ultimate load carried by the joint; the specimen experienced a ductile failure. Welds fabricated using the 5356 filler alloy have a slightly higher load carrying capability than the specimens fabricated with 4043 weld filler alloy.

One baseline specimen fabricated from alloy 6061 was pulled to failure at a ram speed of approximately 4.0 in/sec (102 mm/sec). Ultimate failure load was 23.48 KIP (104.4 kN) or an ultimate stress of 47.0 KSI (324 MPa). Failure loads for the butt weld specimens pulled in tension were approximately 11 KIP (49 kN) or for their nominal cross-sectional area the nominal tensile strength of the welded joints were 34.5 KSI (238 MPa) which is 73 percent of the alloy 6061 plate material's tensile strength.

Two test specimens were fabricated with two longitudinal weld beads that, when loaded, sheared the weld beads. One of these specimens was loaded at maximum ram velocity, 3.38 in/sec (86 mm/sec); the ultimate load carried was 34.0 KIP (151 kN). The second specimen was loaded with a slow ram velocity, 0.0005 in/sec (0.0127 mm/sec) and carried 34.5 KIP (153 kN). The large variation in ram velocity had no effect on the joints load carrying capability when the weld seam was loaded/failed in the shear mode.

1.7 FATIGUE CRACK GROWTH INVESTIGATIONS OF IMPROPERLY-QUENCHED (SOFT) ALUMINUM UNDER A TRANSPORT AIRCRAFT LOAD HISTORY

The Air Force has been concerned with the problem of "soft" aluminum since its discovery in the summer of 1979. The possibility exists that such inferior material might have found its way into any of several Air Force systems. Aluminum plates containing localized regions of substrength material, caused by an improper quench during heat treating, were carefully examined by the Materials Laboratory of AFWAL to determine how properties such as tensile strength, fatigue, fracture, and corrosion sensitivity were affected.^[5-7] In a final effort to understand how such material would behave in a military-type service environment, samples machined from both normal and soft aluminum plates were subjected to two fighter aircraft load histories. Results were reported in References 8 and 9.

Because the problem of possible inferior aircraft components is not confined to Air Force systems alone, the Federal Aviation Administration (FAA) requested the Materials Laboratory to conduct similar spectrum fatigue testing on two commonly-used aluminum alloys, using a load history more representative of a transport type aircraft. The findings of this investigation are reported herein.

Two improperly-quenched aluminum plates were investigated: alloys 7075-T651 and 2024-T351. These two particular alloys were selected since they are used extensively in commercial aircraft and possess different strength-to-toughness characteristics. Aluminum 2024-T351 is a high toughness, low yield strength material, while 7075-T651 possesses low toughness and high strength.

Center-cracked test specimens, as illustrated in Figure 24, were machined from each side of the plate (soft side and properly-quenched side) for test in the longitudinal orientation. Prior to fatigue testing electrical-conductivity measurements were taken in the area where crack propagation was to occur, while after testing hardness readings were obtained, taking care to avoid regions of plastic deformation caused by crack propagation. The purpose of these nondestructive inspections was simply to measure to what extent each material was "affected", since for each material/temper, the strength is related to both electrical conductivity and hardness. An increase in conductivity reflects a decrease in strength, while hardness decreases with decreasing yield strength. For the two test materials in this study, curves relating both electrical conductivity and hardness to yield strength are furnished in Reference 10.

The load spectrum used in this investigation was the Transport Wing Standard (TWIST), developed jointly by the German Federal Republic and the Netherlands, and represents the load sequences for a transport aircraft wing skin near the main landing gear. The sequence of TWIST includes 4,000 different flights

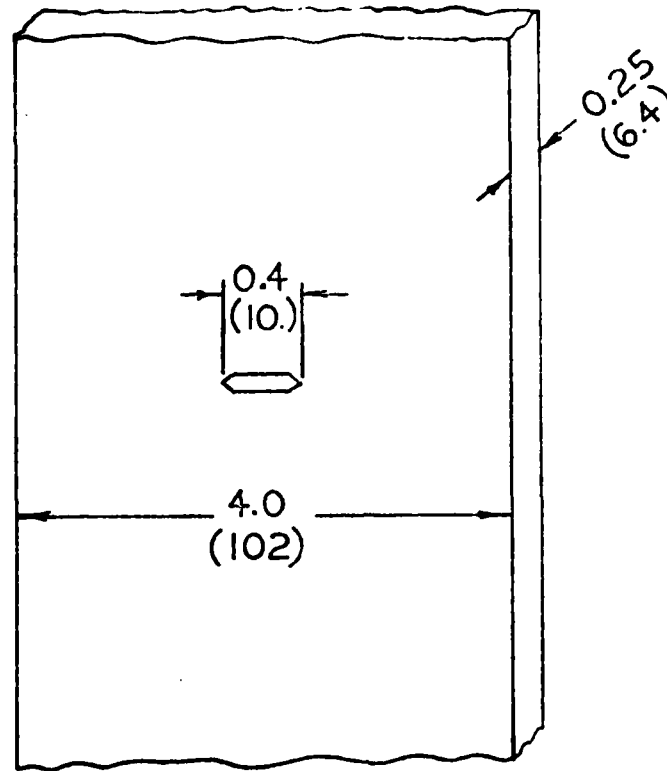


Figure 24. Center-Cracked Panel Test Geometry.

(typically 100 load cycles each), ranging from tranquil to stormy conditions. A portion of the load spectrum is graphically depicted in Figure 25, and can essentially be described as constant amplitude ($R=0.64$) with periodic overloads and underloads of varying magnitude.

Testing was carried out in a 200 KIP (890 kN) electro-hydraulic fatigue machine. A PDP 11-34 minicomputer was interfaced to serve as both control and feedback, creating a complete closed-loop system. Specimens were precracked under constant amplitude loading ($R=0.1$) to an initial crack length ($2a$) of 0.5 inch (13 mm), keeping the maximum precracking stress below any spectrum stress. Crack length was periodically measured via a 30X traveling microscope and recorded as a function of elapsed flights. Maximum spectrum stress was selected so as to yield a convenient crack growth rate for each alloy: 18 KSI (124 MPa) for aluminum 7075-T651 and 23 KSI (158 MPa) for aluminum 2024-T351.

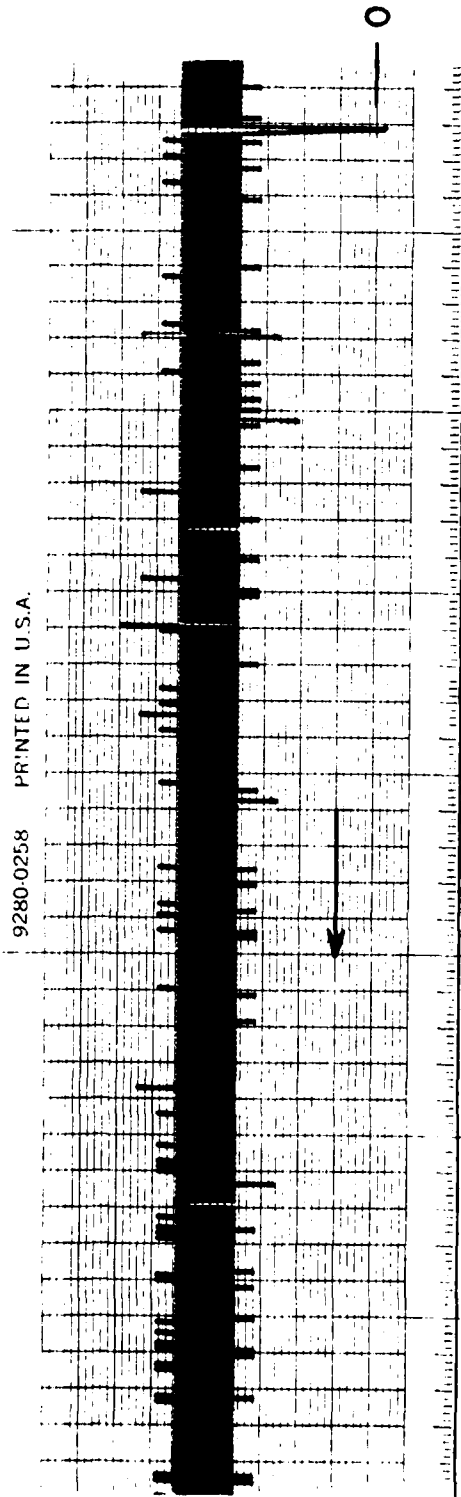


Figure 25. Portion of Load-versus-Time Record for TWIST Load History.

Results obtained for aluminum 2024-T351 are best presented in Figure 26, where total crack length is plotted against elapsed flights. As can readily be observed the two "soft" specimens, TW-2-T and TW-2-B (as indicated by the lower hardness/higher conductivity readings), show a noticeable loss in fatigue life and crack propagation resistance when compared to the properly heat-treated specimen (TW-1-B). This same conclusion was reached in an earlier investigation for 2124-T851 undergoing a fighter aircraft spectrum.^[8] Note also the irregular shape in the data for the normal material, a result of the most severe flight (flight #1656) which occurs only once per pass (4,000 flights) through the spectrum.

Results obtained for aluminum 7075-T651 are presented in Figure 27 and show surprisingly the opposite trend: the "softest" sample (FA-3-T) possessed the greatest life and resistance to crack propagation when compared to the properly heat-treated samples (FA-1-B and FA-3-B). Though sample FA-2-T was removed from the affected regions of the plate, post-test hardness measurements later indicated it was nearly equal in hardness to the properly heat-treated samples. Consequently, it should be regarded as near normal 7075-T651. Thus it appears from these limited results that while 2024-T351 is adversely affected by the improper quench, the fatigue crack growth properties of Al 7075-T651 are actually improved.

To further validate these data, constant amplitude fatigue crack growth data were obtained on CT specimens removed from each previously tested center-cracked panel. The results for both normal and affected 2024-T351 are presented in Figure 28, while the 7075-T651 results are shown in Figure 29. The same trends observed in the spectrum fatigue tests are repeated in the constant amplitude data: for aluminum 2024-T351, the lower strength/higher toughness alloy, the improper quench caused an increase in crack growth rate, while for 7075-T651, the higher strength/lower toughness alloy, the crack growth rates were decreased slightly in the affected regions. For both materials

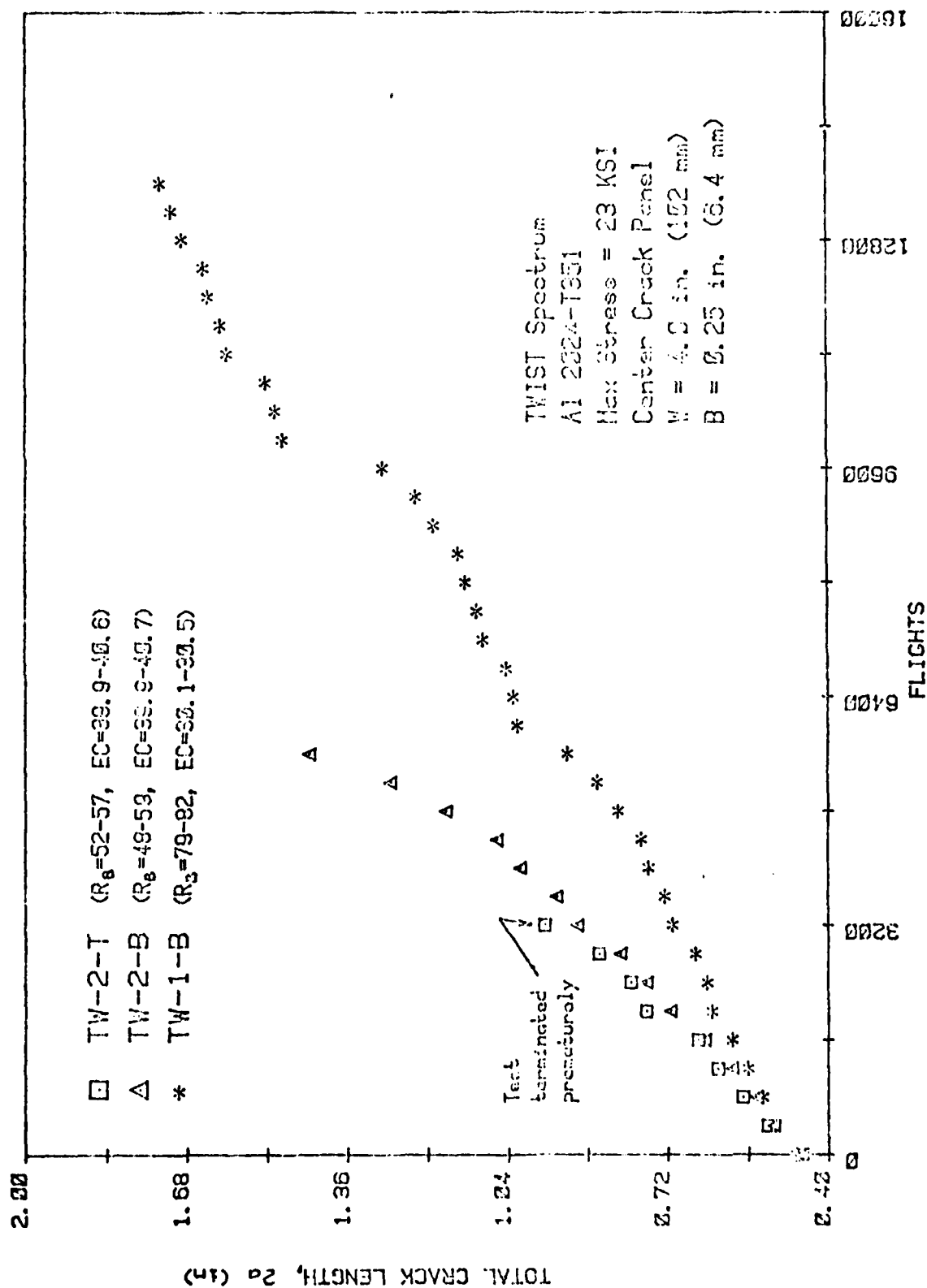


Figure 26. Spectrum Fatigue Crack Growth Data for Normal and "Soft" Aluminum 2024-T351.

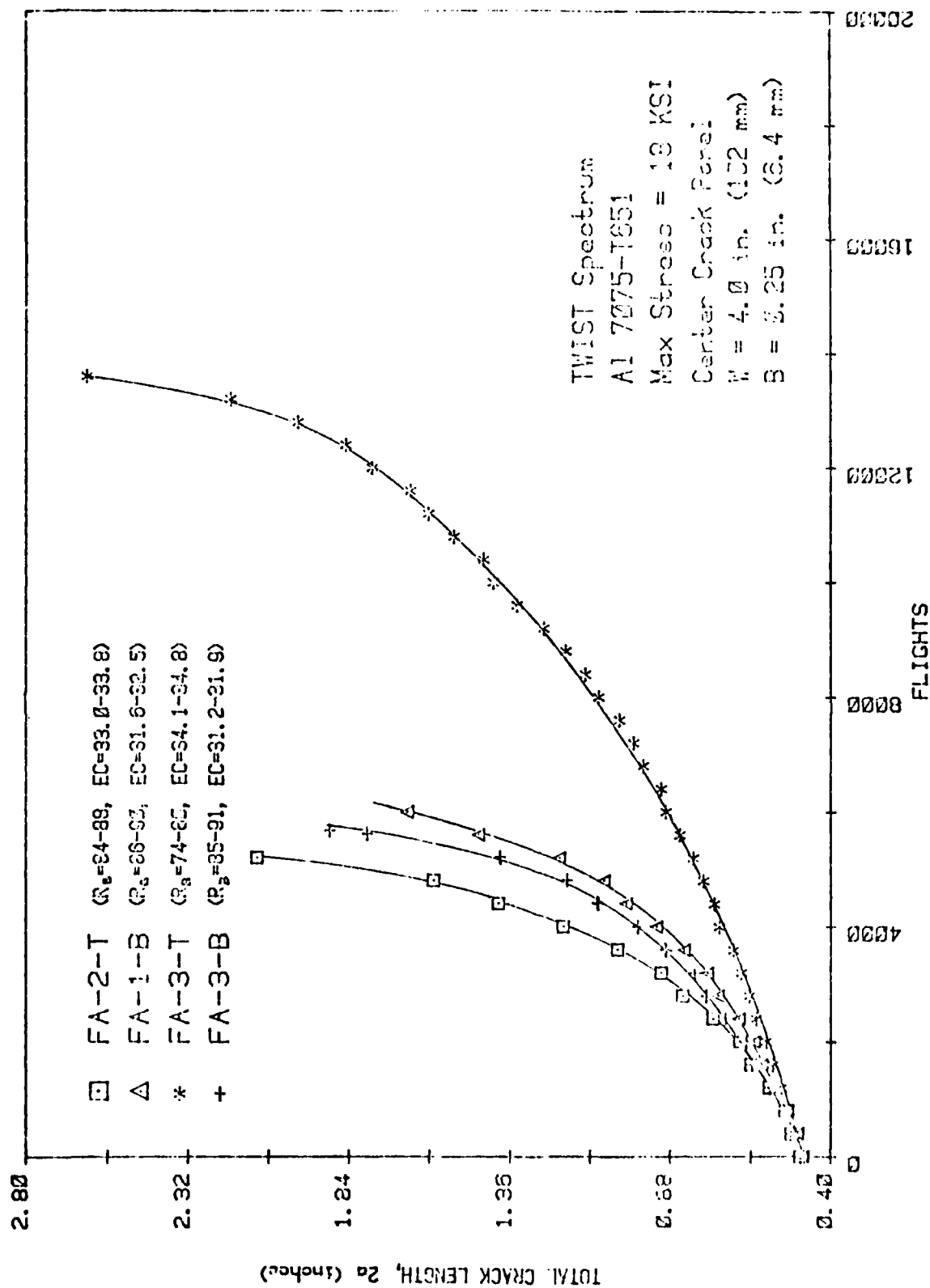


Figure 27. Spectrum Fatigue Crack Growth Data for Normal and "Soft" Aluminum 7075-T651.

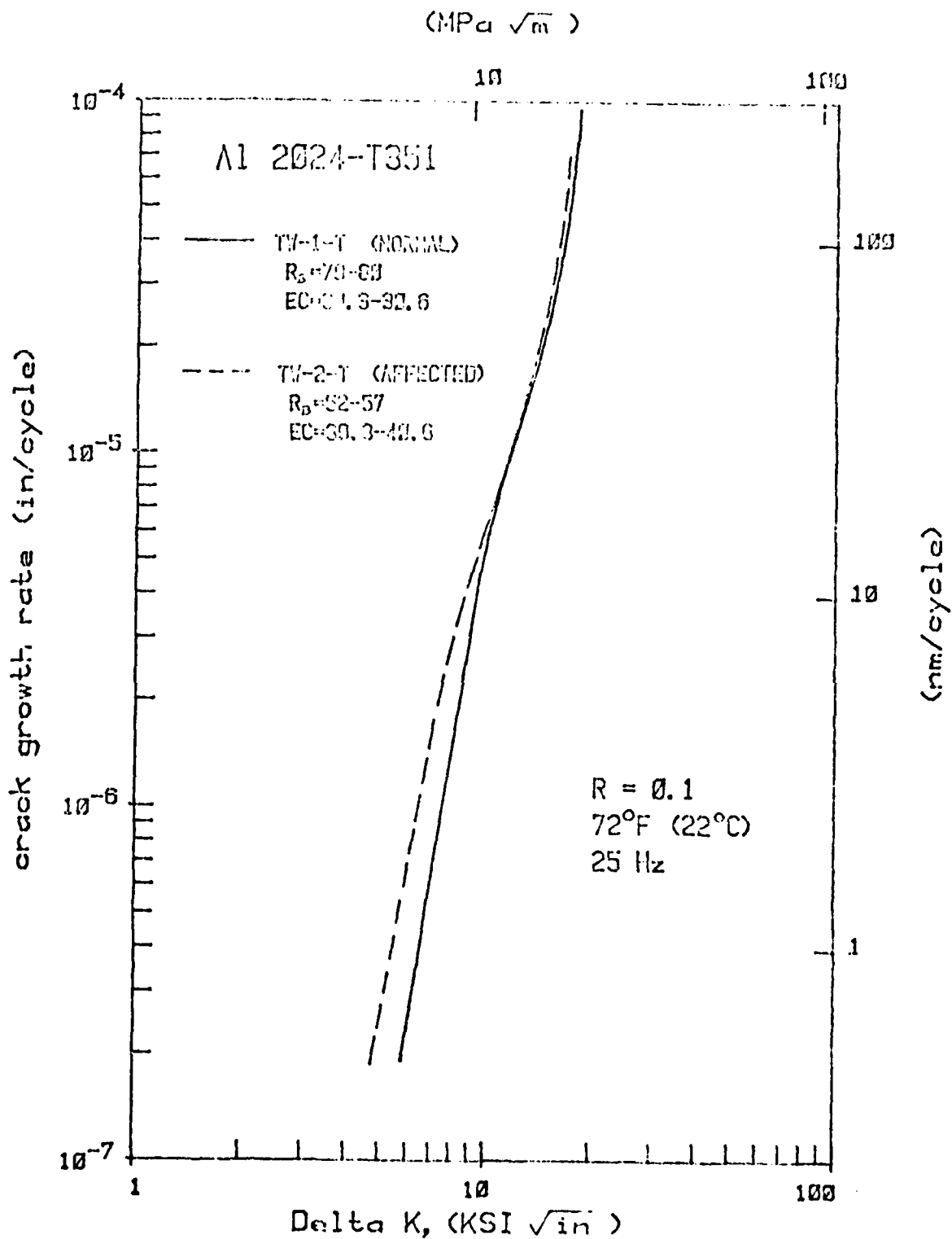


Figure 28. Constant Amplitude FCGR Data for Normal and "Soft" Aluminum 2024-T351.

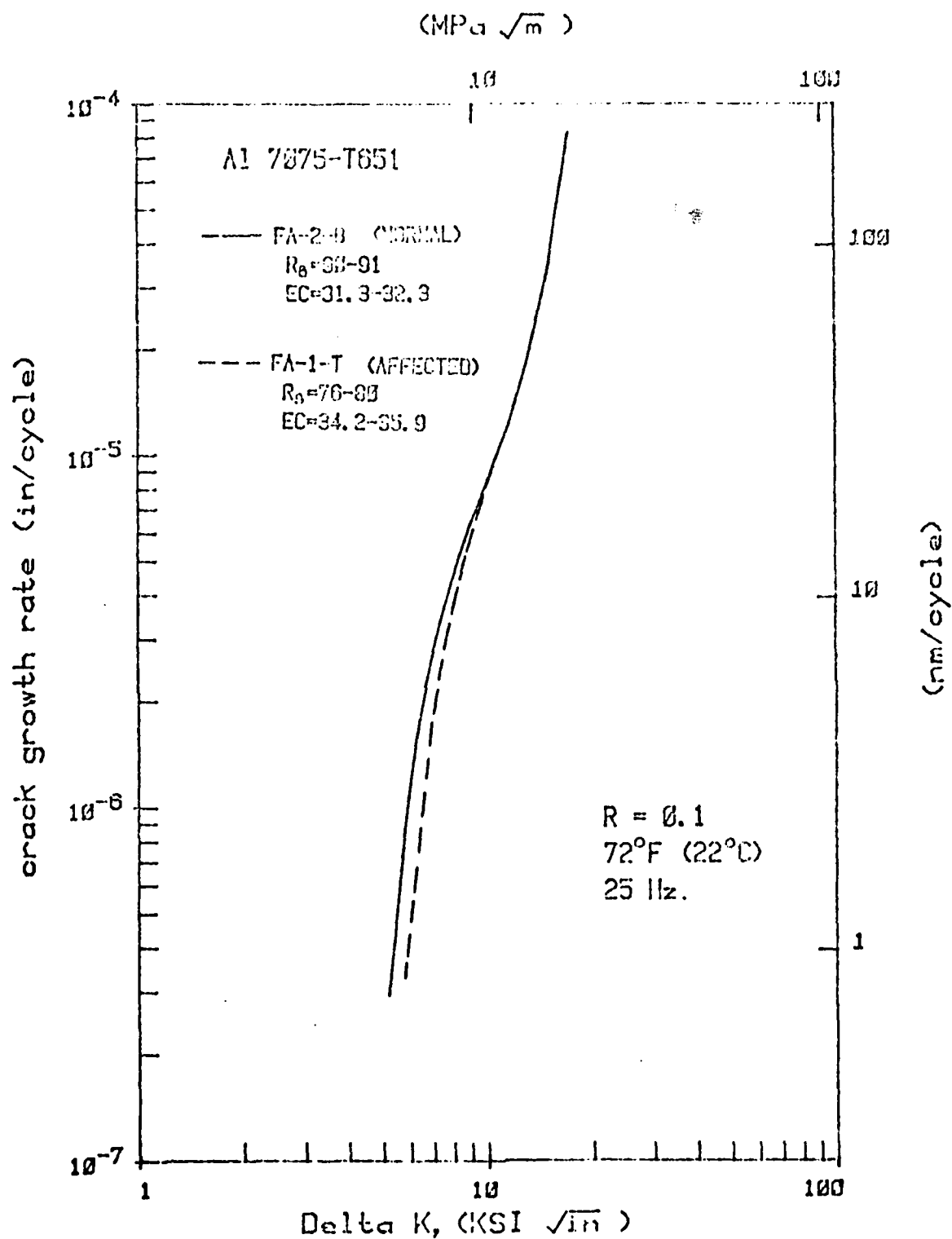


Figure 29. Constant Amplitude FCGR Data for Normal and "Soft" Aluminum 7075-T651.

the effect of the improper quench on fatigue crack growth diminishes at the higher stress intensity ranges [i.e., above 10 KSI/ $\sqrt{\text{in}}$ (10.9 MPa/ $\sqrt{\text{m}}$)].

1.8 MECHANICAL PROPERTY INVESTIGATION OF ALUMINUM X7091-T7E69 EXTRUSION

This investigation was performed to determine mechanical property data for aluminum X7091-T7E69 extrusion, a newly developed alloy produced via powder metallurgy (P/M) methods. Such P/M aluminum alloys are purported to possess superior mechanical and physical properties compared to products produced by conventional cast and wrought ingot technology. Properties examined in this effort are tensile, fracture, smooth and notch fatigue, fatigue crack growth, and stress corrosion cracking. Tensile, fracture, and crack growth properties are established at room temperature and 250°F (121°C).

The test material was provided by the producer, the Aluminum Company of America (ALCOA), in the form of three extruded bars approximately 1.5 x 4.5 x 24 inches long (38 x 114 x 610 mm). All the bars were from the same log (#G79666Al) and were further identified with individual numbers, -20, 21, and 22. A chemical composition was determined for one of the bars with the following results obtained.

CHEMICAL COMPOSITION OF TEST MATERIAL X7091 [Lot-G79666Al]

Wt. %

Zn	Mg	Cu	Co	Si	Fe	B	Mn	Cr	Ti	Al
6.4	2.2	1.4	0.4	~0.2	0.054	0.012	<0.001	<0.02	<0.01	Balance

The material was furnished in the T7E69 condition which is the highest strength temper of the two tempers currently available for this product form.

Tensile specimens, 0.25 inch (6.4 mm) diameter with a 1.0 inch (25 mm) gage length, were removed from the longitudinal orientation of each bar (NOTE: for all test specimens, the first two digits in each I.D. represents from which of the three bars the particular specimen was removed).

Axial fatigue specimens were removed from the longitudinal orientation and machined to two specimen configurations: a smooth fatigue ($K_t = 1$) uniform gage section geometry with a test section diameter of 0.180 inch (4.57 mm), and a cylindrical notched geometry to yield a stress concentration of $K_t = 3.0$.

Fracture, fatigue crack growth, and stress corrosion cracking samples were all compact type (CT) specimens, machined from the L-T orientation of each bar. Fracture and stress corrosion cracking samples were two sizes: 0.75 inch (19 mm) thick (K_{IC} and K_{ISCC}), and 1.5 inch (38 mm) thick (K_{IC} only). The fatigue crack growth specimens were originally 0.5 inch (12.7 mm) thick with a width of 1.5 inches (38 mm); however, because of out-of-plane cracking problems experienced, shallow side grooves were later added, thus reducing the net thickness to 0.4 inch (10.2 mm).

Tensile results performed at room temperature and 250°F (121°C) are listed in Table 14. Results indicate a slight improvement in strength ductility over aluminum 7050-T73651[11] at both temperature ranges. The elevated test temperature of 250°F (121°C) caused a slight decrease in both yield strength (12 percent) and ultimate strength (16 percent).

Fracture test results are listed in Table 15, showing no valid K_{IC} values obtained due to specimen thickness requirements. Fracture appearance, in all cases, was most irregular as shown in Figure 30. Though all specimens precracked straight and flat under relatively low loads, all fractures were roughly 45° to the precracked plane. Measurements performed on one of the three furnished bars failed to reveal any significant degree of residual stress within the bar.

TABLE 14
LONGITUDINAL TENSILE DATA FOR
ALUMINUM X7091-T7E69 EXTRUSION

Spec. I.D.	Test Temp °F (°C)	0.2% Yield Str. KSI (MPa)	Ult. Str. KSI (MPa)	% Elong. lin. (25mm) G.L.	%R.A.
20-T1	70 (21)	75.1 (514)	82.4 (568)	14	40
20-T2		72.1 (497)	76.9 (530)	12	38
21-T1	70 (21)	74.5 (514)	75.6 (521)	13	37
21-T2		77.4 (534)	84.1 (580)	11	34
22-T1	70 (21)	78.7 (543)	84.7 (584)	11	31
22-T2		74.7 (515)	84.2 (580)	14	44
avg.	-	75.4 (520)	81.3 (560)	12.5	37.3
20-T3	250 (121)	67.3 (464)	69.0 (476)	16	45
20-T4		65.4 (451)	67.2 (463)	16	38
21-T3	250 (121)	65.3 (450)	67.4 (465)	17	51
21-T4		67.9 (468)	69.0 (476)	17	44
22-T3	250 (121)	66.3 (457)	67.1 (463)	21	51
22-T4		64.9 (447)	66.1 (456)	18	39
avg.	-	66.2 (456)	67.6 (466)	17.5	44.7

TABLE 15
FRACTURE RESULTS FOR ALUMINUM X7091-T7E69
EXTRUSION (L-T ORIENTATION)

Specimen I.D.	Test Temp °F (°C)	Nom. Thickness in. (mm)	K_{Ic} KSI \sqrt{in} (MPa \sqrt{m})	Invalid K_{Ic} Criteria	
				$2.5 \left(\frac{K_{Ic}}{Y_s} \right)$	$\frac{P_{max}}{P_Q}$
20 K4	70 (21)	0.7 (18)	47.9 (52.6)	1.0	1.21
21 K4	70 (21)	0.7 (18)	52.2 (57.4)	1.2	1.09
22 K2	70 (21)	0.7 (18)	49.8 (54.7)	1.1	1.16
22 TKI	70 (21)	1.5 (38)	68.7 (75.5)	2.3	1.02
20 TKI	250 (121)	1.4 (38)	57.3 (63.0)	1.9	1.46



Figure 30. Typical Fracture Appearance for Aluminum X7091-T7E69 Toughness Specimens.

Smooth and notched fatigue results are presented in Figures 31 and 32, respectively, along with reference data^[11] for aluminum 7050-T73651. These results show a clear improvement in fatigue performance for both stress concentrations over the conventionally produced material.

Precracked CT specimens, loaded in a quiescent 3.5 percent NaCl environment, withstood failures after 1,000 hours when loaded to stress intensities as high as $40 \text{ KSI}/\sqrt{\text{in}}$ ($44 \text{ MPa}/\sqrt{\text{m}}$). Such behavior is clear evidence this material possesses excellent resistance to stress corrosion cracking, thus substantiating the producer's claim.

Constant amplitude fatigue crack growth rate data for X7091-T7E69 are presented in Figure 33 for both room temperature and 250°F (121°C) test environments. Differences between the two data sets are indistinguishable over the range of stress intensities examined, indicating no effect of this temperature on fatigue crack growth properties. Also presented is a data trend line for 7050-T7E69^[11] at room temperature and $R=0.1$. Results show a poorer performance in fatigue crack growth for X7091-T7E69 as compared to the conventional aluminum material, with differences diminishing only at stress intensities approaching the material's fracture toughness limit.

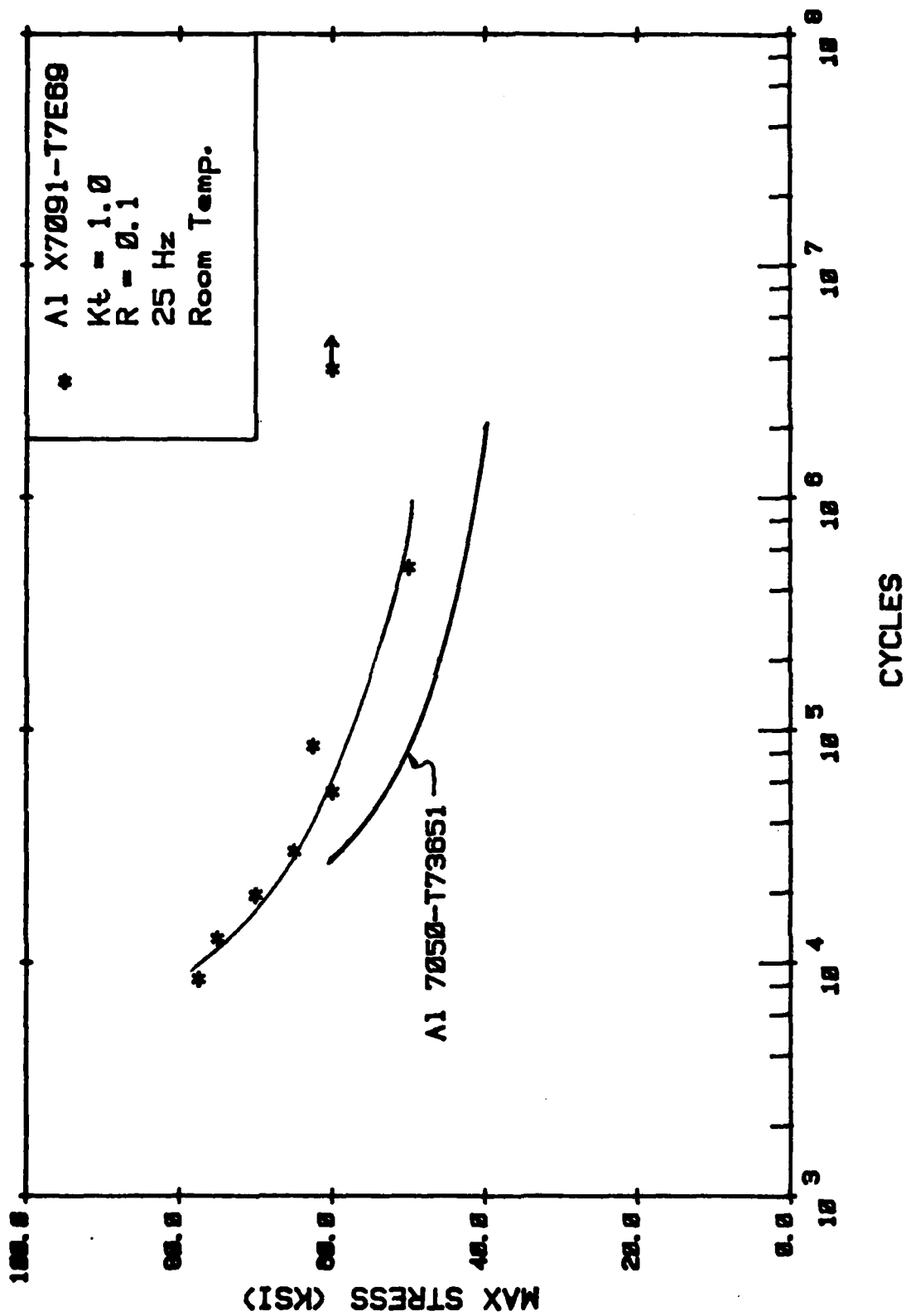


Figure 31. Smooth Axial Fatigue Results for Aluminum X7091-T7E69 Extrusion.

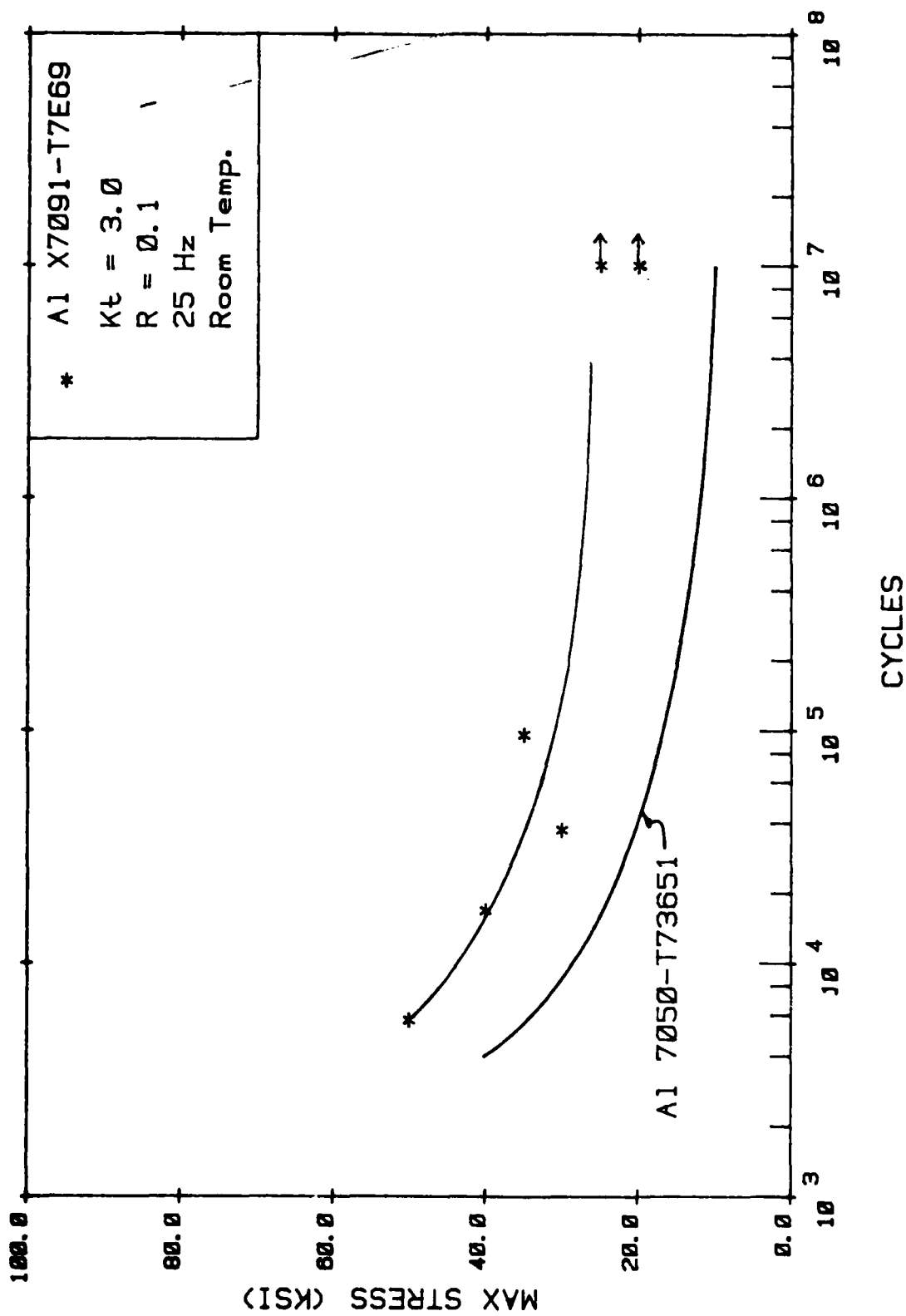


Figure 32. Notched ($D_t = 3$) Axial Fatigue Results for Aluminum X7091-T7E69 Extrusion.

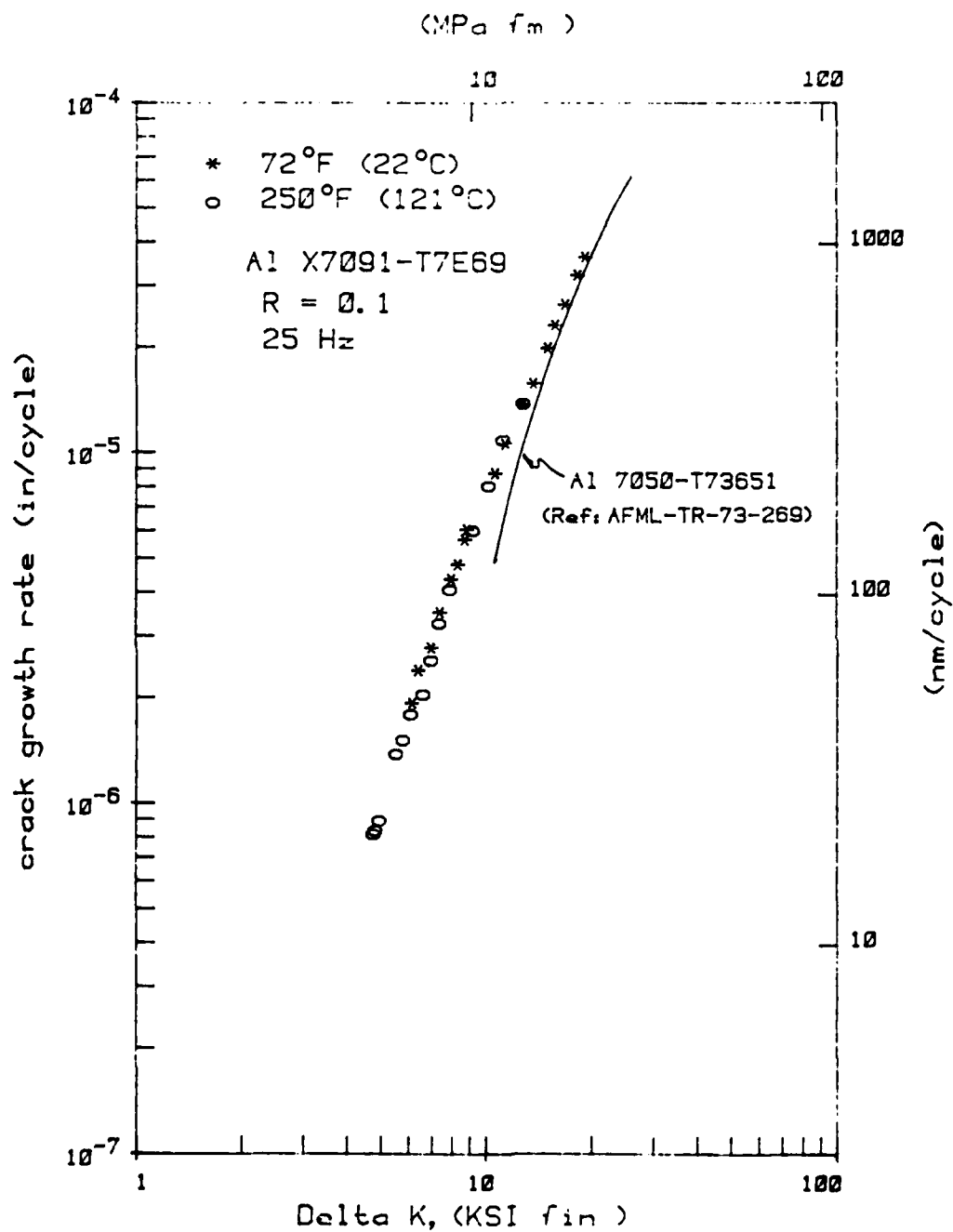


Figure 33. Constant Amplitude Fatigue Crack Growth Data for X7091-T7E69 for Room Temperature and 250°F (121°C) Test Environments.

1.9 FATIGUE CRACK GROWTH RATE DATA ACQUISITION SYSTEM FOR LINEAR AND NONLINEAR FRACTURE MECHANICS APPLICATIONS

Present technology for fatigue crack growth rate (FCGR) testing of materials generally employs visual examination of the specimen surface to determine the crack extension between applied load cycles. Almost all useful FCGR data to date have been obtained in this manner. Such a procedure requires personal supervision, specimen surface preparation for crack tip enhancement, and an adequate optics system (traveling microscope, magnifying glass with reference marks attached to the specimen surface, special lighting, etc.) for accurate crack length measurements. Naturally, the results of the visual procedure hinge on the degree of detail paid to each of the aforementioned elements in the optics system. An ASTM round robin program has determined that the most variability found in FCGR data, obtained from different laboratories, results from the experimental procedures used to obtain the raw test data.[12]

When conducting crack growth rate tests on a material behaving in a nonlinearly elastic manner, the methods employed to collect the raw test data become even more tedious and complex since parameters other than crack length and elapsed cycles must be measured and recorded. Crack tip opening displacement (CTOD), crack tip opening angle (CTOA), and the area under load versus displacement curves represent a few examples of data which are collected and analyzed by investigators to obtain nonlinear fracture parameters. The determination of these parameters are again often subject to operator bias and error, besides demanding constant personal supervision. Data reduction into the final form of crack growth rate versus a crack driving parameter is laborious, often yielding the final conclusions days after actual testing is completed.

Because of such inherent problems in fatigue crack growth testing a completely automated FCGR data acquisition system was developed to provide a nonvisual method for collecting data, such that it would satisfy ASTM Tentative Standard E647-78T.

The system described herein was designed to demonstrate the real-time capabilities of determining the fatigue crack growth rate as a function of either linear elastic fracture mechanics (LEFM) or nonlinear fracture mechanics (NLFM) parameters.

The acquisition system, illustrated in the schematic in Figure 34, utilizes a Hewlett Packard (HP) 9825A desktop calculator having approximately 25K bytes of internal storage. Accompanying it is an HP 6940B Multiprogrammer which is the device which contains the necessary printed circuit boards required for input/output operations. The multiprogrammer contains two voltage monitor cards which are connected by a unique "Y-cable" option to allow simultaneous readings of two channels; in this case, load and displacement. Each voltage monitor card is capable of measuring bipolar dc voltages in the range of ± 10 V, with a least significant bit (LSB) of 5 mV.

A programmable timer card is interfaced to each voltage monitor card to control sampling rate. The period of each time increment is jumper selectable in six decades from 1-4095 μ sec to 0.1 to 409.5 sec. Unfortunately, the fastest sampling rate is currently limited by the voltage monitor card conversion speed and, in the manner in which they are used, is roughly 2,000 conversions/sec.

Additional peripheral equipment to further enhance the system are an HP 9871A impact printer, an HP 7225A plotter, an HP 9885M flexible disk drive unit, and an HP 9878A I/O expander which ties all peripheral devices together.

The test stand to which the acquisition system is interfaced is an MTS electrohydraulic servo-controlled fatigue test machine, capable of cyclic loading up to 30 Hz, with a maximum load range of ± 25 KIP (111 kN). The load signal is obtained by means of a load cell with output voltage range of ± 10 VDC. Estimated signal noise level was approximately 7 mV RMS. Displacement is obtained via a clip gage affixed to the specimen.

AD-A122 004

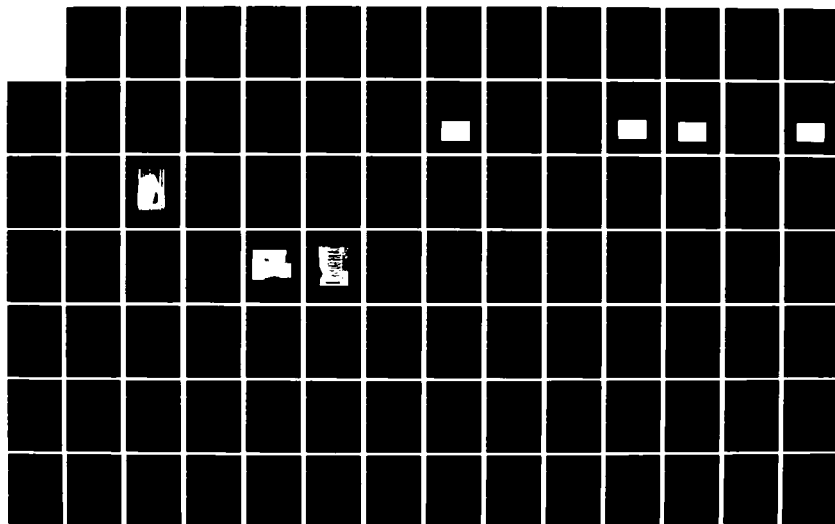
QRC EVALUATION OF MATERIALS AND PROCESSES(U) DAYTON
UNIV OH RESEARCH INST D R ASKINS ET AL. OCT 82
UDR-TR-82-85 AFWAL-TR-82-4104 F33615-80-C-5011

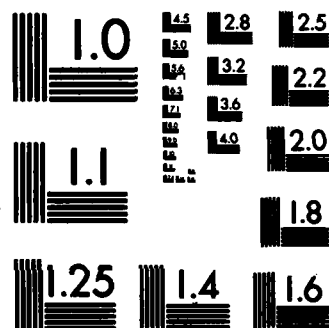
2/4

UNCLASSIFIED

F/G 14/2.

NL





MICROCOPY RESOLUTION TEST CHART
NATIONAL BUREAU OF STANDARDS-1963-A

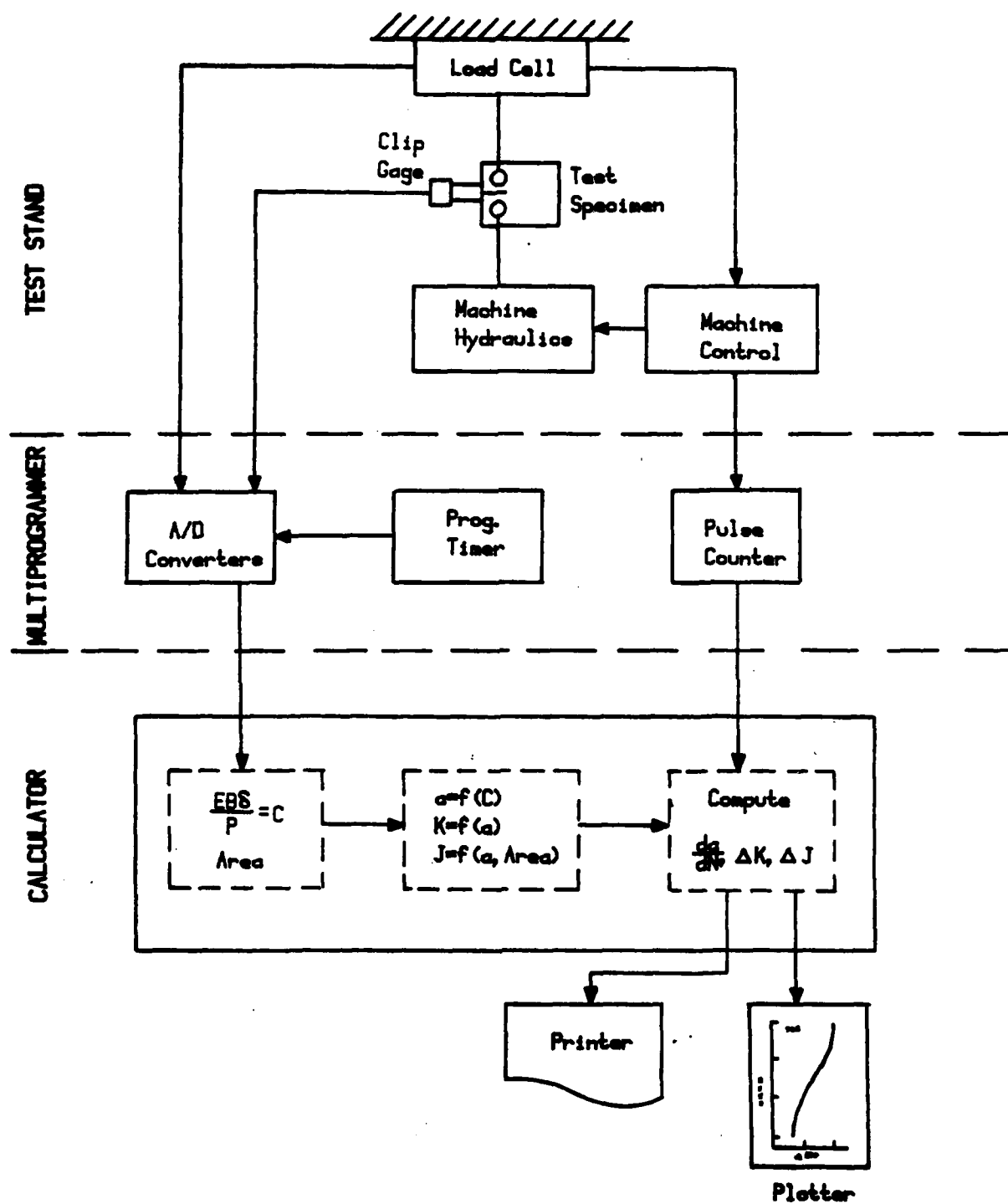


Figure 34. Schematic of FCGR Acquisition System.

and straddling the crack and likewise a ± 10 VDC range, with estimated signal noise levels on the order of 2-3 mV RMS. No attempts were made to further filter these load and displacement signals.

The test specimen geometry for which the system is designed is the compact type, shown in Figure 35, and is one of the two recommended in the present ASTM Standard for FCGR testing, E647-78T. Displacement is measured at the load line by means of the internal machined knife edges as illustrated in Figure 35. (Note: Though this specimen geometry with load-line knife edges is required for NLFM testing, since load-line displacements must be measured, it is not necessary for LEFM testing. For the latter, deflections can be measured at any point for which an accurate compliance expression exists.)

The system software flow chart is provided in Figure 36. Aside from entering the necessary details (specimen dimensions, load ranges, etc.), the program can be described as three basic routines: (1) a scanning routine which continuously scans the displacement signal until the maximum displacement has changed by some predetermined amount, or a sufficient number of load cycles have elapsed from a previous reading; (2) a reading routine which digitizes the load-displacement waveform; and (3) an analysis routine which analyzes this waveform and determines crack length, the crack growth rate, and either the stress intensity range, ΔK , or the change in J , ΔJ . Each of these routines is thoroughly described in the following paragraphs.

Before initiating the fatigue test, certain fixed variables must be entered to provide the basis for subsequent calculations. These include specimen ID and dimensions, load and displacement calibrations (lbf/volt and inches/volt, respectively), material modulus of elasticity, type of analysis desired (K or J), and finally the change in maximum displacement or change in elapsed cycles before a "reading" is taken. After

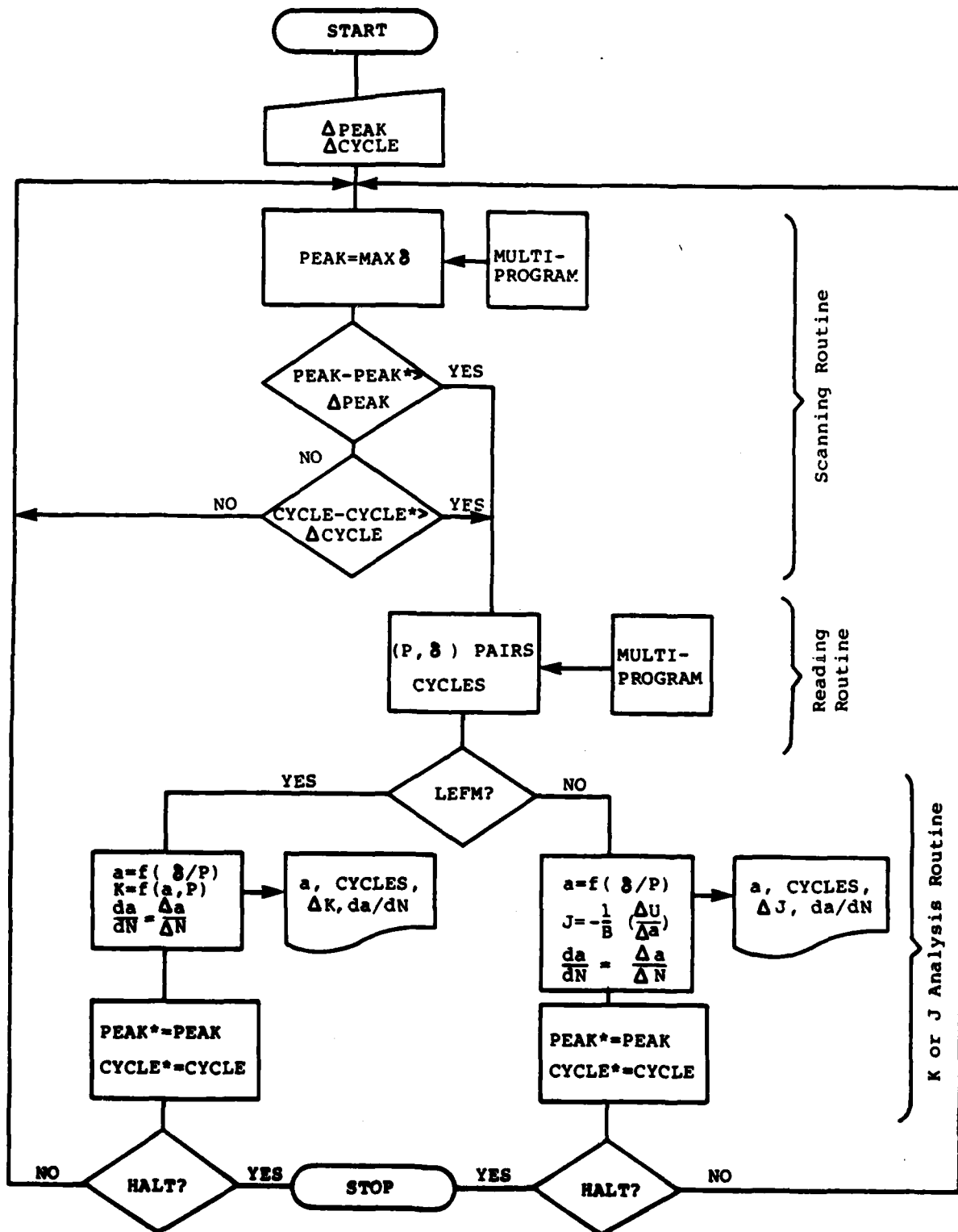


Figure 36. Flow Chart for FCGR Acquisition System.

the fixed data are entered, the computer pauses until the fatigue test is initiated.

When the program is continued the calculator begins by digitizing a displacement-time waveform, representing slightly more than one full cycle with a hundred points. These points are then scanned chronologically for the maximum value of displacement. This displacement value is compared to the previous maximum displacement value established at the last reading. If the difference in the maximum values differs by more than that previously specified by the operator (or if it is the first reading), the program goes to the routine to obtain a reading. If the change in displacement is less, the present cycle count is obtained and likewise compared to the last reading. If this change in cycles is greater than that specified by the user, the program goes to the reading routine. If neither of the two conditions are met, the search to obtain the next maximum displacement or cycle count is reinitiated.

When a significant displacement or cycle count change has occurred, a reading is taken in the following manner: simultaneous values of load and displacement are obtained; a hundred load-displacement pairs representing slightly less than two cycles. This is done to insure a minimum and succeeding maximum value. These points are then converted to the proper units of displacement and load and control then transferred to either the K-analysis or the J-analysis routine.

(1) K-Analysis Routine. If the linear analysis approach was specified, the load-displacement curve is analyzed as follows: the displacement array is scanned for the first minimum value or "valley." Since the load increasing portion consists of approximately 25 points, the first five points (representing 25 percent of the load range) are dropped due to nonlinearities which often exist near the valley of the load-displacement curve. The following ten points are fitted with a straight line using a linear regression analysis to obtain

the loading compliance. The compliance is then used in the following equation^[13] to obtain crack lengths in the range of $0.2 \leq a/W \leq 0.975$:

$$a/W = 1.000 - 4.063u + 11.24u^2 - 106.0u^3 + 464.3u^3 - 650.7u^5 \quad (14)$$

where:

$$u = [\sqrt{BEC} + 1]^{-1}$$

and

a = crack length,

W = specimen width,

B = specimen thickness,

E = elastic modulus, and

C = specimen compliance determined at load-line.

This crack length, along with minimum and maximum loads and specimen dimensions are used to calculate the stress intensity range. Finally, the change in crack length and cycles from the last reading are computed and used to yield the fatigue crack growth rate, da/dN . The secant method for determining crack growth rate was employed rather than the incremental polynomial method described in the tentative ASTM standard for crack growth rate testing (E647) merely for convenience in demonstrating a real time system such as this. Finally, all results are listed and values of da/dN versus ΔK plotted, after which control is transferred back to the scanning routine.

(2) J-Analysis Routine. If the nonlinear analysis approach was specified, control is transferred from the reading routine to the J-analysis routine. In this routine, the displacement array is similarly scanned for the minimum value. Upon determining this minimum point the successive load-displacement points are used to determine the area under the curve. The manner for accomplishing the integration is illustrated in Figure 37.

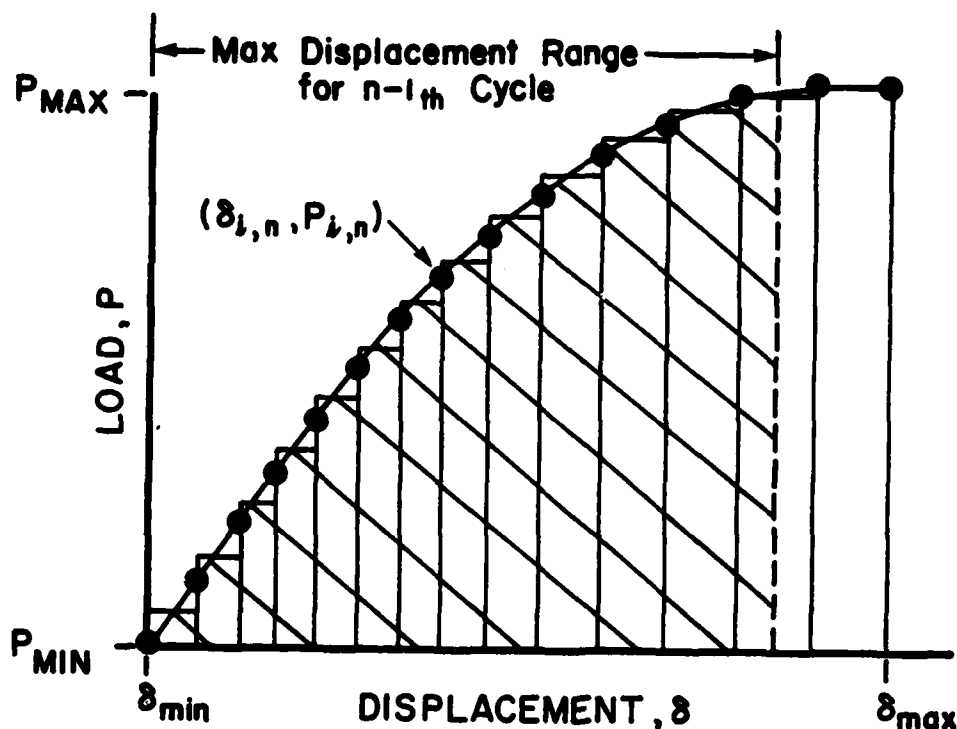


Figure 37. Graphical Method for Determining Area Under Load-Displacement Record for nth Cycle.

In integrating the load-displacement curve, two areas are obtained. First, a partial area is obtained over a displacement range exactly equal to the maximum displacement range of the preceding reading (n-1), since the change in areas between two successive readings must be determined over a constant displacement range. The mathematical routine employed to obtain the area is simply:

$$A_n = \sum_{i=2}^N (\delta_{i,n} - \delta_{i-1,n}) \times \left(\frac{P_{i,n} + P_{i-1,n}}{2} \right) \quad (15)$$

where:

- A_n = area under the curve of nth cycle,
- $\delta_{i,n}$ = ith displacement point, during nth cycle,
- $P_{i,n}$ = corresponding load point in the nth cycle, and
- N = number of divisions in the load-displacement curve (typically 25).

The total area calculation is continued up to the maximum value of load. This total area is then stored, along with the corresponding maximum displacement range over which this area was obtained, for comparison with the next (n+1) reading. The partial area (nth) is subtracted from the previously (n-1th) stored total area of the last reading obtained over the identical displacement range to calculate the change in area ΔU , which in turn is related J through the expression:

$$\Delta J = - \frac{1}{B} \left[\frac{\Delta U}{\Delta a} \right] \Big|_{\delta \text{ constant}} \quad (16)$$

where:

- B = specimen thickness,
- ΔU = the difference in areas under the load-displacement curves at a constant displacement,
- and Δa = crack extension between readings.

To determine the crack length, the maximum or "peak" value of the load-displacement curve is established as the starting point for the unloading compliance analysis. The 25 points subsequent to the peak load-displacement value represents the decreasing portion of the load-displacement curve and are analyzed to determine the unloading compliance. Similar to the K-analysis method, the upper 20 percent of the load range is ignored and a straight line fitted in a least-squares method through the next six points. These six points were selected to be above $0.5 P_{\max}$ because of nonlinearities which might exist in the load-displacement curve near the valley resulting from the crack surfaces coming into contact with each other, as well as other phenomenon upon unloading. The unloading compliance is then used in the appropriate compliance equation to yield crack length. By determining the change in crack length and cycle count from the preceding reading, the crack growth rate and ΔJ are computed. Finally, the crack length, crack count, total area under the curve, crack growth rate, and ΔJ are listed on the line printer and values of da/dN

versus ΔJ plotted, after which control is transferred back to the scanning routine.

Before conducting any crack growth rate testing, certain routines in the acquisition system had to be thoroughly demonstrated for accuracy and precision. These routines include the compliance routine for crack length measurements for both K and J methods, and the integration routine which calculates the area under the load-displacement curve. To accomplish this, a pre-cracked CT specimen, machined from aluminum 7075-T73 plate with a width of 3 inches (76 mm), 0.5 inch (12.7 mm) thick, was cyclically loaded at 1 Hz. A stress ratio (R) of +0.1 was applied at a sufficiently low maximum stress intensity so as not to cause any significant crack extension over 100 to 200 load cycles. Employing the J-analysis routine, 10 crack length and corresponding area measurements were determined via the acquisition system approximately every 10 cycles and compared to the optically measured crack length (three-point, through-thickness average of crack length measured after test) along with the area obtained from a load versus displacement plot from an X-Y recorder. The reconstructed computer printout, along with the optically measured values of crack length and area, is listed in Table 16. As can be seen the average crack length obtained via the acquisition system is within 0.002 inch (0.051 mm) of the visually measured crack length. The precision of the acquisition system is also excellent, as evident by the coefficient of variation (standard deviation/mean) in crack length readings of approximately 0.1 percent. For the area calculation, the average total area under the load-displacement curve obtained via the acquisition system is only slightly less (~ 0.7 percent) than the area measured graphically (average of 10 measurements). The reason for the slight bias is not clear, though certainly the accuracy of the X-Y recorder-generated curve must also be considered. Again, the coefficient of variation is minimal, less than 0.3 percent.

TABLE 16
COMPARISON OF ACQUISITION SYSTEM OUTPUT DATA
TO MEASURE CRACK LENGTH AND AREA FOR J-ANALYSIS

Measured crack length = 1.188 inch (30.18mm)
Measured total area = 6.888 lbf-in. (0.778 N-m)

J-Analysis Routine				
Reading No.*	Crack Length		Total Area	
	inch	(mm)	lbf-in.	(N-m)
1	1.185	(30.10)	6.839	(0.772)
2	1.185	(30.10)	6.840	(0.773)
3	1.187	(30.15)	6.808	(0.769)
4	1.184	(30.07)	6.850	(0.774)
5	1.185	(30.10)	6.869	(0.776)
6	1.186	(30.12)	6.847	(0.773)
7	1.185	(30.10)	6.813	(0.770)
8	1.187	(30.15)	6.849	(0.774)
9	1.187	(30.15)	6.843	(0.773)
10	1.187	(30.15)	6.850	(0.774)
Avg.	1.186	(30.12)	6.841	(0.773)
Std. Dev.	0.0011	(0.028)	0.018	(0.002)

* Readings taken every 10 cycles.

For the K-analysis routine, the results of a similar verification test are listed in Table 17. For this check, the average crack length obtained via the acquisition system is within 0.001 inch (0.025 mm) of the measured crack length with a standard deviation in automated crack length readings of approximately 0.0008 inch (0.02 mm).

Having demonstrated that these data taking routines yield sufficient accuracy, a crack growth rate test was initiated on a 3.0 inch (76 mm) wide, 0.625 inch (15.9 mm) thick, CT specimen machined from aluminum alloy 2124-T851. A sinusoidal waveform with a stress ratio of +0.1 was applied to the specimen at a frequency of 1 Hz. To facilitate rapid data collection, the initial stress intensity range was set at a high level. The change in maximum displacement between crack length readings was set at 0.0005 inch (0.0127 mm); the maximum change in cycles was set at 2,500. Uninterrupted crack length measurements were

TABLE 17
COMPARISON OF ACQUISITION SYSTEM OUTPUT DATA
TO MEASURE CRACK LENGTH FOR K-ANALYSIS

Measured crack length = 1.191 inch (30.25mm)

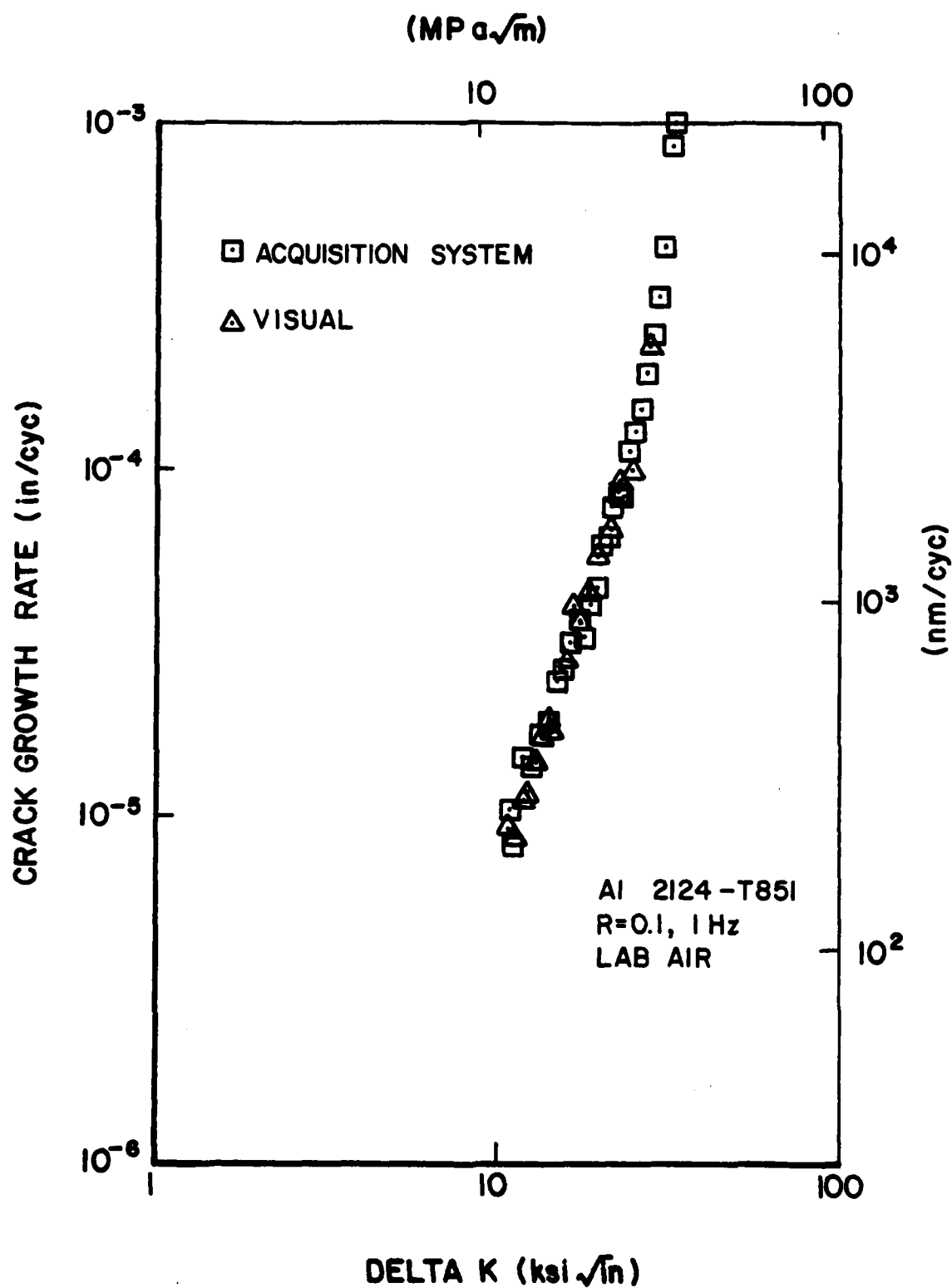
K-Analysis Routine		
Reading No.*	Crack Length	
	inch	(mm)
1	1.192	(30.28)
2	1.192	(30.28)
3	1.192	(30.28)
4	1.192	(30.28)
5	1.193	(30.30)
6	1.192	(30.28)
7	1.191	(30.25)
8	1.192	(30.28)
9	1.193	(30.30)
10	1.194	(30.33)
	Avg. 1.192	(30.28)
	Std. Dev. 0.00082	(0.021)

* Readings taken every 10 cycles.

obtained via a 30X traveling microscope throughout the test for comparison with the acquisition system results.

The test results for the K-analysis method are presented in Figure 38. Note that the results from the visual and automated methods were identical and that data were obtained over a greater range of growth rates with the acquisition system than was achieved by visually monitoring the crack extension due to its faster response at high crack growth rates. The values of crack length versus cycles obtained via computer and visual methods are virtually indistinguishable.

Having proven the linear elastic method successful, the nonlinear, or ΔJ method was employed for a 7075-T73 aluminum CT specimen, 3.0 inch (76 mm) wide and 0.5 inch (12.7 mm) thick. Though 7075-T73 aluminum does not behave as a nonlinear material, it does have the advantage in that for linear elastic materials



the value of J determined is equal to the elastic strain energy release rate, or

$$\Delta J = \frac{\Delta K^2}{E} \quad (17)$$

where ΔK is the stress intensity range, and E is the modulus. Employing this identity as a check for validity, the crack growth was determined as a function of ΔJ and compared to this function of stress intensity calculated over the same interval of crack growth.

The results of this endeavor are presented in Figure 39 (crack growth rate versus ΔJ) for the data generated during a single test. Also shown are the energy values based on ΔK as generated by the system using the compliance crack length. As is evident from the figure, values of ΔJ determined via the acquisition system and the analytical method are in reasonable agreement over the range investigated. A larger scatter, however, exists for the value of ΔJ determined by the computer system versus the analytical values based on stress intensity and elastic modulus. To better estimate the differences between the two data sets, a second degree polynomial was fitted to each set using a least-squares-fit method. Examination of the two curves revealed a difference in ΔJ between each method of less than 5 percent throughout the range of data obtained, and in general, the automated ΔJ values were slightly lower than the analytical results based on K . The source of error or scatter between the acquisition system results and the analytical results are possibly a result of one or both of the following factors.

First, the area calculating routine was demonstrated earlier (Table 16) as possessing sufficient accuracy and precision, the latter evidenced by the small standard deviation of 0.018 lbf-in. (0.002 N-m) for a measured area of approximately 6.84 lbf-in. (0.773 N-m). However, the value of ΔJ is based on the difference in areas between two such records. For

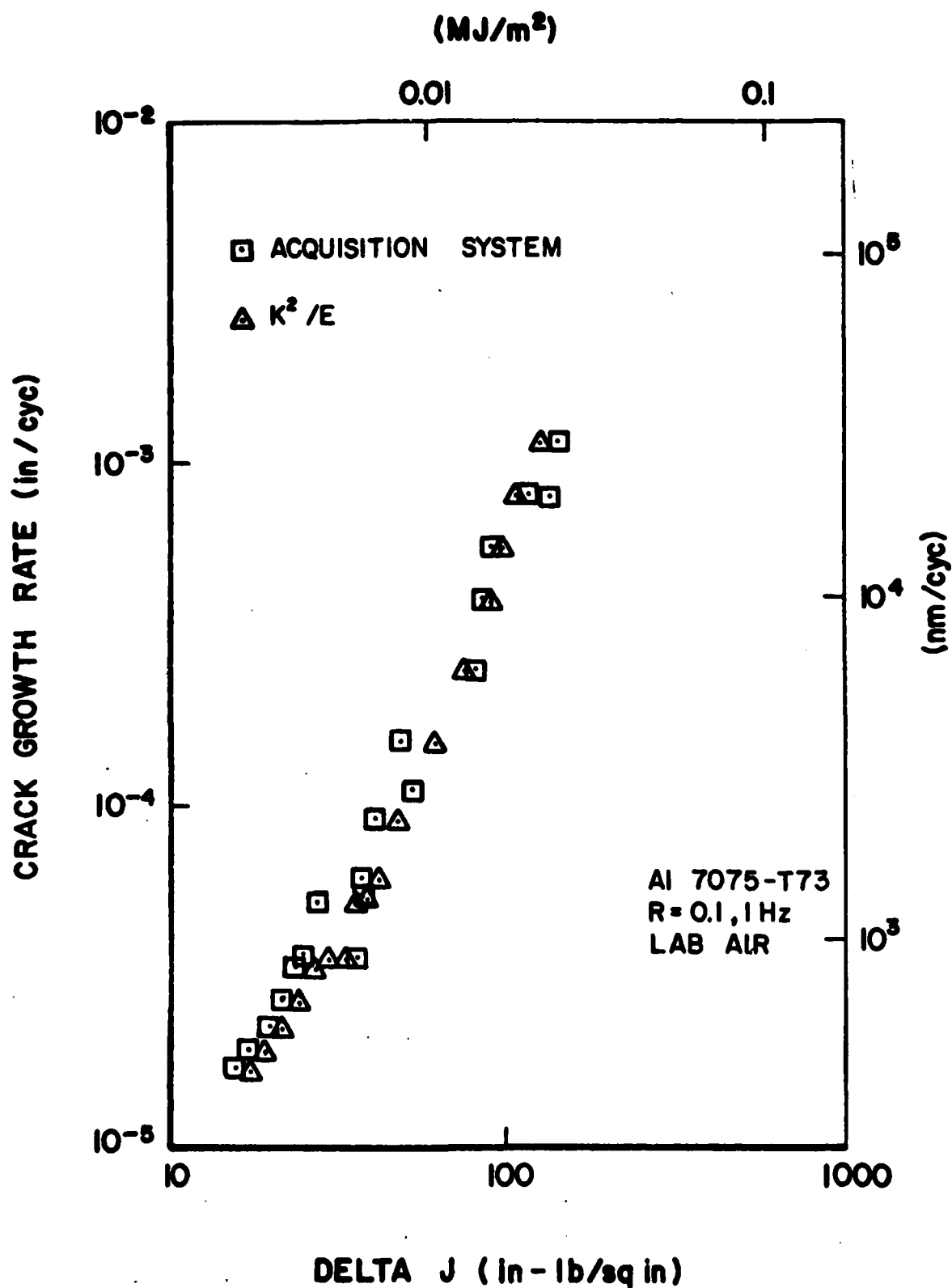


Figure 39. NLFM Crack Growth Data Obtained via Acquisition System and Analytical Methods.

similar test conditions as applied during the earlier verification check, the area difference between two successive readings was on the order of 0.4 to 0.5 lbf-in. (0.045 to 0.056 N-m). Assuming the precision (± 1 standard deviation) remains the same, now a coefficient of variation (standard deviation/avg. area difference) is on the order of 3 to 5 percent. Thus, a seemingly small degree of variation in the total area calculation has a much greater influence on the change in area and subsequently the empirical values of ΔJ .

Secondly, the value of modulus is an important parameter which influences both the compliance crack length and the ΔJ value based on the energy release rate, $\frac{K^2}{E}$. For tests conducted in this program, a handbook value of modulus was chosen at 10.6 msi (73.1 GPa). A 1 or 2 percent error in modulus would create a similar error in both crack length and stress intensity, as well as the analytical expression for ΔJ . Consequently, the difference between the analytic values of ΔJ and the values obtained via the acquisition system might result more from an error in the analytical term and not the automated method.

Finally, as previously stated, the ΔJ data presented in Figure 39 were determined for a linear elastic material. The J-integral method would generally be employed for materials which behave nonlinearly elastic. However, since the routines employed proved quite successful for the elastic material there does not appear any reason why it could not be used for both conditions with equal accuracy.

1.10 EFFECT OF SPECTRUM MODIFICATIONS TO FALSTAFF ON FATIGUE LIFE AND FRACTURE FACE MORPHOLOGY

To best evaluate a material/structure it is necessary to subject it to the same conditions (environment, load, etc.) in laboratory tests that it might be expected to experience in actual service. Such is the purpose of spectrum fatigue testing, where a load history derived either from usage or expected

usage data is applied to a test article and information such as time to failure and crack growth characteristics obtained. Unfortunately, due to test article complexity, it is often impossible or impractical to visually monitor the specimen for fatigue crack initiation and propagation, thus resulting in only one piece of information per test: time to failure. When test specimens are expensive and/or test times lengthy, it often becomes cost prohibitive to completely categorize fatigue and fracture properties for a material/structure of interest.

Because of such test limitations, a member of the Flight Dynamics Laboratory of AFWAL has attempted to modify an existing international standard fighter spectrum, such that a post-test examination of the fracture faces will reveal crack growth rate data from initiation to final catastrophic failure. This report outlines a number of such spectrum modifications and their relative effect on both fracture face topography and fatigue life.

The loading spectrum examined in this effort was the Fighter Aircraft Loading Standard For Fatigue (FALSTAFF), a fighter aircraft load history developed by several European countries and used extensively by participating NATO countries. The FALSTAFF load history is based on data derived from a number of both American-built (Lockheed F-104G and Northrup NF-5A) and European-built (Fiat G-91 and Dassault Mirage IIIS) aircraft and consists of 200 individual flights which represent a variety of exercises such as combat patrol, close air support, reconnaissance, etc. A generation program is used to draw on the exceedance data and properly arrange it to create the various flights. Though each flight is unique, the taxi-load sequences for each one are fixed and represents take-off and landing cycles for two configurations: pylon tank (full) or clear (no external wing stores).

The actual load history endpoints are classed into 32 equi-distant load levels; level 1 is the lowest and level 32 the

highest, with zero load or stress equivalent to a level of 715269. A histogram of the FALSTAFF spectrum is furnished in Table 18.

Spectrum fatigue crack growth investigations were carried out on center-cracked panels machined from aluminum 2024-T3, 0.250 inch (6.4 mm) thick plate. Specimen design is presented in Figure 40. All specimens were machined from the longitudinal direction of the plate.

Fatigue testing was performed in a 160 KIP (712 kN) MTS electrohydraulic fatigue machine. A Digital Equipment Corp. PDP 11-34 computer was interfaced to the test stand to serve as both control and feedback. Crack length measurements were performed after each spectrum pass using a 30X traveling microscope with digital readout.

Restating, the purpose of this effort was to develop modifications to the FALSTAFF load history so that a significant event (i.e., the maximum spectrum stress) will produce some marking on the fracture face, and therefore, by examining the fatigue fracture, one can observe these markings and develop a crack length versus cycles record. At the same time, the modifications must have a minimal effect on fatigue properties.

With this in mind, four spectrum tests were performed: one using the standard FALSTAFF load history, the other three using modified FALSTAFF load histories.

To serve as a baseline for the modified spectra, the first of the four specimens was tested using the standard FALSTAFF spectrum. Results of surface crack length (a) versus passes through the spectrum are shown in Figure 41, along with a 10X photograph of the fracture face. (Note: The quality of this and all other photos of fracture faces suffers with each reproduction.) A through-thickness fatigue crack initiated during the first spectrum pass and propagated until complete fracture at 13.9 passes. As can be viewed from the photograph of the fracture face, marker bands produced by the two, highest

TABLE 18
FALSTAFF LOAD HISTOGRAM
(As Supplied by the Netherlands)

Falstaff Level	Peaks at Level	Troughs at Level	Peaks at or Above Level (in column 1)	Troughs at or Below Level (in column 1)
32	2	0	2	17983
31	0	0	2	↑
30	7	0	9	↓
29	10	0	19	
28	24	0	43	
27	45	0	88	
26	76	0	164	
25	104	1	268	17983
24	193	2	461	17982
23	233	3	694	17980
22	404	4	1098	17977
21	533	12	1631	17973
20	640	23	2271	17961
19	954	37	3225	17938
18	987	69	4212	17901
17	1151	135	5363	17832
16	1282	234	6645	17697
15	1999	327	8644	17463
14	4145	511	12789	17136
13	4058	716	16847	16625
12	493	1445	17340	15909
11	43	4387	17383	14464
10	0	6711	17383	10077
9	0	1941	17383	3366
8	445	543	17828	1425
7	155	36	17983	882
6	0	508	↑	846
5	0	327	↓	338
4	0	6		11
3	0	1		5
2	0	2		4
1	0	2	17983	2

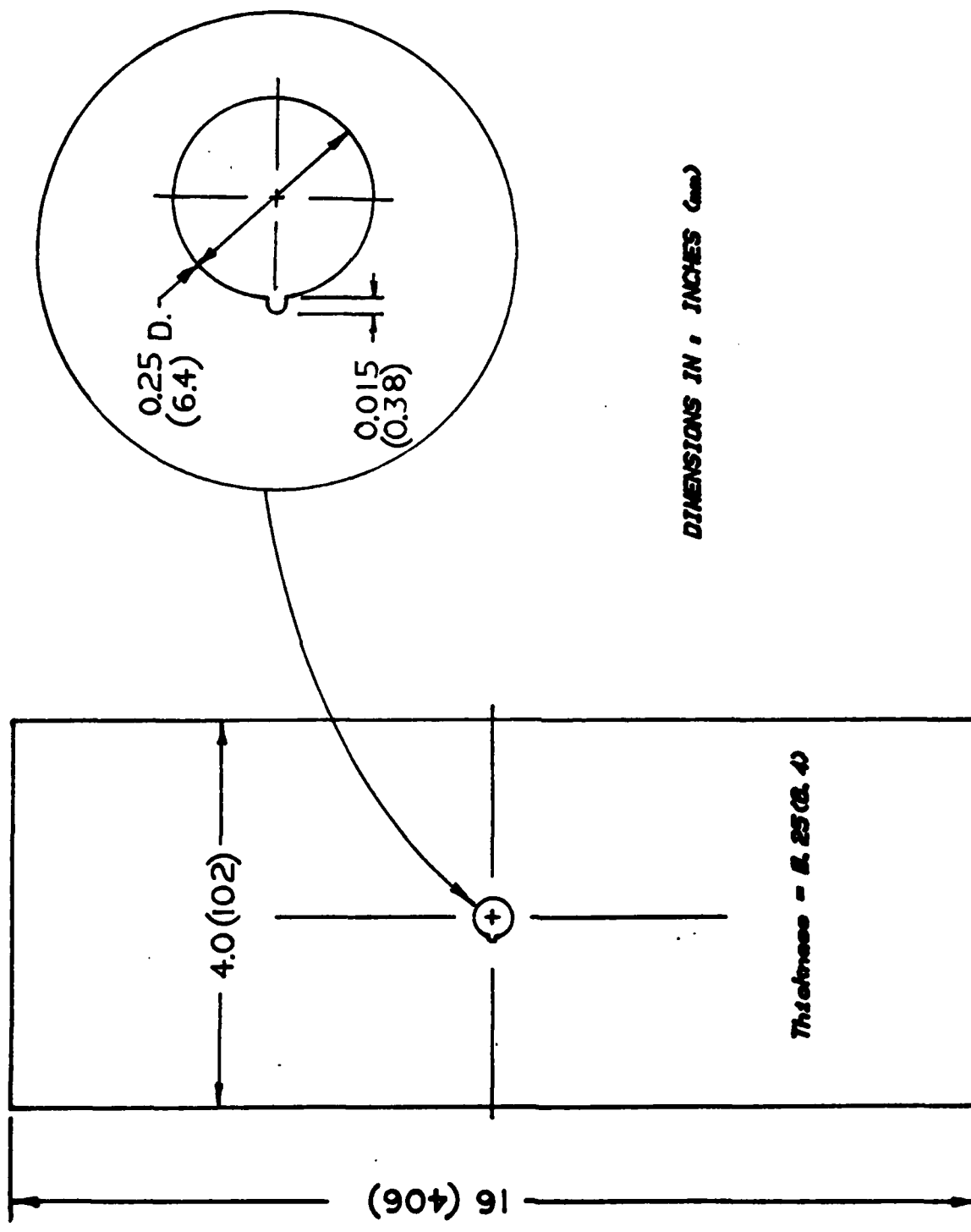
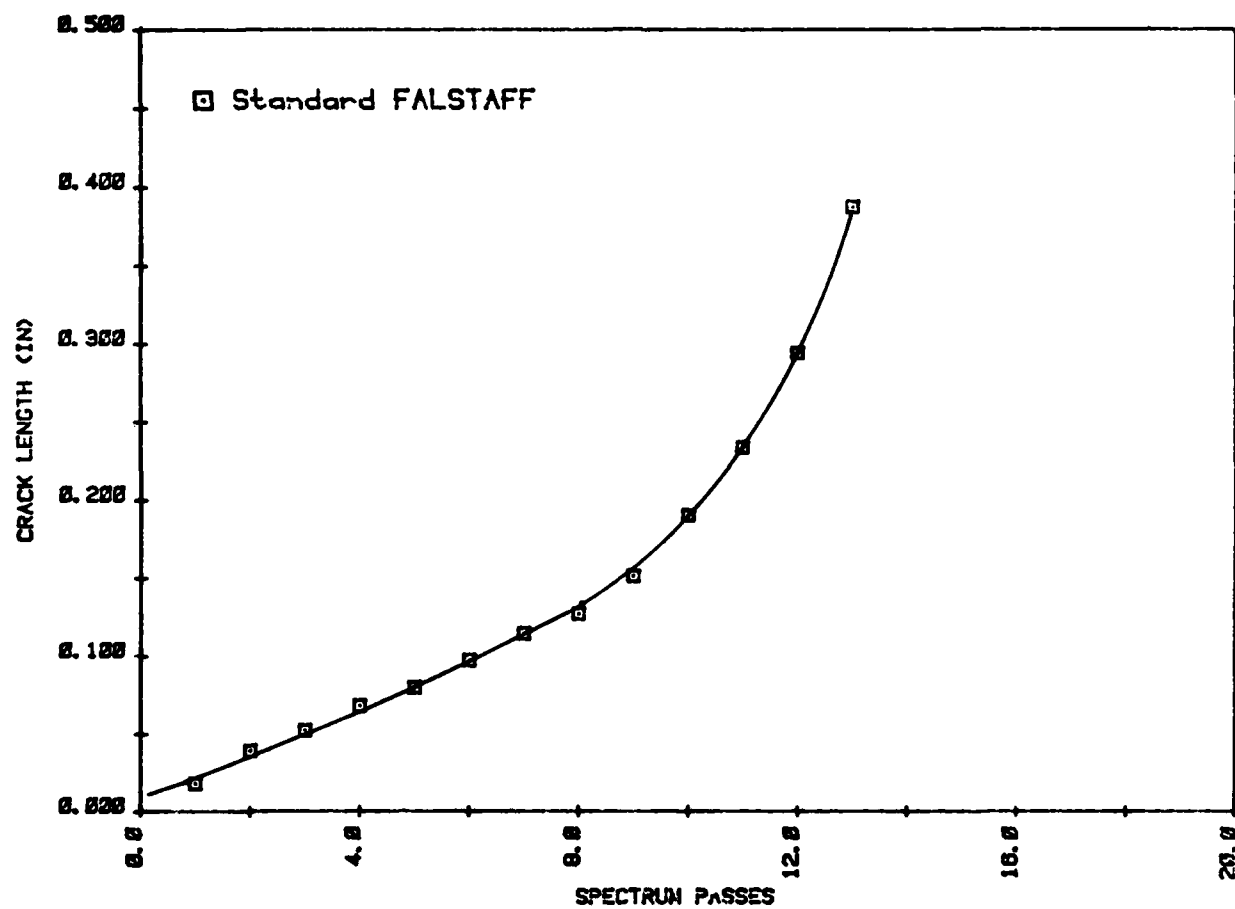


Figure 40. Center-Cracked-Panel Specimen Geometry.



Standard FALSTAFF (SPEC. #1), 10X

Figure 41. Fatigue Crack Growth Data for Standard FALSTAFF.

load levels (level 32) are indistinguishable for the first 0.10 inch (2.54 mm) of crack growth, and only poorly visible beyond 0.10 inch (2.54 mm). At a surface crack length of about 0.1 inch (2.5 mm) the distance between two markings (two load levels 32 per spectrum pass) is approximately 0.02 inch (0.51 mm). The raw test record (a vs. N data) also indicated a surface crack extension of approximately 0.02 inch at the same surface location. Similarly, at a surface location of 0.20 inch (5.1 mm) the spacing between two markings is about 0.060 inch (1.52 mm) and is again in agreement with the crack length measurements.

Thus, when the markings, or more properly described "stretch zones" are visible, they can accurately be used to determine crack extension per spectrum pass. The lack of clear markings in the earlier stages of crack propagation is believed due to the numerous compressive load cycles occurring throughout the spectrum which tend to crush or obliterate fracture face topography. At the higher maximum stress intensities, the markings produced by load level 32 become more pronounced and are not destroyed by the compressive loads.

In an attempt to preserve the markings produced by the high loads, all spectrum loads below level 8 were clipped*, exception being the taxi-load sequences. For the two configurations of taxi-load sequences, the following changes were made:

	<u>Before Take-Off</u>				<u>After Landing</u>		
Configuration #1, from	8	6	8	6	6	8	6
to	8	8	8	6	6	8	8
and							
Configuration #2, from	8	5	7	5	6	8	6
to	8	5	8	8	8	8	8

* Clipping -- Changing all load levels, above or below some defined level to equal that defined level, thus retaining the same number of cycles.

In changing these taxi-loads, the single, greatest compressive load was retained for configuration #1 take-off and landing, and for configuration #2 take-off. All compressive load levels for configuration #2 landing were clipped to level 8.

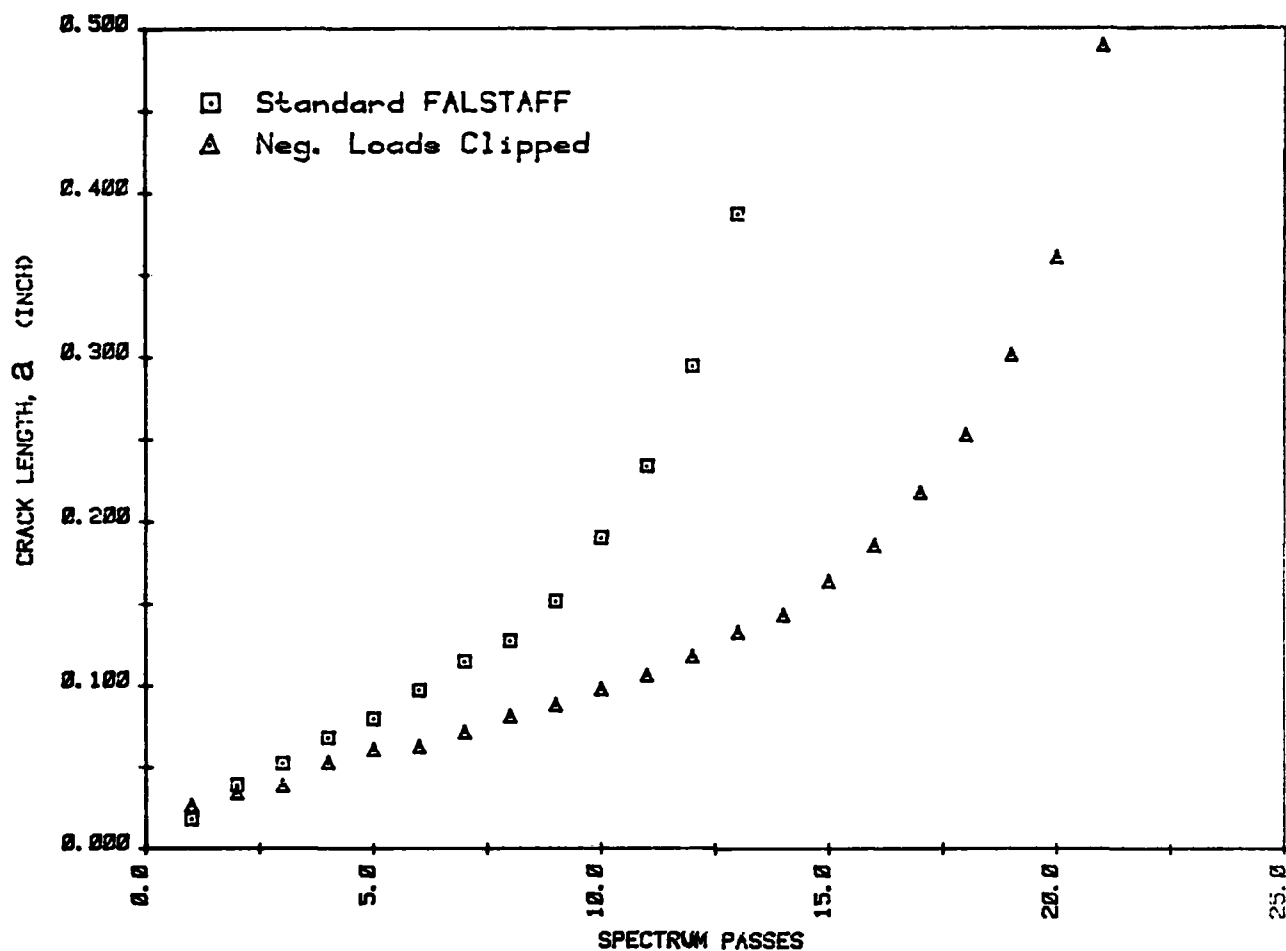
The results for a single specimen (Specimen #2) subjected to this modified spectrum are illustrated in Figure 42. By retaining only a few, small, compressive load cycles, the fatigue life was nearly doubled to 21.6 passes. Again crack initiation occurred during the first pass.

The fracture face of this specimen was similar to the previous specimen: distinguishable markings appeared only at crack lengths greater than about 0.1 inch (2.5 mm). In this region of higher stress intensities, the spacing between two markings coincided with the visual traces of crack length taken during test.

In further attempt to produce visual markings throughout the entire range of crack propagation, the maximum load for the standard spectrum (level 32) was changed to a load level 34, leaving all other load levels the same as were used in the standard FALSTAFF test. Also, in an effort to avoid the fracture faces crushing or smearing during compressive load cycles, a "neat-fit" steel pin was inserted in the starter hole. It was anticipated that this pin would prevent the fracture faces near the hole from coming in contact with each other during the compressive load cycles.

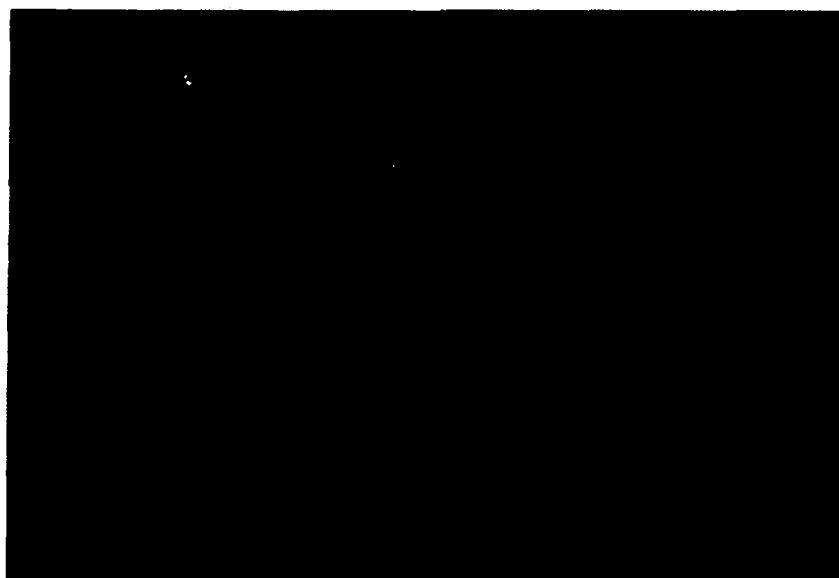
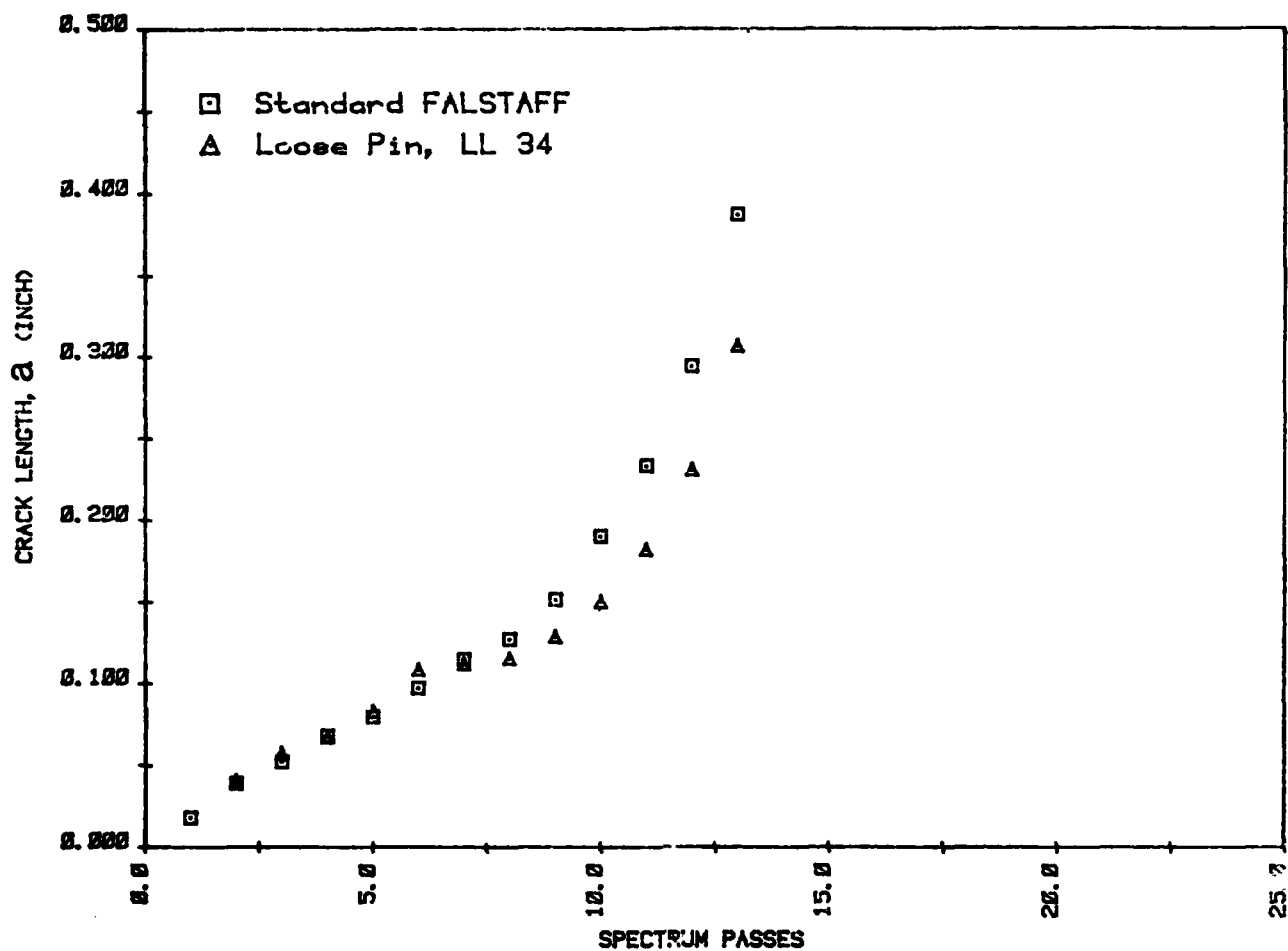
Results of a single specimen (Specimen #3) subjected to this spectrum are presented in Figure 43. Fatigue crack growth characteristics for this test specimen were similar to the standard FALSTAFF specimen, with both specimens failing after approximately 14 spectrum passes.

Fracture face examination revealed barely visible markings at crack lengths greater than 0.050 inch (1.27 mm), a slight improvement over the previous test specimens. Spacing between



Negative Loads Clipped (SPEC. #2), 10X

Figure 42. Fatigue Crack Growth Data for FALSTAFF with Negative Loads Clipped.



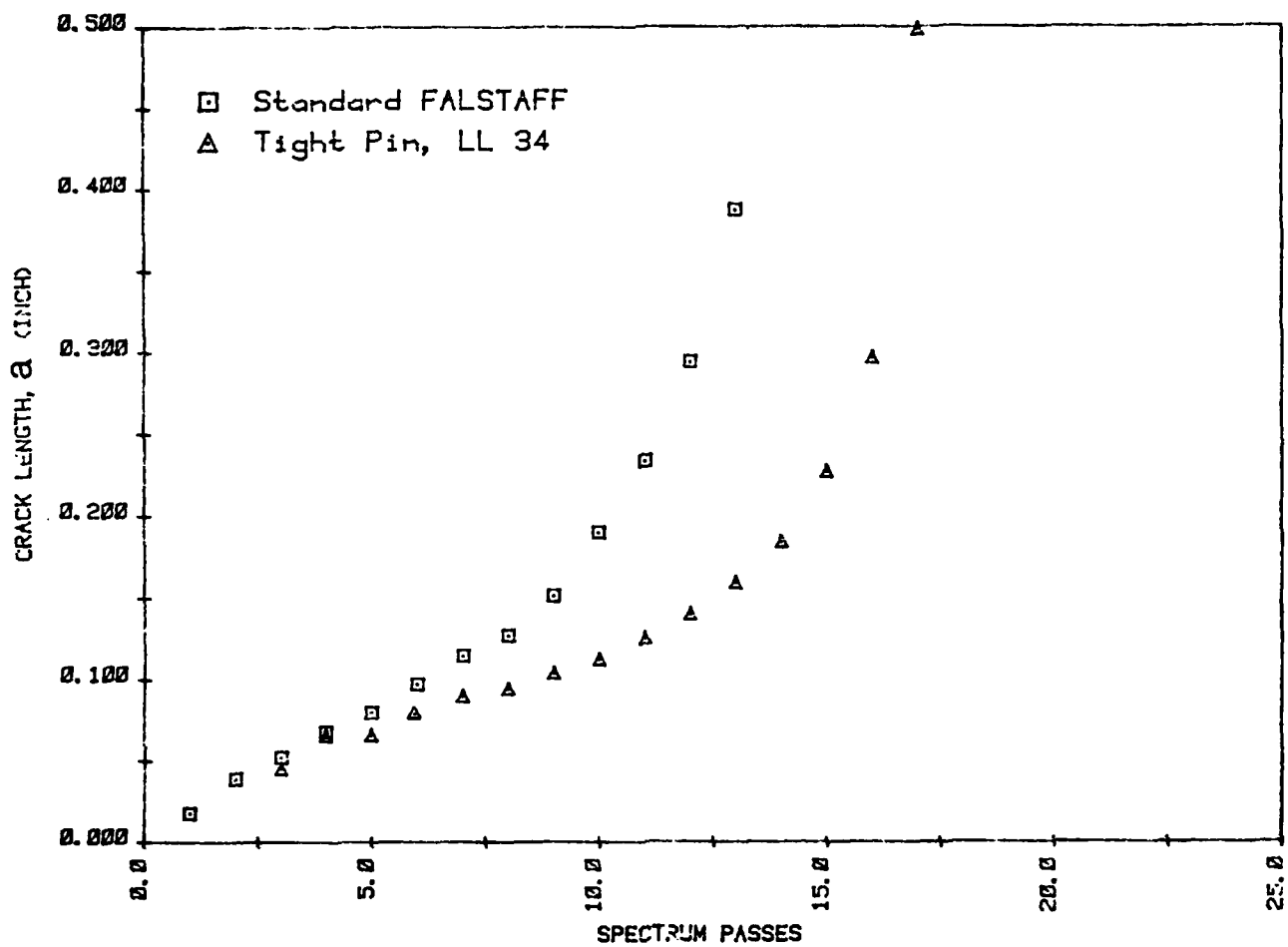
Loose Pin, LL 34 (SPEC. #3), 10X

Figure 43. Fatigue Crack Growth Data for FALSTAFF with Loose Pin at Load Level 34.

two successive markings, when distinguishable, are also in reasonable agreement with surface length measurements taken during test.

Reasons why this combination of spectrum/specimen design did not reveal markings at the shorter crack lengths are two-fold. First, though it was desired to have a neat-fit, zero clearance fastener, a 0.002 inch (0.051 mm) clearance existed, allowing the pin to move freely in the hole during spectrum loading. Consequently, it is believed that the fastener failed to keep the fracture faces apart for the majority of compressive load cycles. Secondly, for the first 48 flights of the fifth spectrum pass [$a \approx 0.05$ inch (1.27 mm)] the pin was erroneously removed, thereby further allowing the fracture faces to come in contact with each other and possibly obliterating any visual markings which might have been present.

For the fourth and final specimen (Specimen #4), the same spectrum modification just described was investigated, this time using a tapered steel pin inserted in the fastener hole rather than the loose fitting pin, thus resulting in a zero clearance fit. Results are illustrated in Figure 44. Unlike the loose-pin specimen, this combination of tight pin and increased load level lead to an increase in fatigue life of approximately 25 percent. Undoubtedly the addition of the tight pin was similar to the clipping of the negative load level; in both situations the detrimental effect of the compressive loads in the crack tip region is removed or lessened and crack propagation rates thus reduced. The effect of the tight pin on the fatigue fracture face was more positive: markings produced by the two high loads (level 34) are visible for the entire range of crack propagation. As with the other specimens' fracture faces, distances between two successive markings are in good agreement with crack extensions per pass based on surface trace measurements.



Tight Pin, LL 34 (SPEC. #4), 10X

Figure 44. Fatigue Crack Growth Data for FALSTAFF With Tight Pin and Load Level 34.

1.11 NAVY ROUND ROBIN CORROSION FATIGUE CRACK GROWTH RATE TEST RESULTS FOR HY-80

To aid in the development of a corrosion fatigue crack growth test standard, the Design Data Group of AFWAL entered into a round-robin test program sponsored by the Navy. Wedge-opening-loaded (WOL) type specimens machined from HY-80 steel were furnished along with necessary data sheets and a draft of the proposed standard to serve as test guidelines. Requested was crack growth rate data in a 3.5 percent NaCl solution, for a stress intensity range from 25 to 80 KSI $\sqrt{\text{in}}$ (27 to 88 MPa $\sqrt{\text{m}}$), at a test frequency of 0.5 Hz. Crack length measurements were to be based on compliance relationships as dictated by the test sponsor, along with any additional methods each participating lab might choose to employ.

Two wedge-open-loaded samples (#X1-41 and #X1-5), machined from HY-80 steel, Lukens Melt No. 09562, were machined to the configuration shown in Figure 45. Location of knife edges, left up to the individual participants, was chosen at a distance of 0.190 inch (4.83 mm) ahead of the front face since an accurate compliance calibration exists for this point.[14]

All testing was performed on a 22 KIP (98 kN) MTS load-frame, equipped with a unique horizontal stressing frame,[15] shown in Figure 46, to achieve the desired horizontal loading conditions. This particular loading frame is essentially a system of lever arms and a tapered element through which a vertical tensile force on the tapered element produces a horizontal tensile load at the specimen. All movement in this frame is effected through roller bearings. A 2.5 KIP (11 kN) fatigue-rated load cell was used, which was calibrated to give a load range of 1000 lbf. (4.45 kN) for 10 VDC full scale. Since the horizontal load frame has a mechanical advantage of 6.52306:1, the actual load range, as applied to test sample, is 6523 lbf (29.0 kN) per 10 VDC full scale. This mechanical advantage is independent of tapered element location in the range used in the tests reported herein.

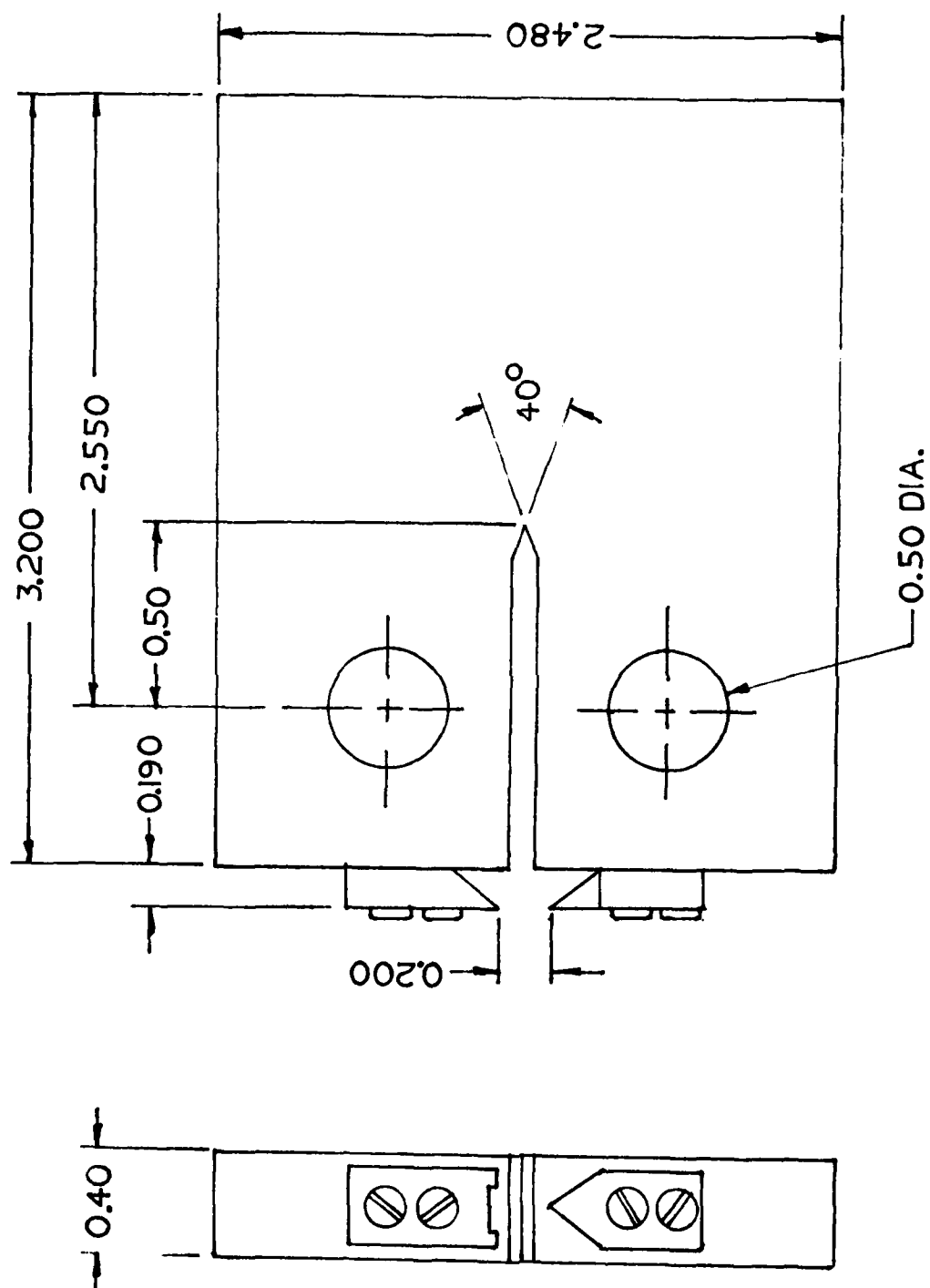


Figure 45. WOL Specimen Geometry.



Figure 46. Horizontal Stressing Frame Installed in Vertical Loading Fatigue Machine.

Crack length measurements were obtained in three manners: First, as requested in the test instructions, load-displacement traces were graphically obtained with an X-Y recorder at intervals established by a specific change in crack-opening-displacement (COD). For slow crack growth, i.e., at ΔK ranges of 20 to 40 KSI $\sqrt{\text{in}}$ (22 to 44 MPa $\sqrt{\text{m}}$), typical intervals were 0.0005 inch (0.0127 mm) change in maximum COD, while at the higher growth rates the interval was 0.001 inch (0.025 mm). From these traces, two load-displacement points per curve were chosen to establish the slope, or compliance: one at one-half maximum load, the other at the maximum load. Each compliance value graphically obtained was then inserted in the following equation to obtain crack length:

$$\begin{aligned} a/W = 1.0020 - 5.1122u + 39.431u^2 - 751.19u^3 \\ + 4928.6u^4 - 10465u^5 \end{aligned} \quad (18)$$

where:

$$u = \frac{1}{(\sqrt{BEC} + 1)}$$

and a = crack length,
 W = specimen width,
 B = specimen thickness,
 E = effective modulus, and
 C = specimen compliance.

A second method chosen to monitor crack length was with a fatigue crack growth rate data acquisition system,[16] developed by UDRI. This system also relies on compliance relationships to obtain crack length. Briefly, the system monitors the COD signal for significant changes in maximum COD. Upon a significant change, the computer then digitizes five sequential load-displacement waveforms and calculates five corresponding compliance values via a best-fit, least-squares analysis through the upper 60 percent of each waveform (load-increasing portion). The highest and lowest values are disregarded and the remaining

three are averaged to obtain an average compliance. This average compliance value is then inserted in equation 18 to yield crack length and corresponding da/dN and ΔK values while the test is in progress.

Finally, the fatigue crack was periodically being visually monitored, using a 30X traveling microscope with digital readout. These values of crack length were to serve as reference points for comparison with the other two methods.

The results of crack growth tests conducted on the two furnished specimens, #X1-41 and #X1-5, are best presented in the plots of crack length versus cycles illustrated in Figures 47 and 48, respectively. Shown in each figure are the crack length measurements obtained with each of the three methods: graphical (as suggested by the test coordinators), acquisition system, and visual monitoring. For specimen #X1-41, crack lengths range from approximately 0.82 inch (21 mm) to 1.70 inch (43 mm) for a maximum load of 2400 lbf (10.7 kN). Corresponding stress intensity range values are 24 KSI/\sqrt{in} (26.4 MPa/\sqrt{m}) at the beginning of test to about 62 KSI/\sqrt{in} (68 MPa/\sqrt{m}) at conclusion. For the second specimen, #X1-5, crack lengths range from 0.86 inch (21.8 mm) to 1.52 inch (38.6 mm) at a maximum load of 4050 lbf (18.0 kN), representing stress intensity ranges from 43 to 80 KSI/\sqrt{in} (47 to 88 MPa/\sqrt{m}).

For each test conducted, there is good agreement between each of the crack length measuring methods employed. Though occasional, noticeable deviations do occur, no one method displayed any clear bias or consistent differences over the others for the entire range of crack lengths. The scatter between readings for specimen #X1-5 is slightly lower than for #X1-41, possibly a result of the higher test load and thus higher signal/noise ratio.

Analyzing first the graphically reduced data, since it was suggested as the primary method to be employed, the fatigue crack growth rate data were obtained for both specimens and is presented in Figure 49. The seven-point incremental polynomial

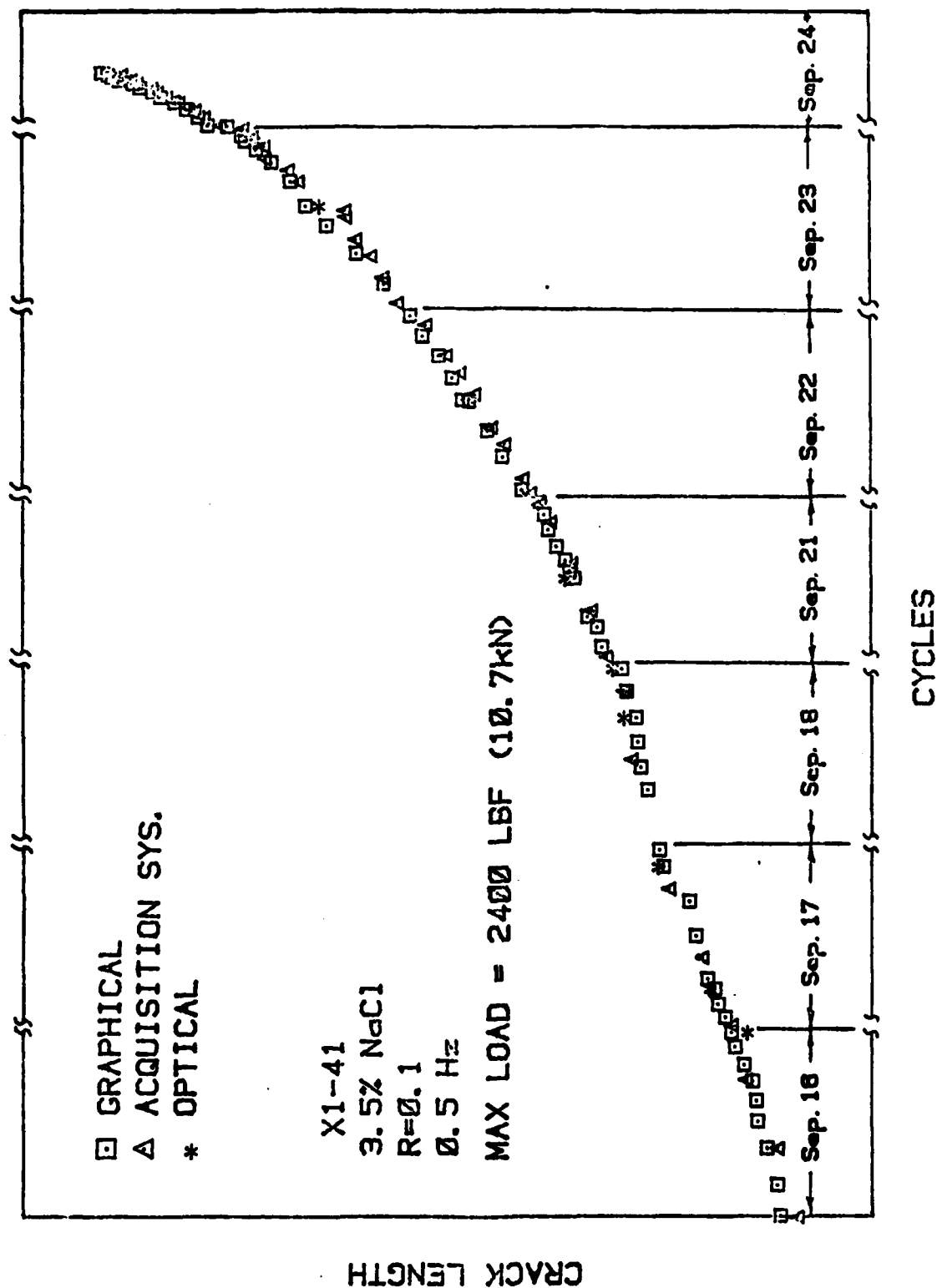


Figure 47. Crack Length vs. Cycles Record for Specimen X1-41.

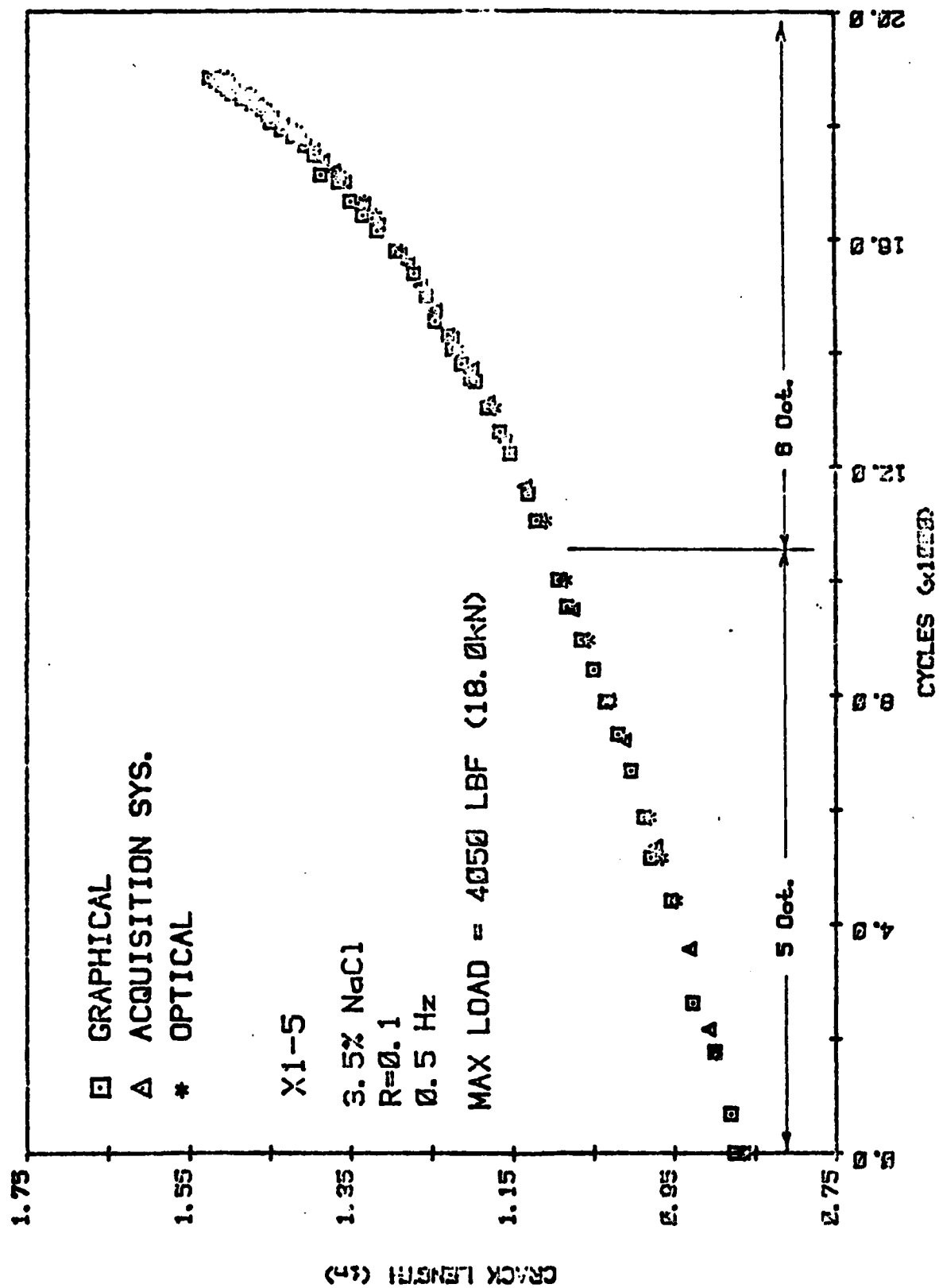
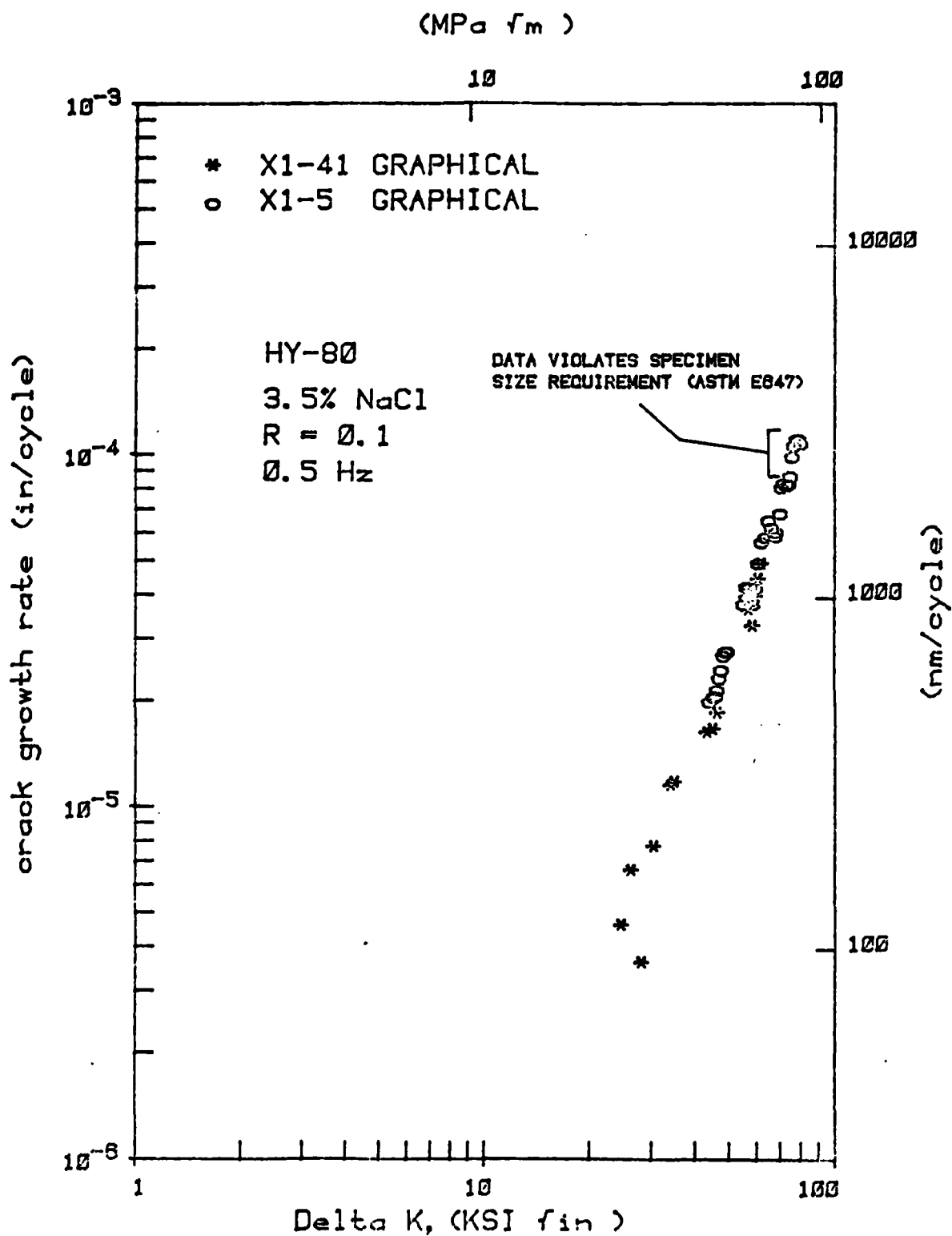


Figure 48. Crack Length vs. Cycles Record for Specimen X1-5.



method described in ASTM E647 was used, treating each day's data as a separate set (when less than seven points were available, a best-fit, straight line was fitted rather than the polynomial). The overlapping data bands indicate the good agreement in corrosion fatigue crack growth response for the two specimens.

The graphically reduced crack growth rate data are also presented in Figure 50 along with the crack growth rate data obtained from optical measurements and data obtained via the crack growth rate data acquisition system. Data derived from the three unique methods indicate excellent agreement throughout the entire range investigated. Data points for each method above 10^{-5} inch/cycle (254 nm/cycle) are virtually indistinguishable.

1.12 EVALUATION OF AEDC C-1 STAGE MATERIAL AND ADHESIVE SYSTEMS

A series of evaluation programs have for some time been conducted on materials proposed for application on the supersonic wind tunnel at the Arnold Engineering and Development Center, Tennessee. The first four compressor stages have all seen composite materials replace former metallic counterparts. Because a new manufacturer has been contracted to make replacement compressor blades for the first (C-1) stage, the Materials Laboratory has been asked to evaluate the new company's fabrication techniques to produce E293/E-glass composite, the material of which the blades are made. Three panels of E293/E-glass composite were delivered for tensile, flexural, and interlaminar shear strength evaluation.

In addition to determining these basic mechanical properties to the composite material, additional panels of E293/E-glass, bonded to such materials as viton, steel, aluminum honeycomb, and even similar E293 composite material, were also delivered for determination of the adhesive shear strength of each bonded joint. The purpose for the latter series of tests is to evaluate the adhesive bonding techniques and capabilities required of the new manufacturer for the compressor reblade effort.

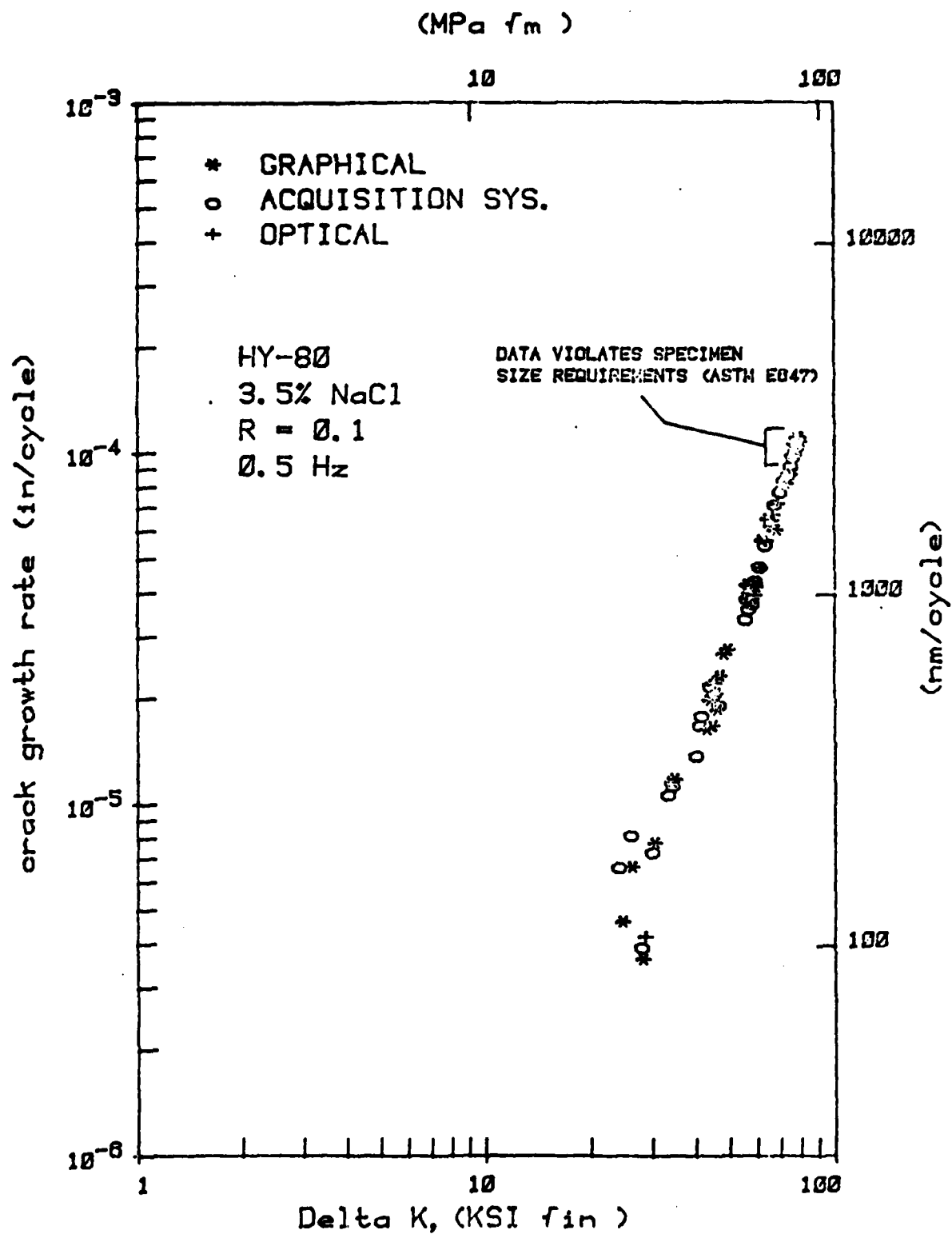


Figure 50. Fatigue Crack Growth Rate Results Based on Graphical, Acquisition System, and Optical Methods.

The following results were obtained on E293/E-glass test panels as fabricated by the Homestead Tool and Machine Inc.

TABLE 19
AVERAGE TENSILE TEST RESULTS FOR
E293/E-GLASS MATERIAL

Dogbone Specimen Geometry					
Panel I.D.	Test Temperature °F (°C)		Ultimate Strength KSI (MPa)		Primary Modulus MSI (GPa)
006	72	(22)	44.8	(309)	3.72 (25.7)
006	280	(138)	33.1	(228)	2.93 (20.2)
007	72	(22)	44.8	(309)	3.72 (25.7)
007	280	(138)	32.0	(220)	2.81 (19.4)
008	72	(22)	45.6 ¹	(314)	3.56 ¹ (24.5)
008	280	(138)	31.9	(220)	2.64 ² (18.2)
Straight-Sided Geometry					
006	72	(22)	46.8	(323)	3.23 (22.3)
006	280	(138)	36.4	(251)	2.85 (19.7)
007	72	(22)	45.9 ²	(316)	3.80 ² (26.2)
007	280	(138)	32.3	(223)	2.71 (18.7)
008	72	(22)	45.1	(311)	3.50 (24.1)
008	280	(138)	30.8	(212)	2.86 (19.7)

NOTES: ¹Average of six tests.

²Average of four tests.

All other results are an average of five tests.

The average tensile properties of each of the panels for two test geometries are presented in Table 19. Listed are average values at room temperature and 280°F (138°C). Results based on both test specimen geometries indicate all panels are nearly identical with regard to tensile strength. The average room temperature tensile strength of this material is about 45 KSI (310 MPa), while the 280°F (138°C) environment caused a loss in ultimate strength of about 30 percent. Primary modulus values were similarly affected by the elevated test temperature.

The effect of specimen geometry is nil, with only slightly higher ultimate tensile strength properties observed for panels #006 and #007. For the dogbone-shaped specimen, all failures occurred where the radius of the grip end blended into the test section. With the straight-sided or uniform test section specimen, all failure occurred very near the edge of the adhesively bonded tab. The different test temperatures had no effect on these failure modes.

The average three-point flexural strength and flexural modulus values for each panel are presented in Table 20. Results indicate all panels are similar with respect to flexural properties. The average room temperature flexural strengths of each panel are nearly identical. For each panel, the effect of the 280°F (138°C) temperature was a reduction in flexural strength of roughly 50 percent of room temperature values. While all the room temperature tests yielded flexural failures, the elevated temperature test specimens all failed as a result of compression in the top plies (beneath the central load point). Some of these specimens also displayed a flex failure mode in conjunction with compression, but it was not apparent which failure occurred first.

The average short-beam-shear (interlaminar) test results for each test panel are furnished in Table 21. Because early test results for panel #006 using a span-to-depth ratio of 5:1 lead to several flexural failures, the ratio was changed to 4:1. The average strength values listed in the table represent only specimens which failed as a result of interlaminar shear.

Results obtained indicate panel #006 possesses slightly higher interlaminar shear strength properties than the other two panels, with panel #007 slightly inferior to panel #008. The test temperature of 280°F (138 °C) reduced the average shear strength of each panel to roughly a third of the room temperature values.

TABLE 20
AVERAGE FLEXURAL TEST RESULTS
FOR E293/E-GLASS MATERIAL

Panel I.D.	Test Temperature °F (°C)		Flexural Str. KSI (MPa)		Flexural Mod. MSI (GPa)	
006	74	(23)	67.3	(464)	2.04	(14.1)
006	280	(138)	38.2	(264)	1.72	(11.9)
007	74	(23)	67.6	(466)	2.13	(14.7)
007	280	(138)	31.0*	(214)	1.75*	(12.1)
008	74	(23)	67.5	(465)	2.28	(15.7)
008	280	(138)	32.3	(223)	1.81	(12.5)

*Average of four tests. All other values are average of five tests.

TABLE 21
AVERAGE INTERLAMINAR SHEAR TEST
RESULTS FOR E293/E-GLASS

Panel I.D.	Test Temperature °F (°C)		Shear Strength KSI (MPa)	
006	74	(23)	82.1 ¹	(56.6)
006	280	(138)	2.89	(19.9)
007	74	(23)	7.64 ²	(52.7)
007	280	(138)	2.15	(14.8)
008	74	(23)	7.99 ³	(55.1)
008	280	(138)	2.20	(15.2)

¹Average of six tests.

²Average of nine tests.

³Average of eight tests.

All other values reflect average of ten tests.

The average results of steel-to-composite single-lap-shear tests are presented in Table 22. Also furnished is the primary failure mode or location, i.e., either the adhesive joint or the composite material being bonded. These limited results indicate panel #B206 (adhesive AF143) possessed the greatest shear strength at room temperature. The lap-joint specimens with no adhesive (#B208) yielded the lowest shear strength values of all adhesive systems, exception being panel #B205 (adhesive HT424) at 280°F (138°C), where the elevated temperature caused a drastic drop in shear strength. Results for the different surface preparations with FM96 adhesive indicate the acid etch had a positive effect for room temperature applications.

TABLE 22
AVERAGE SINGLE-LAP-SHEAR RESULTS
OF STEEL-COMPOSITE SPECIMENS

Panel I.D.	Adhesive System	Test Temperature °F (°C)	Shear Strength psi (MPa)	Predominate Failure Mode ¹
B201	FM96/acid etch, no prime	72 (22)	1647 (11.3)	A
B201	FM96/acid etch, no prime	280 (138)	1295 (8.9)	C
B202	FM96/no etch, no prime	72 (22)	1376 (9.5)	A
B202	FM96/no etch, no prime	280 (138)	1461 (10.1)	C
B203	FM96/acid etch, spray prime	72 (22)	1536 (10.6)	A
B203	FM96/acid etch, spray prime	280 (138)	1280 (8.8)	C
B204	FM96/no etch, spray prime	72 (22)	1236 (8.5)	A
B204	FM96/no etch, spray prime	280 (138)	1539 (10.6)	A
B205	HT424/acid etch, spray prime	72 (22)	1644 (11.3)	A
B205	HT424/acid etch, spray prime	280 (138)	484 (3.3)	ASC ²
B206	AF143/acid etch, spray prime	72 (22)	1732 (11.9)	A
B206	AF143/acid etch, spray prime	280 (138)	1646 (11.3)	C
B207	FM96U/no etch, dip prime	72 (22)	1572 (10.8)	A
B207	FM96U/no etch, dip prime	280 (138)	1388 (9.6)	A
B208	no adhesive/acid etch,	72 (22)	1036 (7.1)	N.A.
B208	spray prime	280 (138)	638 ³ (4.4)	N.A.

NOTES: ¹A=failure of adhesive bond; C=failure of composite material.

²One specimen adhesive failure, one composite failure.

³Results of a single test.

All other results are average of two tests.

It is difficult to draw comparisons for the results at 280°F (138°C), since over half of the panels/adhesive systems yielded interlaminar shear failures in the composite material and not at the adhesive interface. For these results, the adhesive shear strength must obviously be considered in excess of those stresses experienced at failure. One result worth noting is that with the exception of panel #B205 (HT424), the elevated temperature did not significantly reduce the shear strength of any of the adhesives.

The results of single-lap-shear testing on composite-composite specimens are presented in Table 23. As noted in the table, samples from panels #B102 and #B104 were machined with one-half of the lap-shear specimen shorter than the other half: 4 inches (102 mm) as compared to 5.5 inches (140 mm). Since the specimens still maintained the same bond length and width as all other specimens, it was assumed the shorter length of these specimens would have no effect on the adhesive shear strength.

The results shown in Table 23 indicate panel #B101 (FM96) possesses the highest average shear strength at room temperature, with panel #104 (HT424) the lowest. All room temperature tests yielded failures in the adhesive joint. At the elevated temperature, the average shear strength of panels B101, B102, and B103 were roughly two-thirds of the room temperature values, while panel B104 (HT424 adhesive) displayed a loss in shear strength of over 50 percent. This drastic loss in shear strength for HT424 at 280°F (138°C) was similarly witnessed with the steel-composite results.

The results of foam adhesive lap-shear tests are presented in Table 24. For both the 3M and the Hysol 3050 adhesives the room temperature shear strength was in excess of 400 psi (2.76 MPa). Both HT424 adhesive panels show no loss in strength as a result of the higher test temperature, a seemingly contradictory result when viewing the previous thin film adhesive results. Finally,

TABLE 23
AVERAGE SINGLE-LAP-SHEAR RESULTS FOR
COMPOSITE-COMPOSITE SPECIMENS

Panel I.D.	Adhesive System	Test Temperature °F (°C)		Shear Strength psi (MPa)	
B101	FM96	72	(22)	1608	(11.1)
		280	(138)	1115**	(7.7)
B102*	FM96U	72	(22)	1352	(9.3)
		280	(138)	830	(5.7)
B103	AF143	72	(22)	1535	(10.6)
		280	(138)	1145	(7.9)
B104*	HT424	72	(22)	1105	(7.6)
		280	(138)	478	(3.3)

*One-half of specimen machined shorter than other half.

**Failure occurred in composite, not adhesive.

Values reflect average of two tests.

TABLE 24
TEST RESULTS OF SINGLE-LAP-SHEAR
FOAM ADHESIVE SPECIMENS

Panel I.D.	Adhesive System	Test Temperature °F (°C)		Avg. Shear Strength psi (MPa)	
B301	3M 3050	72	(22)	420	(2.90)
		280	(138)	382	(2.63)
B302	FM 41	72	(22)	312	(2.15)
		280	(138)	172	(1.19)
B303	HT424	72	(22)	223	(1.54)
		280	(138)	201	(1.38)
B304	Hysol 3050	72	(22)	470	(3.24)
		280	(138)	306	(2.11)
B305	HT424	72	(22)	215	(1.48)
		280	(138)	229	(1.58)

Values reflect average of two tests.

all failures were cohesive type failures, i.e., the foam adhesive itself failed, rather than an adhesive type failure where the adhesive failed to bond to the material.

Table 25 presents the three-point flexural results for composite-aluminum honeycomb sandwich panels approximately 1 inch (25 mm) thick. It is difficult to draw comparisons for each adhesive system due to the different failure modes experienced. At room temperature, panels #1F, #2F, and #5F experienced a core shear type failure, while at 280°F (138°C), only panel #5F failed in this manner. Tests on both panels #3F and #4F at each temperature yielded an interlaminar shear failure of the composite facing material on the compression side, as shown in Figure 51. Panel #6F failed via compression of the facing panel for both temperatures.

Some results which were notable are that at room temperature panel #2F (3M 3015 adhesive) suffered a core shear failure well below shear stresses withstood by the other five adhesives. At room temperature, panel #6F (FM 96U adhesive) withstood a higher core shear stress than did panels #2F (3M 3015 adhesives) and #5F (Hysol 3050) and may be nearly equal to or superior to panel #1F (FM-41 adhesive). For panel #5F, the 280°F (138°C) test temperature reduced the shear strength of the Hysol 3050 adhesive only slightly, while panel #2F (3M 3015 adhesive) displayed no loss in adhesive shear strength at 280°F (138°C).

Possibly as a result of the smaller, non-standard-sized test specimen, no failures were experienced at any of the adhesive bonded interfaces (i.e., between the facing and core materials). Nearly all failures at both temperatures were a result of crushing the face material at the gripped ends, as shown in Figure 52. However, the maximum loads and associated compressive facing stresses developed for each panel are presented in Table 26. Essentially, the tests amounted to compression testing of the E293 material, with the aluminum honeycomb acting merely as a buckling restraint.

TABLE 25
FLEXURAL TEST RESULTS FOR E293-ALUMINUM
HONEYCOMB SANDWICH PANELS

Panel I.D.	Adhesive System	Test Temperature °F (°C)	Maximum Core Stress psi (Mpa)	Flexural Modulus MSI (GPa)	Failure Mode
1F	FM 41	70 (21)	597 (4.12)	1.32 (9.03)	Core Shear
1F	FM 41	280 (138)	342 (2.36)	0.95 (6.6)	Compression
2F	3M 3015	70 (21)	330 (2.28)	1.35 (9.31)	Core Shear
2F	3M 3015	280 (138)	341 (2.32)	0.97 (6.7)	Compression
3F	HT424, 2 layers	70 (21)	495 (3.41)	1.37 (9.45)	Composite Shear
3F	HT424, 2 layers	280 (138)	78 (0.53)	0.96 (6.6)	Composite Shear*
4F	HT424, 1 layer	70 (21)	439 (3.03)	1.40 (9.65)	Composite Shear
4F	HT424, 1 layer	280 (138)	94 (0.64)	0.89 (6.1)	Composite Shear*
5F	Hysol 3050	70 (21)	465 (3.21)	1.40 (9.65)	Core Shear
5F	Hysol 3050	280 (138)	397 (2.76)	0.95 (6.6)	Core Shear*
6F	FM 96U	70 (21)	556 (3.83)	1.37 (9.45)	Compression
6F	FM 96U	280 (138)	354 (2.44)	1.00 (6.9)	Compression*

*1/8 inch (3.2 mm) x 1 inch (25 mm) aluminum pad under central load point.

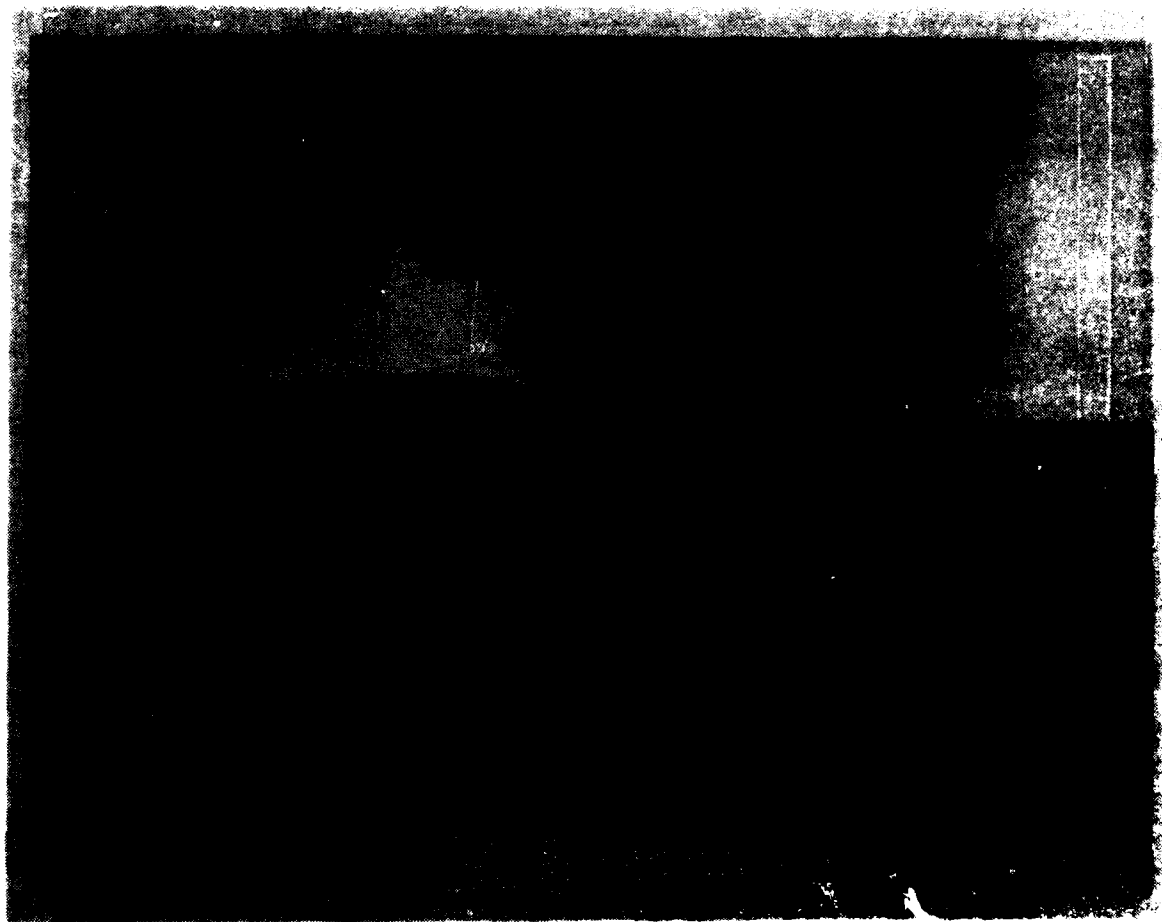


Figure 51. Interlaminar Type Failure Experienced During Flexural Testing for Panels #3F and #4F.



Figure 52. Typical Failure Mode for Edgewise Compression Testing.

TABLE 26
EDGEWISE COMPRESSION RESULTS FOR E293-ALUMINUM
HONEYCOMB SANDWICH PANELS

Panel I.D.	Adhesive System	Test		Maximum Load*		Maximum Compressive Stress		Compressive Modulus NSI (GPa)
		°F	(°C)	KIP	(kN)	KSI	(MPa)	
1C	FM 41	72	(22)	15.1	(67.2)	39.5	(272)	4.5 (31.0)
1C	FM 41	280	(138)	7.1	(31.6)	19.5	(134)	3.2 (22.1)
2C	3M 3015	72	(22)	16.0	(71.2)	41.2	(284)	4.2 (29.0)
2C	3M 3015	280	(138)	5.3	(23.6)	14.9	(103)	3.1 (21.4)
3C	HT424, 2 layers	72	(22)	13.9	(61.8)	35.3	(243)	3.9 (26.9)
3C	HT424, 2 layers	280	(138)	3.6	(16.0)	9.9	(68)	2.8 (19.3)
4C	HT424, 1 layer	72	(22)	12.6	(56.0)	32.4	(223)	3.9 (26.9)
4C	HT424, 1 layer	280	(138)	2.8	(12.4)	7.5	(52)	2.6 (17.9)
5C	Hycol 3050	72	(22)	13.9	(61.8)	36.0	(248)	4.1 (28.3)
5C	Hycol 3050	280	(138)	5.3	(25.8)	16.3	(112)	3.0 (20.7)
6C	FM 96U	72	(22)	15.6	(69.4)	40.8	(281)	4.0 (27.6)
6C	FM 96U	280	(138)	6.9	(30.7)	18.8	(130)	3.0 (20.7)

*At first implication of failure.

A result worth noting is the noticeably lower compression strength values obtained for panels #3C and #4C at 280°F (138°C). This same trend was observed for these two panels/adhesive systems under the three-point flex testing just described; both sandwich panels failed in the facing materials at loads considerably lower than those sustained by the other four sandwich panels.

Finally, for panels #4C at room temperature and #3C at 280°F (138°C), a shear failure between the facing and core was observed along with a crushing of the facing material. It was not possible to discern which occurred first.

After removing the 1-inch (25 mm) wide peel test specimens from each panel, it was discovered that a majority of specimens had deep cuts in the viton sheet, some nearly 90 percent through the thickness. This may have occurred during trimming of the adhesive interface by the manufacturer after bonding to yield the desired bond lengths. As a result, only a few specimens were successfully tested. Limited results obtained are presented in Table 27. All failures occurred in the viton sheet, some near the bonded joint, some near the gripped end. The 280°F (138°C) proved too severe a test temperature for the viton material, where failures occurred below the resolution of the test machine. The only conclusion available regarding these peel tests are that for the specimens furnished, the strengths of the FM 96U adhesive (panel #402) and the HT424 adhesive (panel #404) are superior to the material being bonded, consequently adhesive failure for either system is not a concern.

TABLE 27
INDIVIDUAL PEEL TEST RESULTS FOR
COMPOSITE-VITON PEEL SPECIMENS

Panel I.D.	Adhesive	Test Temperature		Maximum Load	
		°F	(°C)	KIP	(kN)
B402-2	FM 96U	70	(21)	16*	(71)
B402-3	FM 96U	280	(138)	<2**	(<9)
B402-4	FM 96U	280	(138)	<2**	(<9)
B404-2	HT424	70	(21)	23	(102)
B404-3	HT424	70	(21)	24	(107)
B404-4	HT424	70	(21)	22	(98)

*Slight tear in viton sheet prior to testing.

**Below resolution of test machine.

SECTION 2

ELECTRONIC FAILURE ANALYSIS

2.1 FAILURE ANALYSIS OF A LINEAR POSITION TRANSDUCER

A linear position transducer was submitted for testing and analysis. The transducer exhibited low resistance paths from pins A, B, and C to the metal housing which is normally at ground potential. This condition has caused the aircraft to steer erratically during taxi.

The linear position transducer has been previously identified as being "internally shorted". The insulation resistance tests performed by UDRI personnel upon receipt of the transducer indicated the resistance of pins A, B, and C to the metal housing were not shorted but were between 5 and 6 M Ω . The resistance of pin A to B was within its specified limits of 500 Ω \pm 5 percent and the sliding contact moved smoothly and continuously across the fixed resistive element. Upon heating the linear position transducer to approximately 90°F for 20 minutes and allowing it to return to room temperature, the insulation resistance increased by a factor of 100. These tests clearly indicate the transducer had internally trapped moisture.

The corrosion observed on the glass header was primarily crevice corrosion. Neither Auger or XES detected the presence of chlorides among the corrosion products. Several examples of flux-like residues were found on the instrument side of the glass header which probably made a significant contribution to the corrosion process. Recommendations made included a proper cleaning procedure, the correct soldering flux to be used, and a suitable potting compound.

2.2 FAILURE ANALYSIS OF AN EJECTION SEAT ARMING SWITCH

An ejection seat arming switch used in certain aircraft is mounted on the left side of the ejection seat. The only function

of the switch is to activate a light in the cockpit indicating when the ejection seat has been armed. Eight ejection seat arming switches have been submitted for testing due to numerous field failures causing aborted F-16 flights.

The failure analysis of switch samples 1, 3, 7, and 8 revealed two distinct failure patterns. One pattern of failure, seen in samples 1, 3, and 8, was of the diaphragm material at the weld sites inside the annular stiffener. It apparently occurred through a combination of fatigue followed by overload.

The second pattern, seen in sample 7, was the failure of the weld inside the annular stiffener which bonds the button to the diaphragm. This failure did not create a hole or a tear in the diaphragm. It is believed the failure was due to a poor weld in conjunction with the convex diaphragm surface inside the annular stiffener which would not allow the button to be seated squarely during the welding operation.

Sample 4, which was life tested by activating the switch assembly with a motor and cam was cycled in excess of 50,000 times. The switch did not fail either electrically or mechanically. Several significant factors may have influenced its longevity: the diaphragm-button-interface had a good weld, the area of the diaphragm inside the stiffener was not convex, and synergistic environmental effects may be of greater importance.

2.3 FAILURE ANALYSIS OF TWO STEERING CONTROL FEEDBACK POTENTIOMETERS

Two Material Deficiency Report/Teardown Requests were concerned with two nose gear steering control feedback potentiometers. The aircraft was involved in a landing accident as a result of the left main wheel brake being locked. The aircraft departed the runway at an angle resulting in loss of the nose landing gear and collapse of the right main landing gear.

The main nose gear steering control feedback potentiometer and the standby nose gear steering control feedback potentiometer from the affected aircraft were both submitted for investigation. It was requested that these items be examined to determine whether or not they may have contributed to the incident.

Careful visual and electrical inspection of the two submitted nose gear steering control feedback potentiometers was conducted. No evidence of a malfunction which could have contributed to the cause of the mishap was detected. The potentiometers appeared to have been functioning properly at the time of the incident; the only damage observed was that which was inflicted as a result of the mishap.

It is recommended that other aircraft systems be investigated to determine the cause of this particular incident. It is believed that the potentiometers did not contribute to or in themselves cause the mishap.

2.4 INVESTIGATION OF A METHOD FOR THE REMOVAL OF THE RESIDUE IN A FIBER OPTIC TERMINAL

Fiber optics are used to optically transmit signals in a ground-based radar set. The fiber optics units often break, resulting in their complete replacement, including the metal terminals located at the tips. It is reported that the stainless steel ferrules used to terminate certain fiber optics are relatively expensive; it is, therefore, desirable to be able to reuse them. Due to the difficulty of extracting the remains of a broken fiber optic, the terminals have up to now been discarded along with the fiber optic cables. The Productivity, Reliability, Availability and Maintainability (PRAM) Project Office requested that a practical method for removing the remains of the broken fiber optic and saving the ferrule be investigated.

The amount of potting material remaining in the tip was too small to permit practical chemical analysis. It is thought that epoxy is used to cement the fiber bundles in place. Judging

from the appearance of the material holding the fibers in place, the solvents may have had some slight effect on softening or degrading it.

To aid in the removal of the broken fibers and potting compound, it is suggested that the fitting be submerged in methylene chloride for a number of days. This is one of the most potent solvents for epoxies. The remains could possibly be drilled out from the rear. Care should be taken to choose a drill size no larger than the diameter of the orifice where the material is situated.

2.5 REPAIRABILITY ANALYSIS OF AN ENCAPSULATED ELECTRONIC MODULE

A small encapsulated electronic module was submitted for analysis to examine the materials used to encapsulate the module, determining the difficulty in removing them and to recommend a procedure for encapsulating a newly repaired module.

The module was encapsulated in a "rubber-like" material which could be easily cut with a scalpel. It was found to be silicone. The perimeter of the two stacked printed circuit boards was covered with a cloth tape. The tape held a fine white powdery material between the two stacked boards. It could be easily removed with an air gun. It was found to be aluminum oxide. The following reassembly steps are suggested:

- (1) Tape edges of sandwiched printed circuit boards with a suitable cloth tape leaving one of the 5 cm sides exposed.

- (2) Use a sprayer with a low nozzle velocity to blow in the aluminum oxide powder. A powder with a 0.05 micron grain size will pack better than a larger grain size.

- (3) Seal the remaining 5 cm side with the tape.

- (4) Encapsulate the module using a Type I or II, Class 2, Grade B-2 silicone rubber.

The construction of the module makes it an ideal candidate for repair. The materials needed to encapsulate the module following electrical repair offer no significant problems if the proper workmanship and quality control is observed.

2.6 INTEGRATED CIRCUIT LEAD SOLDERABILITY

Twenty integrated circuits (IC) were submitted for analysis of the lead frames due to poor solderability on printed circuit boards repaired at the depot level. The IC leads did not have a bright and shiny surface finish as is the case on the majority of leads on electronic components.

The solderability of the integrated circuit leads was improved by two methods. One method used an H_2SO_4 dip, DI water rinse, isopropyl alcohol rinse followed by a non-activated Type R soldering flux. This method was successful and achieved results similar to that of the second method. The second method involved using a highly activated Type RA soldering flux which is not allowed for use in military electronics.

The following recommendations are made as a result of the completed testing on the integrated circuit leads.

(1) Clean the leads in warm 15 percent H_2SO_4 , DI water rinse, and an isopropyl alcohol rinse. Do not clean and allow the integrated circuits to remain unused for more than one day.

(2) Apply a Type R soldering flux when soldering the integrated circuit to the printed circuit board.

(3) An alternative to the above procedures is the H_2SO_4 cleaning technique, Type R flux, and a dip into a dross-free solder bath. A three to five second dip would be sufficient.

2.7 FAILURE INVESTIGATION OF A CRT GEOMETRY/FOCUS CORRECTION MODULE

Testing and analysis was performed on five CRT correction/focus modules.

The CRT module is from a HUD (Heads-Up-Display) avionics subsystem.

The two observed modes of failure for the CRT module were the out-to-tolerance bias currents and input-output characteristics. Thermograms revealed no significant temperature differences between S/N 1707 (115 mA) and the control module, S/N 1706 (105 mA). Two of the modules (S/N 142 and 1715) which had out-of-tolerance bias currents were instrumented to monitor the change in current as the module was heated. The module was heated with a heat gun which easily raised the boards to approximately 85°C. A change in the bias currents was not observed. These results indicated that no single component was responsible for the out-of-tolerance bias currents. The out-of-tolerance bias currents are probably due to a gradual shift in the DC operating characteristics of the entire module. The reasons for the shift could not be confirmed; often, however, after an article has been in production for a number of years there is an inadvertent relaxation of tolerance requirements for the individual components.

Two of the three modules (S/N 1433 and S/N 1324) which had out-of-tolerance input-output characteristics were traced to a 741 operational amplifier on the output daughter boards. The operational amplifier of S/N 1433 was a catastrophic failure of a current limiting resistor on the chip. The operational amplifier of S/N 1324 was an intermittent failure which could not be identified.

2.8 FAILURE INVESTIGATION OF A PRECISION VARIABLE RESISTOR

Two precision variable resistors failed in a radar altimeter set. The reported failure was no high and low signals and the 9 foot calibrate/self test would not lock-in. The two precision variable resistors are supplied as a set.

The problems observed in the two potentiometers appear to be directly related to the use of a silicone gel to coat the conductive plastic resistive element. The silicone gel acts as an insulative film between the wiper contact and the resistive element. This insulative film can be electrically characterized as an increase in the wiper contact to conductive plastic resistance which will cause a shift in the electrical index point of the reference cup and therefore the output ratios of the remaining cups.

It is not known specifically what purpose the gel serves. One speculation is the gel acts as a lubricant so as to reduce the abrasion between the wiper contact and conductive plastic. Another use would be as a moisture barrier. Conductive plastic potentiometers, however, already exhibit well known and documented rotational life characteristics. Test results indicate that moisture will not cause significant shifts in the electrical index point or output ratios when the silicone is removed. The results of humidity testing show the potentiometers will function satisfactorily without the silicone gel.

2.9 FAILURE ANALYSIS OF LANDING GEAR DOWN LOCK SWITCH

A main landing gear down lock switch was reported to have high electrical contact resistance between two of its terminals. It was requested that the cause of this excessive resistance be determined.

Before disassembly of the switch, resistivity measurements were made between appropriate sets of contacts.

Disassembly of the unit revealed two separately encased microswitches. After matching leads to their respective microswitch and recording the identification, the plastic covers were removed from each switch. A microscopic examination was made of each leaf button contact and its respective stationary lug contact. While all of the contacts exhibited some wear, the two contacts associated with terminals 1 and 3 were

particularly noteworthy. The leaf button contact showed marked pitting and areas where the metal had melted. Carbon deposits were present in this general area as well.

Just as cratering appeared on the moveable leaf contact, a metallic deposit was found on its mating stationary contact. Carbon deposits were found here also.

It is believed that the failure of this microswitch unit was due to excessive wear. This is not considered unusual, especially in view of the age of the unit. According to the date code, the switch was fabricated in 1967. Other than normal replacement of the switch assembly, no further action is warranted. No corrosion or any other factor which could have accelerated failure of the switch was found in the examination.

2.10 FAILURE INVESTIGATION OF AN ANGLE OF ATTACK TRANSMITTER

An Angle-of-Attack Transmitter was submitted for examination because of erratic and intermittent operation. The Angle-of-Attack (AOA) Transmitter directly translates airflow angle changes into rotary mechanical motion. The mechanical rotary motion is converted to analog information by a wiper contact scanning in a resistive element potentiometer. The AOA Transmitter contains five (R1 thru R5) of these potentiometers. The output of the transmitter provides electrical stimulus to several cockpit indicators, a HUD unit, and a slight stabilizing computer.

Three factors appear to be reducing the life expectancy of the AOA Transmitter: the susceptibility of the conductive plastic to abrasion; the pressure exerted by the wiper contact; and the wiper contacts susceptibility to wear. The first factor may be due to variables in the manufacturing process such as the binder material, temperature and rapidity of the curing process, and particle contamination. The second factor is due

to workmanship during the assembly process. As a result of testing, it is believed that the degradation associated with these two factors would be acceptable and the life expectancy increased if the wiper contact was changed.

The following recommendations are made as a result of the completed investigation of the Angle-of-Attack Transmitter.

(1) Initial test results indicate the life expectancy can be improved by switching to a different style wiper contact.

(2) Investigate the possibility of using a flat conductive plastic resistive element as an alternative to the hybrid. The following application and selection guide is included as a reference. The most notable difference between the conductive plastic and the hybrid is the temperature coefficient.

2.11 FAILURE ANALYSIS OF TIP TANK AUTO-DROP SWITCHES

A Material Deficiency Report was issued concerning a microswitch which had electrically shorted, causing a fire on board an aircraft. The microswitch was identified as the right tip tank auto-drop switch. Investigation in the field revealed that the switch had shorted, causing the right wing jettison solenoid and the insulation on the auto drop switch wiring to burn. It was thought that de-icing fluid may have contributed to the switch failure.

It was suspected that the fluid entered the wing fairing and caused the switch to short. A field inspection of the right auto drop switch was made. De-icing fluid was found trapped between the switch housing and the Teflon tape wrapped around the switch housing and the wire bundle. It was requested that the switch be examined to determine if the de-icing fluid caused the right auto drop switch to short out.

The left side auto drop switch from the aircraft was also submitted for evaluation. It was requested that this

switch be examined to determine if the de-icing fluid had caused any internal damage.

The presence of ethylene glycol de-icing fluid could not be confirmed in either of the switches submitted for examination. With respect to the shorted switch assembly, it appeared that the damage was confined to the area immediately under the cover containing the soldering lugs. The two microswitches themselves did not appear to have been damaged.

Concerning the left side switch assembly, there did not appear to be any damage caused by the de-icing fluid. The interior of the switch assembly appeared to be in excellent condition with the exception of a broken wire strand near one of the soldering lugs. This broken wire strand so near the metal base could be a potential problem, particularly in the presence of any liquid which could serve as an electrical conductor. It was reported that de-icing fluid was found under the teflon tape sealing the switch assembly. This mixture could eventually enter the interior through cracks in the potting compound (some were found) and, in an impure form, act as an electrolyte. This condition could cause shorting between an exposed wire adjacent to the metal case.

It is quite possible that the short in the right side switch assembly was caused by the conditions just described. This could not be verified, however, since no trace of glycol could be found in the charred remains of the potting compound or wiring. This is understandable, as the destruction caused by the fire would have obliterated any evidence of broken or exposed wires and liquid contaminants. The damage due to the fire precluded a positive identification of the cause of failure of this switch.

To circumvent such problems, it is suggested that more care be taken in the fabrication of these switches, particularly with respect to soldering the lead wires to the lugs inside the switch assembly case. Steps should also be taken to provide

an effective seal to prevent the entrance of moisture. This could be achieved through the use of a better potting compound, perhaps one with enough flexibility to prevent cracking.

2.12 FAILURE ANALYSIS OF A LINEAR SERVO ACCELEROMETER

Two linear servo accelerometers had been submitted for testing due to one of the accelerometers exhibiting a low output resistance between pin H (output) and pin C (power ground). Additionally, both accelerometers were identified as having unsatisfactory environmental seals in the vicinity of the electrical connector. Finally, both accelerometers were to be subjected to a combined environmental stress test (temperature, humidity, and altitude) to determine if the environmental stresses would adversely affect the electrical performance characteristics of the accelerometer.

The two accelerometers had previously been identified as having unsatisfactory environmental seals. The environmental stresses used during CERT testing highlighted this anomaly. The testing scenario which led to the failure of the accelerometers started during the transition from altitude and the coinciding increase in the dew point temperature. This transition allowed water vapor to be drawn into the accelerometer. Due to the thermal lag between the temperature of the chamber air and the internal temperature of the accelerometer, some of the water vapor will condense in the form of free water. This condensation occurred in the voids between the silicone potting compound, the printed circuit board, and the metal cylinder of both accelerometers. Some of this free water will be evaporated during the high temperature phase of the cycle. Apparently not all the water is evaporated and after repeated cycles water accumulates.

The corrosion observed in the accelerometer is primarily a classical case of crevice corrosion.

The corrosion on the printed circuit board was also primarily a type of crevice corrosion. An EDAX examination of the corrosion products indicated high concentrations of lead with lower concentrations of iron, copper, and zinc. The important point to notice is that no tin was found in the corrosion products. This indicates the lead was being leached from the 60-40 solder alloy. The exact corrosion mechanism is not known but recent literature suggests the formation of lead chlorides and lead carbonates which are white precipitates and possibly lead sulfides which are black precipitates. The ions produced from the corrosion of the aluminum cylinder and the printed circuit board would greatly increase the conductivity of the trapped water leading to stray current leakage paths between various components on the bottom of the printed circuit board.

The following recommendations are made as a result of the completed tests on the linear servo accelerometers.

(1) The bottom of the printed circuit board should be conformally coated to reduce the deleterious effect of water.

(2) Increased care should be taken during the application of the silicone potting compound to ensure no voids exist between the aluminum cylinder and the printed circuit board.

NOTE: The preceding recommendations may be sufficient but further testing would be required to verify the proposed corrective action.

(3) The present method of sealing the aluminum cylinder to the mounting flange of the position detector is a potential source of an environmental leak; use a metallurgical bond to provide a hermetic seal.

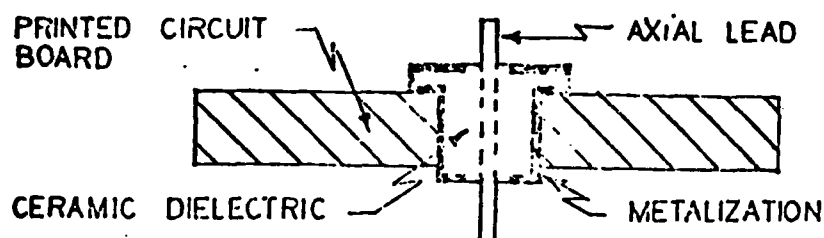
(4) The accelerometer's connector is also a potential source of an environmental leak; use a connector which would provide a hermetic seal.

2.13 CERT (COMBINED ENVIRONMENTS RELIABILITY TEST) FAILURE ANALYSIS

Testing and analysis of four components and two sub-assemblies from IFF Transponders was performed.

The six failures occurred during CERT (Combined Environments Reliability Testing) testing of the IFF Transponder. The CERT testing facility allows environmental stresses such as: temperature, humidity, vibration, altitude, and electrical loading to be combined to simulate aircraft avionics bay environments.

The "feedthrough" type of capacitor was listed as shorted in Failure Report 1. Testing revealed this "shorted" condition



CROSS SECTION OF FEEDTHROUGH CAPACITOR

not to be true. The capacitance, loss tangent and leakage current were found to be quite acceptable. The "feedthrough" capacitor is designed to feed signals through a printed circuit board. During troubleshooting the technician may have mistakenly determined the capacitor was shorted by measuring the resistance of the axial wire lead that protrudes on either side of the printed circuit board.

The carbon composition resistor was reported as burned in Failure Report 1. The resistor did not show any evidence of severe overheating such as discoloration or blistering of the color coded bands. The resistor has, however, increased in value approximately 44 percent. Carbon composition resistors are filled with an organic resin that is moisture sensitive.

These resistors can be subjected to an electrical stress resulting in rapid heating thus increasing the internal pressure. The increased internal pressure can cause rearrangement of the resin particles resulting in a positive permanent resistance change.

In Failure Report 2, the reported failure was an "open" 2 kilo-ohm variable resistor. The wire lead on terminal number 3 had been broken off just inside the plastic case. A microprobe was used to access terminal 3; resistance measurements verified the variable resistor still performed satisfactorily. The broken wire lead of terminal number 3 was removed from the variable resistors plastic case. The wire lead was examined closely under various powers of an optical microscope. The wire lead showed evidence of excess vertical loading due to the elongation at the point of fracture.

Reported failures, Failure Reports 3 and 4, of the solid tantalum capacitors as being "shorted" is not entirely accurate. The capacitor functioned properly; its capacitance and DC leakage current were well within specified tolerances, at room temperature. At temperatures around 65°C, however, the DC leakage current would suddenly increase from approximately 20μA to well over 1.0mA.

The most common operational failure mode of wet slug tantalums is a slow degradation brought about by the loss of electrolyte through the end seal. This results in a loss of capacitance, increase in power factor and a decrease in leakage current. The failure mode observed in these capacitors appeared to be of a more catastrophic nature. Optical microscopy of the tantalum slug revealed holes or faults in the dielectric. The holes which represent low resistance paths, create areas of high current density which will increase leakage current and cause dielectric breakdown of the capacitor. The initiation of these low resistance paths can be due to a crystalline oxide growth inside the amorphous oxide dielectric

or chemical impurities in the electrolyte or tantalum slug. The capacitor of Failure Report 3 showed evidence of crystalline oxide growth. The capacitor of Failure Report 4 showed evidence of a chemical impurity and crystalline oxide growth. Around several of the holes there existed a brownish-red residue later identified as iron. Both of these failure modes can be greatly accelerated by operation at elevated temperatures.

In Failure Report 5, the diode (CR3) which controls the switching action on the lower antenna was found to have a cracked ceramic insulator. A forward and reverse voltage characteristics test performed in situ revealed the diode to be open. Upon removal from the diversity switch, the diode fell in half. A microprobe station was subsequently used to access the anode and cathode on the semiconductor chip. The forward and reverse DC voltage characteristics revealed the diode to be functional. The internal or external stresses which caused the ceramic insulator to crack also may have caused the fine wire lead to become unbonded from the semiconductor anode.

The other anomaly noted during analysis of the diversity switch was the discoloration of the printed circuit board. An analysis using energy dispersive x-rays of the discolored areas revealed them to be similar to residues left by the intrusion of common tap water.

The only anomaly noted on the stripline assembly from Failure Report 6 was the discoloration of the printed circuit foil. The surface analysis using energy dispersive x-rays revealed the residues to be also similar to that of common tap water.

SECTION 3

FIBROUS MATERIALS

3.1 AIRCRAFT CARPETING

Carpeting used in aircraft must meet varying criteria depending on the application. The group of samples tested is under consideration for use in electronic surveillance aircraft. In addition to flame resistance and static control, they must provide adequate wear life. The wool carpeting currently in use (as shown in Table 28, Type A) has a relatively short wear life and may produce lethal combustion by-products. Flammability tests were done according to Federal Standard 191, Test Method 5903.1 (Vertical Flame Test). The wear tests were conducted on a Taber Abraser Model No. 503 according to the test procedures given in ASTM Test Method D-1175 64-T. Abrasion resistance is measured by subjecting the specimen to rotary rubbing action under controlled conditions of pressure and abrasive action. H-18 Calibrade abrasive wheels were used under a 1,000 gram load. This flame resistance and wear life data will be used with static electricity dissipation properties to propose a replacement for the carpeting now being used.

3.2 PARACHUTE CORD

Tensile tests were conducted on Kevlar-29 cords intended for use as parachute suspension lines. Three sample varieties were examined: Braided High Modulus Aramid Cord MIL-C-81729 (USAF) Types VIII, IX, and X. The purpose was to obtain some baseline data for these coreless tubular braids and to determine a test method that was reliable and repeatable. It must be easily duplicated for use by contractors and for government acceptance testing. The testing of Kevlar woven structures presents special problems due to its characteristic high modulus. Improper test configuration that results in uneven sample loading can cause a significant drop in observed tensile strength. The

TABLE 28
AIRCRAFT CARPET TEST DATA

Code Letter and Material	Taber Abrasion		Vertical Flame Test			
	Cycles to Failure	Weight Loss grams	Drip Time sec.	Flame Time sec.	Glow Time sec.	Char Length in. (cm)
A Wool	2200	2.19	None	18.9	0.0	0.4 (0.9)
B Nylon	5300	1.10	None	657.2	0.0	12.0 (30.5)
C Acrylic-Nylon	7500	2.43	None	474.3	0.0	12.0 (30.5)
D Nylon	14500	1.37	40.0	338.5	21.0	12.0 (30.5)
E Nomex	7500	2.06	None	5.1	0.0	0.4 (1.0)
F Nylon	29200	1.91	52.0	368.1	2.0	12.0 (30.5)
G Nylon	33500	1.79	40.5	348.5	33.0	12.0 (30.5)
H FR Nylon	23000	1.60	None	0.0	0.0	0.3 (0.8)
I Nylon	37500	1.39	None	0.0	0.0	0.0 (0.0)
J Nylon	32300	1.56	33.0	76.5	61.3	4.5 (11.4)
J-1 Nylon	--	--	32.7	237.9	191.4	11.0 (27.9)
K Nylon	15400	2.88	None	4.4	0.0	0.1 (0.3)

method chosen utilizes finger-trap eye splices. The ends of each braid sample are folded around and spliced back into itself, forming a loop through which a rod can be inserted to hold the sample during the tests. Consistently high tensile strength values are obtained with this method.

3.3 FLAME RESISTANT MATERIALS

An analysis was done on wear-tested flight suits constructed of (a) PBI (Polybenzimidazole) and (b) E-22 (50 percent Nomex/50 percent Kevlar-29). The areas of interest included post-use physical characteristics, strength retention and any changes in thermal response. These values were compared with the characteristics of similar unused fabrics. The purpose was to ascertain the effects of normal wear and abrasion, laundering, and minor ultraviolet light exposure. This test program was not designed as a competition between the two basic material types, as each has its own specific areas of application, but to determine any adverse effects caused by normal patterns of use.

Aircraft interior materials were tested to determine their relative flammability. Types of materials tested included carpeting, seat covers, and cushion fabrics. Some of these tests were carried out in cooperation with the Air Force investigation of the recent crash of a C-135 aircraft. All data have been relayed to the appropriate government agencies involved.

Physical properties and flame resistance data were determined for two groups of materials proposed for use in protective apparel. The first was a set of three flame-resistant woven fabrics, and the second group consisted of rubber-type materials resistant to chemical exposure. The data will be used to assess any flame hazards associated with the use of these materials.

SECTION 4

ELASTOMERS

4.1 EVALUATION OF SEALANTS AND FOAMS

4.1.1 Fluorosilicone Sealants

Two fluorosilicone sealants, General Electric FRV 1106 and Dow Corning X4-2817, were evaluated in accordance with MIL-S-83430. Both sealants are one part systems. The tests included specific gravity, nonvolatile content, flow, tack-free time, standard curing rate, thermal rupture [at 300°F (149°C) and at 360°F (182°C)], low temperature flexibility, peel strength, corrosion, tensile strength, and hydrolytic stability. All test panels were cured for 14 days at 78°F (24°C) and 50 percent relative humidity.

Both fluorosilicones became tack-free in two hours. This was, however, on the surface only. Uncured sealant remained beneath the tack-free surface. Peel panels were laid up in three layers. The first layer was 0.062 inch thick and was allowed to cure for 14 days at 77°F (23°C) and 50 percent relative humidity. After curing the surface was primed and a second 0.062 inch layer with cloth was applied. This layer was also cured for 14 days at 77°F (23°C) and 50 percent relative humidity then primed. A third layer, 0.031 inch thick, was then applied. This method was used to permit acetic acid to escape the sealant to insure complete cure to avoid thin layer cohesive failures at the panel or at the cloth. The method was satisfactory when unaged panels were tested. It did not, however, prevent the occurrence of poor failure modes on aged panels.

The General Electric FRV 1106 had decreased tensile properties after conditioning except after 72 hours at 140°F (60°C) in Jet Reference Fluid (JRF) plus 7 days at 250°F (121°C). The Dow Corning X4-2817 material showed a decrease in tensile properties after conditioning for 14 days at 140°F (60°C) in JRF and after the MIL-S-83430 heat cycle plus 7 days at 140°F (60°C) in JRF.

Dow Corning Q4-2817 fluorosilicone sealant was evaluated for 180° peel strength using peel panels prepared according to a fabrication procedure supplied by Dow Corning. The rigid substrate was 3 in. by 6 in. by 0.040 in. aluminum coated with MIL-C-27725 urethane coating. The flexible substrate was a 1 in. by 12 in., 30 mesh aluminum screen supplied by Dow Corning. The rigid and flexible substrates were cleaned using MIL-C-28736 four-part solvent. After drying for 30 minutes in air, both the rigid and flexible substrates were primed by wiping with a clean piece of cotton gauze saturated with Dow Corning 1200 primer. The parts were then air dried for 60 minutes at 78°F (26°C), 50 percent relative humidity. The elastomeric material was applied to the rigid substrate and drawn to 1/16 in. thickness using a template, then the flexible substrate was immediately applied. A second layer of sealant was applied over the flexible substrate. A template was again used to control the top layer to 1/16 in. thickness. The sealant was then wiped from the edges of the flexible substrate. This provided two 1 in. x 6 in. peel strength laminates. The laminates were cured for 14 days at 78°F (26°C) at 50 percent relative humidity. Two panels were then conditioned for seven days at 140°F (60°C) in JRF and two panels were conditioned for seven days at 140°F (60°C) in JRF/SW. After conditioning, the panels in JRF had an average load of 7.4 lbs/in (13.0 N/cm) with 100 percent cohesive failures, and in the JRF/SW the panels had loads of 10.6 lbs/in (18.6 N/cm)/8.4 lbs/in (14.7 N/cm), respectively, with 100 percent cohesive failure.

4.1.2 Polysulfide Sealants

Four classes of PS-890, a MIL-S-8802E fuel tank sealant, were evaluated for tack-free time and standard curing rate. The sealants consisted of ten different batches with six different manufacturing dates. The types of sealant included four batches of Class A-2, and two batches each of Classes B-1/2, B-2, and B-4. Of the four batches of Class A-2 sealant, only

one batch, C98431-12, manufactured in February 1980 and supplied as Semkits, did not meet specification requirements for standard cure time. It was noted, however, that lumps were present in the sealant portion of the Semkit.

Of the two Class B-1/2 sealants, Batch No. C86434, manufactured in May 1979 but updated on June 1980, did not meet tack-free time or standard cure time requirements. After 48 hours, however, it did attain a Shore A hardness of 37 points. This batch had a heavy skin on the sealant. The two batches of Class B-2 sealant both met MIL-S-8802E specification requirements. The two batches of Class B-4 sealant both failed to meet specification requirements. Batch C000232, manufactured in February 1980, was slightly slow in standard cure time and failed tack-free time. Batch C97272 was manufactured in April 1979 and was updated to June 1980. This batch, supplied in Semkit form, just failed to meet tack-free requirements, but had only 16 points hardness after 90 hours.

4.1.3 Channel Sealants

General Electric G651, a groove sealant, was evaluated for corrosion characteristics on QQ-A-250/12 aluminum by subjecting coated panels in air, Jet Reference Fluid (JRF), and saltwater at 140°F (60°C) for 20 days. The compatibility of G651 with Dow Corning 94-031 was also evaluated using the seal efficiency jigs. No discoloration or pitting of the QQ-A-250/12 aluminum panel occurred on the Jet Reference Fluid, saltwater, or air portions of the panel. To evaluate G651 compatibility with DC94-031, seal efficiency jigs with 5 mil spacers were used. One jig was injected with G651 and one with DC94-031. They were then conditioned for 72 hours at 140°F (60°C) with JRF at atmospheric pressure. The jigs were then subjected to the conditioning cycle three times, 16 hours at 140°F (60°C) with JRF at 5 psig plus 2 hours at 180°F (82°C) with JRF at 5 psig plus 4 hours at 260°F (127°C) with vapor at 0 psig plus 40 minutes at 320°F (160°C) with vapor at 0 psig plus 60 minutes at 360°F (182°C) with vapor at 0 psig. After three cycles, the

G651 jig was injected with DC94-031 and the DC94-031 jig was injected with G651. The original cycle was then repeated using both test jigs. Neither jig showed any signs of leakage during the entire six cycles.

The following tests were performed on Dow Corning X4-2805-130 channel sealant: nonvolatile content, hydrolytic stability, and adhesion to titanium. Nonvolatile content was measured after conditioning seven days at 158°F (70°C), hydrolytic stability after 120 days at 160°F (71°C)/95 percent relative humidity. Specimens were tested for adhesion to titanium, MIL-T-9046, after the following aging was completed.

96 hrs at 140°F (60°C) in JRF +
 2 hrs at 180°F (82°C) in JRF +
 4 hrs at 260°F (127°C) in air +
 40 min at 320°F (160°C) in air +
 60 min at 360°F (182°C) in air.

The specimens were then bonded to blocks and tested in flatwise tension. Five control specimens were also tested in flatwise tension. The results are shown below:

Nonvolatile Content	99.3%	
Hydrolytic Stability	no reversion	
Adhesion to Titanium	<u>Controls</u>	<u>Aged</u>
	6.42 psi	8.7 psi
	6.31 psi	8.6 psi
	7.15 psi	9.1 psi
	6.3 psi	8.34 psi
	4.5 psi	10.00 psi
	6.1 psi	

4.1.4 Firewall Sealants

GE RTV 144, a sealant, was evaluated for flame resistance according to MIL-S-38249. Four panels, 0.040 in. x 2-7/8 in. x 6 in. with a 1/4-in. hole in the center, were coated with an 1/8-in. thick layer of RTV 133 sealing compound and cured for 14 days at standard conditions. Two control panels were tested in the original condition and two were tested after immersion in AMS 3021 (Stauffer's 7700) for 72 hours at

140°F (60°C). Testing consisted of exposure to a bunsen burner flame at a temperature of $2000 \pm 100^\circ\text{F}$ ($1093 \pm 38^\circ\text{C}$) for 15 minutes, with the flame directed at the center of the coated side of the panel at an angle of 45° and at a distance of 1 inch.

All panels passed, as no burning through the 1/4-in. hole in the center of the panel to the uncoated side occurred. There was, however, a large difference in the effect of the flame on the material between the original and aged panels. The control panels were heavily oxidized, cracked, and charred but the sealant remained largely intact and did not itself ignite. The aged panels burst into flames shortly after exposure to the bunsen burner. The material peeled off in layers and fell off the panel in large pieces.

Dapcocoat 18-4 (Type I) and 18-4F (Type II) firewall sealants were also evaluated to selected tests according to MIL-S-38249. These tests included flow, tack-free time, curing rate, thermal rupture, low temperature flexibility, peel strength, corrosion, and flame resistance. The Type I and Type II were mixed at a one-to-one ratio and all test panels were primed with Dapco #1-100 primer which was allowed to dry a minimum of one hour before application of the sealant. The material met all specification requirements except for peel strength after conditioning for 72 hours at 400°F (204°C). The first set of peel panels were fabricated using aluminum screen. After conditioning, however, the screen cut the sealant causing the failure mode to be at the screen and the loads were below 10 lbs. The panels were refabricated using PBI cloth instead of screen. A control panel using PBI cloth was fabricated to check the ability of the sealant to bond to the PBI prior to conditioning. Failures occurred in the sealant on the control panel. After being conditioned for 72 hours at 400°F (204°C) the failure mode was at the PBI/sealant interface at loads less than 10 lbs. These cloth/sealant failures may be due to the effects of the 400°F (204°C) temperature on the sealant.

4.1.5 Air Content in Sealant

Chem Seal CS3204-B-2 sealant has been supplied through GSA to Tinker AFB for use as an integral fuel tank sealing compound. Tinker personnel experienced problems with excessive air in the sealant mix. An inspection of the drums of base compound also indicated excessive air content to be present.

Sealant evaluations were conducted by UDRI to determine the properties of the material from Tinker AFB and from Chem Seal Corporation. Four samples were supplied by Tinker and four samples containing the same four batch numbers were supplied by Chem Seal. Another sample from a fifth batch was also supplied by Chem Seal. A sample of Pro Seal 890B-2 was supplied by Tinker for the evaluation. All batch numbers are identified in Table 29.

The following tests were conducted on the four batches of CS3204-B-2 from Tinker and on the PS890 B-2 from Tinker:

- Viscosity of base and accelerator
- Application time
- Tack-free time
- Flow
- Standard cure
- Peel strength
- Air content of base
- Nonvolatile content
- Specific gravity
- Volatile mercaptans and hydrogen sulfide

The initial four batches from Chem Seal were evaluated for:

- Tack-free time
- Standard cure
- Air content
- Nonvolatile content
- Specific gravity
- Volatile mercaptans and hydrogen sulfide

The fifth batch from Chem Seal was evaluated only for air content, nonvolatile content, specific gravity, and volatile mercaptans and hydrogen sulfide.

TABLE 29

VISUAL APPEARANCE OF CS 3204 B-2 SEALANT BASE

Batch #035140 - Mfd 3/80

The sealant received from Tinker AFB was very air filled and had a much greater amount of air than the material from Chem Seal. The sealant from Chem Seal looked very good.

Batch #045310 - Mfd 4/80

The material from Tinker AFB had slightly more air than the material from Chem Seal, although the material from Chem Seal had a fair amount of air.

Batch #055130 - Mfd 5/80

The material from Tinker AFB was very air filled and had more air than the material from Chem Seal. The material from Chem Seal had more air than Batch #035140 from Chem Seal.

Batch #065420 - Mfd 7/80 (Refrigerated)

The material from Tinker AFB had considerably more air than the material from Chem Seal. The sealant from Chem Seal was very good.

Conclusions:

- 1) Batch 045310 from Tinker AFB was the best of all four batches but contained air. The remaining three batches contained large quantities of air and were very similar in appearance.
- 2) Batches 045310 and 055130 from Chem Seal were very similar to each other with small amounts of air.
- 3) Batches 035140 and 065420 from Chem Seal were very similar to each other and were as air free as PS-890 batch C008768.

Batch 035140/035130 from Tinker AFB failed viscosity of accelerator, flow at all three times, and peel strength in Jet Reference Fluid. Batch 045310/045090 from Tinker failed application rate, and 50 and 90 minute flow. Batch 055130/055180 from Tinker failed flow at 90 minutes. Batch 065420/075070 from Tinker which had been kept in refrigerated storage failed application rate. The PS-890 B-2 from Tinker passed all tests. Three batches of CS3204 B-2 sealant supplied by Chem Seal, 045310/045090, 055130/055180, and 095380/095530 failed non-volatile content.

The Chem Seal 3204B-2 did not have generally bad physical properties. The material received from Chem Seal indicated lower air content; however, they also indicated greater amounts of volatiles and lower densities. If these volatiles were given off by the CS3204 B-2 sealant while in storage or shipment to Tinker AFB, this could explain the higher percentage of air in Tinker AFB CS3204 B-2.

During this evaluation a need arose for a more repeatable type of test for air content in polysulfide sealants. The first method, an analytical method for air in base materials, yielded very scattered data points for percent air content in the samples. The evaluation was made by placing 20 gms of base sealant into a 500 ml flask and filling the flask with trichloroethylene. A 0.5 ml graduated tube was installed on the mouth of the flask then trichloroethylene was added to a recordable level. The flask and tube was capped then agitated at 10 minute intervals for three hours. The drop in the level of the trichloroethylene was recorded and percent air content calculated.

Another method that was used in air content determination involved mixing the sealant on a rotary of dasher mixer and then placing the sealant in a cartridge where it is allowed to cure. After curing, cross-sectional cuts are made through the sealant and the sectioned areas are inspected for voids caused by the presence of air during cure.

A third attempt to achieve consistent air content evaluations utilized the following procedure.

- (1) Tare off a standard weight per gallon (wt/gal) cup and lid.
- (2) Fill the wt/gal cup with sealant, squeeze out excess.
- (3) Take weight of material in cup. This is a direct readout.
- (4) Remove material from wt/gal cup, putting it into a 1 pint can, about 125-150 grams. Add about 20-30 grams extra from original container. Heat pint can in 180°F (82°C) oven 10 to 15 minutes to facilitate the degassing process. Degas the pint can with material under 28-30 inches of vacuum for 15-20 minutes or until "head" breaks.
- (5) After degassing is complete, remove material from vacuum chamber. Refill wt/gal cup from 1 pint can and weigh.
- (6) Calculate - difference before and after degassing.

The difficulty with this method was avoiding the trapping of air when filling the cup with sealant both prior to and after evacuating the air. The results can be found in Table 30.

The fourth method used was to calculate the density of the sealant before degassing and after degassing. The specific volumes were then determined for each sample by taking the reciprocal of the density. The difference in specific volumes were then divided by the specific volume of the material before degassing to calculate percent air content.

$$v_0 = \frac{1}{\rho_{avg}}$$

$$v_1 = \frac{1}{\rho_{evacuated}}$$

$$\text{Air content, \% vol.} = \frac{v_0 - v_1}{v_0}$$

The results of these tests are presented in Table 30.

TABLE 30
SEALANT AIR CONTENT DETERMINATIONS

Chem Seal 3204 B-2
BN. 045310

Specific Gravity of Non Vac. - 1.44
Specific Gravity of Vac. - 1.54
Specific Vol. of Non Vac. - 0.694
Specific Vol. of Vac. - 0.649

$$\% \text{ Air by Vol.} - \frac{0.694-0.649}{0.694} \times 100 = 6.48\%$$

Chem Seal 3204 B-2
BN. 055130

Specific Gravity of Non Vac. - 1.48
Specific Gravity of Vac. - 1.54
Specific Vol. of Non Vac. - 0.676
Specific Vol. of Vac. - 0.649

$$\% \text{ Air by Vol.} - \frac{0.676-0.649}{0.676} \times 100 = 3.99\%$$

Chem Seal 3204 B-2
BN. 125630

Specific Gravity of Non Vac. - 1.52
Specific Gravity of Vac. - 1.52
Specific Vol. of Non Vac. - 0.658
Specific Vol. of Vac. - 0.658

$$\% \text{ Air by Vol.} - \frac{0.658-0.658}{0.658} \times 100 = 0.00\%$$

PS-899B-2
BN. C11812

Specific Gravity of Non Vac. - 1.51
Specific Gravity of Vac. - 1.51
Specific Vol. of Non Vac. - 0.6641
Specific Vol. of Vac. - 0.6641

$$\% \text{ Air by Vol.} - \frac{0.6641-0.6641}{0.6641} \times 100 = 0.00\%$$

In a fifth evaluation, two sealants, Goal Chemical GC-408B-2, Batch No. CP38, and Chem Seal CS3204B-2, Batch No. 025321, were evaluated for air content using the specific gravity method. Four specimens of each sealant were prepared with 15 minutes heat soak at 180°F (82°C) for 15 minutes prior to exposing to a vacuum of 29 inches of mercury for 15 minutes and another five specimens of each sealant without the 180°F (82°C) soak prior to vacuum exposure.

No significant difference between the average air content of the specimens with heat soak and those without heat soak was noted. GC408B-2 measured 1.3 percent air with heat and 1.9 percent without heat. The Chem Seal had 0.7 percent with heat and 0.0 percent without heat.

4.1.6 Foam Materials

Hydrolytic stability evaluations of MIL-B-83054 Type II yellow and Types IV and V blue reticulated foams were conducted to complement data previously obtained on Types I and III fuel tank foams.

Testing of yellow foam was performed at 120°F (49°C) and 95 percent relative humidity to duplicate conditions under which Type I orange and Type III red polyester polyurethanes were previously tested. The blue polyether polyurethane foams were subjected to 200°F (93°C) and 95 percent relative humidity to compare the quality of present foam with that of blue foam tested previously.

Accelerated hydrolytic reversion data have been used to predict the service life of elastomeric compounds. The results of testing of yellow foam indicated that the useful service life for Type II foam is greater than that for Type I orange but less than that for Type III red foam. These data are shown in Figures 53, 54, and 55.

Comparison of the most recent test data at 200°F (93°C) for Types IV and V blue foams indicated improved hydrolytic

FIGURE 53

HYDROLYTIC STABILITY OF
MIL-B-83054, TYPE I (ORANGE) FOAM

○ 120°F (49°C), 95% R.H. (TMP)
△ 120°F (49°C), 95% R.H. (Non-TMP)

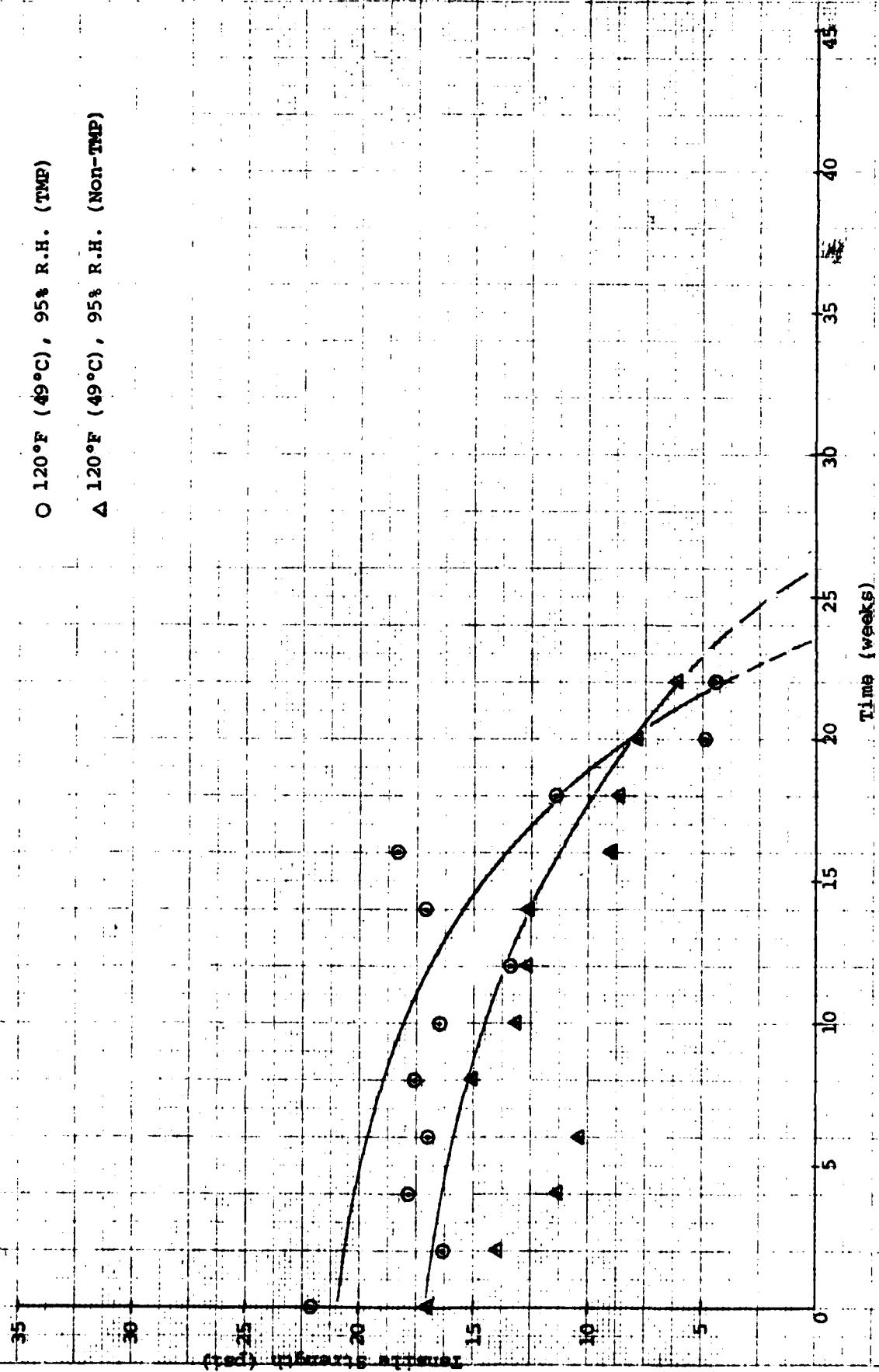


FIGURE 54

HYDROLYTIC STABILITY OF
MIL-B-83054, TYPE II (YELLOW) FOAM

◊ 120°F (49°C), 95% R.H.

○ 160°F (71°C), 95% R.H.

△ 200°F (93°C), 95% R.H.

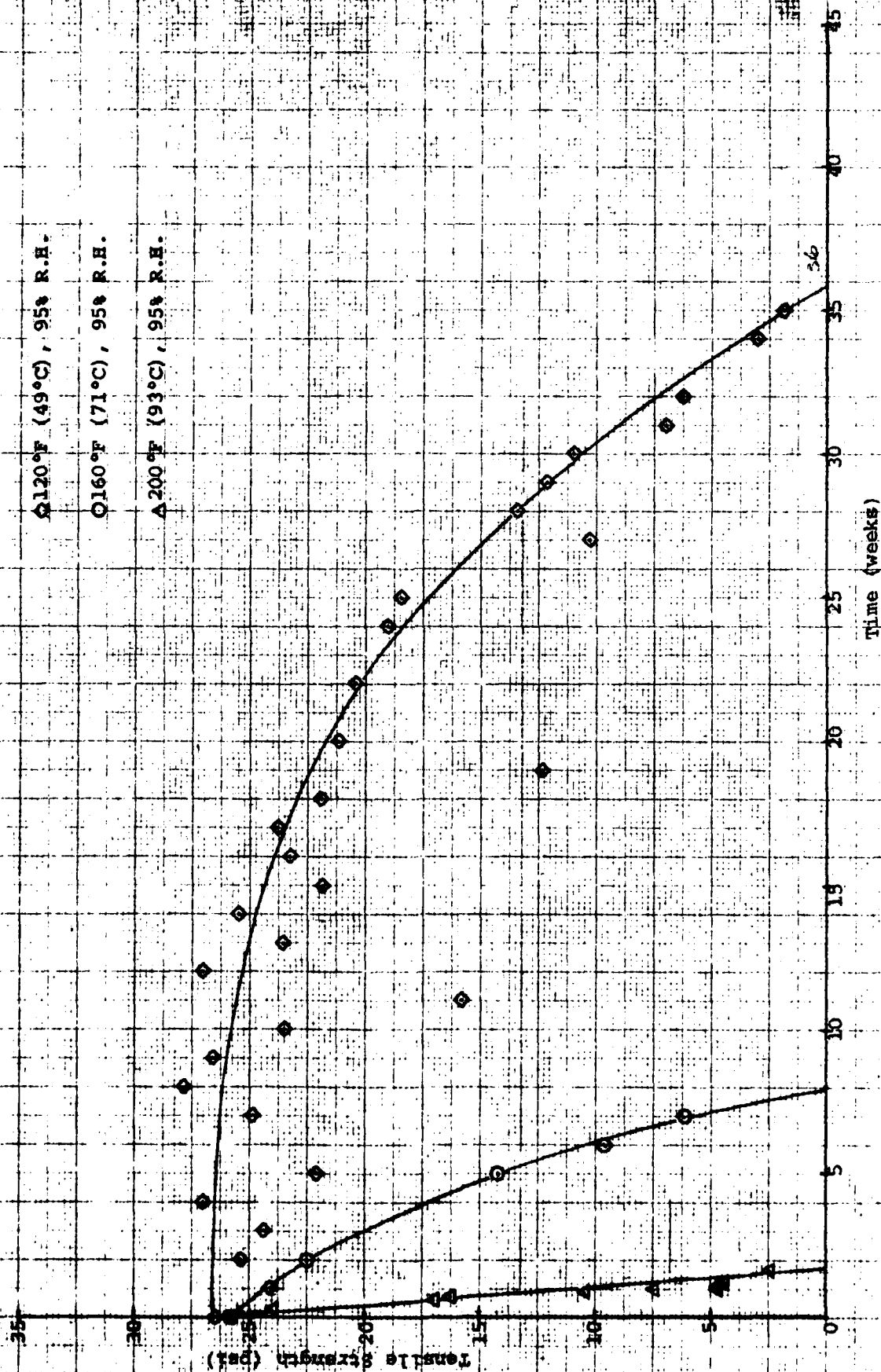


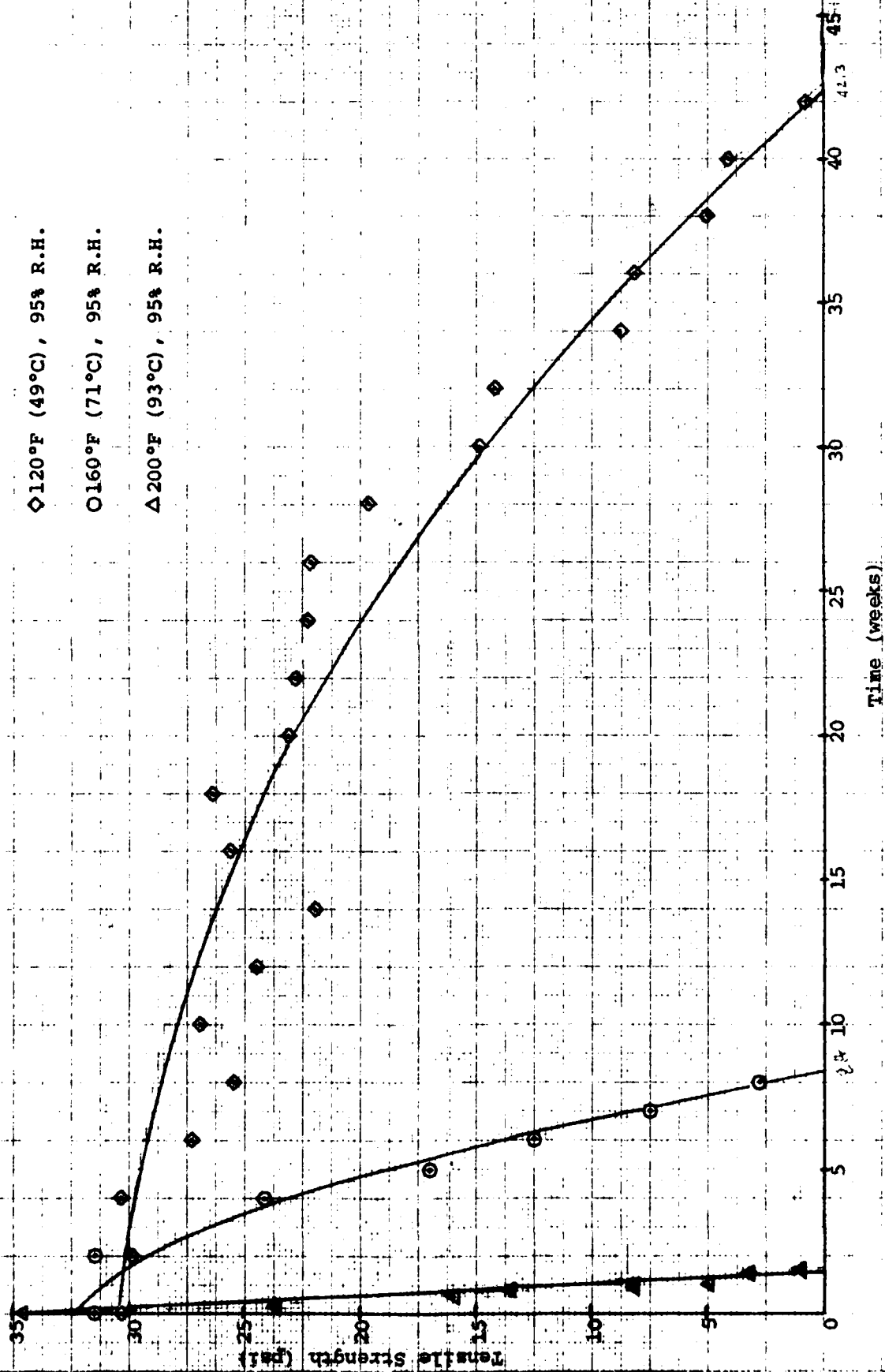
FIGURE 55

HYDROLYTIC STABILITY OF
MIL-B-83054, TYPE III (RED) FOAM

◇ 120°F (49°C), 95% R.H.

○ 160°F (71°C), 95% R.H.

△ 200°F (93°C), 95% R.H.



stability for the present foams. Different methods were used, however, to maintain conditions under which the materials were tested. The use of mason jars containing liquid to maintain the high humidity may have introduced a more severe environment than the use of controlled humidity cabinets for the present foam materials. The data are shown in Figures 56 and 57.

The density of an earcap pad fabricated from a foam material was determined according to MIL-R-5001A, Paragraph 4.5.3. The density of a foam is obtained by dividing the weight by the volume. The volume of the foam specimen was obtained by placing it in a graduated cylinder and filling the cylinder with flax seed to 1 inch over the specimen. The specimen was then removed from the cylinder and the difference in height measured. This difference was considered the volume. Three specimens were measured from the earpad and their densities were 0.002 lbs/in³.

The density of an earcap pad fabricated from a foam material was determined according to MIL-R-5001A, Paragraph 4.5.3. The density of a foam is obtained by dividing the weight by the volume. The volume of the foam specimen was obtained by placing it in a graduated cylinder and filling the cylinder with flax seed to 1 inch over the specimen. The specimen was then removed from the cylinder and the difference in height measured. This difference was considered the volume. Three specimens were measured from the earpad and their densities were 0.002 lbs/in³.

A block of reticulated fuel tank foam from an F-15 aircraft with approximately 7.5 years service was evaluated for residual tensile strength at room temperature. The tensile specimens were 4 inches long with a 1/2 inch square test area. Test results are shown in Table 31.

FIGURE 56

HYDROLYTIC STABILITY OF
MIL-B-83054, TYPE IV (DARK BLUE) FOAM

- ◇ 160°F (71°C), 95% R.H.
- 200°F (93°C), 95% R.H.
- △ 200°F (93°C), 95% R.H.

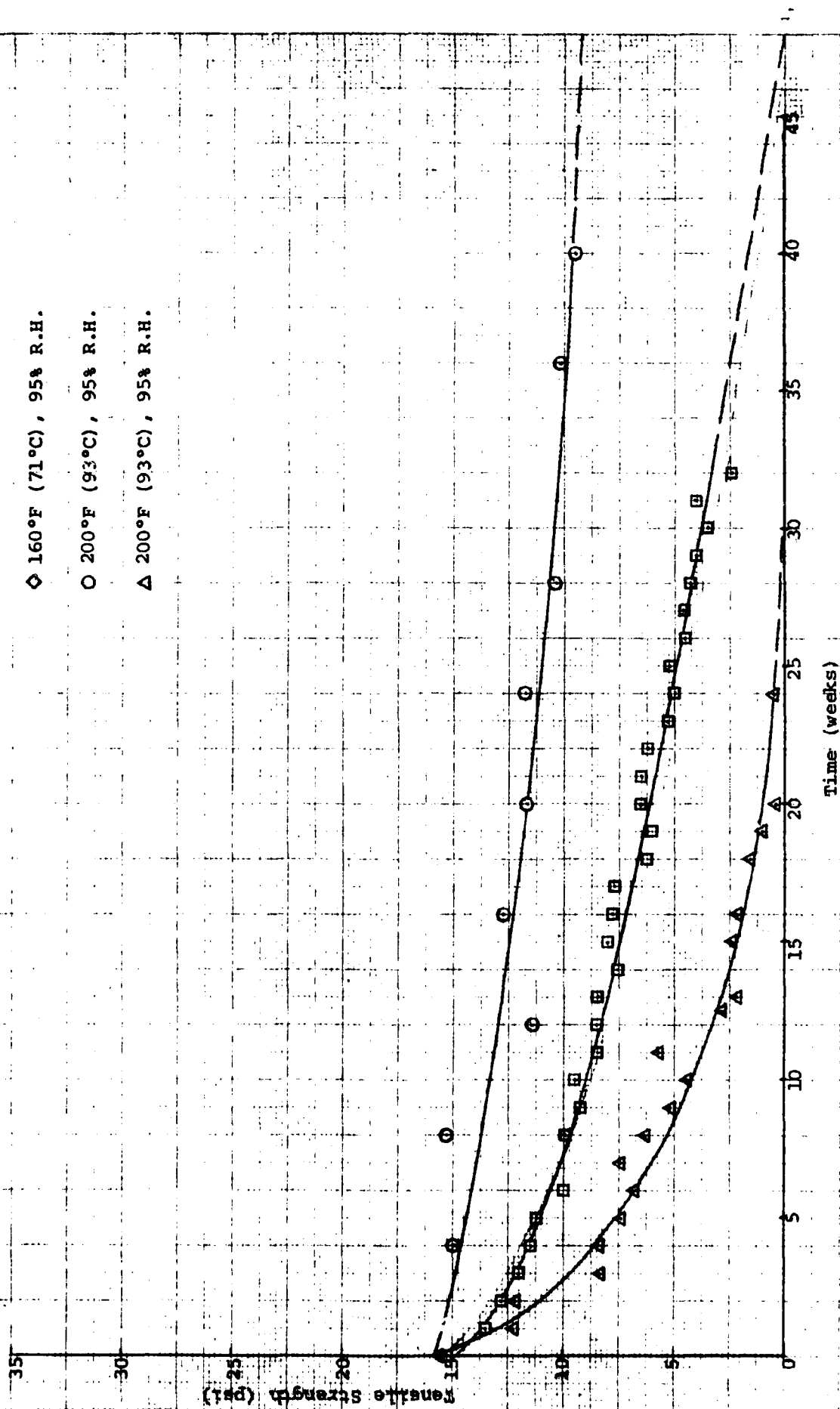


FIGURE 57

HYDROLYTIC STABILITY OF
MIL-B-83054, TYPE V (LIGHT BLUE) FOAM

○ 160°F (71°C), 95% R.H.
 □ 200°F (93°C), 95% R.H.
 △ 200°F (93°C), 95% R.H.

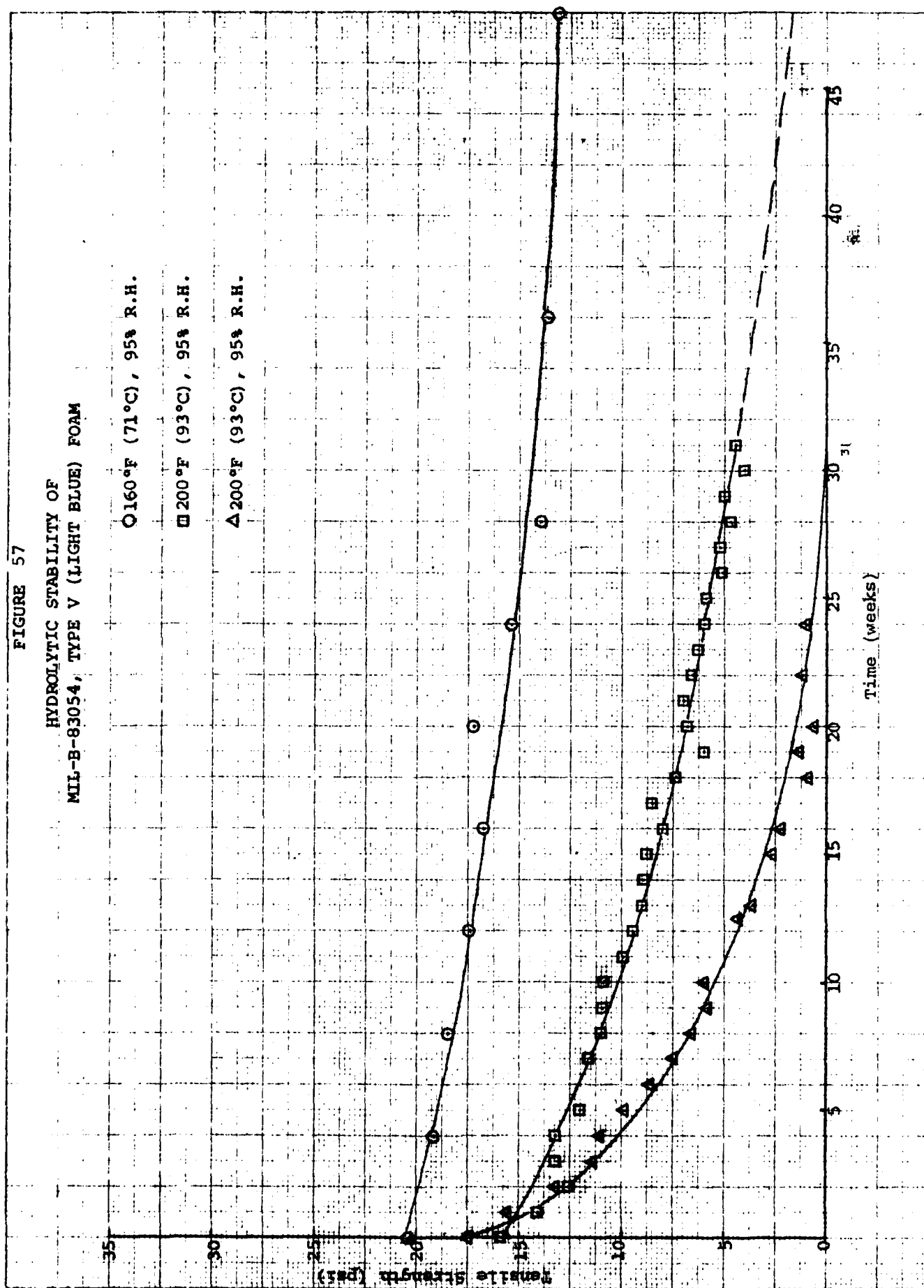


TABLE 31
F-15 FOAM

Condition	100% Modulus		Ultimate Tensile Strength		Elongation (%)
	psi	(MPa)	psi	(MPa)	
7 years in wing vent box	14.0	(0.10)	27.7	(0.19)	230
	14.3	(0.10)	24.9	(0.17)	235
	15.3	(0.11)	32.7	(0.23)	320
	14.3	(0.10)	29.7	(0.20)	305
	<u>15.2</u>	<u>(0.10)</u>	<u>25.5</u>	<u>(0.18)</u>	<u>230</u>
Avg.	14.6	(0.10)	28.1	(0.19)	260

4.2 EVALUATION OF CLEANING SOLVENTS AND ADHESION PROMOTERS

MIL-C-38736 cleaning solvent contains 50 percent aromatic naphtha (TT-N-97, Type II). Aliphatic naphtha (TT-N-95B, Type II) from BWI Plastics and Chemicals was substituted for the aromatic naphtha to make a solvent blend similar to MIL-C-38736. Peel specimens on new MIL-C-27725 coated panels and on C-130 panels were fabricated using PS 899B-2, a MIL-S-83430 manganese dioxide cure sealant. Two panels of each type were scrubbed with the cleaning solvent and the cleaner was allowed to evaporate from the panel surfaces. Two more panels of each type were scrubbed with the cleaner and wiped dry. After fabrication the panels were exposed to an accelerated cure of 48 hrs at 78°F (26°C) and 50 percent relative humidity plus 24 hrs at 140°F (60°C) and then conditioned for seven days at 140°F (60°C) in Jet Reference Fluid and saltwater (JRF/SW) prior to testing.

PS899-B-2 sealant exhibited 100 percent cohesive failure on the new MIL-C-27725 coated panels, both wiped and unwiped. PS899-B-2 also underwent 100 percent cohesive failures in JRF on both wiped and unwiped C-130 panels. After saltwater aging, both wiped panels had 100 percent cohesive sealant failure. One unwiped panel, however, showed only 60 percent cohesive failure; the other unwiped panel showed 100 percent cohesive failure.

Another cleaning solution, DAP Inc. XMH-1-5, was compared to MIL-C-38736 cleaner in a program in which four adhesion promoters were also evaluated on artificially aged MIL-C-27725 polyurethane coated panels. The MIL-C-27725 coatings were subjected to an artificial aging procedure which eliminates free-isocyanates from the panel surfaces, thereby inhibiting adhesion of polysulfide sealants.^[17] MIL-C-27725 coatings were artificially aged by conditioning for 48 hrs at 250°F (121°C) in air followed by soaking in distilled water for 48 hrs at 140°F (60°C). After artificial aging, all MIL-C-27725 coatings with the exception of one set, were wiped with MIL-C-38736 cleaner before applying the respective promoters. The remaining set was wiped with XMH-1-5 cleaner only.

The adhesion promoters evaluated included Products Research PR-148, Essex Chemical Pro Seal 152, and Eldorado Chemical Bond Aid #6 and Bond Aid #7. Two sealants, PR-1422B-2, dichromate cure, and PS-890B-2, manganese cure, were applied to the panels containing the adhesion promoters. After fabrication, the peel panels were subjected to an accelerated cure of 48 hrs at 78°F (26°C) in 50 percent relative humidity plus 24 hrs at 140°F (60°C), then conditioned for seven days at 140°F (60°C) in JRF/SW prior to peel testing.

Products Research PR1422 B-2 was 100 percent cohesive on all panels, both aged and unaged, with and without the use of an adhesion promoter. Cohesive failure of Essex Chemical PS890-B-2 on aged panels, however, was dependent on the use of adhesion promoters. PS890-B-2, was 100 percent cohesive on unaged urethane and on aged panels treated with any of the adhesion promoters. With the exception of a 50 percent cohesive failure in the salt-water portion of an aged panel cleaned with XMH-15-1, all failures of aged panels cleaned with MIL-C-38736 and coated with PS890-B-2 were 100 percent adhesive.

Tests of the four adhesion promoters mentioned above, plus tests of three additional adhesion promoters, were conducted on

artificially aged MIL-C-27725 (DeSoto 832-011) coated panels. The adhesion promoters included DAP Clean and Prime Blue, Pro Seal 151 Red and Pro Seal 152 Blue, Product Research PR-147 and PR-148, and Eldorado Chemical Bond Aid #6 and Bond Aid #7. The coatings were again aged for 48 hrs at 250°F (121°C) in air plus 48 hrs at 140°F (60°C) in distilled water. After conditioning, the coatings were wiped with a selected adhesion promoter, and PS890-B-2 sealant was applied. Peel panels were given a standard 14 day cure at 78°F (24°C) and 50 percent relative humidity and then conditioned for seven days at 140°F (60°C) in JRF/SW solution.

The sealant on all artificially aged panels prepared without an adhesion promoter failed 100 percent adhesively during peel testing. All test panels containing one of the adhesion promoters exhibited 100 percent cohesive failure with the exception of one panel prepared with DAP Clean and Prime Blue, which had 80 percent cohesive failure in JRF.

Because of work being conducted in the sealant industry, other artificial agings were recommended. MIL-C-27725 urethane coated panels were artificially aged using two different processes, then used in an evaluation of eight adhesion promoters. The two artificial agings used were 120 hours in an open-arc weatherometer and the second aging was five days at 250°F (121°C) in air followed by two days at 140°F (60°C) in distilled water. The promoters evaluated were PS-152, red and blue, DAP red and blue, PR-147 (red) and PR-148 (blue), Bond Aid #6 (red) and #7 (blue). The two MIL-S-8802E sealants used were PS890-B-2, manganese dioxide cure, and PR1422 B-2, dichromate cure. After fabrication, the panels were conditioned at 140°F (60°C) in JRF/SW for seven days.

As in previous evaluations, PR1422 B-2 exhibited 100 percent cohesive failure with all adhesion promoters for both agings. Weatherometer aged panels with PS890-B-2 sealant over both Bondaid #6 and Bondaid #7 adhesion promoters, failed 100 percent

adhesively in both JRF and saltwater. All other aged panels with PS890-B-2 and all other adhesion promoters failed 100 percent cohesively in JRF. Panels containing PS890-B-2 with PR-147 and PS-152 had cohesive failures of 100 percent and 30 percent, respectively, in saltwater. The remaining panels failed 100 percent adhesively in saltwater.

Further evaluations of the performance of adhesion promoters in conjunction with a manganese dioxide cure sealant (PS899-B-2) and a dichromate cure sealant (PR1422 B-2) were initiated. Two types of adhesion promoters were used, Type I, in which no chlorinated materials are permitted, color coded blue; and Type II, which contains no restrictions concerning formulation, color coded red. There were two adhesion substrates, Acrylic sheet per MIL-P-5425A, 0.220 inch thick, and aluminum panels coated with MIL-C-27725 urethane which had been exposed to either of two different agings:

- (1) 12 days at 140°F (60°C) + 60 hours at 160°F (71°C) + 6 hours at 180°F (82°C) while immersed in Jet Reference Fluid (JRF) followed by 66 hours at 200°F (93°C) + 5 hours at 255°F (125°C) + 4 hours at 280°F (138°C) + 1.2 hours at 300°F (149°C) in an air circulating oven, and
- (2) 3 days at 140°F (60°C) in JRF + 4 hours at 250°F (121°C) in air circulating oven followed by 3 days at 140°F (60°C) in JRF.

All eight adhesion promoters were evaluated on the acrylic substrates using both sealants. The eight promoters evaluated were Bond Aid No. 6 and No. 7, Pro Seal PS-151 and PS-152, Product Research PR-147 and PR-148, and DAP Clean and Prime Blue and Clean and Prime Red. PS899-B-2 had 100 percent cohesive failure in peel strength testing for all adhesion promoters except Bond Aid No. 7 and PS-152. The panels with Bond Aid No. 7 achieved cohesive failures of 95 and 90 percent, respectively; these values, however, may have been due to nonuniformity of the primer on the panel surface. With PS-152, one panel had 100 percent cohesive failure and the other 75 percent cohesive

failure. This failure may also have been due to primer thickness and uniformity. PS899-B-2 failed 100 percent adhesively with no adhesion promoter. The PR1422 B-2 underwent 100 percent cohesive failure on the control panel and on all panels except Bond Aid No. 6 (40 percent cohesive), Clean and Prime Red (65 percent cohesive), Clean and Prime Blue (67 percent cohesive), and PR-147 (90 percent cohesive).

Four promoters only were evaluated on MIL-C-27725 coated panels, Bond Aid No. 6 and No. 7, and PS-151 and 152. For aging (1) on the MIL-C-27725 coating, PS899-B-2 had 100 percent adhesive failure on the unprimed panel but 100 percent cohesive failure on all primed panels after the peel panels were conditioned for seven days at 140°F (60°C) in JRF/SW. PR1422 B-2 had 100 percent cohesive failure on the unprimed panels and 100 percent cohesive failure on the primed panels after the peel panels were conditioned for seven days at 140°F (60°C) in JRF/SW.

For aging (2) on the MIL-C-27725 coating PS899-B-2 had 100 percent adhesive failure on the unprimed panels and 100 percent cohesive failure on all primed panels after the peel panels were conditioned for seven days at 140°F (60°C) in JRF/SW. PR1422 B-2 had 100 percent cohesive failure on the unprimed panel and 100 percent cohesive failure on all promoters except PS-151 in the JRF portion in which one panel had 40 percent cohesive and one had 95 percent cohesive failure. All peel panels were conditioned for seven days at 140°F (60°C) in JRF/SW.

4.3 PEEL STRENGTH EVALUATIONS

4.3.1 MIL-C-5541 Alodine Coating

Panels coated with an alodine coating conforming to MIL-C-5541 were evaluated for peel strength using Pro Seal 890B-2, batch C00244/C00245 and Pro Seal 890A-2, batch C9714812/C97149112. The MIL-C-5541 coatings were supplied by AAA, Arodite Corp., and the University of Dayton. The peel panels were cured using an accelerated cure of 48 hours at 78°F (26°C)/50 percent relative humidity plus 24 hours at 140°F (60°C).

After curing, the PS890-B-2 panels were conditioned for seven days at 140°F (60°C) in Jet Reference Fluid and saltwater (JRF/SW) and the PS890-A-2 panels were conditioned for seven days at 140°F (60°C) in JRF only and for seven days at 140°F (60°C) in JRF/SW.

The PS890-B-2 underwent 100 percent cohesive failure in both JRF and SW on MIL-C-5541 from AAA, and 100 percent cohesive failure in JRF on the Arodite coating. One panel containing Arodite coating, however, had 10 percent adhesive failure in SW. On Arodite coatings primed with PR-148, PS890-B-2 had 100 percent cohesive failure in both JRF and SW. A 100 percent cohesive failure was obtained on the University of Dayton MIL-C-5541 coating in JRF; however, one SW panel had 25 percent adhesive failure. Pro Seal 890A-2 sealant was evaluated on UD coated panels only and had 100 percent cohesive failures in both JRF and in JRF/SW.

4.3.2 Ion Vapor Deposited Coating

Steel panels with Ion Vapor Deposited (IVD) aluminum on one surface were evaluated for peel strength using three types of sealants. The sealants used were PS890-B-2, MIL-S-8802E, manganese cured; PS899-B-2, MIL-S-83430, manganese cured; and PR1422 B-2, MIL-S-8802E, dichromate cured. The sealants were applied to the panel surfaces containing a 0.4 mil IVD coating. The test panels were cured for 14 days at 78°F (26°C) and 50 percent relative humidity. After curing, the panels were conditioned for seven and 70 days, respectively, at 140°F (60°C) in JRF/SW with the test fluid being changed every 14 days. After conditioning for seven days in JRF/SW the PS890-B-2 had 100 percent adhesive failure in SW and 100 percent cohesive failure in the JRF. PS899-B-2 had 100 percent cohesive failure in JRF; however, one panel had a 20 percent adhesive failure in SW. The PR1422-B-2 had 100 percent cohesive failure in JRF and one panel had 20 percent adhesive failure in SW. After conditioning for 70 days at 140°F (60°C) in JRF/SW, the PS890-B-2

had 100 percent cohesive failure in JRF and 100 percent adhesive failure in the SW. The PS899-B-2 also had 100 percent cohesive failure in JRF and 100 percent adhesive failure in the SW, and the PRL422 B-2 had 100 percent cohesive failure in the JRF and SW. The portions of the IVD panels that were not coated with sealant were very badly corroded and pitted after aging for 70 days in SW.

4.3.3 Peel Test Methods

The Materials Research Laboratories of the Australian Department of Defense utilizes a metal adapter in place of the mesh or fabric overhang called out in test procedures for determining peel strength of sealants. Figures 58 and 59 depict the method used by the Australians for Instron testing.

A similar adapter has been used by UDRI to test peel panels in which the mesh or cloth tabs have failed before sealant peeling was initiated. No significant differences in peel strength performance were recorded during past testing between use of the cloth extension and use of the adapter.

The Australian method left some question as to which end of the panel was installed in the movable jaw of the test instrument. Two peel panels were tested at UDRI to determine if any differences in peel strength would result from the method of installation in the test apparatus. One panel was installed in the Scott test machine with the cloth extension in the lower, movable jaw and the metal panel in the upper, stationary jaw. Peel strength of the sealant was determined to be 31.5 pounds per inch width with 100 percent cohesive failure. The second panel was installed in the Scott tester with the cloth extension in the upper, stationary jaw and the metal panel in the lower, movable jaw. Measured peel strength was determined to be 28.6 pounds per inch with 100 percent cohesive failure. More scatter between peak loads was also noted with the latter method.

This end clamped in the lower jaw of the testing machine.

Cloth or Screen

Sealant

This end clamped in the upper jaw of the testing machine.

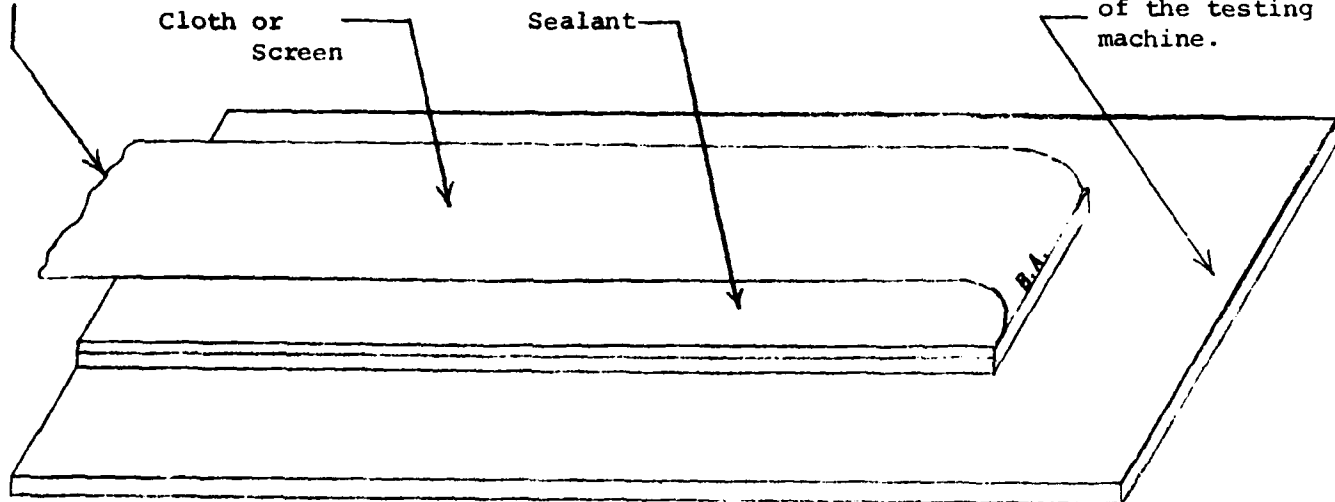


Figure 58. Standard Peel Test Panel.

This end clamped in the upper jaw of the testing machine.

Clamping attachment

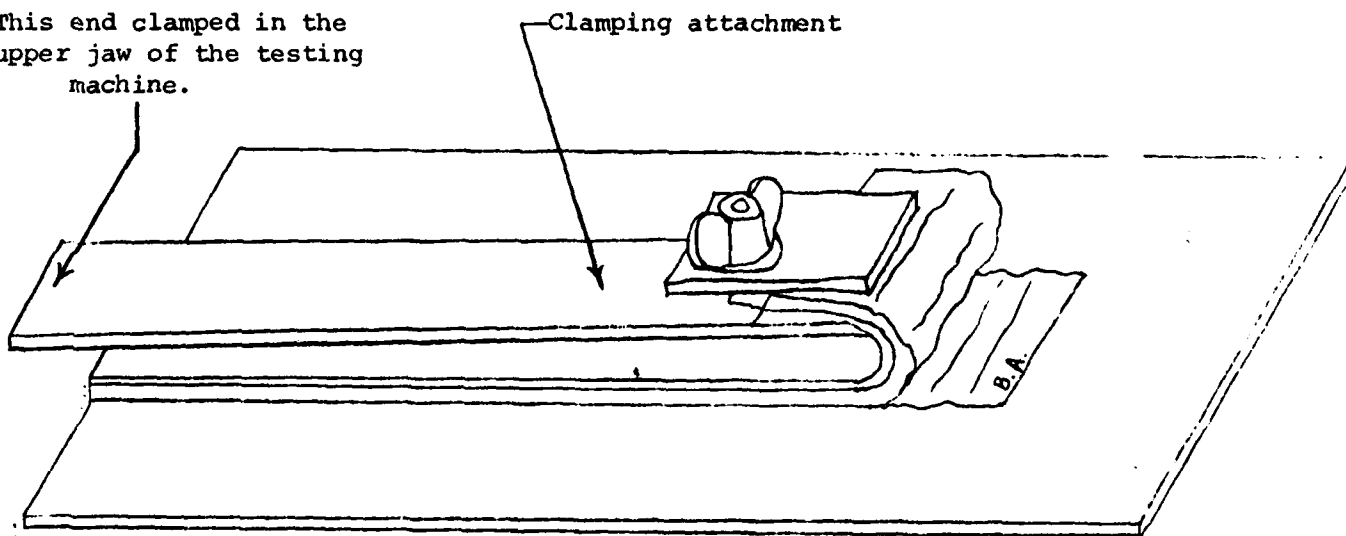


Figure 59. Peel Test Panel and Adapter.

4.3.4 Peel Test Differences

Because of reported differences between peel strength data obtained by certain sealant manufacturers and by UDRI, a peel test program to compare test methods was initiated with Products Research and Chemical Corporation (PRC). PRC supplied the University of Dayton with six peel panels and a quantity of unmixed sealant from each of PR1422 B-2 (Batch C67833) of PR1422-B-1/2 (Batch C33396). Three panels of each class fabricated by PRC were aged at PRC using PRC blended JRF. One peel strip on each test panel was tested at PRC. A second peel strip on each panel was later tested after receipt at UDRI. The remaining three unaged panels of each sealant fabricated by PRC were sent to UDRI. Two of these panels were conditioned for seven days at 140°F (60°C) in UD blended JRF and one panel was conditioned for seven days at 140°F (60°C) in UD-JRF/SW.

Eight peel panels of each PR1422 B-2 and PR1422 B-1/2 were fabricated at UDRI using the unmixed sealant supplied by PRC. Of these, four panels of each class were cured for 14 days at 78°F (26°C) and 50 percent relative humidity and four were subjected to an accelerated cure of 48 hours at 78°F (26°C) and 50 percent relative humidity plus 24 hours at 140°F (60°C). Two standard cure panels and two accelerated cure panels were then conditioned for seven days at 140°F (60°C) in UD blended JRF and the remaining two panels of each cure were conditioned at 140°F (60°C) in UD-JRF/SW.

The PR1422 B-2 peels fabricated and conditioned at PRC had an average load of 24.6 lbs. Panels fabricated at both PRC and UD and aged at UD in JRF had loads of approximately 13.0 lbs. The panels aged in JRF/SW at UD had loads of approximately 17.0 lbs in JRF and 21.0 lbs in SW. All panels had 100 percent cohesive failures.

PR1422 B-1/2 fabricated and conditioned at PRC had a load of 22 lbs. The panels fabricated at both PRC and UD and aged at UD in JRF had loads of approximately 13.0 lbs. The PR1422 B-1/2 panel fabricated at PRC but aged in the UD JRF/SW had loads of 28.3 lbs/35.3 lbs, respectively. These loads were higher than the loads attained on UD fabricated panels, both standard and accelerated cured. The 14-day standard cure in JRF/SW had loads of 19.0/21.6 lbs, respectively, and the accelerated cure in JRF/SW had loads of 20.5/27.8 lbs, respectively. All panels again exhibited 100 percent cohesive failures.

Because of the above differences, further peel tests were planned to evaluate any differences in mixing and fabrication techniques between PRC and UDRI. PRC supplied PR1422 B-2 sealant (Batch C37614) in both rotary pre-mixed frozen cartridges and in un-mixed kits. Peel panels were fabricated at UDRI by personnel from both PRC and UDRI. All panels were cured for 14 days at standard conditions and then aged for 7 days at 140°F (60°C) in JRF.

Peel test values obtained were consistent for all panels. They were, however, substantially lower than specification minimum. Subsequent evaluations of the sealant by the manufacturer indicated that an incorrect ratio of catalyst to base was incorporated into the sealant.

Thirty-two additional panels of PR1422 B-2 from a number of different batches, both hand and machine mixed, were prepared by PRC. Sixteen of these panels were tested at PRC and the remaining 16 panels were sent to UDRI for aging and testing. Results of testing at both PRC and UDRI were again consistent, most values within specification.

Two additional sealant kits in un-mixed form were supplied for fabrication at UDRI. Batch 40044 was supplied for direct comparison to the same batch prepared at PRC. Batch 40593 was an updated kit from Batch C37614 originally submitted and found to be below specification limits. Data for PR1422 B-2 are summarized in Table 32.

TABLE 32
PEEL TEST RESULTS
PR1422 B-2

Batch No.	Where Mixed	How Mixed	Cure Cycle	Where Conditioned	Conditioning Fluid	Peel Strength (lbs)	Cohesive Failure (%)
C67833	UDRI	Hand	Accel.	UDRI	UDRI-JRF	12.6	100
C67833	UDRI	Hand	Accel.	UDRI	UDRI-JRF/SW	18.4/21.5	100/100
C67833	UDRI	Hand	STD	UDRI	UDRI-JRF	13.0	100
C67833	UDRI	Hand	STD	UDRI	UDRI-JRF/SW	15.5/21.3	100/100
C67833	PRC	--	STD	PRC	UDRI-JRF	24.6	100
C67833	PRC	--	STD	UDRI	UDRI-JRF	13.6	100
C67833	PRC	--	STD	UDRI	UDRI-JRF/SW	16.7/20.8	100/100
C37614	PRC	Hand	STD	UDRI	PRC-JRF	9.0	100
C37614	PRC	Hand	STD	UDRI	UDRI-JRF	7.8	100
C37614	PRC	Rotary	STD	UDRI	PRC-JRF	10.5	100
C37614	PRC	Rotary	STD	UDRI	UDRI-JRF	12.7	100
C37614	UDRI	Hand	STD	UDRI	PRC-JRF	12.6	100
C37614	UDRI	Hand	STD	UDRI	UDRI-JRF	9.8	100
C37614	UDRI	Rotary	STD	UDRI	PRC-JRF	12.8	100
C37614	UDRI	Rotary	STD	UDRI	UDRI-JRF	16.8	100
H68564	PRC	Hand	STD	UDRI	UDRI-JRF	22.0	100
H40044	PRC	Hand	STD	UDRI	UDRI-JRF	22.4	100
40670	PRC	Rotary	STD	UDRI	UDRI-JRF	25.7	100
36973	PRC	Rotary	STD	UDRI	UDRI-JRF	27.3	100
40593	PRC	Rotary	STD	UDRI	UDRI-JRF	26.8	100
68361	PRC	Rotary	STD	UDRI	UDRI-JRF	26.8	100
H68361	PRC	Hand	STD	UDRI	UDRI-JRF	19.9	100
40044	PRC	Rotary	STD	UDRI	UDRI-JRF	25.8	100
H68564	PRC	Hand	Accel.	PRC	PRC-JRF	23.5	100
H40044	PRC	Hand	Accel.	PRC	PRC-JRF	19.5	100
H68361	PRC	Hand	Accel.	PRC	PRC-JRF	17.3	100
36973	PRC	Rotary	Accel.	PRC	PRC-JRF	25.0	100
68361	PRC	Rotary	Accel.	PRC	PRC-JRF	26.5	100
40044	PRC	Rotary	Accel.	PRC	PRC-JRF	25.5	100
40593	PRC	Rotary	Accel.	PRC	PRC-JRF	28.5	100
40670	PRC	Rotary	Accel.	PRC	PRC-JRF	25.0	100
H40044	UDRI	Hand	STD	UDRI	UDRI-JRF	18.3	100
H40593	UDRI	Hand	STD	UDRI	UDRI-JRF	34.4	100

4.4 EVALUATION OF O-RINGS

4.4.1 MIL-P-25732 O-Ring Seals

A series of tests to determine the effects of various fluid agings were conducted on MIL-P-25732 O-rings. The O-rings were aged 70 hours at 275°F (135°C) in MIL-H-5606C and MIL-H-5606C with MLO-79-483 additive, one part additive to eight parts of MIL-H-5606 by volume. The properties to be determined included hardness, tensile strength, percent elongation, volume change, 25 percent compression set, and low temperature retraction (TR-10).

The original set of data were obtained by conditioning Parker N304 O-rings to MIL-H-5606C from PENRECO. The O-rings aged in the MIL-H-5606C had a volume swell of 7.2 percent. Since N304 compound is qualified to MIL-P-25732 in which the requirement for volume swell is 10 to 20 percent, the O-rings were retested using MIL-H-5606C from Margolis and Sons. The O-rings had a volume swell of 15.0 percent in Margolis MIL-H-5606C. To check these data, Parco 4067 O-ring compound was evaluated in each batch of MIL-H-5606C. The 4067 compound had a swell of 14.9 percent in the PENRECO oil and an 18 percent volume swell in the oil from Margolis and Sons. To verify that both the Margolis and PENRECO oils were within MIL-H-5606C specification limits, fresh "L" stock was aged in each oil for 168 hours at 158°F (70°C). After conditioning, the "L" stock had a volume swell of 25.1 percent in the Margolis oil and had a volume swell of 20.8 percent in PENRECO oil. Since the MIL-H-5606C specification calls for "L" stock to have a swell of 19 to 30 percent, both fluids were determined to be within specification. Since the Parker N304 compound was not within specification in the PENRECO oil, it was reevaluated in the Margolis fluid with the MLO-79-483 additive. As shown in Table 33, the additive in both MIL-H-5606C fluids caused an increased volume swell of the O-ring compound.

AD-A122 004

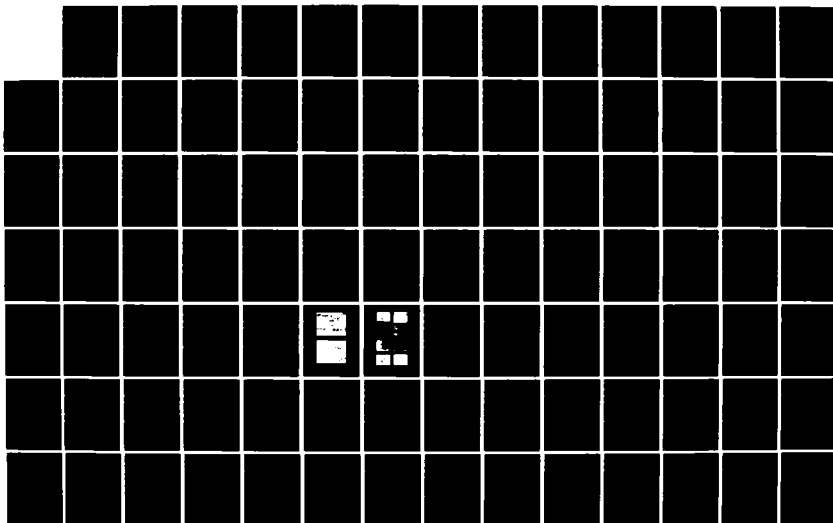
ARC EVALUATION OF MATERIALS AND PROCESSES(U) DAYTON
UNIV OH RESEARCH INST D R ASKINS ET AL. OCT 82
UDR-TR-82-85 AFWAL-TR-82-4104 F33615-80-C-5011

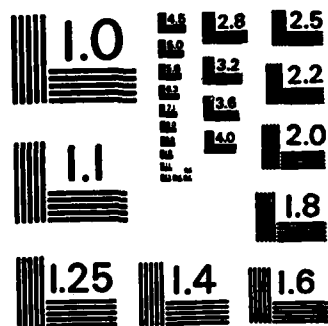
3/4

UNCLASSIFIED

F/G 14/2

NL





MICROCOPY RESOLUTION TEST CHART
NATIONAL BUREAU OF STANDARDS-1963-A

TABLE 33

PHYSICAL PROPERTIES OF O-RINGS IN MIL-H-5606
WITH AND WITHOUT MLO-79-483 ADDITIVE AFTER
AGING FOR 70 hrs AT 275°F(135°C)

Material	Oil	Additive	Hardness O-Ring Button	Elongation (%)	50% Modulus (psi)	Tens.Str. (psi)	Vol.Swell (%)	25% Comp. Set(%)	TR-10
Parker N304 Batch 239541	MIL-H-5606 (WPAPB)	---	70 76	106	352	986	7.2	42.9	-49°C (-56°F)
Parker N304 Batch 239541	MIL-H-5606 (WPAPB)	MLO-79-483	62 71	141	207	1190	21.1	34.3	-50°C (-58°F)
Parker N304 Batch 239541	MIL-H-5606 (WPAPB)	---	-- --	120	328	1093	9.0	---	
Parker N304 Batch 239541	MIL-H-5606 (Margolis)	---	-- --	125	288	985	15.0	---	
Parker N304 Batch 239541	MIL-H-5606 (Margolis)	MLO-79-483	-- --	137	---	1074	20.4	40.0	-51°C (-60°F)
Parco 4067	MIL-H-5606 (WPAPB)	---	-- --	152	292	1446	14.9	---	
Parco 4067	MIL-H-5606 (Margolis)	---	-- --	151	221	1277	18.0	---	
"L" Stock*	MIL-H-5606 (WPAPB)	---	-- --	---	---	---	20.8	---	
"L" Stock*	MIL-H-5606 (Margolis)	---	-- --	---	---	---	25.1	---	

* Aged at 158°F(70°C).

4.4.2 PNF O-ring Seals

Phosphazine (PNF) materials from Firestone were evaluated in O-ring and sheet stock form under a variety of different aging conditions. The three O-ring materials, identified as PNF 280-001R, PNF 270-003R, and PNF 290-003 were evaluated at seven different aging conditions. Properties evaluated were tensile strength, percent elongation, hardness, specific gravity, TR-10, percent compression set, percent volume swell, and percent weight loss. Not all properties were evaluated at each condition. The tensile strength, elongation, weight loss, TR-10, and hardness properties were evaluated on the original O-rings, on O-rings conditioned 70 hours at 347°F (175°C) in air, 70 hours at 392°F (200°C) in air, 70 hours at 347°F (175°C) in Stauffer Blend 7700, and aging for 22 hours at 77°F (23°C) in TT-S-735, Type III fluid. The compression set properties were evaluated after conditioning for 70 hours at 77°F (23°C), 22 hours at 347°F (175°C) in air, and 70 hours at 347°F (175°C) in Stauffer Blend 7700.

Three PNF sheet stock materials, PNF 270-003, PNF 280-009, and PNF 290-003 representing three hardness values, were evaluated for original properties; after 22 hours at 75°F (25°C) in TT-S-735, Type III fluid; after 22 hours at 347°F (175°C) in air (compression set only); after 70 hours at 302°F (150°C) in Stauffer 7700; after 70 hours at 347°F (175°C) in air; and after 70 hours at 275°F (135°C) in MIL-H-5606.

The PNF 280-001R O-rings showed a slight increase in tensile strength, elongation, and hardness after aging 70 hours at 347°F (175°C) in air. The PNF 270-003R and PNF 290-003 O-rings exhibited a slight increase in hardness and a decrease in elongation under the same conditions. All three O-ring compounds underwent a decrease in properties after aging 70 hours at 392°F (200°C) in air.

After 70 hours at 302°F (150°C) in Stauffer Blend 7700, all compounds underwent decreases in tensile

strength and hardness, and showed some increase in elongation and percent volume swell.

Both the PNF 280-001R and PNF 270-003R compounds also showed decreases in tensile strength and hardness, and an increase in elongation after aging for 70 hours at 347°F (175°C) in Stauffer Blend 7700. PNF 290-003 showed a decrease in tensile strength and elongation with a slight decrease in elongation. All three materials exhibited high volume swell and compression set in Stauffer's Blend 7700.

After aging for 22 hours in TT-S-735, Type III fluid, the PNF 280-004R, PNF 270-003R, and PNF 290-003 O-rings showed a loss in tensile strength and hardness, but indicated little change in elongation.

The tensile strength measurements for all three sheet stock materials were lowest after conditioning in the TT-S-735, Type III fluid, although the Stauffer 7700 caused almost as much damage to all the tensile strengths. All the materials had less elongation and higher volume swells in the TT-S-735, Type III fluid. The fluid that was the least degrading to all three materials was the MIL-H-5606. The swell was approximately half the other two fluids, with minimal effect on the elongations, tensile strength, and hardness of all three materials. The PNF 280-009 showed no loss of properties after being conditioned for 70 hours at 347°F (175°C) in air. The PNF 290-003 and PNF 280-003 lost tensile strength at 347°F (175°C) in air for 70 hours; however, the elongations and hardness properties did not change. All three materials had approximately a 1 percent weight loss after 70 hours at 347°F (175°C) in air.

The compression set properties of all three materials were evaluated at three conditions: 75 hours at 275°F (135°C) in MIL-H-5606, 70 hours at 302°F (105°C) in Stauffer 7700, and 22 hours at 347°F (175°C) in air. The PNF 270-003 had the lowest compression set at all three conditions. The

PNF 270-003 had its greatest compression set in Stauffer 7700 fluid. Compression set of PNF 280-009 and PNF 290-003 was the greatest in MIL-H-5606.

Evaluation of the materials as controls in TR-10 were not available because the specimens broke while being elongated. At the other three conditions, 70 hours at 302°F (150°C) in Stauffer 7700, 70 hours at 347°F (175°C) in air, and 70 hours at 275°F (135°C) in MIL-H-5606, TR-10 data were obtained. The PNF 290-003 had the highest TR-10 in all fluids; PNF 270-003 and PNF-280-009 had the same TR-10 values except at 70 hours at 275°F (135°C) in MIL-H-5606 where the PNF 280-009 would not elongate to 50 percent without breaking. TR-10 measurements were attempted on six specimens of PNF 280-009.

4.4.3 Corrosion Test of Hydraulic Seals

There is a potential problem of corrosion of elastomeric seals in MIL-H-83282 hydraulic fluid. To provide comparative data, three seal materials were tested for corrosion in accordance with MIL-P-25732C using MIL-H-6083, Type I fluid. The same three materials were also evaluated for corrosion on 4130 steel using MIL-H-5606 hydraulic fluid and using MIL-H-83282 hydraulic fluid. The three materials evaluated included T-seals manufactured by Green-Tweed, T-seals manufactured by Parker, and Precision 7377-214 O-rings previously qualified to MIL-P-25732C. The T-seals showed no corrosion, pitting, or discoloration or any of the metals specified in MIL-P-25732C, except on 4130 steel after 14 days at 77°F (25°C) in 95 percent relative humidity. The Green-Tweed T-seals had slight pitting and corrosion on 4130 steel with MIL-H-5606C, slight pitting and discoloration with MIL-H-83282, and no change with the MIL-H-6083. The Parker T-seals showed slight pitting and discoloration on 4130 steel with MIL-H-5606, severe pitting and corrosion with MIL-H-83282, and no change with MIL-H-6083. The Precision 7377 O-rings exhibited slight corrosion on 4130 steel with MIL-H-5606, and severe pitting and corrosion with

each of the MIL-H-83282 and MIL-H-6083 fluids. Additional corrosion tests of Parker T-seals were then conducted on both 4130 steel and 304 stainless steel after conditioning for 70 hours at 180°F (82°C) at 95 percent relative humidity using each of the three hydraulic fluids, MIL-H-5606C, MIL-H-83282, and MIL-H-6083. 4130 steel showed severe pitting and corrosion. No change was noted on 304 stainless steel. Precision 7377 O-rings were also evaluated at 180°F (82°C) in 95 percent relative humidity on 4130 steel and 304 stainless steel using MIL-H-5606C and MIL-H-83282. There was severe corrosion and pitting on the 4130 steel and no change on the 304 stainless steel. Because of the limited number of seals available, Green-Tweed seals were not evaluated at the elevated temperature.

4.5 MATERIALS COMPATIBILITY IN JP-10 FUEL

The compatibility of seven different seal and sealant materials in JP-10 aircraft fuel was determined during a 12-month evaluation program. The materials included Parker N602-70, MIL-P-5315 Buna-N O-rings; Parker L677-70, MIL-R-25988 Type I, Class 1, Grade 70 fluorosilicone O-rings; Parker V747-75, MIL-R-83248, Type I, Class 1 fluoroelastomer O-rings; C-147-70, MIL-R-1149, Type II, Class 1 (65 hardness) neoprene O-rings; Pro Seal 890B-2, MIL-S-8802 polysulfide sealant; Ultraseal PC 504 impregnant from Imprex; and Loctite PMS 10E impregnant from Loctite Corp.

The four O-ring materials were evaluated for tensile strength and elongation, hardness, volume swell, TR-10, and compression set properties. The polysulfide sealant was evaluated for tensile strength and elongation, hardness, volume swell, and peel strength on MIL-C-27725 coated panels. The two impregnants were observed for softening, tackiness, and cracking. The following agings in JP-10 fuel were used for the evaluation:

- (1) 7 days at 75°F (23°C) in JP-10;
- (2) 6 months at 75°F (23°C) in JP-10;

- (3) 7 days at 140°F (60°C) in JP-10;
- (4) 1 month at 140°F (60°C) in JP-10;
- (5) 3 months at 140°F (60°C) in JP-10;
- (6) 6 months at 140°F (60°C) in JP-10;
- (7) 9 months at 140°F (60°C) in JP-10; and
- (8) 12 months at 140°F (60°C) in JP-10.

The test data are summarized in Tables 34 through 40. C-147-70 neoprene was the most severely affected O-ring material after aging in JP-10 fuel. The material lost approximately two-thirds of its original tensile strength and exhibited very large volume swell after just seven days in JP-10. Loctite PMS10E impregnant became badly cracked after aging six months in JP-10.

4.6 MATERIALS COMPATIBILITY WITH SHALE OIL DERIVED FUEL

An extensive program to evaluate the effect of JP-4 derived from shale oil on elastomeric materials, structural adhesives, and coating was conducted. Properties of the materials were determined after various agings in petroleum JP-4 and shale oil derived JP-4 for up to six months.

Results of the evaluation indicated that Buna-N O-ring materials are seriously affected by the shale oil derived fuel. All other materials underwent comparable performance in both petroleum and shale oil derived JP-4. Data are to be summarized in a technical report describing the entire program.

4.7 POLYURETHANE POTTING COMPOUND

A low density polyurethane potting compound was evaluated in the laboratory for the feasibility of replacing the filler, Saran Micropheres, with water to obtain a 10 percent foam. Calculations of the required water content to provide the 10 percent foam were made and it was determined that 0.03 grams of water were required for 300 grams of resin. The material was subsequently evaluated at four levels: no water, 0.03 grams

TABLE 34
MATERIALS COMPATIBILITY IN JP-10 FUEL
MIL-P-5315 BUNA-N N602 O-RINGS

Conditioning	Tensile Strength		Elong. (%)	Vol. Change (%)	Comp. Set (%)	TR-10		Hardness (pts)
	(psi)	(MPa)				(°F)	(°C)	
None	1440	9.93	360	---	---	-44	-42	70
7 days @ 75°F (24°C) in JP-10	1160	8.00	320	30.8	-3.7	-51	-46	61
6 mths. @ 75°F (24°C) in JP-10	1240	8.55	340	29.5	-0.3	-53	-47	60
7 days @ 140°F (60°C) in JP-10	1200	8.27	320	37.8	-2.2	-51	-46	59
1 mth. @ 140°F (60°C) in JP-10	1170	8.07	315	35.6	1.5	-54	-48	60
3 mths. @ 140°F (60°C) in JP-10	1170	8.07	295	37.5	3.6	-54	-48	55
6 mths. @ 140°F (60°C) in JP-10	1170	8.07	295	37.3	2.9	-51	-46	56
9 mths. @ 140°F (60°C) in JP-10	1190	8.2	285	36.2	5.1	-56	-49	60
12 mths. @ 140°F (60°C) in JP-10	1120	7.72	260	37.8	8.8	-58	-50	60

TABLE 35

MATERIALS COMPATIBILITY IN JP-10 FUEL
MIL-R-83248 FLUOROELASTOMER V747-75 O-RINGS

Conditioning	Tensile Strength		Elong. (%)	Vol. Change (%)	Comp. Set (%)	TR-10		Hardness (pts)
	(psi)	(MPa)				(°F)	(°C)	
None	1680	11.56	200	---	---	1	-17	75
7 days @ 75°F (24°C) in JP-10	1400	9.65	170	0.3	2.2	-8	-22	79
6 mths. @ 75°F (24°C) in JP-10	1550	10.69	200	0.7	4.0	1	-17	84
7 days @ 140°F (60°C) in JP-10	1360	9.38	165	1.3	2.5	-18	-28	77
1 mth. @ 140°F (60°C) in JP-10	1800	12.41	230	1.5	2.5	0	-18	77
3 mths. @ 140°F (60°C) in JP-10	1820	12.55	215	2.7	2.9	-4	-20	82
6 mths. @ 140°F (60°C) in JP-10	1800	12.41	220	1.4	2.2	0	-18	80
9 mths. @ 140°F (60°C) in JP-10	1660	11.44	200	3.0	3.6	-10	-23	79
12 mths. @ 140°F (60°C) in JP-10	1760	12.15	365	2.8	2.2	-4	-20	75

TABLE 36
MATERIALS COMPATIBILITY IN JP-10 FUEL
MIL-R-25988 FLUROSILICONE L677-70 O-RINGS

Conditioning	Tensile Strength		Elong. (%)	Vol. Change (%)	Comp. Set (%)	TR-10		Hardness (pts)
	(psi)	(MPa)				(°F)	(°C)	
None	1100	7.58	300	---	---	-74	-59	70
7 days @ 75°F (24°C) in JP-10	860	5.93	270	8.7	0.6	-83	-64	69
6 mths. @ 75°F (24°C) in JP-10	940	6.48	300	8.1	2.2	-80	-62	69
7 days @ 140°F (60°C) in JP-10	950	6.55	300	10.1	0.0	-83	-64	70
1 mth. @ 140°F (60°C) in JP-10	950	6.55	295	9.5	0.7	-83	-64	69
3 mths. @ 140°F (60°C) in JP-10	1040	7.17	330	10.2	2.6	-85	-65	69
6 mths. @ 140°F (60°C) in JP-10	900	6.20	290	10.0	3.3	-80	-62	69
9 mths. @ 140°F (60°C) in JP-10	940	6.48	275	10.2	2.2	-85	-65	71
12 mths. @ 140°F (60°C) in JP-10	980	6.8	275	9.9	3.0	-83	-64	70

TABLE 37
MATERIALS COMPATIBILITY IN JP-10 FUEL
MIL-R-1149 NEOPRENE O-RINGS

Conditioning	Tensile Strength		Elong. (%)	Vol. Change (%)	Comp. Set (%)	TR-10		Hardness (pts)
	(psi)	(MPa)				(°F)	(°C)	
None	2230	15.37	285	---	---	-33	-36	70
7 days @ 75°F (24°C) in JP-10	725	5.00	180	97.9	-5.8	---*	---	60
6 mths. @ 75°F (24°C) in JP-10	640	4.41	190	100.7	-2.1	---*	---	52
7 days @ 140°F (60°C) in JP-10	740	5.10	190	110.7	-5.8	-85**	-65	59
1 mth. @ 140°F (60°C) in JP-10	580	4.00	180	116.0	-2.5	---*	---	55
3 mths. @ 140°F (60°C) in JP-10	590	4.07	195	120.8	2.5	---*	---	55
6 mths. @ 140°F (60°C) in JP-10	540	3.72	205	128.0	3.9	-94	-70	47
9 mths. @ 140°F (60°C) in JP-10	510	3.52	215	134.0	6.2	---*	---	52
12 mths. @ 140°F (60°C) in JP-10	440	3.03	210	140.5	10.6	---*	---	53

* Broke in test fixture -- Very high swell.

** Better than -85°F (-65°C) -- Very high swell.

TABLE 38
MATERIALS COMPATIBILITY IN JP-10 FUEL
MIL-S-8802 POLYSULFIDE PS-890B-2

Conditioning	Peel Strength		Failure Mode (% Coh)	Tensile Strength		Elong. (%)	Vol. Change (%)	Hardness (pts)
	(lbs/in)	(N/cm)		(psi)	(MPa)			
None	40.3	70.6	100	350	2.41	275	---	55
7 days @ 75°F (24°C) in JP-10	40.2	70.4	100	300	2.07	370	1.8	54
6 mths. @ 75°F (24°C) in JP-10	37.3	65.3	100	550	3.80	270	4.9	51
7 days @ 140°F (60°C) in JP-10	41.3	72.3	100	290	2.00	325	4.0	50
1 mth. @ 140°F (60°C) in JP-10	29.6	51.8	100	300	2.07	285	6.9	49
3 mths. @ 140°F (60°C) in JP-10	30.3	53.1	100	290	2.00	345	11.0	50
6 mths. @ 140°F (60°C) in JP-10	22.4	39.2	100	530	3.65	230	12.4	50
9 mths. @ 140°F (60°C) in JP-10	20.7	36.2	100	250	1.72	220	---	48
12 mths. @ 140°F (60°C) in JP-10	17.0	29.8	100	240	1.66	230	14.3	45

TABLE 39
MATERIALS COMPATIBILITY IN JP-10 FUEL
IMPREX (ULTRASEAL PC504 IMPREGNANT)

Conditioning	Observations
7 days @ 75°F (24°C) in JP-10	No change
6 months @ 75°F (24°C) in JP-10	No change
7 days @ 140°F (60°C) in JP-10	Softened; no tackiness or cracking
1 month @ 140°F (60°C) in JP-10	Softened; no tackiness or cracking
3 months @ 140°F (60°C) in JP-10	Softened; no tackiness or cracking
6 months @ 140°F (60°C) in JP-10	Softened; no tackiness or cracking
9 months @ 140°F (60°C) in JP-10	Softened; no tackiness or cracking
12 months @ 140°F (60°C) in JP-10	No tackiness or cracking

TABLE 40
MATERIALS COMPATIBILITY IN JP-10 FUEL
LOCTITE (LOCTITE PMS 10E IMPREGNANT)

Conditioning	Observations
7 days @ 75°F (24°C) in JP-10	No change
6 months @ 75°F (24°C) in JP-10	No change
7 days @ 140°F (60°C) in JP-10	No change
1 month @ 140°F (60°C) in JP-10	No change
3 months @ 140°F (60°C) in JP-10	No change
6 months @ 140°F (60°C) in JP-10	Cracked badly
9 months @ 140°F (60°C) in JP-10	Cracked badly; softened; being attacked
12 months @ 140°F (60°C) in JP-10	Cracked badly; softened; surface flaking

of water per 300 grams resin, 0.06 grams water per 300 grams resin, and 0.1 grams of water per 300 grams of resin. The material was evaluated for density, brittleness temperature, tensile strength, compression set, and long term properties at 160°F (71°C) and 95 percent relative humidity. In the formulation specification, the cure time for the foam was given as 16 hours at 78°F (26°C). It was determined in the laboratory, however, that this was not adequate time for the material to reach full properties. To obtain full properties, the foam had to be postcured for 48 hours at 160°F (71°C).

4.8 BOSTIK NO. 7102 USING THE "MERCER HOT MELT APPLICATOR"

Bostik 7102, a hot melt polyester, was evaluated for curing rate, tensile strength, hardness, thermal rupture, low temperature flexibility, peel strength, corrosion, and resistance to humidity. All the specimens were prepared using a "Mercer Hot Melt Applicator." Specimens for all the above tests were originally fabricated with an applicator supplied from General Dynamics. Because of a design change, a second applicator gun was supplied by General Dynamics, and tensile, low temperature flexibility, and thermal rupture specimens were fabricated using the newly designed gun. To evaluate the curing rate of the hot melt sealant, hardness measurements were taken every hour for eight hours, then 24 hours later at which time the hardness leveled off. The material was evaluated for tensile strength after six hours at 78°F (26°C), 24 hours at 78°F (26°C), 96 hours at 78°F (26°C), 7 days at 78°F (26°C), 14 days at 78°F (26°C), 14 days at 160°F (71°C), and 14 days at 160°F (71°C) in distilled water. The material was also evaluated after conditioning at 160°F (71°C)/95 percent relative humidity for 7 days, 30 days, 60 days, 90 days, and 120 days. The material deteriorated after being conditioned for 120 days at 160°F (71°C)/95 percent relative humidity. Gun No. 2 tensile specimens were evaluated at 160°F (71°C)/95 percent relative humidity and at 160°F (71°C). The peel strength

qualities of the Bostik 7102 were evaluated on MIL-P-23377 epoxy coated panels after curing 96 hours at 78°F (26°C). Both the control specimens and specimens conditioned for 14 days at 160°F (71°C) exhibited 100 percent adhesive failure. The panels conditioned in JP-4, water, and MIL-A-8243B deicer underwent 100 percent cohesive failure. Low temperature flexibility specimens were also evaluated on the MIL-P-23377 coating after curing 96 hours at 78°F (26°C) and the specimens made with the original applicator gun failed after all preconditioning. Specimens made with the redesigned gun, however, did not fail when tested as controls only. Similar results were obtained for the thermal rupture specimens. All specimens that were fabricated with the old design gun failed, and all specimens that were fabricated with the new gun passed. Although no temperature profile was measured for the first gun used for applying the Bostik adhesive, the gun did give off smoke during application. The redesigned gun did not emit smoke during use. The temperature of the metal block on the applicator gun was measured using a thermocouple and the temperature ranged from 170°F (77°C) to 350°F (177°C).

4.9 GENERAL ELECTRIC TUFEL SILICONE

General Electric Tufel silicone materials SE845 and SE875 were evaluated for original properties, after aging for 70 hours at 392°F (200°C) in air, and after aging for 70 hours at 212°F (100°C) in water. Tests conducted at all three conditions were hardness, tensile strength, percent elongation, 100 percent modulus, tear strength, and TR-10. Specific gravity was also measured for the unaged materials. Compression set was determined after aging 22 hours and after aging 70 hours at 392°F (200°C) in air and after aging 70 hours at 212°F (100°C) in air.

The SE875 was a much harder material than SE845 and exhibited lower percent elongation with higher modulus and tear strength although SE875 and SE845 had the same tensile strength. Except for a decrease in percent elongation, all properties of SE845 showed increased values after aging for 70 hours at

392°F (200°C). SE875, however, showed an increase in 100 percent modulus but other properties were considerably lower after aging.

No major effects on either material were noted after aging for 70 hours at 212°F (100°C) in water. SE875 did show a slight decrease in tensile strength and percent elongation.

Both materials exhibited large compression set values after air aging at both temperatures. SE875 had the greater compression set in each case.

4.10 EVALUATION OF F-16 FUEL BLADDER

A leaking fuel bladder taken from an F-16 aircraft was received by the University of Dayton for evaluation. The bladder was evaluated for permeability, puncture resistance, weight per unit area, and thickness of construction plies. The permeability samples were taken from both the mandrel area and at several other ply build-up areas. According to MIL-T-6396C, permeability must be less than 0.025 fl.oz./ft²/24 hrs. The highest value determined for the selected bladder samples was 0.022 fl.oz./ft²/24 hrs. Puncture resistance was also conducted according to MIL-T-6396C where the minimum allowable puncture load is 15 pounds. The measured load was 65.2 pounds on two bladder specimens. The weight of a single thickness of inner fuel tank construction was specified to be 0.210 lbs/ft². An average weight per area of 0.179 lbs/ft² was determined from five specimens of bladder construction. The thickness was measured by photographing bladder cross-sections from the mandrel area and then photographing a scale at the same magnification. The specification requires the bladder construction to be 0.035 inch thick. Measured thicknesses, however, ranged from 0.030 inch to 0.034 inch. The photographs also contained evidence of some low quality fabrication causing large voids between plies and some wrinkling when one ply was rolled upon the next. The data for all tests are summarized in Table 41.

TABLE 41
F-16 FUEL BLADDER EVALUATION

Puncture Resistance

65.2 lbs
65.2 lbs

Permeability*

<u>Location</u>	<u>Results</u> <u>Fl.oz./ft²/24 hrs.</u>
Mandrel	0.022 0.007
Mandrel	0.022 0.000
Connector	0.000
Buildup	0.015
Connector	0.015
Buildup	0.022

Weight Per Unit Area

0.181 lbs/ft²
0.185
0.176
0.177
0.178

Thickness

0.031 in.
0.034 in.
0.031 in.
0.030 in.

* Scatter may be due to irregularity of specimen thickness.

4.11 EXTERIOR FUEL TANK COATINGS

Two materials used as exterior coatings on fuel tanks of commercial aircraft were evaluated for potential use on military aircraft. PR-1196 is a two-part sprayable polyurethane coating from Products Research Corporation, and 473-13 is a two component epoxy system from Bostik.

These two materials were evaluated for tensile strength, percent elongation, volume change, adhesion to MIL-P-23377 primer (cured two hours at 200°F (93°C)), adhesion to MIL-S-8802D sealant, low temperature flexure on MIL-P-23377 (cured two hours at 200°F (93°C)) and on MIL-S-8802D sealant, and for performance under dynamic cycling.

The tensile strength, volume change, and elongation were evaluated after conditioning at each of the following: 7 days at 140°F (60°C)/JRF; 7 days at 140°F (60°C) in H₂O; or 120 days at 160°F (71°C)/95 percent relative humidity. The data are shown in Tables 42 and 43, respectively, for PR-1196 and Bostik 473-13.

Both materials were evaluated for low temperature flexibility characteristics on MIL-P-23377 primer (two hours at 200°F (93°C) cure) and on MIL-S-8802D sealant. The material was tested prior to aging and after aging 7 days at 250°F (121°C). Results are shown in Table 44. The materials were also evaluated with a functional test using 14-1/2 inch split discs with MIL-P-23377 primer cured two hours at 200°F (93°C). The discs were spray coated with either PR-1196 or Bostik 473-13, then placed in a fuel test fixture. The fixture was then filled with JP-4 and pressure was applied to the panel in 30 second intervals starting at 0.5 psi pressure. The panel was cycled for one week at pressure with pressure increases in 0.5 psi increments until leakage occurred. Test results are given in Table 45.

The PR-1196 and Bostik 473-13 were evaluated for adhesion to a MIL-S-8802D fuel tank sealant and for adhesion to MIL-P-23377 cured two hours at 200°F (93°C). The test panels were laid up as

TABLE 42

PR-1196

TENSILE STRENGTH, ELONGATION AND VOLUME SWELL

Conditioning	Ultimate Tensile Str. psi (MPa)		Elongation (%)	Volume Swell (%)
Control	317	(2.19)	120	
Control	318	(2.19)	120	
Control	312	(2.15)	135	
Control	<u>314</u>	<u>(2.16)</u>	<u>135</u>	
Avg.	315	(2.17)	128	
7 days @ 140°F (60°C) in JRF	185	(1.28)	65	15.47
	175	(1.21)	50	17.79
	<u>184</u>	<u>(1.27)</u>	<u>70</u>	<u>16.49</u>
Avg.	181	(1.25)	62	16.58
7 days @ 140°F (60°C) / H ₂ O	189	(1.30)	30	2.09
	214	(1.48)	80	1.81
	241	(1.66)	100	1.85
	<u>244</u>	<u>(1.68)</u>	<u>95</u>	<u>1.81</u>
Avg.	222	(1.53)	76	1.89
120 days @ 165°F (74°C) / 95% R.H.	247	(1.70)	80	
	241	(1.66)	80	
	242	(1.67)	70	
	<u>495</u>	<u>(3.41)</u>	<u>90</u>	
Avg.	306	(2.11)	80	

TABLE 43
BOSTIK 473-13
TENSILE STRENGTH, ELONGATION AND VOLUME SWELL

Conditioning	Ultimate Tensile Str. psi (MPa)		Elongation (%)	Volume Swell (%)
Control	2164	(14.92)	40	---
Control	2219	(15.30)	40	---
Control	<u>2000</u>	<u>(13.79)</u>	<u>25</u>	---
Avg.	2128	(14.67)	35	
7 days @ 140°F (60°C)/JRF	800	(5.52)	40	19.49
	926	(6.38)	50	19.04
	710	(4.89)	30	19.88
	767	(5.29)	25	19.88
	<u>819</u>	<u>(5.65)</u>	<u>20</u>	<u>19.78</u>
Avg.	804	(5.54)	33	19.61
7 days @ 140°F (60°C)/H ₂ O	1774	(12.23)	45	0.071
	1717	(11.84)	50	0.210
	1582	(10.91)	40	0.209
	1727	(11.91)	60	0.040
	<u>1424</u>	<u>(9.82)</u>	<u>45</u>	<u>0.211</u>
Avg.	1645	(11.34)	48	0.148
120 days @ 160°F (74°C)/95% R.H.	778	(5.36)	35	---
	855	(5.89)	32	---
	803	(5.54)	20	---
	<u>954</u>	<u>(6.58)</u>	<u>40</u>	---
Avg.	848	(5.85)	32	

TABLE 44
LOW TEMPERATURE FLEXIBILITY

SPECIMEN			RESULTS
7075 Clad/PR-1422/PR-1196	orig.	#1	Failed
	orig.	#2	Passed
	aged	#1	Passed
	aged	#2	Passed
23377 (200°F)/PR-1196	orig.	#1	Passed
	orig.	#2	Passed
	aged	#1	Passed
	aged	#2	Passed
7075 Clad/PR-1422/Bostik	orig.	#1	Failed
	orig.	#2	Failed
	aged	#1	Failed
	aged	#2	Failed
2337 (200°F)/Bostik	orig.	#1	Passed
	orig.	#2	Passed
	aged	#1	Passed
	aged	#2	Passed

Aging Conditions: 7 days @ 250°F (121°C).

TABLE 45
DYNAMIC CYCLING - WITH JP-4

PR-1196

Date Started	Pressure lbs.	kgs.	Results
1-8-80	0.5	0.23	No Leakage
1-15-80	1.0	0.05	No Leakage
1-22-80	2.0	0.90	Leakage after 24 hours at seam and one fastener.
Bostik 473-13			
1-22-80	0.5	0.23	No Leakage
1-29-80	1.0	0.05	Leakage after 6 days at two connectors.

shown in Figure 60, Type I, to evaluate adhesion to the sealant. Peel panels were constructed as shown in Type II of Figure 60 to evaluate the coating on MIL-P-23377 (200°F (93°C) cure). As shown in Table 46, PR-1196 failed cohesively after conditioning in H₂O for both types of layups. After aging in JRF, however, the PR-1196 failed 100 percent adhesively at the PR-1422 interface in both Type I and Type II layup.

As indicated in Table 47, the Type II Bostik 473-13 layup failed 50 percent cohesively after aging in H₂O and 100 percent adhesively in JRF. The Type I configuration of Bostik 473-13 had 100 percent cohesive failure in H₂O and 100 percent adhesive failure at the PR-1422 interface in JRF.

In order to eliminate adhesive failures at the sealant/coating interface, additional peel panels were fabricated using thin layered construction similar to Class A-2 sealant per MIL-S-83430. PR-1196 again failed in the layered areas prior to peel testing. Bostik 473-13 exhibited cloth failure at less than ten pounds per inch width.

TYPE ONE

8802 D SEALANT
EXTERIOR COATING
8802 D SEALANT
7075 CLAD

TYPE TWO

8802 D SEALANT
EXTERIOR COATING
23377 (200°F)

Figure 60. Peel Panel Lay-Up Order.

TABLE 46
PR-1196
PEEL STRENGTH

Specimen No.	Type Layup	Conditioning	Load		Failure Mode
			Lbs.	Kgs.	
1	2	7 Days @ 140°F/H ₂ O	51.1	23.18	100% Cohesive
2	2	7 Days @ 140°F/H ₂ O	<u>51.4</u>	<u>23.32</u>	100% Cohesive
Avg.			51.3	23.27	
1	2	7 Days @ 140°F/JRF	0		100% Failure of PR-1422 from PR-1196
2	2	7 Days @ 140°F/JRF	<u>0</u>		100% Failure of PR-1422 from PR-1196
Avg.			0		
1	1	7 Days @ 140°F/H ₂ O	23.9	10.84	100% Cohesive failure in PR-1196
2	1	7 Days @ 140°F/H ₂ O	<u>22.0</u>	<u>9.98</u>	100% Cohesive failure in PR-1196
Avg.			23.0	10.43	
1	1	7 Days @ 140°F/JRF	0		Failed @ PR-1196
2	1	7 Days @ 140°F/JRF	<u>0</u>		PR-1422 Interface
Avg.			0		

TABLE 47
BOSTIK 473-13
PEEL STRENGTH

Specimen No.	Type Layup	Conditioning	Load		Failure Mode
			Lbs.	Kgs.	
1	2	7 Days @ 140°F/JRF	0		100% Adhesive
2	2	7 Days @ 140°F/JRF	0		100% Adhesive
Avg.			0		
1	2	7 Days @ 140°F/H ₂ O	14.25	6.46	50% Cohesive/ 50% Adhesive
2	2	7 Days @ 140°F/H ₂ O	16.50	7.48	50% Cohesive/ 50% Adhesive
Avg.			15.38	6.98	Cohesive Failure in PR 1422
1	1	7 Days @ 140°F/JRF	0		Failed @ 1422 - Bostik
2	1	7 Days @ 140°F/JRF	0		473 Interface
Avg.			0		
1	1	7 Days @ 140°F/H ₂ O	25.1	11.39	100% Cohesive Failure
2	1	7 Days @ 140°F/H ₂ O	19.4	8.80	@ First layer of PR-1422
Avg.			22.3	10.12	

SECTION 5

PLASTICS, ADHESIVES, AND COMPOSITES

5.1 SHELTER HONEYCOMB CORE SHEAR TESTING

In recent years, there has been a growing need for the hardening of honeycomb constructed shelters against both small arms fire and nuclear blast. In the case of nuclear blast the honeycomb core may be subjected to very high shear stresses. Therefore, a program was initiated to determine the shear strength of existing and candidate shelter honeycomb core materials. The testing variables of prime interest were strain rate, temperature, and high humidity degradation.

Three strain rates were used to measure the core shear strengths: 0.05, 4, and 300 inches/min. (0.127, 10.2, and 762 cm/min., respectively). Four test conditions were selected: -65°F (-54°C), 72°F (22°C), 200°F (93°C), and 200°F (93°C) after 14 days at 200°F (93°C) and 95-100 percent relative humidity.

Initially, two types of honeycomb core were to be characterized. The first, WR-II, is a core fabricated from resin impregnated Kraft® paper which is designed primarily for use in the construction of portable shelters. The second, HRP-10, is resin impregnated DuPont NOMEX® aramid fiber designed for high strength and toughness. These two core materials were supplied by Hexcel. Later in the program two additional types of core were added. These honeycomb core materials were supplied by the Shelter Repair Depot at McClellan Air Force Base in Sacramento, California. The additional materials were HRP, manufactured by Hexcel, and HTP, manufactured by Orbitex (Ciba-Geigy Corporation). The characteristics of the four different types of core which were tested are presented in Table 48.

Shear tests were performed in both the "L" and "W" directions, at all four test conditions and three strain rates, on each of the types of core listed in Table 48.

TABLE 48
SHELTER CORE MATERIAL CHARACTERISTICS

Material Designation	Cell Size		Density		Thickness	
	(inch)	(mm)	(lb/ft ³)	(kgs/m ³)	(inch)	(mm)
HRH-10	0.25	6.4	4.8	76.9	0.5	12.7
	0.25	6.4	4.8	76.9	2	50.8
	0.25	6.4	4.8	76.9	3	76.2
WR-II	0.38	9.5	3.8	60.9	0.5	12.7
	0.38	9.5	3.8	60.9	2	50.8
HRP	0.38	9.5	4.5	72.1	1.5	38.1
HTP	0.38	9.5	3.2	51.3	0.87	22.2
HTP	0.38	9.5	4.5	72.1	0.87	22.2

Two different tests can be conducted to determine core shear properties; plate shear (ASTM C273), and beam shear (ASTM C393). Either test was initially felt to be acceptable but both were to be conducted on some materials for comparison of data.

After some preliminary testing, however, it was clear that for high strain rates and after high humidity aging, in particular for thick core, the plate shear method was unsatisfactory because the plates would debond from the core before the core failed in shear. Most of the data were consequently obtained using the beam shear method.

The core shear properties which were obtained using the plate shear method are shown in Table 49. Comparable data for the same material and test conditions using the beam shear method are presented in Table 54.

The data obtained using the beam shear method are shown in Tables 50 through 64. Some of the data points for the HTP core were not obtained because an insufficient amount of this type core was supplied.

The following is a summary of the observations which can be made upon examination of the data:

(a) the measured shear strength appears to be unaffected by strain rate;

(b) shear strength measured with the beam method is slightly higher than that measured by the plate method;

(c) core shear strength decreases as temperature increases and moisture absorption further reduces shear strength; and

(d) although the data are limited, it appears that glass/phenolic (HRP and HTP) cores are less affected by temperature than WR-II and HRH-10.

TABLE 49

HRH-10 CORE SHEAR STRENGTH BY
PLATE TEST METHOD

Plate Shear, HRH-10, "L" Direction						
Core Thickness (in)	Core Thickness (cm)	Condition of Test (°F) (°C)	Testing Speed (in/min) (cm/min)	Ultimate Strength (psi) (MPa)	Standard Deviation (psi) (MPa)	Standard Deviation (MPa)
0.5	1.27	72	0.05	333.5	3.5	0.02
0.5	1.27	72	4	350.2	11.9	0.08
0.5	1.27	-65	0.05	365.6	22.3	0.15
0.5	1.27	-65	4	402.0	17.3	0.12
0.5	1.27	200	0.05	285.3	20.0	0.14
0.5	1.27	200	4	318.2	31.0	0.21
Plate Shear, HRH-10 Core, "W" Direction						
0.5	1.27	72	0.05	174.2	5.8	0.04
0.5	1.27	72	4	176.7	5.2	0.04
0.5	1.27	-65	0.05	200.6	11.8	0.08
0.5	1.27	-65	4	195.8	15.4	0.11
0.5	1.27	200	0.05	145.6	7.7	0.05
0.5	1.27	200	4	159.2	6.5	0.04

TABLE 50

WR-II CORE SHEAR STRENGTH BY BEAM METHOD,
"L" DIRECTION, 0.5 inch (1.27 cm) THICK

Condition of Test (°F)	Condition of Test (°C)	Testing Speed (in/min)	Testing Speed (cm/min)	Ultimate Strength (psi)	Ultimate Strength (MPa)	Standard Deviation (psi)	Standard Deviation (MPa)
-65	-54	0.05	0.13	391.7	2.70	6.7	0.05
-65	-54	4	10.16	297.3	2.05	15.4	0.11
-65	-54	300	762	353.5	2.44	7.4	0.05
72	22	0.05	0.13	334.6	2.31	20.5	0.14
72	22	4	10.16	271.6	1.87	11.6	0.08
72	22	300	762	406.3	2.80	17.7	0.13
200	93	0.05	0.13	241.7	1.67	8.7	0.06
200	93	4	10.16	168.1	1.16	3.6	0.02
200	93	300	762	274.0	1.89	8.5	0.06
HHA ¹		0.05	0.13	178.9	1.23	5.6	0.04
HHA		4	10.16	186.5	1.28	3.2	0.02
HHA		300	762	114.9	0.79	4.9	0.03

¹HHA (Hot Humid Aging) = 200°F (93°C) after two weeks at 200°F (93°C)
and 95-100% Relative Humidity.

TABLE 51

WR-II CORE SHEAR STRENGTH BY BEAM METHOD,
"W" DIRECTION, 0.5 inch (1.27 cm) THICK

Condition of Test (°F)		Testing Speed (in/min) (cm/min)		Ultimate Strength (psi) (MPa)		Standard Deviation (psi) (MPa)	
-65	-54	0.05	0.13	206.2	1.42	12.5	0.09
-65	-54	4	10.16	137.4	0.95	6.5	0.04
-65	-54	300	762	227.8	1.57	9.3	0.06
72	22	0.05	0.13	175.6	1.21	3.6	0.02
72	22	4	10.16	142.7	0.98	1.3	0.01
72	22	300	762	188.7	1.30	3.2	0.02
200	93	0.05	0.13	101.6	0.70	1.6	0.01
200	93	4	10.16	116.5	0.80	2.1	0.01
200	93	300	762	154.8	1.07	5.9	0.04
HHA ¹		0.05	0.13	115.8	0.80	5.4	0.04
		4	10.16	126.6	0.87	11.5	0.08
		300	762	94.6	0.65	1.7	0.01

¹HHA (Hot Humid Aging) = 200°F (93°C) after two weeks at 200°F (93°C)
and 95-100% Relative Humidity.

TABLE 52

WR-II CORE SHEAR STRENGTH BY BEAM METHOD,
"L" DIRECTION, 2 inch (5.08 cm) THICK

Condition of Test (°F)	Condition of Test (°C)	Testing Speed (in/min)	Testing Speed (cm/min)	Ultimate Strength (psi)	Ultimate Strength (MPa)	Standard Deviation (psi)	Standard Deviation (MPa)
-65	-54	0.05	0.13	248.7	1.71	12.2	0.08
-65	-54	4	10.16	166.7	1.15	15.5	0.11
-65	-54	300	762	218.3	1.50	11.1	0.08
72	22	0.05	0.13	213.2	1.47	15.6	0.11
72	22	4	10.16	190.7	1.31	3.5	0.02
72	22	300	762	294.6	2.03	31.5	0.22
200	93	0.05	0.13	187.1	1.29	2.4	0.02
200	93	4	10.16	117.3	0.81	3.5	0.02
200	93	300	762	191.7	1.32	11.6	0.08
	HHA ¹	0.05	0.13	138.0	0.95	1.7	0.01
	HHA	4	10.16	139.8	0.96	1.2	0.01
	HHA	300	762	157.5	1.09	5.1	0.04

¹HHA (Hot Humid Aging) = 200°F (93°C) after two weeks at 200°F (93°C)
and 95-100% Relative Humidity.

TABLE 53

WR-II CORE SHEAR STRENGTH BY BEAM METHOD,
"W" DIRECTION, 2 inch (5.08 cm) THICK

Condition of Test (°F)		Testing Speed (in/min) (cm/min)		Ultimate Strength (psi) (MPa)		Standard Deviation (psi) (MPa)	
-65	-54	0.05	0.13	154.7	1.07	9.5	0.07
-65	-54	4	10.16	115.2	0.79	0.7	0.00
-65	-54	300	762	144.7	1.00	15.9	0.11
72	22	0.05	0.13	140.0	0.96	2.2	0.02
72	22	4	10.16	107.1	0.74	2.6	0.02
72	22	300	762	125.1	0.86	4.2	0.03
200	93	0.05	0.13	98.6	0.68	4.6	0.03
200	93	4	10.16	74.0	0.51	0.7	0.00
200	93	300	762	95.6	0.66	1.1	0.01
	HHA ¹	0.05	0.13	56.7	0.39	2.5	0.02
	HHA	4	10.16	64.2	0.44	1.4	0.01
	HHA	300	762	98.1	0.68	3.5	0.02

¹HHA (Hot Humid Aging) = 200°F (93°C) after two weeks at 200°F (93°C)
and 95-100% Relative Humidity.

TABLE 54

HRH-10 CORE SHEAR STRENGTH BY BEAM METHOD,
"L" DIRECTION, 0.5 inch (1.27 cm) THICK

Condition of Test (°F)		Testing Speed (in/min) (cm/min)		Ultimate Strength (psi) (MPa)		Standard Deviation (psi) (MPa)	
-65	-54	0.05	0.13	480.5	3.31	5.4	0.04
-65	-54	4	10.16	363.2	2.50	13.1	0.09
-65	-54	300	762	490.1	3.38	20.9	0.14
72	22	0.05	0.13	420.7	2.90	61.1	0.42
72	22	4	10.16	328.0	2.26	2.2	0.02
72	22	300	762	439.6	3.03	8.2	0.06
200	93	0.05	0.13	306.8	2.11	13.4	0.09
200	93	4	10.16	312.6	2.15	9.4	0.06
200	93	300	762	366.0	2.52	1.9	0.01
HHA ¹ HHA HHA		0.05	0.13	172.4	1.19	15.0	0.10
		4	10.16	295.2	2.03	2.5	0.02
		300	762	364.4	2.51	5.6	0.04

¹HHA (Hot Humid Aging) = 200°F (93°C) after two weeks at 200°F (93°C)
and 95-100% Relative Humidity.

TABLE 55

HRH-10 CORE SHEAR STRENGTH BY BEAM METHOD,
"W" DIRECTION, 0.5 inch (1.27 cm) THICK

Condition of Test (°F) (°C)		Testing Speed (in./min) (cm/min)		Ultimate Strength (psi) (MPa)		Standard Deviation (psi) (MPa)	
-65	-54	0.05	0.13	223.8	1.54	2.9	0.02
-65	-54	4	10.16	183.1	1.26	3.2	0.02
-65	-54	300	762	237.1	1.63	4.8	0.03
72	22	0.05	0.13	202.9	1.40	2.8	0.02
72	22	4	10.16	173.6	1.20	1.4	0.01
72	22	300	762	196.3	1.35	8.9	0.06
200	93	0.05	0.13	167.2	1.15	2.9	0.02
200	93	4	10.16	169.3	1.17	3.7	0.03
200	93	300	762	192.8	1.33	3.5	0.02
	HHH ¹	0.05	0.13	170.6	1.18	1.5	0.01
	HHH	4	10.16	175.4	1.21	3.0	0.02
	HHH	300	762	136.7	0.94	3.2	0.02

¹HHH (Hot Humid Aging) = 200°F (93°C) after two weeks at 200°F (93°C)
and 95-100% Relative Humidity.

TABLE 56

HRH-10 CORE SHEAR STRENGTH BY BEAM METHOD,
"L" DIRECTION, 2 inch (5.08 cm) THICK

Condition of Test (°F)		Testing Speed (in/min) (cm/min)		Ultimate Strength (psi) (MPa)		Standard Deviation (psi) (MPa)	
-65	-54	0.05	0.13	294.5	2.03	6.0	0.04
-65	-54	4	10.16	254.0	1.75	8.4	0.06
-65	-54	300	762	309.0	2.13	4.8	0.03
72	22	0.05	0.13	281.5	1.94	0.4	0.00
72	22	4	10.16	241.4	1.66	0.8	0.01
72	22	300	762	265.0	1.83	9.0	0.06
200	93	0.05	0.13	257.0	1.77	3.9	0.03
200	93	4	10.16	187.4	1.29	1.2	0.01
200	93	300	762	241.5	1.66	10.1	0.07
HHA ¹		0.05	0.13	194.4	1.34	0.5	0.00
HHA		4	10.16	192.6	1.33	4.3	0.03
HHA		300	762	250.9	1.73	8.2	0.06

¹HHA (Hot Humid Aging) = 200°F (93°C) after two weeks at 200°F (93°C)
and 95-100% Relative Humidity.

TABLE 57

HRH-10 CORE SHEAR STRENGTH BY BEAM METHOD,
"W" DIRECTION, 2 inch (5.08 cm) THICK

Condition of Test (°F)		Testing Speed (in/min) (cm/min)		Ultimate Strength (psi) (MPa)		Standard Deviation (psi) (MPa)	
-65	-54	0.05	0.13	142.2	0.98	1.1	0.01
-65	-54	4	10.16	117.8	0.81	5.4	0.04
-65	-54	300	762	180.7	1.26	5.4	0.04
72	22	0.05	0.13	147.0	1.01	4.2	0.03
72	22	4	10.16	113.7	0.78	3.1	0.02
72	22	300	762	---	---	---	---
200	93	0.05	0.13	106.5	0.73	3.4	0.02
200	93	4	10.16	103.8	0.72	2.7	0.02
200	93	300	762	152.8	1.05	3.2	0.02
HHA ¹		0.05	0.13	127.0	0.88	2.1	0.01
HHA		4	10.16	104.6	0.72	1.9	0.01
HHA		300	762	143.3	0.99	4.0	0.03

¹HHA (Hot Humid Aging) = 200°F (93°C) after two weeks at 200°F (93°C)
and 95-100% Relative Humidity.

TABLE 58

HRH-10 CORE SHEAR STRENGTH BY BEAM METHOD,
"L" DIRECTION, 3 inch (7.62 cm) THICK

Condition of Test (°F) (°C)		Testing Speed (in/min) (cm/min)		Ultimate Strength (psi) (MPa)		Standard Deviation (psi) (MPa)	
-65	-54	0.05	0.13	242.2	1.67	5.5	0.04
-65	-54	4	10.16	198.1	1.36	3.1	0.02
-65	-54	300	762	263.8	1.82	1.8	0.01
72	22	0.05	0.13	195.8	1.35	4.4	0.03
72	22	4	10.16	172.4	1.19	6.7	0.05
72	22	300	762	259.3	1.79	11.2	0.08
200	93	0.05	0.13	206.8	1.42	4.5	0.03
200	93	4	10.16	190.4	1.31	4.3	0.03
200	93	300	762	236.0	1.63	3.3	0.02
HHA ¹ HHA HHA		0.05	0.13	197.7	1.36	13.4	0.09
		4	10.16	183.5	1.26	9.2	0.06
		300	762	234.9	1.62	4.6	0.03

¹HHA (Hot Humid Aging) = 200°F (93°C) after two weeks at 200°F (93°C)
and 95-100% Relative Humidity.

TABLE 59

HRH-10 CORE SHEAR STRENGTH BY BEAM METHOD,
"W" DIRECTION, 3 inch (7.62 cm) THICK

Condition of Test (°F)	Condition of Test (°C)	Testing Speed (in/min)	Testing Speed (cm/min)	Ultimate Strength (psi)	Ultimate Strength (MPa)	Standard Deviation (psi)	Standard Deviation (MPa)
-65	-54	0.05	0.13	147.9	1.02	6.2	0.04
-65	-54	4	10.16	118.4	0.82	2.1	0.01
-65	-54	300	762	171.6	1.18	6.0	0.04
72	22	0.05	0.13	137.2	0.95	4.7	0.03
72	22	4	10.16	113.1	0.78	1.9	0.01
72	22	300	762	156.7	1.08	0.7	0.00
200	93	0.05	0.13	117.9	0.81	1.8	0.01
200	93	4	10.16	112.2	0.77	2.4	0.02
200	93	300	762	149.7	1.03	1.5	0.01
HHA ¹		0.05	0.13	117.7	0.81	0.1	0.00
HHA		4	10.16	102.3	0.70	1.9	0.01
HHA		300	762	140.0	0.96	8.9	0.06

¹HHA (Hot Humid Aging) = 200°F (93°C) after two weeks at 200°F (93°C)
and 95-100% Relative Humidity.

TABLE 60

HRP CORE SHEAR STRENGTH BY BEAM METHOD,
"L" DIRECTION, 1.5 inch (3.81 cm) THICK

Condition of Test (°F) (°C)		Testing Speed (in/min) (cm/min)	Ultimate Strength (psi) (MPa)		Standard Deviation (psi) (MPa)	
-65	-54	0.05	270.5	1.86	11.5	0.08
-65	-54	4	207.7	1.43	9.2	0.06
-65	-54	300	293.4	2.02	11.2	0.08
72	22	0.05	264.8	1.82	7.0	0.05
72	22	4	211.2	1.46	1.8	0.01
72	22	300	289.4	1.99	19.3	0.13
200	93	0.05	246.8	1.70	3.4	0.02
200	93	4	206.9	1.43	7.2	0.05
200	93	300	271.5	1.87	17.5	0.12
HHA ¹ HHA HHA		0.05	220.1	1.52	10.8	0.07
		4	146.8	1.01	11.1	0.08
		300	281.1	1.94	11.7	0.08

¹HHA (Hot Humid Aging) = 200°F (93°C) after two weeks at 200°F (93°C)
and 95-100% Relative Humidity.

TABLE 61

HRP CORE SHEAR STRENGTH BY BEAM METHOD,
"W" DIRECTION, 1.5 inch (3.81 cm) THICK

Condition of Test (°F)	Condition of Test (°C)	Testing Speed (in/min)	Testing Speed (cm/min)	Ultimate Strength (psi)	Ultimate Strength (MPa)	Standard Deviation (psi)	Standard Deviation (MPa)
-65	-54	0.05	0.13	165.4	1.14	5.8	0.04
-65	-54	4	10.16	122.9	0.85	2.8	0.02
-65	-54	300	762	171.4	1.18	10.6	0.07
72	22	0.05	0.13	181.1	1.25	5.2	0.04
72	22	4	10.16	133.5	0.92	1.8	0.01
72	22	300	762	187.7	1.29	0.8	0.01
200	93	0.05	0.13	178.2	1.23	4.7	0.03
200	93	4	10.16	140.6	0.97	2.4	0.02
200	93	300	762	190.9	1.32	7.9	0.05
HHA ¹		0.05	0.13	148.8	1.03	22.2	0.15
HHA		4	10.16	128.4	0.88	7.8	0.05
HHA		300	762	160.2	1.10	6.2	0.04

¹HHA (Hot Humid Aging) = 200°F (93°C) after two weeks at 200°F (93°C)
and 95-100% Relative Humidity.

TABLE 62

HTP CORE SHEAR STRENGTH BY BEAM METHOD,
 "L" DIRECTION, 0.87 inch (2.22 cm) THICK,
 3.2 lbs/ft³ (51.3 kg/m³) DENSITY

Condition of Test (°F)	Condition of Test (°C)	Testing Speed (in/min)	Testing Speed (cm/min)	Ultimate Strength (psi)	Ultimate Strength (MPa)	Standard Deviation (psi)	Standard Deviation (MPa)
-65	-54	0.05	0.13	164.4	1.13	9.4	0.06
-65	-54	4	10.16	138.2	0.95	5.2	0.04
-65	-54	---	---	---	---	---	---
72	22	0.05	0.13	170.1	1.17	1.0	0.01
72	22	4	10.16	131.3	0.90	7.0	0.05
72	22	300	762	190.5	1.31	5.5	0.04
200	93	0.05	0.13	158.7	1.09	4.8	0.03
200	93	4	10.16	134.6	0.93	7.0	0.05
200	93	300	762	178.8	1.23	11.9	0.08
HHA ¹		4	10.16	127.1	0.88	10.3	0.07
HHA		300	762	155.1	1.07	3.1	0.02
HHA		---	---	---	---	---	---

¹HHA (Hot Humid Aging) = 200°F (93°C) after two weeks at 200°F (93°C)
 and 95-100% Relative Humidity.

TABLE 63

HTP CORE SHEAR STRENGTH BY BEAM METHOD
 "W" DIRECTION, 0.87 inch (2.22 cm) THICK,
 3.2 lbs/ft³ (51.3 kg/m³) DENSITY

Condition of Test (°F)	Condition of Test (°C)	Testing Speed (in/min)	Testing Speed (cm/min)	Ultimate Strength (psi)	Ultimate Strength (MPa)	Standard Deviation (psi)	Standard Deviation (MPa)
-65							
72	22	0.05	0.13	103.7	0.7	0.0	0.00
72	22	4	10.16	98.1	0.7	0.2	0.00
72	22	300	762	113.9	0.8	1.3	0.01
200	93	300	762	106.3	0.7	7.7	0.05
HHH ¹		300	762	90.6	0.6	1.3	0.01

¹HHH (Hot Humid Aging) = 200°F (93°C) after two weeks at 200°F (93°C)
 and 95-100% Relative Humidity.

TABLE 64

HTP CORE SHEAR STRENGTH BY BEAM METHOD,
0.87 inch (2.22 cm) THICK,
4.5 lbs/ft³ (72.1 kg/m³) DENSITY

Condition of Test (°F) (°C)		Testing Speed (in/min) (cm/min)	Ultimate Strength (psi) (MPa)		Standard Deviation (psi) (MPa)
-65 HHA ¹	-54	300	762		3.7
		0.05			
	-54	300	762		3.7
		0.05			
-65 HHA ¹	-54	300	762		3.7
		0.05			
	-54	300	762		3.7
		0.05			
200 HHA ¹	93	300	762		3.7
		0.05			
	93	300	762		3.7
		0.05			

¹HHA (Hot Humid Aging) = 200°F (93°C) after two weeks at 200°F (93°C) and 95-100% Relative Humidity.

5.2 TENSILE PROPERTIES OF NORYL EN-265

Several pieces of plastic parts were submitted for evaluation in tension. The parts were believed to be from inside the A-10 aircraft and were a thermoplastic identified as Noryl EN-265. For comparison, both virgin Noryl EN-265 and polycarbonate, of equal thickness, were also tested. The results obtained are shown in Tables 65 and 66.

5.3 CHARACTERIZATION OF NEAT RESIN MATRIX SYSTEMS

A request was received to formulate and characterize two epoxy resin matrix systems which offer the potential of both high strength and high elongation. The resin matrix systems are:

(1) Epon 828	100 pts	(2) Epon 826	100 pts
DEN 438	100 pts	Diethyl MDA	35 pts
Diethyl MDA	73 pts		

The Diethyl MDA is a noncrystalline liquid derivative of methylenedianiline (MDA). The results of the mechanical tests on neat resin castings are presented in Table 67.

5.4 ASTM-E-TBD-5 PRIMER SPECIFICATION

A standard specification for "Corrosion-Inhibiting Adhesive Primer for Aluminum Alloys to be Adhesively Bonded in Honeycomb Shelter Panels" was being prepared by ASTM Subcommittee E6.23 with assistance from AFWAL and UDRI. After reviewing the document, a list of 21 technical and editorial changes were recommended and submitted to the subcommittee in the January 1981 meeting. All of the changes were reviewed and accepted as proposed.

5.5 FIELD PERFORMANCE PANELS

A request was made to assist in the planning and testing of 4-foot (1.22m) by 8-foot (2.44m) shelter panels which will be exposed to both controlled environments and outside weathering (in Panama) for periods up to five years. The first

TABLE 65
TENSILE PROPERTIES OF A-10 PLASTIC PARTS

Part Identification	Yield Strength		Breaking Strength		% Elongation at Break
	(psi)	(MPa)	(psi)	(MPa)	
Green, no number	4730	32.6	4100	28.2	3.6
Black, no number	4090	28.2	3510	24.2	2.6
Black, 160D180551-3	3900	26.9	3360	23.2	2.7
2nd Black part	7320	50.4	6660	45.9	19.2
2nd Black part, transverse	7490	51.6	6970	48.0	16.6
Small part on 2nd Black part	7980	55.0	6570	45.3	28.4

TABLE 66

TENSILE PROPERTIES OF VIRGIN EN-265 AND POLYCARBONATE

Test Direction	Test Speed	Strength		% Elongation at Break
		Yield	Breaking	
Noryl EN-265				
longitudinal	0.05 in/min 0.13 cm/min	8630 psi 59.5 MPa	6180 psi 42.6 MPa	15.6
	2 in/min 5.1 cm/min	10080 psi 69.5 MPa	8190 psi 56.4 MPa	9.8
transverse	0.05 in/min 0.13 cm/min	7370 psi 50.8 MPa	7370 psi 50.8 MPa	7.2
	2 in/min 5.1 cm/min	8530 psi 58.8 MPa	8530 psi 58.8 MPa	5.8
Polycarbonate				
longitudinal	0.05 in/min 0.13 cm/min	8970 psi 61.8 MPa	8720 psi 60.1 MPa	110.0
	2 in/min 5.1 cm/min	9570 psi 65.9 MPa	9890 psi 68.1 MPa	140.0
transverse	0.05 in/min 0.13 cm/min	8940 psi 61.6 MPa	8780 psi 60.5 MPa	105.0
	2 in/min 5.1 cm/min	9570 psi 65.9 MPa	9940 psi 68.5 MPa	145.0

TABLE 67
PROPERTIES OF CAST EPOXY RESIN SYSTEMS

Resin Properties	Resin System	
	826/438/ Diethyl MDA	828 Diethyl MDA
Tensile Modulus, 10^6 psi (10^6 KPa)	0.44 (3.03)	0.41 (2.82)
Stress at Proportional Limit, 10^3 psi (10^3 KPa)	4.3 (29.6)	3.9 (26.9)
Strain at Proportional Limit, %	1.00	0.98
Tensile Strength, 10^3 psi (10^3 KPa)	9.8 (67.0)	8.5 (58.1)
Ultimate Elongation, %	2.93	2.79
Toughness, 10^3 in- lbf/in ³ (MPa)	0.17 (1.17)	0.14 (0.96)
Fracture Toughness, 10^3 lbf/in ² x in ^{1/2} (MPa/ \sqrt{m})	0.55 (0.60)	0.65 (0.71)

consideration was the type tests to be performed. Four have been recommended; flatwise tension, flatwise compression, beam shear, and climbing drum peel. Beam shear and peel tests may be performed in the "L" and "W" directions. Each panel is divided into six sections, with each having constructed repairs, hinges, and inserts in addition to some plain areas with no hardware. Also, some panels may contain humidity indicators built into the construction of the panel. Two of the humidity indicators were placed in a laboratory constructed WR-II honeycomb core. One indicator is such that changes take place at 20, 30, 40, and 50 percent relative humidity. The other indicator changes at 30 percent relative humidity only. The panel has been placed in a humidity chamber at 140°F (60°C) and 95 to 100 percent relative humidity.

The indicators did indeed show when moisture was building inside the constructed honeycomb panels. The test plan was submitted to the AFWAL Project Engineer and the Shelter Engineering Division of the U.S. Army at Natick Research Labs for discussion and approval.

5.6 OPTICAL PROPERTIES OF TRANSPARENT SPECIMENS

Twenty-four (24) samples of aircraft windshields in varying sizes were received with a request to determine the percent haze of each. The samples were machined into sizes appropriate to the hazemeter. All tests have been completed and the results are listed in Table 68.

5.7 EVALUATION OF REINFORCED RIM 120

A request was received to evaluate RIM 120, a Union Carbide reinforced injection molded urethane resin, for its tensile properties at 0°, 45°, and 90° to the direction of flow. The material was tested in tension for strength, modulus, and elongation. The results are presented in Table 69.

TABLE 68
WINDSHIELD HAZE MEASUREMENTS

Sample I.D.	Diffuse	Luminous	% Haze
S/N 659 Control	39	795	4.9
S/N 879 Control	22	797	2.8
S/N 742 Control	21	798	2.6
S/N F111 Sprayed	166	639	26.0
S/N F111 Non-Sprayed	58	667	8.7
S/N F111 Stripped	72	672	10.7
F111/1	61	670	9.1
S/N 659/2	82	785	10.4
S/N 742 Stripped	60	790	7.6
S/N 742 Non-Sprayed	32	795	4.0
S/N 742 Sprayed	98	784	12.5
F111	103	663	15.5
S/N 659/1	72	786	9.1
S/N 879/1	37	789	4.7
S/N 879 Stripped	23	798	2.9
S/N 879 Sprayed	173	761	22.7
S/N 879 Non-Sprayed	23	799	2.9
S/N F111/2	68	658	10.3
S/N 742/1	18	778	2.3
S/N 742/2	27	795	3.4
S/N 879/2	51	778	6.6
S/N 659 Sprayed	32	792	4.0
S/N 659 Non-Sprayed	23	797	2.9
S/N 659 Stripped	23	798	2.9

TABLE 69
TENSILE PROPERTIES OF
RIM 120 (6LPT97-18) WITH
25% GLASS REINFORCEMENT

Testing Temp.		Orientation (to flow)	Elongation (%)	Strength		Modulus	
(°F)	(°C)			(psi)	(MPa)	(psi) 10 ⁶	(MPa) 10 ³
72	22	0°	21	6540	45	0.29	1.9
225	107	0°	35	2780	19	0.07	0.5
-65	-54	0°	5	16080	111	0.74	5.0
72	22	45°	29	6290	43	0.22	1.5
72	22	90°	32	5810	40	0.18	1.2
225	107	90°	49	2100	15	0.04	0.3
-65	-54	90°	5	13740	95	0.56	4.0

5.8 COLD TEMPERATURE TESTS FOR EXPANDABLE SLEEVING

A request was received to determine a suitable cold temperature test for plastic expandable sleeving. Several candidate methods have been investigated. One which appeared to work and was acceptable to the AFWAL Project Engineer was ASTM-D-2137, "Low Temperature Impact Test for Coated Fabrics." The specimens were tested and passed the requirements.

5.9 POLYETHERIMIDE (G.E.) TENSILE TESTING

Tensile tests were conducted on General Electric's polyetherimide material on an Instron Universal testing machine at a constant crosshead travel of 2 in./min. (5.08 cm/min.). The strain was measured with an Instron strain gage extensometer with a 1-inch (2.54 cm) gage length (50 percent maximum strain) in accordance with ASTM Method D-638. Two specimens were tested at 225°F (107°C) and two were tested at -65°F (-54°C). Table 70 presents the results of the tests.

5.10 KEVLAR-29 RECOVERY SYSTEMS

A program to evaluate the effects of elevated temperature air agings on the tensile properties of Kevlar-29 has been conducted.

Tests were performed in accordance with ASTM Method D2256 on an Instron Universal testing machine using a 0 to 50 pound (0 to 22.7 Kg) load cell. Test samples were secured in cord capstan grips allowing an effective gage length of 10 inches (25.4 cm). All tests were conducted at room temperature using a crosshead speed of 2 inches/minute (5.08 cm/minute).

The average tensile strength and load loss at each test condition are reported in Table 71.

TABLE 70
POLYETHERIMIDE (G.E.) TENSILE SPECIMENS

Condition of Test		Tensile Stress at Yield		% Elong. at Yield	Tensile Stress at Break		% Elong. at Break
(°F)	(°C)	(10 ³ psi)	(MPa)		(10 ³ psi)	(MPa)	
225	107	10.04	69.2	5.6	7.86	54.1	45.8+
-65	-54	22.32	153.8	7.8	21.20	146.1	10.25

NOTE: Specimens were held at the test temperature for 30 minutes before tests were started.

TABLE 71
TENSILE STRENGTH AND LOAD LOSS OF
KEVLAR-29 RECOVERY SYSTEMS

Temperature °F (°C)	Aging Conditions					
	1 Hour		8 Hours		24 Hours	
	(lbs)	(N)	(lbs)	(N)	(lbs)	(N)
R.T.	17.02	(75.71)	17.02	(75.71)	17.02	(75.71)
302 (150)	15.16	(67.43)	15.55	(69.17)	14.57	(64.81)
347 (175)	14.96	(66.54)	14.15	(62.94)	13.40	(59.60)
392 (200)	14.24	(63.34)	13.31	(59.20)	11.34	(50.44)
437 (225)	12.71	(56.53)	11.76	(52.31)	9.76	(43.41)
482 (250)	11.49	(51.11)	10.14	(45.10)	8.58	(38.16)
Load Loss	32.5%		40.4%		49.6%	

Temperature °F (°C)	Aging Conditions							
	7 Days		14 Days		28 Days		42 Days	
	(lbs)	(N)	(lbs)	(N)	(lbs)	(N)	(lbs)	(N)
R.T.	17.02	(75.71)	17.02	(75.71)	17.02	(75.71)	17.02	(75.71)
302 (150)	13.56	(60.32)	12.56	(55.87)	12.00	(53.38)	10.94	(48.66)
347 (175)	11.75	(52.26)	10.67	(47.46)	11.16	(49.64)	9.89	(43.99)
392 (200)	10.64	(47.33)	9.81	(43.65)	9.09	(40.43)	8.59	(38.21)
437 (225)	8.39	(37.32)	8.41	(37.41)	6.38	(28.38)	5.42	(24.11)
482 (250)	7.04	(31.31)	5.51	(24.51)	3.95	(17.57)	2.03	(9.03)
Load Loss	58.6%		67.6%		76.8%		88.05%	

- NOTES: 1. All values represent average of ten (10) specimens.
2. Load loss represents decrease in strength from R.T. to 482°F (250°C) condition for each aging period.

5.11 ANISOTROPY OF GLASS FILLED POLYPHENYLENE SULFIDE

The objective of this effort was to show that, in glass filled injection molded specimens, as thickness increases, the anisotropy or directionality in tensile properties will decrease. Specimens of various thicknesses were molded into 4-inch (10.2 cm) diameter discs. Tensile specimens were then cut longitudinal and transverse to the flow direction.

The imbalance in tensile strength did indeed decrease with increasing thickness for the two thinner sections. However, at the largest thickness, the strength directionality seemed to reverse itself. Modulus data did not indicate this anomaly. Table 72 summarizes the data.

5.12 STANDARD WORK PROCEDURE REQUESTS

Numerous "Standard Work Procedure Requests" were received and have been completed. These include such tasks as machining and tabbing of test specimens and physical property determinations. The specific tasks include the following:

- physical properties of glass/P.I. laminates;
- composite machining - shear and flexure specimens;
- machining adhesive bonded panels;
- machining honeycomb panels;
- machining and physical property determination of glass/epoxy laminates; and
- machining of tensile specimens from high temperature laminates.

5.13 SUPPORT OF JANAF FIBERGLASS LAMINATE TESTING

The objective of this program was to determine mechanical, physical, and thermophysical properties of various types of glass reinforced composite materials used in radome construction.

The Air Force Weapons Laboratory (AFWL) supplied UDRI with a series of glass reinforced composites that were representative of both flat and curved radome materials. The materials were:

TABLE 72

TENSILE PROPERTIES¹ OF INJECTION MOLDED POLYPHENYLENE SULFIDE

Flow Direction	Thickness		Tensile Strength		Tensile Modulus	
	Inch	mm	psi	MPa	x10 ⁶ psi	x10 ⁶ Pa
Transverse	0.057	1.45	5,572 S.D. 440	38.4 3.0	1.04 0.04	7.17 0.30
Longitudinal	0.057	1.45	8,297 S.D. 470	57.2 3.2	1.22 0.09	8.41 0.59
Transverse	0.093	2.36	7,147 S.D. 572	49.2 3.9	1.04 0.05	7.17 0.37
Longitudinal	0.093	2.36	7,825 S.D. 627	53.9 4.3	1.14 0.07	7.86 0.50
Transverse	0.125	3.18	7,753 S.D. 637	53.4 4.4	1.15 0.12	7.92 0.79
Longitudinal	0.125	3.18	4,667 S.D. 1,002	32.2 6.9	1.16 0.12	7.99 0.89

¹Average of 10 specimens.

- | | |
|------------------------|-------------------------------|
| (1) Cordopreg (flat) | (5) SG/Epoxy Type I |
| (2) Cordopreg (curved) | (6) SG/Epoxy Type II |
| (3) EG/Epoxy Type I | (7) Quartz/Polyimide (curved) |
| (4) EG/Epoxy Type II | (8) Stypole (curved) |

In addition to these eight materials, UDRI also fabricated eight flat laminates of Quartz 581/Polyimide (PMR 15). Five of these laminates were shipped to AFWL for further evaluation. The remaining three were used for this program.

Two physical properties of each type of composite material were measured; specific gravity and laminate resin content. Three types of thermophysical property measurements were conducted on the subject materials; specific heat, thermal conductivity, and thermogravimetric analysis (TGA). One other, heat of pyrolysis, was desired. A suitable method for determining this property was not available.

Table 73 presents the specific gravity and resin content values obtained on the various reinforced composite materials used in this program. There was a substantial difference in the specific gravity of the AFWL supplied curved polyimide/quartz panel and that of the UDRI fabricated flat polyimide/quartz laminate. Photomicrographs were obtained on these two laminates and are presented in Figure 61. It is clear from the photomicrographs that the AFWL supplied curved panel was of very poor quality and has a very high void content while the UDRI fabricated flat panel was essentially void-free.

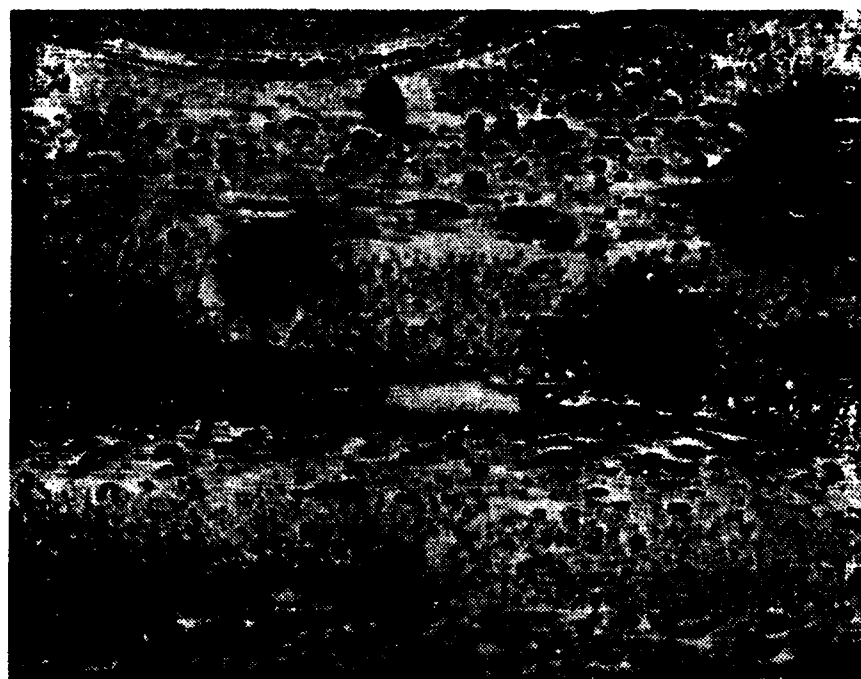
Figure 62 presents 150X photomicrographs of the seven materials not illustrated in Figure 61 which were tested in this program. The following observations can be made from these photographs.

(a) Both the flat and curved cordopreg laminates were void-free and of apparent high quality. The white areas in the photo probably indicate the presence of some sort of particulate filler.

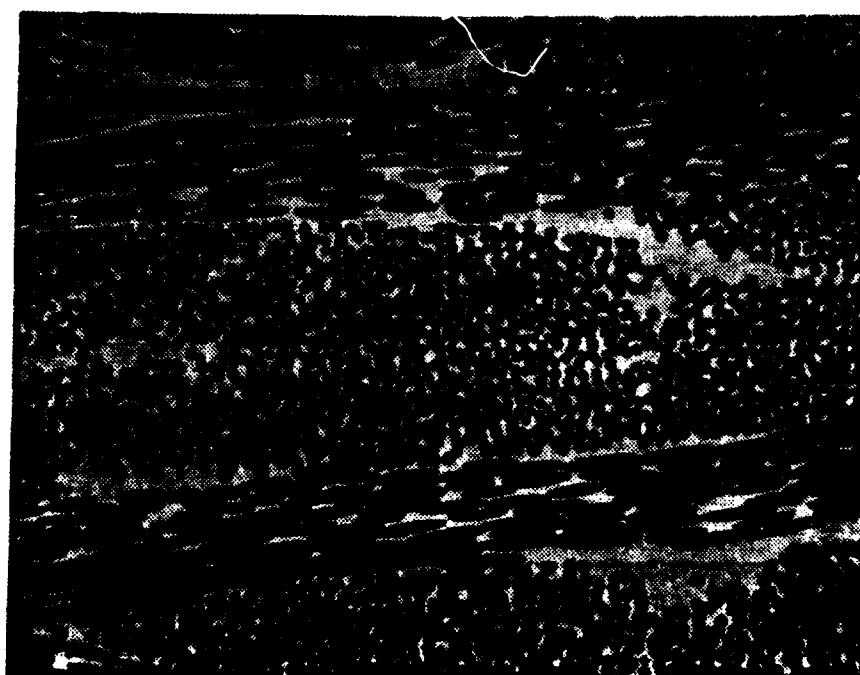
TABLE 73
PHYSICAL PROPERTIES¹ OF JANAF LAMINATES

Materials	Specific Gravity	% Resin Content
Cordo (flat)	1.97	34.15
Cordo (curved)	1.93	34.93
EG/Epoxy Type 1	1.83	36.48
EG/Epoxy Type 2	1.94	31.86
SG/Epoxy Type 1	1.90	31.93
SG/Epoxy Type 2	1.90	29.38
Stypole	2.00	33.95
Polyimide/Quartz (curved)	1.60	26.65
Quartz 581/Polyimide (flat - UDRI)	1.82	27.82

¹Average of three specimens.



(a) AFWL Supplied Curved Panel, Specific Gravity = 1.60



(b) UDRI Fabricated Flat Panel, Specific Gravity = 1.82

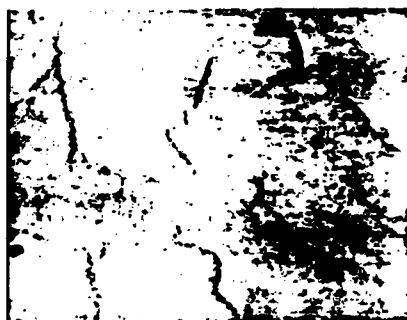
Figure 61. Photomicrographs of Quartz/Polyimide Laminates.



(A) CORDOPREG, FLAT



(B) CORDOPREG, CURVED



(C) STYPOLE, CURVED



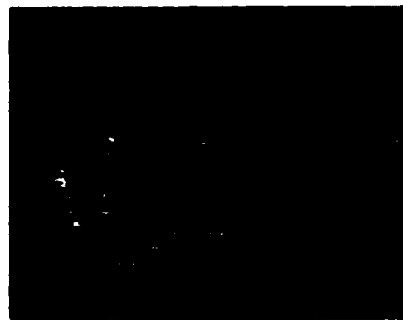
(D) SG/EPOXY, TYPE I



(E) SG/EPOXY, TYPE II



(F) EG/EPOXY, TYPE I



(G) EG/EPOXY, TYPE II

Figure 62. Laminate Photomicrographs.

(b) The styrole curved laminate was void-free but contained numerous cracks.

(c) The SG/epoxy laminates both contained some voids, with the Type I material having numerous small voids uniformly distributed throughout, and the Type II material having fewer voids. In both cases the porosity is within the fiber bundles rather than being concentrated between the plies. This would indicate that the most probable source of the porosity is the release and entrapment of a volatile resin constituent during processing.

(d) The EG/epoxy laminates both exhibit some porosity also, although the Type II material is very nearly void-free. The same observation regarding void location and probable source as was made for the SG/epoxy laminates would seem to apply to these as well.

The specific heat data measured for each material are presented in Table 74.

Thermal conductivity was measured on the six flat laminates evaluated in this program. These results are presented graphically in Figures 63 and 64. A quadratic least-squares fit of each set of data is plotted for each material in these figures.

TGA curves were obtained on all nine materials evaluated in this program. The weight versus temperature graphs obtained in both air and nitrogen atmospheres are presented in the Interim Technical Report AFWAL-TR-81-4129 and are not included here.

Mechanical properties were obtained on the six flat laminates characterized in this investigation. These materials were tested for tensile and flexural strength and modulus at room temperature, 350°F (177°C), and 600°F (316°C), depending on the resin matrix in the laminates. The tensile and flexural properties of these materials are presented in Tables 75 and 76, respectively. Not only are there very marked differences between

TABLE 74
SPECIFIC HEAT¹ OF JANAF LAMINATES

Temp. (°C)	Cordopreg (flat)	Cordo Precurved	EG/Epoxy Type 1	EG/Epoxy Type 2	SG/Epoxy Type 1	SG/Epoxy Type 2	Stypole	Quartz PI (curved)	Quartz 581 PI (UDRI)
100	0.199	0.217	0.207	0.300	0.234	0.221	0.157	0.123	0.234
125	0.228	0.255	0.209	0.275	0.234	0.224	0.151	0.129	0.242
150	0.262	0.269	0.196	0.307	0.238	0.223	0.155	0.138	0.256
175	0.275	0.279	0.225	0.315	0.243	0.234	0.168	0.145	0.261
200	0.290	0.297	0.234	0.326	0.251	0.239	0.167	0.151	0.270
225	0.303	0.312	0.234	0.329	0.258	0.247	0.170	0.165	0.275
250	0.321	0.331	0.232	0.335	0.249	0.251	0.177	0.158	0.279
275	0.322	0.334	0.256	0.337	0.263	0.253	0.178	0.186	0.284
300	0.331	0.340	0.266	0.348	0.271	0.254	0.201	0.198	0.289 ²

¹Units are (cal/gm-°C). All tests were run in a nitrogen atmosphere.

²This data point was extrapolated.

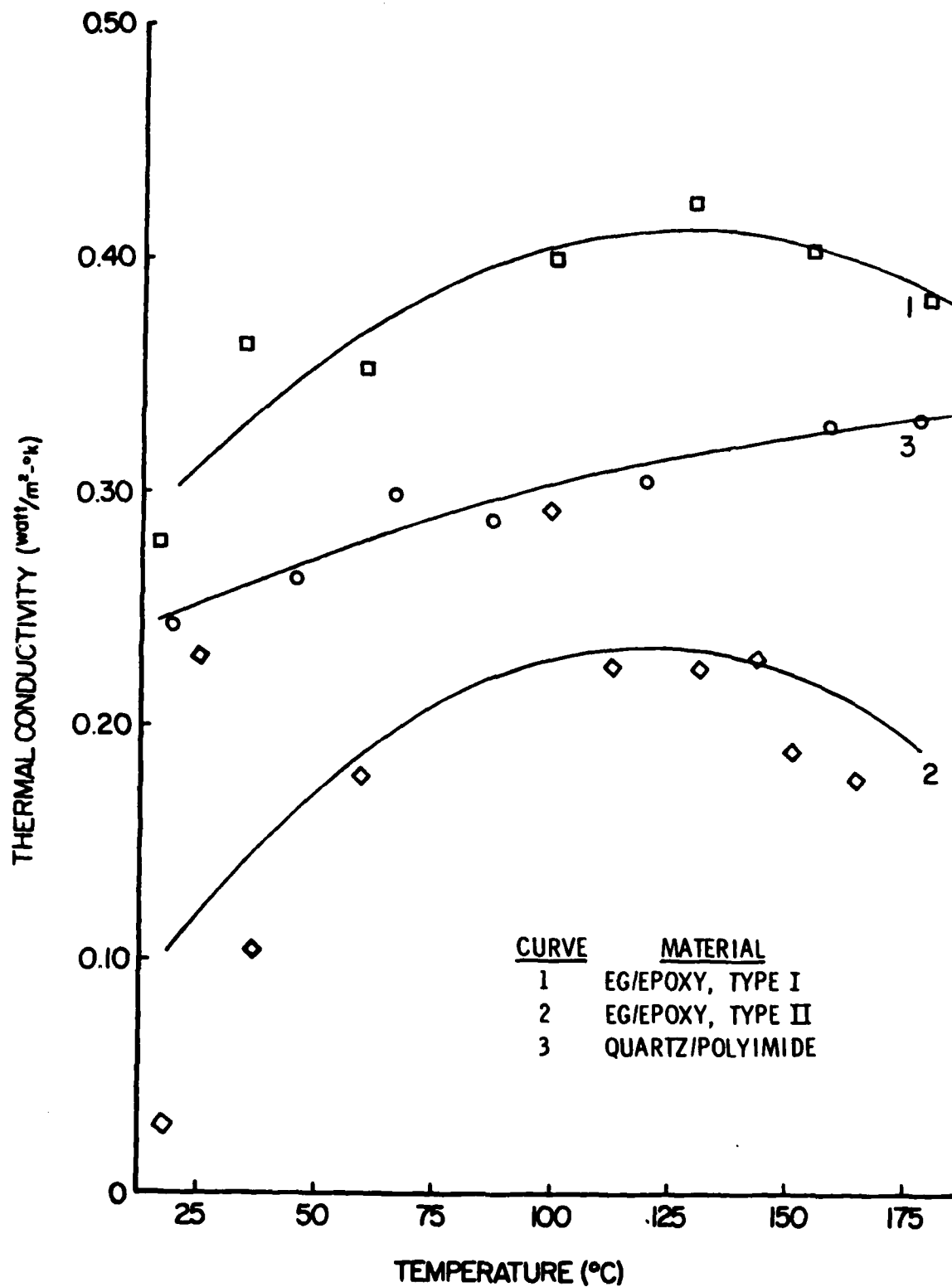


Figure 63. Thermal Conductivity Curves on EG/Epoxy Type 1 and 2 and Quartz 581/PMR-15 Laminates.

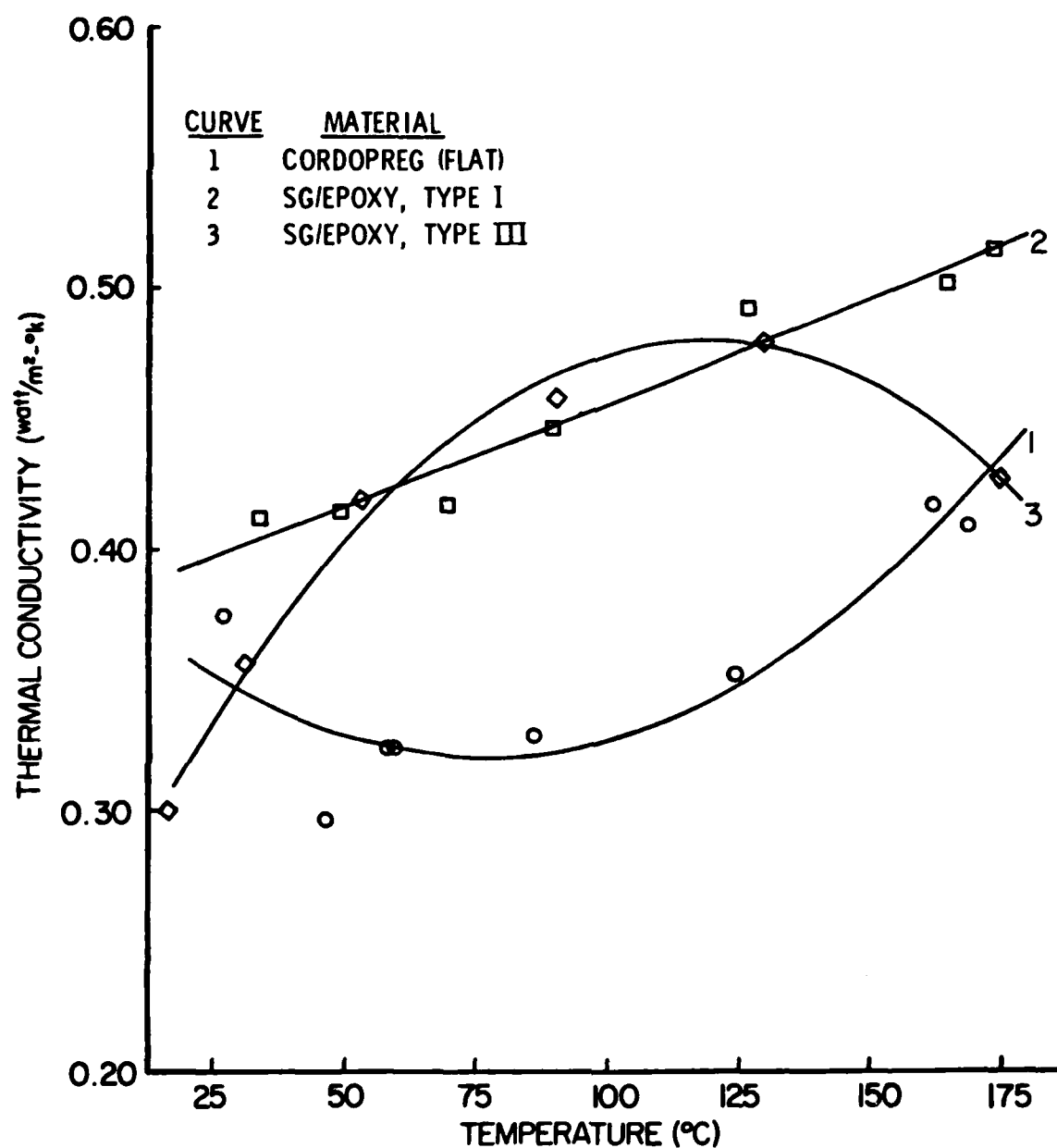


Figure 64. Thermal Conductivity Curves on SG/Epoxy Type 1 and 2 and Cordopreg Laminates.

TABLE 75
TENSILE PROPERTIES OF JANAF LAMINATES

Material	72°F (22°C)		350°F (177°C)		600°F (316°C)	
	Ult. Strength	Initial Modulus	Ult. Strength	Initial Modulus	Ult. Strength	
	psi (10 ³) MPa (10 ²)	psi (10 ⁶) MPa (10 ⁴)	psi (10 ³) MPa (10 ²)	psi (10 ⁶) MPa (10 ⁴)	psi (10 ³) MPa (10 ²)	
Cordopreg (flat)	35.1 2.42	2.07 1.43	15.4 1.06	1.31 0.90	---	---
EG/Epoxy Type 1	92.8 6.40	3.89 2.68	67.0 4.60	4.40 3.00	---	---
EG/Epoxy Type 2	88.1 6.07	4.13 2.85	67.3 4.64	3.28 2.25	---	---
SG/Epoxy Type 1	147 10.1	5.83 4.02	90.3 6.22	4.56 3.14	---	---
SG/Epoxy Type 2	135 9.30	5.50 3.80	20.5 1.41	4.24 2.92	---	---
Quartz 581/ PMR-15	92.8 6.40	2.65 1.83	81.8 5.63	2.50 1.72	74.0	5.1

Values represent an average of specimens.

TABLE 76
FLEXURAL PROPERTIES OF JANAF LAMINATES^{1,2}

Material	72°F (22°C)			350°F (177°C)			600°F (316°C)		
	Ult. Strength		Initial Modulus	Ult. Strength		Initial Modulus	Ult. Strength		Initial Modulus
	psi (10 ³)	MPa (10 ²)	psi (10 ⁶)	MPa (10 ²)	psi (10 ³)	MPa (10 ²)	psi (10 ³)	MPa (10 ²)	psi (10 ⁶) MPa (10 ⁴)
Cordopreg (flat)	52.7 T	3.6	2.5	1.7	16.7 C	1.2	0.84	0.58	0.95 0.65
EG/Epoxy Type 1	176.9 C&S	12.0	4.7	3.2	12.8 C&S	0.88	0.93	0.64	0.50 0.34
EG/Epoxy Type 2	153.8 T&S	11.0	5.6	3.6	74.1 C&S	5.1	2.63	1.8	N/A N/A
SG/Epoxy Type 1	215.0 C&S	15.0	5.2	3.5	98.0 C&S	6.8	3.50	2.4	N/A N/A
SG/Epoxy Type 2	207.5 C&S	14.0	5.1	3.5	17.5 S	1.2	1.23	8.5	N/A N/A
Quartz 581/ PMR-15	110.0 T	7.6	2.7	1.8	103.0 T&C	7.1	2.4	1.7	82 C 2.4 1.7

¹Values represent an average of three specimens.

²Letters below strength values indicate failure mode.

T - tensile failure on bottom

C - compressive failure on top

S - shear failure along midplane

the various materials, the relative degree of degradation at elevated temperatures also varies quite significantly from material to material.

5.14 NEW SURFACE TREATMENTS

Two bonded panels utilizing a reacted surface preparation on 2024-T3 bare aluminum adherends were submitted for evaluation. One panel was bonded with polypropylene with a lap of 1 inch (2.54 cm) and the other was bonded with Epon 828/Versamid 125 with a lap of 1/2 inch (1.27 cm). The latter panel was cured on a hot plate. For comparison, UDRI fabricated a standard lap-shear panel using an optimized FPL adherend etch and the Epon 828/Versamide 125 adhesive system with a 1/2 inch (1.27 cm) lap and cured at room temperature for seven days.

Table 77 reports the results obtained on these three adhesive panels. Examination of the data shows a difference in the control data obtained on the two panels which were bonded with the Epon 828/Versamide 125 adhesive system. The difference in the cure cycles of these two panels could account for this variation in the control data. The exposure of test specimens to 14 days at 140°F (60°C), 95-100 percent R.H. seemed to continue the cure of the UDRI fabricated panel, improving its strength considerably to the unaged controls.

Perhaps a better method to evaluate this reacted surface preparation is to perform a wedge-type of test comparing it to other standard surface preparation such as optimized FPL and phosphoric acid anodized.

5.15 BONDING PANELS FOR STRESS-DURABILITY

A request for the fabrication of stress-durability specimens was received. The purpose of this effort was to furnish test coupons to determine the effects of temperature-humidity and stress on the mechanical properties of adhesives. This project consisted of the fabrication of 960 samples using 6061-T6 bare

TABLE 77
LAP SHEAR PROPERTIES OF BONDS INCORPORATING
REACTED SURFACE VS. OPTIMIZED FPL
ETCHED SURFACE TREATMENTS

Specimen Type ¹	Aging Condition	Test Temperature		Ultimate Strength		Failure Mode % Adh-% Coh
		(°F)	(°C)	(psi)	(MPa)	
Reacted Surface Polypropylene Adhesive 1-inch Lap	None	72	22	1000	6.9	65-35
	14 days @ 140°F(60°C) 95-100% R.H.	140	60	1300	9.0	90-10
Reacted Surface 828/125 Adhesive Hotplate Cure 1/2-inch Lap	None	72	22	3890	26.8	80-20
	14 days @ 140°F(60°C) 95-100% R.H.	140	60	2690	18.5	80-20
Opt. FPL Etch 825/125 Adhesive 72°F(22°C) Cure 1/2-inch Lap	None	72	22	1510	10.4	95-5
	14 days @ 140°F(60°C) 95-100% R.H.	140	60	2720	18.8	85-15

¹All adherends were 2024-T3 bare aluminum.

aluminum adherends, surfaces of which were prepared with optimized FPL etch and primed with BRL27 primer. The five film adhesives were: Narmco M1117, Hysol EA9652 and EA9601NW, McCann MA429, and 3M AF180. Table 78 reports the lap-shear control data obtained on each adhesive system. These data along with the 900 test coupons were forwarded to the initiator for stress-durability testing at ARRADCOM.

5.16 EVALUATION OF SCAR SPECIMEN DESIGN

The objective of this program was to compare the stress-durability behavior of multi-joint adhesive (SCAR-Stress Continuous Adhesive Replicate) specimens with regular single-lap specimens in both the spring-loaded "Sharp" jigs and the hydraulically-loaded cells in the Durability Test Apparatus (see AFML-TR-78-35). Figure 65 shows these joint configurations.

Three standard (ASTM D1002) single lap shear panels were prepared (designated 011-1,2,3). Twenty-one specimens were obtained from these three panels. These were divided into four groups of five specimens each, with one or two specimens from each panel in each group of five. Two groups were tested for static lap shear strength at 72°F (22°C) and 140°F (60°C), respectively. One group was tested in a stress-durability mode in the spring-loaded Sharp fixtures. The fourth group was tested in a stress-durability mode in the hydraulically-loaded cells of the Durability Test Apparatus. The results of these tests are presented in Tables 79, 80, and 81, respectively. There is little apparent difference between the two different stress-durability test method results, either in the times-to-failure, residual strength, or failure modes.

Two SCAR panels (designated 011-4,5) were prepared. Each was prepared in a two-inch width and sliced lengthwise to provide two five-specimen gangs each. One-half of panel 011-4 was tested statically at 140°F (60°C) to provide baseline data. These data are presented in Table 79. The other half of panel

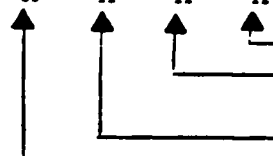
TABLE 78
LAP-SHEAR CONTROL PROPERTIES OF
BONDED PANELS FOR STRESS-DURABILITY

Adhesive System	Test Temperature ¹	Lap-Shear Strength ²		Failure ³ Location
		psi (S.D.)	MPa (S.D.)	
McCann's MA 429 T	R.T.	4960 (275)	34.2 (0.2)	10-0-60-30
	140°F (60°C)	4870 (193)	33.6 (0.2)	0-0-10-90
	200°F (93°C)	3820 (115)	26.3 (0.2)	0-0-10-90
Hysol's EA 9601 NW	R.T.	4070 (130)	28.0 (0.9)	20-10-0-70
	140°F (60°C)	4330 (160)	29.8 (1.1)	15-10-0-75
	200°F (93°C)	3740 (240)	25.8 (1.7)	20-10-0-70
Hysol's EA 9652	R.T.	4350 (420)	30.0 (2.9)	10-25-0-65
	140°F (60°C)	4310 (182)	29.7 (1.3)	5-15-0-80
	200°F (93°C)	3690 (208)	25.4 (1.4)	5-0-15-80
Narmco's MB 1117	R.T.	3990 (370)	27.5 (2.5)	0-0-10-90
	140°F (60°C)	4440 (190)	30.6 (1.3)	0-0-30-70
	200°F (93°C)	4220 (220)	29.0 (1.5)	0-0-10-90
3M's XA 180	R.T.	4700 (165)	32.4 (1.1)	0-0-0-100
	140°F (60°C)	4020 (206)	27.7 (1.4)	0-0-0-100
	200°F (93°C)	3250 (197)	22.4 (1.4)	0-0-0-100

¹Specimens tested at elevated temperature were held at temperature for 10 minutes before testing.

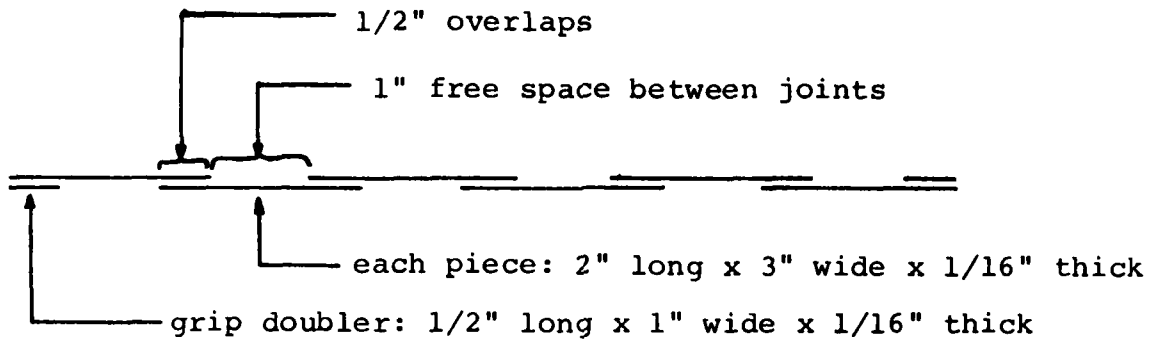
²Average of 10 specimens.

³X - X - X - X



 cohesive failure within the adhesive layer.
 adhesive (interfacial) failure between the
 adhesive and the primer.
 cohesive failure within the primer layer.
 adhesive (interfacial) failure between the
 primer and the substrate oxide.

SCAR Specimen (Stress Continuous Adhesive Replicate Specimen)



When a joint fails, drill the joint so it can be bolted back together and the chain returned to the aging chamber. Develop a guide or method so the holes are drilled on the specimen centerline. Use some sort of washer under the bolts to spread the load and prevent bearing failures.

Standard Single Lap Shear Specimen

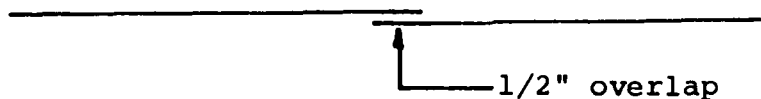


Figure 65. Specimen Configurations for SCAR Design Evaluation.

TABLE 79
STATIC LAP-SHEAR TEST RESULTS
FOR SCAR DESIGN EVALUATION

Specimen Number	Test Temperature		Ultimate Strength		Failure Sequence	Failure Mode
	(°F)	(°C)	(psi)	(MPa)		M/P-P-P/A-A
SCAR						
011-4-2-4	140 ¹	60	3080	21.2	1	0-0-80-20
011-4-2-5	↓	↓	3080	21.2	1	0-0-60-40
011-4-2-3			2810	19.4	2	0-0-70-30
011-4-2-1			2980	20.5	3	0-0-80-20
011-4-2-2			2780	19.2	4	0-0-60-40
Average	↓	↓	2950	20.3		
Std. Dev.			140	1.0		
Standard Lap Shear						
011-1-1	72	22	3180	21.9	N.A.	0-0-90-10
011-1-5	↓	↓	3260	22.5	↓	0-0-90-10
011-2-2			2980	20.5		0-0-100-0
011-2-6			3450	23.8		0-0-100-0
011-3-3			3040	20.9		0-0-90-10
Average	↓	↓	3180	21.9	↓	
Std. Dev.			186	1.3		
011-1-2	140 ¹	60	3180	21.9	N.A.	0-0-90-10
011-1-6	↓	↓	3300	22.7	↓	0-0-90-10
011-2-3			3010	20.7		0-0-90-10
011-2-7			3380	23.3		0-0-80-20
011-3-4			3120	21.5	↓	0-0-80-20
Average	↓	↓	3200	22.0		
Std. Dev.			145	1.0		

¹- Specimens tested @ 140°F (60°C) after 10 minutes @ 140°F (60°C).

TABLE 80

STRESS-DURABILITY TEST RESULTS USING THE SHARP FIXTURE
FOR SCAR DESIGN EVALUATION @ 140°F (60°C), 95-100% R.H.

Specimen Number	Exposure Stress Level		Stress-Durability		Residual Lap Shear Results		
	(psi)	(MPa)	Time to Failure (hours)	Failure Mode M/P-P-P/A-A	Strength (psi) (MPa)	% of Baseline	Failure Mode M/P-P-P/A-A
Baseline @ 140°F = 3080 psi							
011-4-1-2	1600	11.0	2400+	-----	2350 16.19	76	0-0-0-100
011-4-1-3	1633	11.3	2400+	-----	1990 13.71	65	0-0-0-100
011-4-1-4	1600	11.0	2400+	-----	1920 13.23	62	0-0-0-100
011-4-1-5	1600	11.0	2400+	-----	2450 16.88	80	0-0-0-100
011-4-1-1	1600	11.0	2400+	-----	2300 15.85	75	0-0-20-80
Average			2400+		2200 15.16	72	
Std. Dev.			-0-		233 1.61	8	
Baseline @ 140°F = 3200 psi							
011-5-2-1	1600	11.0	69	0-0-0-100	---	--	-----
011-5-2-3	1600	11.0	144	0-0-0-100	---	--	-----
011-5-2-4	1600	11.0	144	0-0-0-100	---	--	-----
011-5-2-2	1570	10.8	162	0-0-0-100	---	--	-----
011-5-2-5	1600	11.0	162.5	0-0-0-100	---	--	-----
Average			136				
Std. Dev.			39				
Baseline @ 140°F = 3200 psi							
011-1-4	1600	11.0	2400+	-----	2440 16.81	76	0-0-30-70
011-2-1	1600	11.0	2400+	-----	2360 16.26	74	0-0-20-80
011-2-5	1600	11.0	2400+	-----	2440 16.81	76	0-0-30-70
011-3-2	1600	11.0	2069	0-0-0-100	---	--	-----
011-3-6	1600	11.0	1478	0-0-5-95	---	--	-----
Average			2150+		2410 16.60	75	
Std. Dev.			402		46 0.32	1	

NOTES: 1. Residuals tested at 140°F (60°C) after 10 minutes @ 140°F (60°C).

2. SCAR specimens listed in the order of failure.

3. SCAR Lap 011-5-2-4 failed while being reloaded and the failure time has been recorded the same as the previous failure times.

TABLE 81

**STRESS-DURABILITY TEST RESULTS USING THE DURABILITY TEST APPARATUS
FOR SCAR DESIGN EVALUATION @ 140°F (60°C), 95-100% R.H.**

Specimen Number	Exposure Stress Level		Stress-Durability		Residual Lap Shear Results		
	(psi)	(MPa)	Time to Failure (hours)	Failure Mode M/P-P-P/A-A	Strength (psi)	% of Baseline	Failure Mode M/P-P-P/A-A
SCAR	Baseline @ 140°F = 3080 psi						
011-5-1-1	1600	11.0	243.1	0-0-0-100	-----	-----	-----
011-5-1-2	1568	10.8	259.1	0-0-0-100	-----	-----	-----
011-5-1-4	1633	11.2	360.1	0-0-0-100	-----	-----	-----
011-5-1-5	1600	11.0	370.85	0-0-0-100	-----	-----	-----
011-5-1-3	1600	11.0	370.85	0-0-0-100	-----	-----	-----
Average			321				
Std. Dev.			64				
NOTE: Listed in the order of failure.							
Standard Lap Shear	Baseline @ 140°F = 3200 psi						
011-1-3	1600	11.0	2400+	-----	2050	64	0-0-0-100
011-1-7	1600	11.0	2400+	-----	2170	68	0-0-0-100
011-2-4	1600	11.0	2400+	-----	2590	81	0-0-0-100
011-3-1	1600	11.0	2009	0-0-0-100			
011-3-5	1600	11.0	2400+	-----	2460	77	0-0-0-100
Average			2322+		2320	73	
Std. Dev.			175		250	8	

NOTE: Residuals tested at 140°F (60°C) after 10 minutes @ 140°F (60°C).

011-4 was tested in a stress-durability mode in a Sharp fixture. These results are presented in Table 80. One-half of panel 011-5 was tested in a stress-durability mode in one of the hydraulically-loaded cells of the Durability Test Apparatus. The results for this specimen gang are presented in Table 81.

It will be readily observed that the stress-durability behavior of panel 011-5 in the Durability Test Apparatus was substantially inferior to that of panel 011-4 in the Sharp fixture or to that of the standard lap shear specimens in either device. At this point, it was decided to test the remaining half of panel 011-5 in the Sharp fixtures. These data are presented in Table 82. The time-to-failure for the second half of panel 011-5, tested in the Sharp fixture, was also dramatically shorter than that for panel 011-4 or for the standard lap shear specimens tested in either device. This would indicate that, for some unknown reason, panel 011-5 did not have good bonded joints. Disregarding the results of panel 011-5, one notes that there is little apparent difference between the two different stress-durability loading modes or between the two different specimen types. The problem arising with panel 011-5, however, indicates the need to assess bond quality prior to testing on the SCAR specimen. This is of particular concern because one cannot mix specimens from different panels in a SCAR specimen chain. One possibility may be to make a wider SCAR panel so more than two chains can be cut from a single panel.

5.17 CHARACTERIZATION OF A "SILICADIZED COATING" AS A BONDING SURFACE

The purpose of this project was to evaluate silicadized coatings as an adhesive bonding surface. The seven types of coated adherends were cut into two halves and wiped clean with methanol. They were dried for two hours at 200°F (93°C) and stored in a dessicator until bonded. The halves were bonded together with FM 73 and tested for lap shear strength at room temperature. Table 82 shows the results of this evaluation.

TABLE 82
LAP SHEAR RESULTS ON SILICADIZED
COATINGS TESTED AT ROOM TEMPERATURE

Specimen Type	Lap Shear Strength		Failure Mode (%)			
	(psi)	(MPa)	M/C	C	C/A	A
A1D1	2360	16.3	80	0	20	0
A1C6	3490	24.0	0	0	95	5
A2C0	1480	10.2	50	0	50	0
A7B1	4350	30.0	30	0	60	10
B1C0	1900	13.1	20	0	75	5
B2C6	3440	23.7	0	0	100	0
B2D2	2120	14.5	80	0	20	0

The failure mode column describes where the failure occurred in percentage form.

- M/C Adhesive (interfacial) failure between the silicadized coating and the substrate oxide.
- C Cohesive failure within the silicadized coating.
- C/A Adhesive (interfacial) failure between the adhesive and the silicadized coating.
- A Cohesive failure within the adhesive layer.

One can expect to obtain about 6000 psi (41 MPa) lap shear strength at room temperature with FM 73. Examination of the test results reveals that none of the silicadized specimens achieved this strength level. Most of the failures occurred interfacially between the silicadized coating and the substrate oxide or between the silicadized coating and the adhesive rather than in the adhesive layer.

5.18 DURABILITY TESTING OF FM400/BR400 ADHESIVE JOINTS

The object of this program is to evaluate the effect of powdered aluminum filler upon the environmental degradation of adhesive joints exposed to elevated temperature and high humidity. The three adhesive systems being investigated are: Commercial FM400 (with scrim and aluminum filler), UD formulated FM400 (with aluminum filler and no scrim), and UD formulated FM400 (with no scrim or aluminum filler). The two special UD FM400 formulations are:

UD1 - MY720I	100 pbw
Dicyandiamide X	10 pbw
MD105 Aluminum Powder	175 pbw
UD2 - MY720I	100 pbw
Dicyandiamide X	10 pbw

2024-T81 bare aluminum adherends were used with the optimized FPL surface preparation and BR400 primer.

The test matrix which was followed is presented in Table 83. The test results obtained for the seven static lap shear conditions are presented in Tables 84-86. Table 87 presents the environmental stress-durability behavior of three adhesive systems. These results will be analyzed and discussed more thoroughly in an upcoming technical report.

5.19 COMPATIBILITY OF PHOSPHORIC ACID ANODIZING WITH 350°F (177°C) CURING ADHESIVE PRIMERS

A program was undertaken to determine the compatibility of phosphoric acid anodized (PAA) aluminum surfaces with 350°F

TABLE 83
FM400 ADHESIVE DURABILITY TEST MATRIX

Test Type	Test Temperature		Test or Pretest Conditioning	Replicates
	(°F)	(°C)		
Lap shear	72	22	None	5
Lap shear	160	71	None	5
Lap shear	250	121	None	5
Lap shear	72	22	30 days @ 160°F(71°C) & 95-100% R.H., unstressed	5
Lap shear	72	22	100 days @ 160°F(71°C) & 95-100% R.H., unstressed	5
Lap shear	160	71	100 hr soak in water @ 160°F(71°C), unstressed	5
Lap shear	160	71	1,000 hr soak in water @ 160°F(71°C), unstressed	5
Stressed durability	160	71	20% of 160°F(71°C) dry ultimate stress & 95-100% R.H.	4 ¹
Stressed durability	160	71	30% of 160°F(71°C) dry ultimate stress & 95-100% R.H.	4
Stressed durability	160	71	40% of 160°F(71°C) dry ultimate stress & 95-100% R.H.	4
Stressed durability	160	71	50% of 160°F(71°C) dry ultimate stress & 95-100% R.H.	4

¹Four replicates derive from chamber ability to accommodate specimens.

TABLE 84

STATIC THICK ADHEREND LAP-SHEAR STRENGTH OF
COMMERCIAL FM400 ADHESIVE SYSTEM

Test Temperature ¹		Aging Condition	Strength		% Cohesive Failure
(°F)	(°C)		(psi)	(MPa)	
72	22	None	7440	51.3	10
160	71	None	6410	44.2	20
250	121	None	5470	37.7	40
72	22	28 days @ 160°F (71°C), 95-100% R.H.	5860	40.9	40
72	22	100 days @ 160°F (71°C), 95-100% R.H.	4600	31.7	40
160	71	100 hours soak in water @ 160°F (71°C)	5790	39.9	40
160	71	1000 hour soak in water @ 160°F (71°C)	4380	30.2	70

¹Dry specimens held at test temperature 30 minutes prior to test. Aged specimens held at test temperature 10 minutes prior to test.

TABLE 85
 STATIC THICK ADHEREND LAP-SHEAR STRENGTH OF
 UD-1 (with aluminum filler and
 no scrim)

Test Temperature ¹		Aging Condition	Strength		% Cohesive Failure
(°F)	(°C)		(psi)	(MPa)	
72	22	None	6020	41.5	10
160	71	None	4800	33.1	10
250	121	None	3480	24.0	10
72	22	28 days @ 160°F (71°C), 95-100% R.H.	5200	35.8	0
72	22	100 days @ 160°F (71°C), 95-100% R.H.	4860	33.5	10
160	71	100 hour soak in water @ 160°F (71°C)	4800	33.1	10
160	71	1000 hour soak in water @ 160°F (71°C)	4476	30.8	20

¹Dry specimens held at test temperature 30 minutes prior to test. Aged specimens held at test temperature 10 minutes prior to test.

TABLE 86
 STATIC THICK ADHEREND LAP-SHEAR STRENGTH OF
 UD-2 (with no scrim or aluminum
 filler)

Test Temperature ¹		Aging Condition	Strength		% Cohesive Failure
(°F)	(°C)		(psi)	(MPa)	
72	22	None	2870	19.8	10
160	71	None	2660	18.4	10
250	121	None	2540	17.5	10
72	22	28 days @ 160°F (71°C), 95-100% R.H.	3170	21.8	10
72	22	100 days @ 160°F (71°C), 95-100% R.H.	3100	21.3	10
160	71	100 hour soak in water @ 160°F (71°C)	3430	23.6	10
160	71	1000 hour soak in water @ 160°F (71°C)	3170	21.8	10

¹Dry specimens held at test temperature 30 minutes prior to test. Aged specimens held at test temperature 10 minutes prior to test.

TABLE 87
ENVIRONMENTAL STRESS-DURABILITY BEHAVIOR
OF LAP-SHEAR ADHESIVE JOINTS

Adhesive	Joint Shear Stress During Exp.			Time to Failure (hours)	Residual Lap-Shear Strength	
	(psi)	(MPa)	% of 160°F (71°C) dry ultimate		(psi)	(MPa)
FM400	3200	22.0	50	22.0	---	---
	3200	22.0	50	64.0	---	---
	3200	22.0	50	180.5	---	---
	3200	22.0	50	173.6	---	---
	2590	17.8	40	66.0	---	---
	2590	17.8	40	203.3	---	---
	2590	17.8	40	263.6	---	---
	2590	17.8	40	444.3	---	---
	1920	13.2	30	2423+ ³	3470	23.9
	1920	13.2	30	2423+ ³	3110	21.4
	1920	13.2	30	2423+ ³	3530	24.3
	1920	13.2	30	2423+ ³	Broke in handling	
UDRI-1	3360	23.2	70	1.1	---	---
	3360	23.2	70	1.2	---	---
	3360	23.2	70	6.8	---	---
	3360	23.2	70	2.5	---	---
	3120	21.5	65	126.0	---	---
	3120	21.5	65	180.8	---	---
	3120	21.5	65	3.1	---	---
	3120	21.5	65	210.4	---	---
	2880	19.8	60	500.0	---	---
	2880	19.8	60	664.7	---	---
	2880	19.8	60	336.4	---	---
	2880	19.8	60	1919.5+ ³	4840	33.3
	2400	16.5	50	2400.0+ ³	4600	31.7
	2400	16.5	50	2400.0+ ³	4950	34.1
	2400	16.5	50	2400.0+ ³	5080	35.0
	2400	16.5	50	2400.0+ ³	5100	35.1
UDRI-2	2260	15.6	85	2.3	---	---
	2260	15.6	85	2263.7+ ³	2300	15.8
	2260	15.6	85	1944.0+ ²	---	---
	2130	14.7	80	9.7	---	---
	2130	14.7	80	24.9	---	---
	2130	14.7	80	2419.0+ ³	Broke in handling	
	2130	14.7	80	2424.0+ ³		
	1860	12.8	70	2419.0+ ³	3360	23.2
	1330	9.17	50	2419.0+ ³	3480	24.0
	1330	9.17	50	2400.0+ ³	3230	22.3
	1330	9.17	50	2400.0+ ³	3310	22.8
	1330	9.17	50	2400.0+ ³	3370	23.2

¹ Exposure at 160°F (71°C), 95-100% R.H.

² Means the sample is still being stressed to failure or 2400 hours time limit.

³ Specimens survived the 2400 hour time limit without failure and were removed for residual strength testing (one specimen inadvertently removed and tested after only 1919.5 hours).

(177°C) curing adhesive primers. Some past investigations (Schwartz, Marceau) indicated that the environmental durability of 350°F (177°C) adhesive/primer systems was greater on an FPL etched surface than on a PAA surface. The program reported here consisted of conducting surface examinations, lap shear, peel, wedge, and stress-durability tests on a variety of joint combinations. The following alloy/surface preparations/primers/ and adhesives are involved:

1. Adherend alloy - 2024-T81 bare;
2. Surface preparations - optimized FPL (OFPL) and PAA;
3. Adhesive/primer combinations - No primer/R398; RB500/R398; No primer/MB329; RB500;MB329; and MB-6725-1/MB329.

The program was organized into three tasks; namely,

- Task I - Surface Examination;
- Task II - Baseline Values; and
- Task III - Surface Effects Tests.

Task I involved preparing both OFPL etched and PAA surfaces and spraying both primers on the surfaces. Scanning electron micrographs (SEM) of both cured and uncured primer samples on each type surface were to be obtained.

Task II involved the preparation of bonds with each combination of alloy/surface prep/adhesive-primer listed above and testing for lap shear and peel strength according to the following test plan:

- (a) Lap shear strength at 72°F (22°C) - ASTM D1002;
- (b) Lap shear strength at 350°F (177°C) - ASTM D1002;
- (c) Peel strength at 72°F (22°C) - ASTM D3167; and
- (d) Peel strength at -65°F (-54°C) - ASTM D3167.

Three replicates of each material combination were tested, requiring a total of 120 test specimens in Task II (two surface preps x five adhesive/primer combinations x four test conditions x three replicates).

Task III involved the preparation of bonds with each combination of materials listed above and testing for wedge crack-propagation and environmental stress-durability according to the following test plan:

(a) Wedge crack-propagation in a 95°F (35°C)/five percent salt spray environment, and

(b) Stress-durability in a 95°F (35°C)/five percent salt spray environment at a stress level equal to 50 percent of the 72°F (22°C) lap shear strength.

Five replicates of each material combination were tested, requiring a total of 100 test specimens in Task III (two surface preps x five adhesive/primer combinations x two test conditions x five replicates).

The surface examinations conducted in Task I provided no evidence of non-wetting for either surface preparation method or for either the cured or non-cured primer condition for the RB500 primer. No evidence of rubber inclusions was present either. Small lumps which were dispersed throughout the primer were shown to be strontium chromate particles, which are blended into the primer to impart corrosion resistance. Surface inspection for the MB-6725-1 primer were not obtained.

The results of the lap-shear and peel tests conducted in Task II are presented in Tables 88 and 89. It will be noted in these two tables that two different data values are presented for some of the adhesive/primer combinations. These represent values obtained from specimens made about three months apart but with the same materials and processing procedures. As can be observed, the data differs substantially in some cases. The places where the data differs most substantially are also those where the failure mode differed markedly. No explanation for this variability can be offered.

The results of wedge crack-growth tests in Task III are reported in Figures 66 and 67. These specimens were exposed to

TABLE 88
LAP SHEAR PROPERTY SUMMARY

Adhesive	Surface Prep.	Primer	72°F (22°C) Strength		350°F (177°C) Strength	
			(psi)	(MPa)	(psi)	(MPa)
R398	OPT	None	3320	22.9	2300	15.8
		500	3300	22.7	2380	16.4
R398	PAA	None	3890	26.8	2840	19.6
		500	2490	17.2	2300	15.8
		500	3130	21.6	2570	17.7
MB329-1	OPT	None	3150	21.7	2710	18.7
		500	2610	18.0	2880	19.4
		500	2690	18.5	3230	22.3
		6725-1	3260	22.5	3110	21.4
MB329-1	PAA	None	3370	23.2	3250	22.4
		500	2690	18.5	3170	21.8
		500	3020	20.8	3250	22.4
		6725-1	3040	20.9	3200	22.0

NOTES: 1. All tests were on 2024T81 aluminum adherends.
2. The two surface preparations are:
OPT - optimized FPL etch
PAA - phosphoric acid anodized.

TABLE 89
FLOATING ROLLER PEEL DATA SUMMARY

Adhesive	Surface Prep.	Primer	Peel Strength (lb/in width) [N/cm width]	
			72°F (22°C)	-65°F (-54°C)
R398	OPT	None	(8.31) [14.55] - 4	(6.99) [12.24] - 4
		500	(6.58) [11.52] - 3	(5.50) [9.63] - 3
R398	PAA	None	(5.62) [9.84] - 2	(5.34) [9.35] - 2
		None	(8.98) [15.72] - 2	(8.03) [14.06] - 2
		500	(12.94) [22.66] - 3	(13.93) [24.39] - 2
		500	(3.66) [6.41] - 3	(3.40) [5.95] - 2
MB329-1	OPT	None	(5.60) [9.81] - 4	(8.60) [15.06] - 4
		500	(5.03) [8.81] - 4	(3.14) [5.50] - 4
		6725-1	(4.88) [8.54] - 4	(6.23) [10.91] - 4
MB329-1	PAA	None	(5.01) [8.77] - 2	(4.38) [7.67] - 2
		None	(8.20) [14.36] - 2	(5.58) [9.77] - 2
		500	(6.43) [11.26] - 3	(5.92) [10.37] - 2
		500	(3.97) [6.95] - 3	(5.94) [10.40] - 2
		6725-1	(4.95) [8.67] - 4	(4.74) [8.30] - 4

- NOTES: 1. Numbers behind hyphens in each column represent the numbers of specimens tested.
2. All tests were on 2024T81 aluminum adherends.
3. The two surface preparations are:
 OPT - optimized FPL etch
 PAA - phosphoric acid anodized.

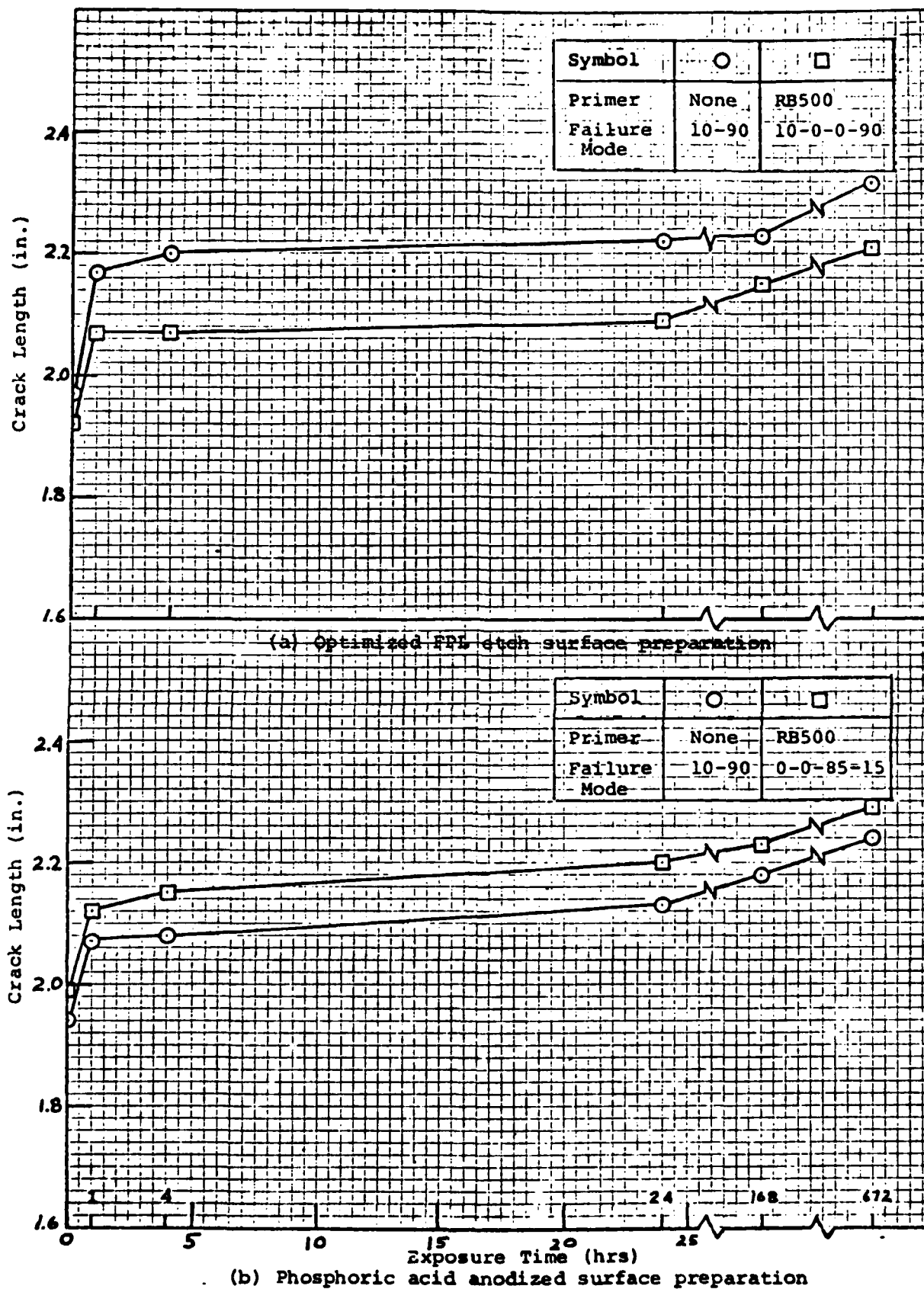
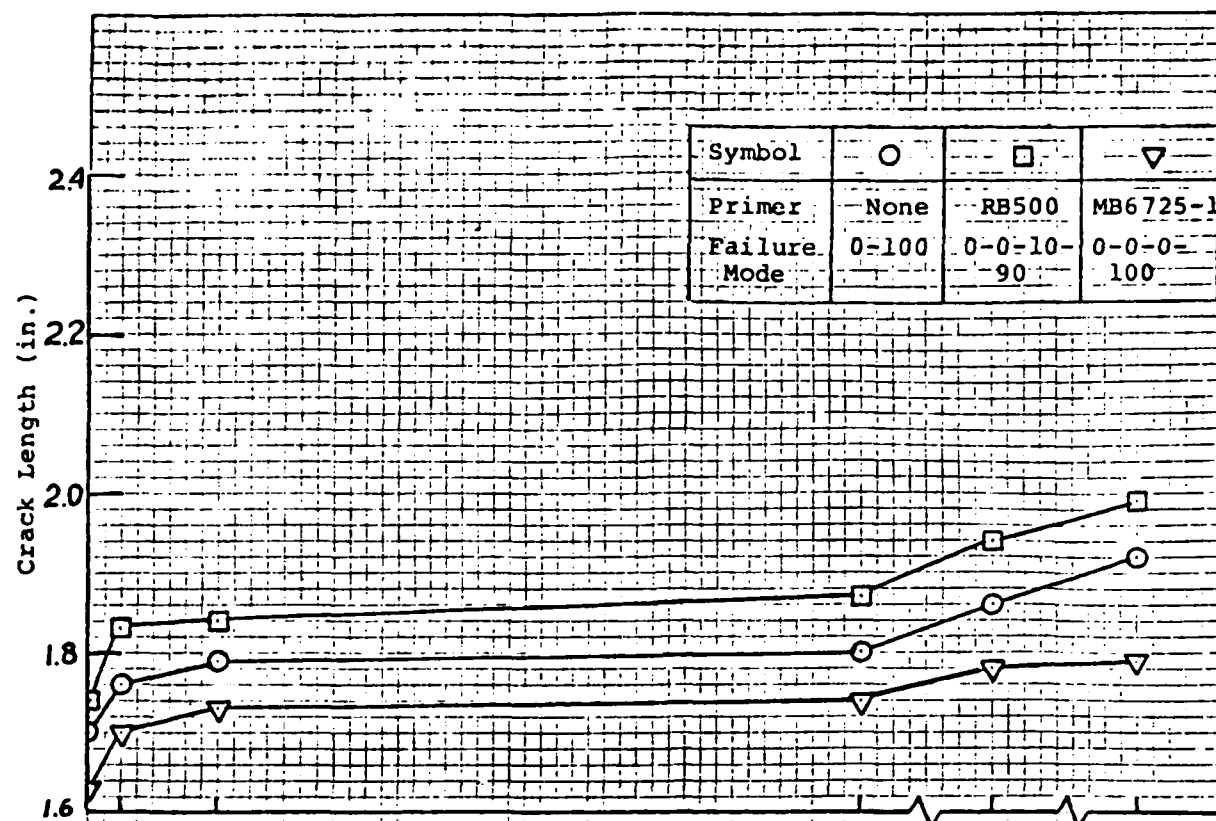
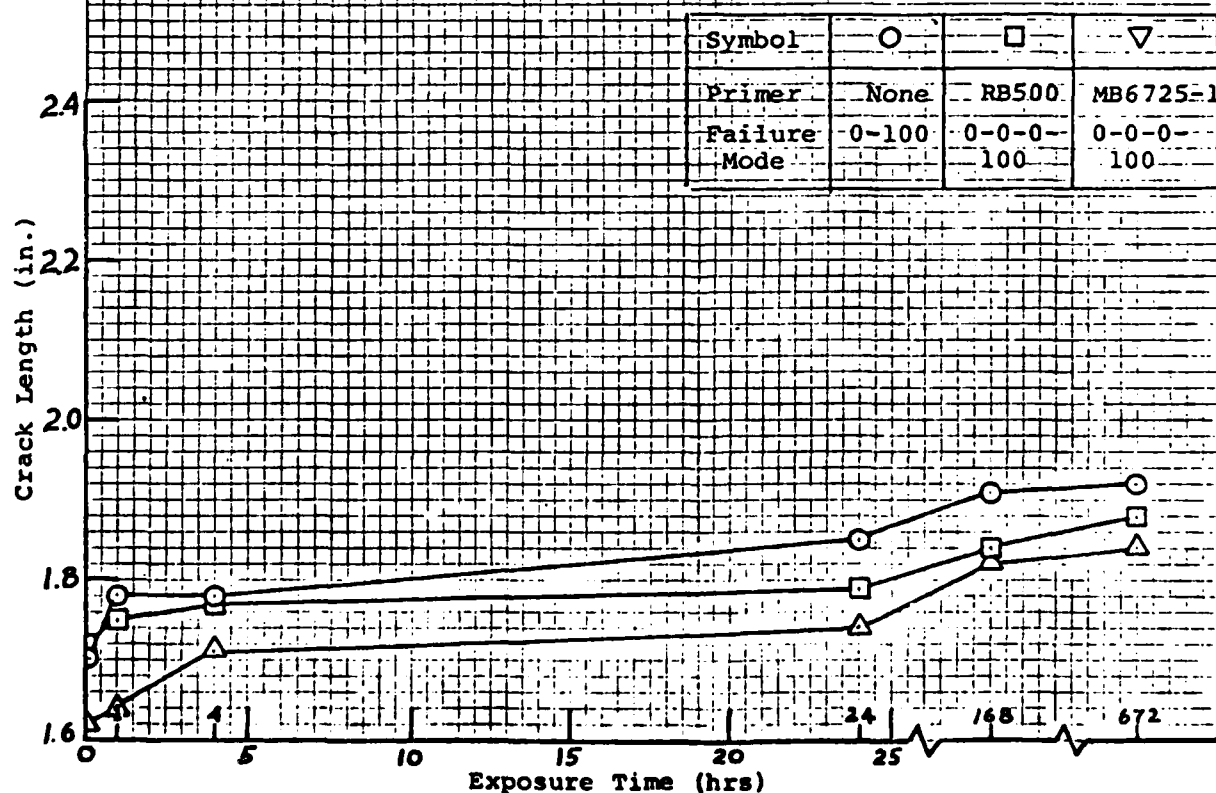


Figure 66 . Wedge Crack Propagation Results for Reliabond 398 Adhesive on 2024T81 Aluminum Adherends in Salt Fog Environment.



(a) Optimized FPL etch surface preparation



(b) Phosphoric acid anodized surface preparation

Figure 67 . Wedge Crack Propagation Results for MB329-1 Adhesive on 2024T81 Aluminum Adherends in Salt Fog Environment.

a 95°F (35°C)/5 percent NaCl salt fog environment and crack lengths were measured as a function of exposure time up to 28 days (672 hours). It will be noted in these figures that MB329-1 appears to be more resistant to this cleavage type crack propagation than RB398. The MB329-1 adhesive exhibits a shorter initial crack length than RB398 (~1.70 inch versus ~1.95 inch) (4.3 cm versus 5.0 cm) and also undergoes less crack growth during salt spray exposure than the RB398 (~0.2 inch versus ~0.3 inch) (0.5 cm versus 0.8 cm). Practically no difference in crack growth could be observed to distinguish between the two different surface preparations or the three different primer conditions.

The salt spray stress-durability testing required in Task III necessitated coating the gripped area of each specimen with a corrosion inhibiting coating before assembly into the loading fixture. The results of exposing the three lap-shear SCAR specimens to 95°F (35°C)/5 percent salt spray environment at a 50 percent stress level are reported in Table 90. All of the joints survived the 2400-hour exposure and were tested for residual strength at room temperature.

5.20 TENSILE SHEAR EVALUATION OF FUEL TANK ADHESIVES

The purpose of this task was to screen three adhesive systems for possible use as a fuel tank adhesive. The three adhesives evaluated were Hysol's 1664, and 3M's EC1838 and EC2216 Gray. These materials were tested for lap-shear strength at two conditions: room temperature and at room temperature after exposure to Type II hydrocarbon fuel at 140°F (60°C) for 60 days. The control data for these adhesives are presented in Table 91. Table 91 also reports the results obtained on these materials after being exposed to the hydrocarbon fuel. Several types of failure modes were observed due to the quality and configuration of the test specimen (Figure 68). Ninety-three (93) samples were tested in this evaluation, of these, 38 were good failures occurring in the lap area. Twenty-three (23) of

TABLE 90

STRESS-DURABILITY TEST RESULTS AFTER 2400-HOUR EXPOSURE TO
95°F (35°C), 5% SALT SPRAY ENVIRONMENT

Adhesive	Surface Prep.	Primer	Exposure Stress			Stress Durability		Residuals			
			% of Base-line	Level		Time (hours)	Failure Mode ¹	Ult. Strength		% of Base-line	Failure Mode ¹ M/P-P-P/P/A-A
				psi	MPa			psi	MPa		
R398	OPT	NONE	50	1670	11.5	2400+	-----	3390	23.4	102	90-10
		500	50	1650	11.4	2400+	-----	3020	20.8	91	0-0-20-80
R398	PAA	NONE	50	1940	13.4	2400+	-----	2450	16.9	63	20-80
		500	50	1240	10.8	2400+	-----	2570 ²	17.7	82	0-0-80-20
MB329-1	OPT	NONE	50	1590	10.9	2400+	-----	2930	20.2	93	60-40
		500	51	1380	9.5	2400+	-----	2620 ³	18.1	97	0-0-50-50
MB329-1	PAA	6725-1	50	1630	11.2	2400+	-----	3160	21.8	97	0-0-90-10
		NONE	51	1710	11.8	2400+	-----	1810	12.5	54	0-100
		500	50	1500	10.3	2400+	-----	2810	19.4	93	0-0-50-50
		6725-1	50	1540	10.6	2400+	-----	3310 ²	22.8	109	0-0-100-0

NOTE: 1. Failure Mode=M/P-Metal to Primer, P-within Primer, P/A-Primer to Adhesive, A-within Adhesive.

2. Test results of 1 specimen, 2 specimens failed in adherend.

3. Test results of 2 specimens, 1 specimen failed in adherend.

TABLE 91
FUEL TANK ADHESIVE DATA

Materials	Test Condition	Ultimate Strength ¹				Failure Mode (% Coh.)
		Avg (psi)	S.D. (psi)	Avg (MPa)	S.D. (MPa)	
3M 1838 Glass to Glass	R.T.	600	200	4.16	1.38	Note 3
	R.T. after aging ²	240	70	1.63	0.48	Note 4
3M 1838 Hytrel to Hytrel	R.T.	830	200	5.71	1.38	Note 5
	R.T. after aging	60	30	0.43	0.19	Note 6
Hysol 1664 Glass to Glass	R.T.	980	190	6.73	1.30	Note 3
	R.T. after aging	300	50	2.08	0.32	Note 7
Hysol 1664 Hytrel to Hytrel	R.T.	950	300	6.55	2.08	Note 8
	R.T. after aging	80	20	0.53	0.17	Note 9
3M 2216 Glass to Glass	R.T.	520	150	3.59	1.05	Note 3
	R.T. after aging	250	60	1.73	0.39	Note 10
3M 2216 Hytrel to Hytrel	R.T.	1080	320	7.47	2.19	Note 11
	R.T. after aging	30	---	0.21	---	Note 12

¹Average of 7 or 8 samples.

²60 days in Type II hydrocarbon fuel at 140°F (60°C).

³Failure within adherend.

⁴Six samples failed in lap-joint, one failure at bond between adherend and Al backing, adherend elongated at low load, and one sample had both adhesive and adherend failure.

⁵Four samples failed in lap-joint, three failures at bond between adherend and Al backing, adherend elongated at low load, and one failed first in adherend/Al bond, then in lap area.

⁶Four samples failed in lap-joint, four samples failed in bond area during exposure to hydrocarbon fuel, average of four samples.

⁷Failure at bond between adherend and Al backing, adherend elongated at low load.

⁸Four samples loaded in lap joint, four failures were at the bond between adherend and Al backing, adherend elongated at low load.

⁹All failure in lap-joint.

¹⁰Six samples failed in lap-joint, one sample failed at bondline between adherend and Al backing elongated at low load.

¹¹Five samples failed in lap-joint, two samples failed at bondline between adherend and Al backing elongated at low load.

¹²One sample failed in lap-joint, six samples failed in aging.

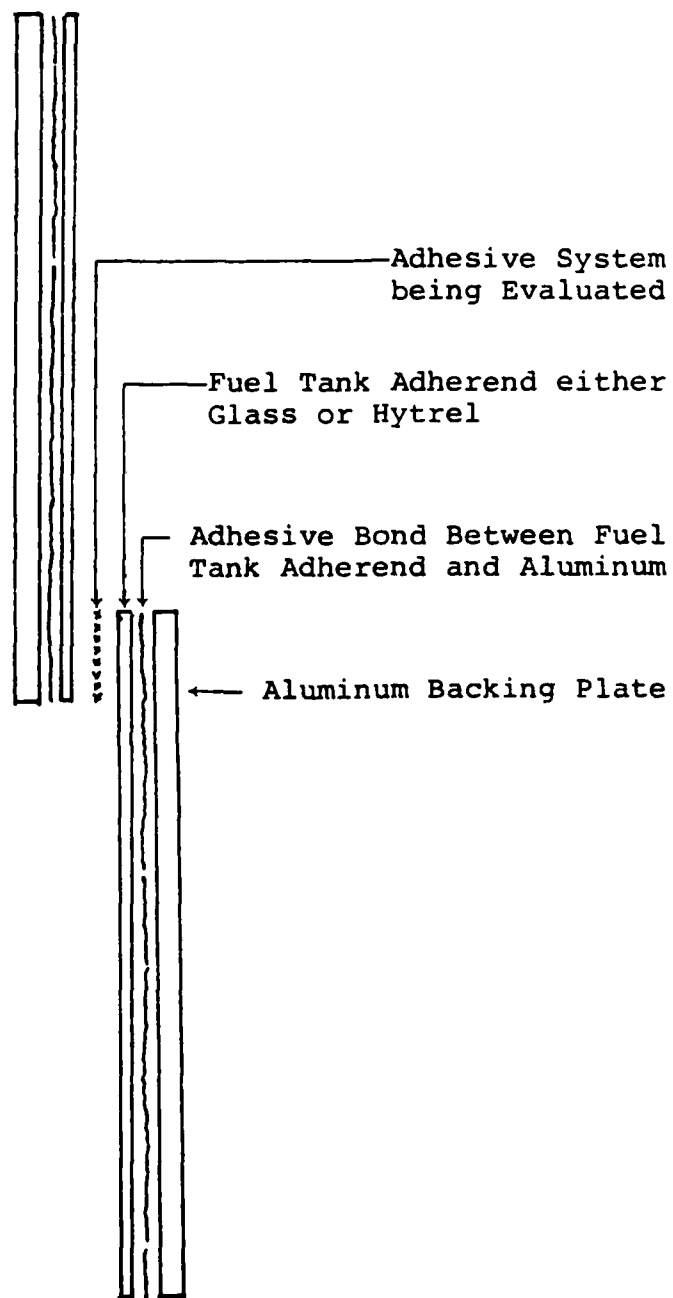


Figure 68. Fuel Tank Lap Shear Specimen.

the specimens failed within the fuel tank adherend, because the aluminum backing plate was either loose or not attached to the fuel tank adherend. Nineteen (19) samples failed along the bondline between the fuel tank adherend and the aluminum backing plate. When this occurred, the load would drop off and the fuel tank adherend would elongate. Ten (10) specimens failed in the bond area during the time of exposure to the hydrocarbon fuel. Of the three remaining samples, two of them failed both in the lap area and at the fuel tank adherend and aluminum backing plate bondline. The last type of failure occurred in the lap area and in the fuel tank adherend.

The data indicate that there is some lap shear strength when the three adhesive systems were used to bond the glass to glass adherends. Better test specimens are needed to obtain actual lap shear values since many of the failures occurred outside the lap area. It also indicates that none of the adhesive systems, when used to bond Hvtrel to Hytrel adherends, had any lap shear integrity after the fuel agings.

5.21 SHELTER REPAIR ADHESIVES

The primary objective of this investigation was to measure the lap-shear and stress-durability behavior of several shelter repair adhesive candidates as a function of temperature and environmental exposure. Eight different two-part paste adhesives were tested at temperatures up to 200°F (93°C).

Of these eight, three withstood the combined elevated temperature, high humidity exposure conditions very well relative to the other five. Three of the eight performed quite poorly.

A technical report (AFWAL-TR-81-4081) has been submitted for publication which describes all of the procedures and results of this program in considerable detail.

5.22 COPPER CONTENT OF FPL ETCH SOLUTIONS

A standard FPL sulfuric acid-sodium dichromate etch bath is optimized by the addition of copper to the initial etch

solution. This "sweetening" procedure produces a bonding surface which is much more durable in hot, wet environments than one produced with an "unsweetened", or standard FPL etch bath.

During the course of our work on the Shelter Adhesive investigations, a question was raised as to whether an optimized or initially sweetened FPL etch bath becomes depleted in copper after etching non-copper containing aluminum alloys such as 5052. If the copper content of the solution was reduced with age, one would eventually be left with an unsweetened or standard FPL etch rather than the optimized solution one started with.

A standard operating procedure in using optimized FPL etch baths is to periodically analyze the bath solution for pH, sulfuric acid concentration, and sodium dichromate concentration. The acid and dichromate concentrations are adjusted by the addition of the appropriate amounts of each constituent to return the bath to within its prescribed limits. No such analysis for copper has been specified.

This investigation was directed toward determining whether the copper content of an optimized FPL etch solution remained stable or steadily diminished with use when a non-copper containing aluminum alloy (5052) was being treated.

A standard FPL etch solution was prepared. Two samples of this solution were then withdrawn and "sweetened" with 0.12 ounce and 0.05 ounce of 2024 aluminum alloy per gallon of solution, respectively, by dissolving the aluminum in the etch solutions. The remainder of the main etch solution was "sweetened" with 0.25 ounce of 2024 aluminum alloy per gallon.

Four liters of the sweetened main etch solution were placed in the etch pan. A series of 60 four-inch by nine-inch 5052 aluminum sheets were then immersed in the solution (one at a time) and subjected to the standard etch process called for in ASTM D2651.

Twenty-five milliliter samples of this solution were withdrawn for subsequent copper analysis after etching 2, 5, 10,

20, 40, and 60 panels. Small specimens for chemical surface analysis for copper were cut from the first, 20th, and 60th panel etched. Throughout the etching process, the pH, sulfuric acid concentration, and sodium dichromate concentration of the etch solution were periodically measured and adjusted as discussed earlier.

The copper concentrations of the nine sample solutions (three originals and six in process) were measured by atomic absorption. The surface analysis of the three etched panels was accomplished with energy dispersive x-ray analysis (EDAX). The results of the solution analyses are presented in Table 92.

TABLE 92
ATOMIC ABSORPTION ANALYSES OF ACID
SOLUTIONS FOR COPPER

Identification	Scale Reading	Fraction of Primary Control
Initial solution 0.25 oz/gal	51.2	1.000
Initial solution 0.12 oz/gal	24.2	0.473
Initial solution 0.05 oz/gal	10.5	0.205
In-process solutions		
2nd panel	53.3	1.041
5th panel	52.1	1.018
10th panel	54.3	1.061
20th panel	53.8	1.051
40th panel	53.1	1.037
60th panel	53.9	1.053

No copper was detectable on any of the three samples submitted for EDAX. Detection limits with this technique are 0.1-0.5 percent.

Based on the above results, it appears that the copper originally added to the etch solution is not depleted with use for a non-copper-containing alloy and that one need not

AD-A122 004

ARC EVALUATION OF MATERIALS AND PROCESSES(D) DAYTON
UNIV OH RESEARCH INST D R ASKINS ET AL OCT 82
UDR-TR-82-85 AFWAL-TR-82-4104 F33615-80-C-5011

474

UNCLASSIFIED

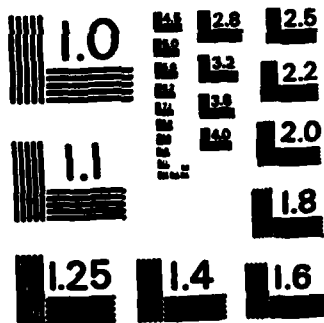
F/G 14/2

NL

END

FILMED

DTIC



MICROCOPY RESOLUTION TEST CHART
NATIONAL BUREAU OF STANDARDS-1963-A

be concerned with analyzing the solution for copper content as one must for changes in pH, acid or dichromate concentrations. Further, the copper does not seem to be deposited on the etched oxide surface in any detectable quantities.

It would be informative to ascertain the mechanism of participation for the copper in the etching process. This knowledge would be of value in guiding future studies of surface preparations leading to durable bonding surfaces.

Several possible mechanisms can be speculated on. One might be that the copper acts as a wetting agent, reducing interfacial tension and enhancing but not participating in the surface oxidation reactions. A second might be that the copper forms complexes which are organically soluble and thereby acts as a coupling agent between the oxide and the primer. This would be in trace amounts too small to be detectable. A third might be that the copper participates in some sort of electrochemical reaction which leads to a more durable oxide formation. In this case copper in some form would be deposited on the oxide surface, but in amounts too small to be detectable by EDAX.

While further investigations aimed at defining the exact chemical mechanism of oxide formation appear warranted, they were not within the scope of this particular effort.

5.23 STATISTICAL STUDY OF RYTON R-4 INJECTION MOLDING

The objective of this investigation was to determine whether molding similar specimens at different times and from different resin batches causes significant differences in Ryton tensile properties. Eight sets of ASTM D638, Type I tensile specimens were injection molded at one-week intervals and from two different resin batches. One set from each batch was dried before molding while the other three were molded "as-is". The various sets were divided into subsets and tested at different times. Tensile strength, modulus, and

ultimate elongation were recorded and the results were statistically analyzed to ascertain the significance of the various fabrication and testing variables on tensile properties.

The only factor that had a consistent effect on tensile properties of Ryton R-4 was the date of testing. The molding date did not have a significant effect on any of the three properties measured (strength, modulus, or ultimate elongation). The only batch-to-batch difference that was significant was in modulus. This difference was on the order of 10 percent. It must be recalled, however, that modulus values are very susceptible to individual interpretation of the slope of load-strain recordings. Differences of ± 10 percent are not at all uncommon.

The effect of test date on tensile properties appears to be such that the tensile strength and elongation decrease with increasing time between molding and testing. While the observed decreases are statistically significant the actual decreases, which range from 2 to 5 percent for strength and 8 to 35 percent for elongation, may not be practically significant.

One other effect not addressed statistically but which was built into the project was the effect of predrying the Ryton before molding. While predrying appears to have no effect on either modulus or elongation, the strength appears to be reduced by about 5 percent when the material is not predried before molding.

5.24 TENSILE CREEP TESTING OF RYTON R-4

The objective of this investigation was to study the effects of fiber orientation on tensile and creep properties of Phillips Ryton R-4. Fiber orientation in injection molded articles results from melt flow patterns in the mold and is related to part thickness.

Four inch discs of two different thicknesses were molded. Tensile specimens were cut in both the longitudinal and transverse

directions (with respect to the fiber flow pattern) from these discs and tested for static strength, modulus, and elongation and tensile creep behavior. Table 93 presents the static tensile properties.

TABLE 93
ROOM TEMPERATURE TENSILE PROPERTIES
OF RYTON R-4

Molded Thickness		Test Direction	Strength		Modulus		Elong. (%)
(inch)	(mm)		(10 ³ psi)	(MPa)	(10 ⁶ psi)	(GPa)	
0.064	1.63	Longitudinal	12.79	88.1	1.73	11.9	0.93
0.064	1.63	Transverse	5.97	41.1	1.34	9.2	0.63
0.082	2.08	Longitudinal	11.36	78.3	1.61	11.1	0.88
0.083	2.08	Transverse	6.20	42.7	1.40	9.6	0.56

Creep testing is currently underway but no data are yet available.

5.25 HIGH TEMPERATURE ADHESIVE EVALUATION

With the supersonic compressor section (C-4) of the 16S wind tunnel at AEDC (Arnold AFS, Tennessee) currently being rebladed with composites, the need for an adequate high-temperature adhesive for long-term structural use has become the limiting factor for bonding the composite (polyimide-glass) reblade shell to steel spar used to complete the blade-disk attachment. In response to this need a program was initiated to evaluate several candidate adhesive systems and processing approaches in order to satisfy the need for establishing a design data base on which to make high-temperature adhesive selections.

Three material variables and one process variable were examined in the program. The material variables were: (a) adherend material, (b) type of surface primer, and (c) adhesive. The process variable was the type of surface preparation used on the adherend.

Two adherend materials were used: (a) AISI 4130 steel and (b) E-glass/polyimide (PMR15/7781) composite material. Each of these are in current use in the compressor blade bonding application mentioned earlier.

Three surface primer conditions were examined: (a) none, (b) BR34, a companion primer for FM34 for American Cyanamide, and (c) a PMR15 varnish.

Basically, only two adhesives were evaluated, FM34 and PMR15, although late in the program, a brief look was taken at Thermid 600.

Five different surface preparations were examined, two specific to the glass/polyimide composite adherends, and three specific to the steel adherends. These were:

(a) Composite adherends

- (1) Nomex peel ply, and
- (2) Mechanical, consisting of a glass bead blasting treatment;

(b) Steel adherends

- (1) Mechanical, consisting of a glass bead blasting treatment (ASTM D2651, method A for stainless steel),
- (2) Mechanical abrasion followed by etching in a phosphoric acid-ethanol solution, and
- (3) Mechanical abrasion followed by etching in Metex T-103 solution and passivation in a sodium dichromate solution.

Two types of tests were used for the adhesive evaluations conducted during this program, wedge crack-extension and lap shear. The first was employed to screen candidate surface preparations for their ability to retain a high level of interfacial adhesion during high temperature exposure. The second was utilized to assess the resistance of the adhesives themselves to degradation during long-term high temperature aging.

The investigation was conducted in two phases. The first was aimed at identifying the best of several candidate surface

preparation procedures. When this phase was completed, only the best surface preparation procedure for each type of adherend was used for specimen fabrication in the second phase. The second phase was aimed at determining which adhesive provided the best lap shear properties during long-term high temperature aging.

During the screening of surface preparation procedures in Phase I, a total of 19 combinations of adherend type, surface preparation method, primer and adhesive were used to prepare wedge crack-extension specimens. These specimens were exposed to 450°F (232°C) for seven days and crack growth measured as a function of time. The results indicated that for the composite adherends, the mechanical abrasion was the better of the two methods examined, while for the steel adherends, the chemical cleaning procedure involving Metex T-103 was the best of the three methods examined.

During Phase II, all lap joint panels were made with one steel and one composite adherend whose surface were prepared with the respective treatments determined best in Phase I. Two adhesive/primer systems were used (FM34/BR34 and PMR15/PMR15). Table 94 presents the results of these tests.

TABLE 94
LAP SHEAR PROPERTIES OF FM-34 AND PMR-15
STEEL-TO-COMPOSITE PANELS

Test Temperature (°F) (°C)	FM-34		PMR-15	
	Lap Shear Strength (psi) (MPa)		Lap Shear Strength (psi) (MPa)	
0 -18	1760	12.1	2010	13.8
72 22	1650	11.4	2240	15.4
550 288	570	3.9	2365	16.3
72 22 [after 500 hrs. @ 550°F (288°C)]	1110	7.6	1860	12.8
550 288 [after 500 hrs. @ 550°F (288°C)]	760	5.2	1680	11.6
72 22 [after 1000 hrs. @ 550°F (288°C)]	860	5.9	1010	7.0
550 288 [after 1000 hrs. @ 550°F (288°C)]	650	4.5	1330	9.2

A technical report is being prepared describing all of the procedures and results of this investigation in detail.

SECTION 6 LUBRICANTS

6.1 HYDRAULIC FLUID

A hydraulic fluid, MLO 81-72, was characterized by determining its (1) viscosity at -54°C, -40°C, 40°C, and 100°C; (2) flash point; (3) four-ball wear; and (4) oxidation-corrosion characteristics. The sample passed all the MIL-H-5606D specifications except the -40°C specification. This data point was rechecked and the data were repeatable.

A hydraulic fluid, MLO 80-70, was characterized by oxidation-corrosion analysis. The fluid passed the MIL-H-5606D specification for oxidation-corrosion.

Four hydraulic fluids, MLO 81-13, MLO 81-14, MLO 81-70, and MLO 81-72 were analyzed by determining oxidation-corrosion studies per MIL-H-5606 specification. MLO 81-13, MLO 81-70, and MLO 81-72 met the MIL-H-5606 requirements. MLO 81-14 does not pass due to the fluid's excessive weight loss and excessive viscosity change. A different sample (MLO 81-70) of this fluid was analyzed and it met the requirements of the MIL-H-5606 specification. The question was--Why did MLO 81-14 have such an excessive weight loss? A study was conducted to determine the effect on the fluid and metals by varying certain test conditions.

Hydraulic fluid samples, MLO 80-490 thru MLO 80-493 were analyzed to determine their viscosities at -54°C, -40°C, 40°C, and 100°C, flash points, pour points, acid numbers, four-ball wear scars, and water content. Oxidation-corrosion data were also obtained on MLO 80-490 and MLO 80-491.

A hydraulic fluid (MLO 80-494) was characterized by determining viscosities at -53.9°C, 37.8°C and 40°C, water content, and chlorine content.

Several hydraulic fluids, MLO 80-467 thru MLO 80-470, were analyzed to determine their viscosities at -54°C, -40°C, 40°C, and 100°C, flash points, pour points, acid numbers, four-ball wear scars and water contents. Oxidation-corrosion data were also obtained on MLO 80-467 thru MLO 80-468.

An experimental hydraulic fluid (MLO 80-328) was characterized by determining its viscosity at 40°C, flash point, and acid number. Oxidation-corrosion data were also obtained on this fluid. The oxidation-corrosion analysis showed poor repeatability. This could be due to the marginal nature of the formulation.

An unknown sample (MLO 80-429) was analyzed by determining its acid number and viscosity at 37.8°C (100°F) and 98.9°C (210°F). Capillary gas chromatography and high pressure liquid chromatography were also used. These analyses showed that the fluid may be a MIL-H-5606 type hydraulic fluid.

An experimental hydraulic fluid (MLO 80-299) was characterized by determining its kinematic viscosities at various temperatures, flash point, pour point, and acid number. Oxidation-corrosion data were also obtained on this fluid. This fluid was characterized using methods specified in the MIL-H-5606 specification.

Several experimental hydraulic fluids were characterized by determining their flash point, Shell four-ball wear scars, pour points, and viscosities at various temperatures. Oxidation-corrosion data were also obtained on these fluids. These fluids were characterized using methods specified in MIL-H-5606 specification.

A hydraulic fluid MLO 81-399 was analyzed for viscosity, acid number, flash point, four-ball wear, and oxidative stability. The sample passed the requirements for viscosity, flash point, and Shell four-ball wear. However, the sample did not pass the viscosity change and weight loss requirements in the MIL-H-5606 specification for hydraulic fluids.

Three samples (MLD 81-271 thru MLD 81-273) were analyzed by determining their viscosities at 37.8°C (100°F) and 98.9°C (210°F), pour points, flash points, Shell four-ball wear, and oxidation-corrosion characteristics.

A hydraulic fluid, MLO 82-21, was characterized by determining its flash point (closed and open cup), fire point, pour point, acid number, wear scar, water content, and kinematic viscosities at -54°C, -40°C, +40°C, and 100°C. This fluid meets the MIL-H-5606 specification requirements for these characteristics.

A hydraulic fluid, MLO 82-24, was characterized by the same methods as those described for characterizing MLO 82-21 with the addition of the oxidation-corrosion test. This fluid also meets the MIL-H-5606 specification requirements for these characterizations.

Two hydraulic fluid base stocks (MLO 82-22 and MLO 82-23) were characterized by determining their flash points, pour points, and viscosities at -40°C, +40°C, and 100°C. The data show that MLO 82-23 is more viscous than MLO 82-24.

Two hydraulic fluids, MLO 82-57 and MLO 82-58, were analyzed by determining viscosities, flash points, and MIL-H-5606 content by gas chromatography. MLO 82-57 is a mixture containing approximately 50 percent by GC of MIL-H-5606 hydraulic fluid. The flash point and -40°C viscosity also confirm this. MLO 82-58 appears to be all MIL-H-5606 by GC methods, flash point, and -40°C viscosity.

6.2 LUBRICATING FLUIDS

A lubricating oil (MLO 82-25) was characterized by determining its flash point, pour point, acid number, and viscosities at -40°C and +40°C. This fluid does not meet the MIL-L-7870 requirements for the +40°C viscosity. Oxidation-corrosion data were also obtained on this sample and the acid number change is higher than the limits set forth in the MIL-L-7870 specification.

A grade M lubricating oil, MLO 82-68, was characterized by determining its flash point, pour point, and viscosity at 38°C (100°F) and 99°C (210°F). The pour point does not meet the requirement set forth in the MIL-L-6086C specification for grade M lubricating oils. This pour point determination was repeated using another sample, MLO 82-136, obtained from the same batch of oil as MLO 82-68 and there was not a significant change in the pour point.

MLO 82-263 was characterized by determining its flash point, acid number, viscosities at -54°C (-65°F) and 38°C (100°F). Oxidation-corrosion data were obtained at 121°C (250°F). This liquid lubricant was characterized using procedures specified in MIL-L-6085 specification.

MLO 80-454 was characterized by determining its flash point, fire point, pour point, and viscosities at various temperatures.

MLO 80-461 was characterized by determining flash point, fire point, pour point, acid number, and viscosities at 37.8°C and 98.9°C.

A fresh lubricating oil (MLO 81-159) and the same type oil (MLO 81-160) which overheated were compared with each other by determining acid numbers and viscosities at 37.8°C. There was no change between the oils by acid number or by viscosity at 37.8°C.

A flash point by Cleveland open cup and a viscosity at 54.4°C (130°F) were determined on a lubricating oil (MLO 81-161) to see if these determinations meet the MIL-L-6085 specification requirements. This oil did meet these two requirements.

MLO 81-84 was analyzed by determining its viscosities at -54°C and 54.4°C, acid number, and oxidation-corrosion studies (per MIL-L-6085 specification). The fluid passed the MIL-L-6085 specification requirements.

MLO 81-120 (KG80) and MLO 81-121 (SRG-160) were analyzed by determining their viscosities at 37.8°C and 98.9°C, acid numbers, Shell four-ball wear studies and oxidation-corrosion studies per MIL-L-83176 specifications. The data reported were within the MIL-L-83176 specification. It was noted that the SRG-160 sample (MLO 81-121) was cloudy. The sample was warmed to 70°C for four hours and the sample became cloudy. The sample was then dried over calcium chloride and after 24 hours the sample was still cloudy. This phenomenon is typical of paraffinic based mineral oils containing wax.

6.3 ADDITIVES

An additive (MLO 81-162) was characterized by infrared spectroscopy and gas chromatography (FID). These analyses show that the sample is a light grade synthetic or natural hydrocarbon.

6.4 INSTRUMENT OIL CANDIDATE FLUIDS

MLO 80-216 and MLO 80-217 were characterized by determining their flash points, Shell four-ball wear scars at different loads, acid numbers, wettabilities, and viscosities at 38°C (100°F) and 99°C (210°F). Oxidation-corrosion data were also obtained on both fluids. These fluids were characterized using procedures specified in MIL-H-83176 specification.

Two petroleum based instrument oils, MLO 80-485 and MLO 80-486 were characterized by determining flash points, viscosities at 37.8°C and 98.9°C, water content, wettabilities and four-ball wear scars. Two synthetic hydrocarbon based instrument oils, MLO 80-487 and MLO 80-488, were analyzed by determining viscosities at 98.9°C, wettabilities and four-ball wear scars. A base oil used in formulating synthetic instrument oils was analyzed by determining viscosity at 98.9°C and wettability.

SECTION 7
REFERENCES

1. ASTM E-399-78, "Plane-Strain Fracture Toughness of Metallic Materials," Part 10.
2. Cervay, Russell R., "An Empirical Model for Loading Ratio Effect on Fatigue Crack Growth Rate Data," University of Dayton Research Institute Technical Report AFWAL-TR-81-4140, November 1981.
3. Goodwin, S. L. and Abbott, N. J., "Kevlar Properties Investigation Development of Kevlar Tensile Test Methods," Air Force Flight Dynamics Laboratory (FET), Wright-Patterson AFB, Ohio, Technical Report AFFDL-TR-79-3019, March 1979.
4. Cervay, Russell R., "Mechanical Property Evaluation of Aluminum Alloy 7010-T73651," University of Dayton Research Institute, Technical Report AFWAL-TR-80-4094.
5. Harmsworth, C. L. and Petrak, G. J., "An Investigation of Improperly Quenched (Soft) Aluminum Plate," AFML-TR-79-4205, December 1979.
6. Ruschau, J. J., "A Thorough Mechanical Property Investigation of Slack-Quenched (Soft) Aluminum Alloy 2124-T851 Plate," UDR-TM-80-02, January 1980.
7. Cervay, R. R., "Tensile Properties of Six Slack-Quenched Aluminum Alloy Rolled Plates," UDR-TM-79-23, November 1979.
8. Ruschau, J. J., "Crack Growth Investigation of "Soft" Aluminum Undergoing the F-16 Spectrum," UDR-TM-80-20, June 1980.
9. Petrak, G. J. and Ruschau, J. J., "Fatigue and Fatigue Crack Growth Characteristics of Improperly Quenched (Substrength) Aluminum," Accepted for publication in Engineering Fracture Mechanics, January 1980.
10. Petrak, G. J. and Gunderson, A. W., "Compilation of Mechanical Property Data for Improperly Quenched (Soft) Aluminum Plates," AFWAL-TR-81-4112.
11. Jones, R. E. and Fudge, K. A., "Engineering Design Data for Aluminum Alloy 7050-T73651 Plate," AFML-TR-73-269, November 1973.

12. Clark, Jr., W. G. and Hudak, Jr., S. J., "Variability in Fatigue Crack Growth Rate Testing," Journal of Testing and Evaluation, Vol. 3, No. 6, November 1975, pp. 454-476.
13. Hudak, Jr., S. J., et al., "Development of Standard Methods of Testing and Analyzing Fracture Crack Growth Rate Data," Third Semiannual Report, Westinghouse Research Labs, March 1977.
14. Hudak, S. J., et al., "Development of Standard Methods of Testing and Analyzing Fatigue Crack Growth Rate Data," AFML-TR-78-40, May 1978, pp. 14-16.
15. U.S. Patent #3,919,884.
16. Ruschau, John J., "Fatigue Crack Growth Rate Data Acquisition System for Linear and Nonlinear Fracture Mechanics Applications," AFWAL-TR-81-4011, March 1981.
17. Usmani, A. M., et al., "Development of High Adhesion Integral Fuel Tank Sealants," AFWAL-TR-80-4195, January 1981.

END

FILMED

1-83

DTIC